FRONT UNDERRIDE PROTECTION DEVICES:
DESIGN METHODOLOGY FOR HEAVY VEHICLE CRASHWORTHINESS

by

Adam George Mount Cook

A Thesis Presented in Partial Fulfillment
of the Requirements for the Degree of

Master of Applied Science

In

Mechanical Engineering

Faculty of Engineering and Applied Science
University of Ontario Institute of Technology
Oshawa, Ontario, Canada

April 2016

© 2016 Adam G. M. Cook

ABSTRACT

North American Heavy Vehicles contribute to a third of all road fatalities in Canada. Head on collisions are one of the most severe, as the mismatch of vehicle weight and sizing intensifies when a passenger vehicle is impacted. To improve crash safety, Front Underride Protection Devices (FUPDs) are a proposed solution to establishing a compatible collision between a passenger vehicle and a heavy vehicle. The European Union is among numerous administrations to regulate FUPDs, yet FUPDs are nonexistent in North America. Current regulations conform to European Cab-over Engine Tractors designs. Implementation of current regulations in North American conflicts with the widely driven Conventional Style Tractor due to the different design space for a FUPDs. This study builds on developing regulations for North America, and establishes a design methodology to developing and optimizing FUPDs for the Conventional Style Tractor enlightening the crashworthy importance of front underride protection devices to improving road safety. Advanced two stage optimization methodology was outlined to ensure industry targets are embedded with in the design to develop lightweight and cost effective devices. Recommendations for the modifications of the ECE R93 for Conventional Style Tractor are outlined; P1 load magnitudes requirements for FUPD stiffness should be increased from the regulated 80 kN to 160 kN to improve small overlap collisions. Regulated geometric parameters were recommended to have a minimal frontal contact height of 240mm, with ground clearance set between 350mm to 400mm. Geometric configurations were outlined and restricted to conform to the aerodynamic curvatures of the tractors bumper. After validation of the National Crash Analysis Center (NCAC) Toyota Yaris finite element analysis (FEA) model for side impact, the addition of a FUPD enhanced the survivability of passenger vehicle. The work achieved in enhancing the design methodology for industrial implementation and outlining regulations for North America.

TABLE OF CONTENTS

ABSTRACT ..... **ii**

TABLE OF CONTENTS ..... **iii**

LIST OF FIGURES ..... **x**

LIST OF TABLES ..... **xviii**

ABBREVIATIONS ..... **xix**

ACKNOWLEDGEMENTS ..... **xx**

CHAPTER 1: INTRODUCTION **1**

1.1 MOTIVATION 1

1.2 LITERATURE REVIEW 7

1.2.1 Variants of Tractor Styles 7

1.2.2 Frontal Crash Testing 9

1.2.3 Current FUPD Regulations 10

1.2.4 Rear Underride Protection Devices 12

1.3 WORKING FOUNDATION – METHODS FOR DESIGN AND TESTING 14

1.3.1 Design Methodology 15

1.3.2 Ground Clearance and Contact Section Height 17

1.3.3 Modified ECE R93 19

1.3.4 Dual Spring System Testing Method 19

1.3.5 Dual Stage Front Underride Protection Device (dsFUPD) 21

1.3.6 Additional Consideration 22

1.3.6.1 Angled Collisions 22

1.3.6.2 Heavy Braking of the Passenger Vehicle 22

1.4 DEVELOPMENT SOFTWARE 24
1.4.1 LS DYNA 24
1.4.2 LS-DYNA Tool Box - Topology, Shape and Size Optimization 25
1.4.3 Mechanical Simulation Software - Vehicle Behavior Simulation 26
1.5 OPTIMIZATION TECHNIQUES 26
1.5.1 Metaheuristics Optimization 26
1.5.2 Optimization Strategies 27
1.5.2.1 Direct Simulation 27
1.5.2.2 Metamodel Optimization 27
1.5.3 Optimization Algorithm Methods 28
1.5.3.1 Genetic Algorithm (GA) 28
1.5.3.2 Adaptive Simulated Annealing (ASA) 31
1.5.3.3 Hybrid Algorithms with Leap Frog Optimizer for Constrained Minimization 32
1.5.4 Metamodeling Techniques 33
1.6 CRASHWORTHY MATERIALS 34
1.7 CLOSING REMARKS 36

CHAPTER 2: TESTING METHODS & EVALUATION METRICS 37
2.1 FINITE ELEMENT ANALYSIS VEHICLE MODELS 39
2.1.1 Passenger Vehicle Models 39
2.1.2 Tractor-Trailer Models 41
2.1.2.1 Full Tractor-Trailer Model 41
2.1.2.2 Component Level VNL Tractor Model 42
2.1.2.3 Dual Stage FUPD F9 Model 43

2.2 VIRTUAL ENVIRONMENT SETUP 44
2.2.1 FEA Solver Environments 44
2.2.2 Quasistatic Point Load Experiment 45
2.2.3 Dynamic Collision Experiments 46
2.3 EVALUATION METRICS 48
2.3.1 Compatibility Profile of the Collision 48
2.3.2 Contour of Interface Resultant Forces 49
2.3.3 Insurance Institute for Highway Safety - Rating Occupant Compartment Intrusion 50
2.4 INITIAL ENVIRONMENT CONDITIONS CONSIDERATION 52

CHAPTER 3: GEOMETRIC PARAMETERS & LOADING CONDITIONS ... 54
3.1 VIRTUAL EXPERIMENT I – DYNAMIC IMPACT WITH A RIGID BAR .. 54
3.1.1 Virtual Experiment I – Setup 57
3.1.2 Virtual Experiment I – Results 58
3.1.2.1 Results I – Collision Compatibility Profiles – Toyota Yaris 59
3.1.2.2 Results I – Collision Compatibility Profiles – Ford Taurus 60
3.1.2.3 Results II – IIHS Intrusion Matrices – Toyota Yaris 61
3.1.2.4 Results II – IIHS Intrusion Matrices – Ford Taurus 62
3.1.2.5 Results III – Impact Force Contour – Toyota Yaris 63
3.1.2.6 Results III – Impact Force Contour – Ford Taurus 66
3.2 GROUND CLEARANCE AND CROSS SECTION HEIGHT 67
3.3 IMPACT FORCES & LOADING CONDITIONS 71
3.4 VIRTUAL EXPERIMENT II – VERIFYING RESULTS ON A DEFORMABLE FUPD 74
3.4.1 Virtual Experiment II – Setup 74

3.4.2 Virtual Experiment II – Results 76
3.4.2.1 Results III – Impact Force Contour – Toyota Yaris 77
3.4.3 Virtual Experiment II – Conclusions 78
3.5 CHAPTER SUMMARY 79

CHAPTER 4: DESIGN OPTIMIZATION METHODOLOGY & CRASHWORTHY MATERIALS 81
4.1 DESIGN OPTIMIZATION METHODOLOGY 82
4.2 MULTIOBJECTIVE OPTIMIZATION APPROACH TO DEVELOPING FUPDs 83
4.2.1 OPTIMIZATION TESTING ENVIRONMENT 84
4.2.2 EXPERIMENT I – OPTIMIZATION APPORACH 85
4.2.2.1 Virtual Experiment I – Results 86
4.2.2.2 Virtual Experiment I – Discussion & Conclusions 91
4.2.3 Virtual Experiment II – Dynamic Collision Testing 94
4.2.3.1 Virtual Experiment II – Setup 94
4.2.3.2 Virtual Experiment II – Results 95
4.2.3.3 Virtual Experiment I – Discussion & Conclusions 96
4.2.4 Design Optimization Methodology Conclusions 98
4.3 CRASHWORTHY MATERIALS 100
4.3.1 Optimization Stage I – Single Material Consideration 101
4.3.1.1 Stage I Optimization – Results 103
4.3.1.2 Stage I Optimization – Discussion & Conclusions 105
4.3.2 Stage II Optimization – Material Collection Optimization 105
4.3.2.1 Stage II Optimization – Results 106
4.3.2.2 Stage II – Discussion & Conclusions 107

4.3.3 Design Verification – Dynamic Collision Testing 108
4.3.3.1 Design Verification – Setup 108
4.3.3.2 Design Verification – Toyota Yaris 109
4.3.3.3 Design Verification – Ford Taurus 110
4.3.3.4 Design Verification – Discussion & Conclusions 111
4.3.4 Crashworthy Materials Conclusions 111
4.4 CHAPTER SUMMARY 112

CHAPTER 5: DESIGN FOR ENHANCED CRASHWORTHINESS COMPATIBILITY 114
5.1 VIRTUAL EXPERIMENT I – IMPACT VERTICAL SECTION HEIGHT .. 115
5.1.1 Virtual Experiment I – Setup 116
5.1.2 Virtual Experiment I – Results 117
5.1.3 Virtual Experiment I – Discussion & Conclusions 118
5.2 VIRTUAL EXPERIMENT II – BASE CURVE SECTION ANGLE 118
5.2.1 Virtual Experiment II – Setup 118
5.2.2 Virtual Experiment II – Results 120
5.2.3 Virtual Experiment II – Discussion & Conclusions 121
5.3 VIRTUAL EXPERIMENT III – OUTER CURVE SECTION ANGLE 121
5.3.1 Virtual Experiment III – Setup 122
5.3.2 Virtual Experiment III – Results 122
5.3.3 Virtual Experiment III – Discussion & Conclusions 123
5.4 VIRTUAL EXPERIMENT IV – SIDE OVERLAP SUPPORT 123
5.4.1 Virtual Experiment IV – Setup 124
5.4.2 Virtual Experiment IV – Results I: IIHS Occupant Compartment Intrusion.. 126

5.4.3 Virtual Experiment IV – Results II – 30% Overlap: Plastic Strain 127
5.4.4 Virtual Experiment IV – Discussion & Conclusions 128
5.5 CHAPTER SUMMARY 129

CHAPTER 6: ADDITIONAL CONSIDERATIONS FOR FUPDs PERFORMANCE 130
6.1 HEAVY BRAKING AND PITCHING 130
6.1.1 Virtual Experiment I – Impact Velocity and Pitch Angle 131
6.1.1.1 Virtual Experiment I – Setup 132
6.1.1.2 Virtual Experiment I – Results 132
6.1.1.3 Virtual Experiment I – Discussion & Conclusions 134
6.1.2 Virtual Experiment II – Heavy Braking Dynamic Collision 135
6.1.2.1 Virtual Experiment II - Setup 136
6.1.2.2 Virtual Experiment II – Results 136
6.1.2.3 Virtual Experiment II – Discussion & Conclusions 138
6.1.3 Virtual Experiment III – Heavy Braking Dynamic Collision 139
6.1.3.1 Virtual Experiment III - Setup 139
6.1.3.2 Virtual Experiment III – Results 140
6.1.3.3 Virtual Experiment III – Discussion & Conclusions 140
6.1.4 Section Discussion 141
6.2 SIDE IMPACT OF PASSENGER VEHICLE 142
6.2.1 Virtual Experiment I - Structurally Validating the Toyota Yaris for IIHS Side Impact Crashworthiness Evaluation 145
6.2.1.1 Virtual Experiment I - Setup 147
6.2.1.2 Virtual Experiment I - Results 148
6.2.1.3 Discussion & Conclusions 148

6.2.2 Virtual Experiment II – Dynamics Side Impact Crashworthiness of the FUPDs 149
6.2.2.1 Virtual Experiment II - Setup 149
6.2.2.2 Virtual Experiment II - Results 150
6.2.2.3 Virtual Experiment II - Discussion & Conclusions 152
6.2.3 Section Discussion 152
6.3 REAR IMPACT OF PASSENGAR VEHICLE 154
6.3.1 Virtual Experiment I – Dynamic Rear Impact Setup 156
6.3.2 Virtual Experiment I - Results 160
6.3.3 Virtual Experiment I – Discussion 161
6.3.4 Section Discussion 162
6.4 CHAPTER SUMMARY 163

CHAPTER 7 CONCLUSION AND FUTURE WORK 164
7.1 ACCOMPLISHMENTS & RECOMMENDATIONS 164
7.2 CONCLUSIONS 165
7.3 FUTURE WORK 167

PUBLICATIONS 169
REFERENCES 170

LIST OF FIGURES

Figure 1-1 Head-on Collision between a Passenger Vehicle and Tractor-Trailer [4] 1
Figure 1-2 Front-Front Collision of the Toyota Yaris (Blue – Pink Chassis rail) Underriding a Tractor-trailer (Red – Green Chassis rail) 2
Figure 1-3 Deaths in Crashes Involving Large Trucks, 1975-2014 [14]..... 4
Figure 1-4 Overall Average Collision Statistic for Fatalities and Injuries in Canada Between 2001-2005 [7]..... 5
Figure 1-5 Tractor-Trailers: Average Collision Statistic for Fatalities and Injuries in Canada Between 2001-2005 [7]..... 5
Figure 1-6 Heavy Trucks: Average Collision Statistic for Fatalities and Injuries in Canada Between 2001-2005 [7]..... 6
Figure 1-7 Tractor-trailer Variants [20]..... 7
Figure 1-8 Conventional Tractor (North America) and Cab-over Engine Tractor (EU) Measurement Standards [21] 7
Figure 1-9 Axel Position Variants in Conventional Tractors [23, 24]..... 8
Figure 1-10 Front Bumper Height Classification [23]..... 9
Figure 1-11 CMVSS/FMVSS 208 [29] 10
Figure 1-12 IIHS Small-Overlap Frontal Impact [29] 10
Figure 1-13 ECE R93 Geometry and Point Loading Testing [32] 11
Figure 1-14 RUPDs on a Manac Trailer [37] 12
Figure 1-15 Post-Impact of Passenger Vehicles and the Trailer Rear end a with a .RUPD [37]..... 13
Figure 1-16 CMVSS 223 Loading Points for RUPDs [35] 13
Figure 1-17 MacDonald's Three Tier Design Strategy [5]..... 15
Figure 1-18 Tier 2: FUPD Design Map [5] 16
Figure 1-19 Topology Optimization of a FUPD Design Envelope [5]..... 17
Figure 1-20 64km/h-100%-120mm with 350mm Ground Clearance at Time of Primary (Left) and Secondary (Right) Impact Force Peaks [5]..... 18
Figure 1-21 Force Height Comparison with ECE R93 (inner range - blue) and MacDonald (broad range - red) Recommended Geometry [5]..... 18

Figure 1-22 Simplified FUPD Constrained by Dual Spring System [5] 20
Figure 1-23 Compatibility Profile of Yaris 64km/hr – 100% Overlap: Justification of Utilizing Spring System Simplification [5] 20
Figure 1-24 Concept 2 with Extension Variations: 0mm, 100mm and 200mm (Bottom View) [5] 21
Figure 1-25 FUPD Model F8 [5] 22
Figure 1-26 dsFUPD Model F9 [5] 22
Figure 1-27 CarSim and LS-DYNA Deceleration Profiles (Wheels Locked) [5] 23
Figure 1-28 Yaris 55km/h vs J11 Concept FUPD Compatibility Profile 23
Figure 1-29 Visual Environment of LS-DYNA – Multiple Car Rear Impact [43] 25
Figure 1-30 Elitism Procedure in NSGA-II [47] 30
Figure 1-31 Simulate Annealing Probability & Local Minima [51] 31
Figure 1-32 Metallurgical Designation Range of Steel Alloys Grades [52] 34
Figure 2-1 Design Methodology Structure 38
Figure 2-2 Tier 2 and 3 – In detailed Process Map 39
Figure 2-3 2010 Toyota Yaris FEA model provided by NCAC 40
Figure 2-4 Impact Comparison of the Toyota Yaris in NCAP Test 5677 and simulation [55] 40
Figure 2-5 2001 Ford Taurus FEA model provided by NCAC 41
Figure 2-6 NTRCI Tractor-trailer Validation with a Roadside Barrier 42
Figure 2-7 Primary (left) and Secondary (right) Component Level VNL Tractor Models [5] 42
Figure 2-8 Comparisons of Collisions Involving Toyota Yaris with Closing Speed of 64km/h and 50% Overlap versus the Primary Component Level VNL Tractor (left) and complete NTRCI Tractor-Trailer Model (right) [5] 43
Figure 2-9 dsFUPD F9 model 43
Figure 2-10 Quasistatic Loading Environment 45
Figure 2-11 Overlap Coverage with Respect to the Passanger Vehicle 47
Figure 2-12 Simplified FUPD (in red) Constrained by Dual Spring System 47
Figure 2-13 Impact Force vs. Relative Displacement/Deformation 49
Figure 2-14 Impact Forces Relation to Visual Contour Force Displace 49

Figure 2-15 IIHS Intrusion Measuring Reference Points [28] 50
Figure 2-16 IIHS Guidelines for Rating Occupant Compartment Intrusion [52] 51
Figure 2-17 Toyota Yaris IIHS test comparisons [17] 52
Figure 2-18 Ford Taurus IIHS test comparisons [17] 52
Figure 3-1 Vertical Measurements 55
Figure 3-2 Rigid Bar Front Profile with ECE R93 Point Load Placements 57
Figure 3-3 Experiment Setup –Head-On 100% Coverage 58
Figure 3-4 Yaris – 100% – 120CH 59
Figure 3-5 Yaris – 100% – 240CH 59
Figure 3-6 Yaris – 50% – 120CH 59
Figure 3-7 Yaris – 50% – 240CH 59
Figure 3-8 Yaris – 30% – 120CH 59
Figure 3-9 Yaris – 30% – 240CH 59
Figure 3-10 Taurus – 100% – 120CH 60
Figure 3-11 Taurus – 100% – 240CH 60
Figure 3-12 Taurus – 50% – 120CH 60
Figure 3-13 Taurus – 50% – 240CH 60
Figure 3-14 Taurus – 30% – 120CH 60
Figure 3-15 Taurus – 30% – 240CH 60
Figure 3-16 Yaris – 100% – 120CH 61
Figure 3-17 Yaris – 100% - 240CH 61
Figure 3-18 Yaris – 50% – 120CH 61
Figure 3-19 Yaris – 50% – 240CH 61
Figure 3-20 Yaris – 30% – 120CH 61
Figure 3-21 Yaris – 30% – 240CH 61
Figure 3-22 Taurus – 100% – 120CH 62
Figure 3-23 Taurus – 100% – 240CH 62
Figure 3-24 Taurus – 50% – 120CH 62
Figure 3-25 Taurus – 50% – 240CH 62
Figure 3-26 Taurus – 30% – 120CH 62
Figure 3-27 Taurus – 30% – 240CH 62

Figure 3-28 100% Overlap for 120mm Height at 350mm Ground Clearance..... 63
Figure 3-29 100% Overlap for 120mm Height at 400mm Ground Clearance..... 63
Figure 3-30 100% Overlap for 240mm Height at 350mm Ground Clearance..... 63
Figure 3-31 50% Overlap for 240mm Height at 350mm Ground Clearance 64
Figure 3-32 30% Overlap for 240mm Height at 350mm Ground Clearance 64
Figure 3-33 100% Overlap for 240mm Height at 400mm Ground Clearance..... 65
Figure 3-34 50% Overlap for 240mm Height at 400mm Ground Clearance 65
Figure 3-35 30% Overlap for 240mm Height at 400mm Ground Clearance 65
Figure 3-36 100% Overlap for 240mm Height at 350mm Ground Clearance..... 66
Figure 3-37 50% Overlap for 240mm Height at 350mm Ground Clearance 66
Figure 3-38 30% Overlap for 240mm Height at 350mm Ground Clearance 66
Figure 3-39 100% Overlap for 240mm Height at 400mm Ground Clearance..... 66
Figure 3-40 50% Overlap for 240mm Height at 400mm Ground Clearance 67
Figure 3-41 30% Overlap for 240mm Height at 400mm Ground Clearance 67
Figure 3-42 120mm Cross Section Height – 500mm Ground Clearance 68
Figure 3-43 120mm Cross Section Height – 300mm Ground Clearance 68
Figure 3-44 240mm Cross Section Height – 350mm Ground Clearance 69
Figure 3-45 240mm Cross Section Height – 400mm Ground Clearance 70
Figure 3-46 Toyota Yaris Impact to the Rigid Bar Compatibility Profile for 240mm Height at 350mm Ground Clearance..... 72
Figure 3-47 100% Overlap – F9 76
Figure 3-48 100% Overlap – F9 – IIHS..... 76
Figure 3-49 50% Overlap – F9 76
Figure 3-50 50% Overlap – F9 – IIHS..... 76
Figure 3-51 30% Overlap - F9 76
Figure 3-52 30% Overlap – F9 – IIHS..... 76
Figure 3-53 100% Overlap Impact from the Toyota Yaris..... 77
Figure 3-54 50% Overlap Impact from the Toyota Yaris..... 77
Figure 3-55 30% Overlap Impact from the Toyota Yaris..... 78
Figure 4-1 Optimization Selection Path 83
Figure 4-2 Computational Results of Phase 3 Optimization Solving CPU time. 87

Figure 4-3 Feasible Results from Phase 3 NSGA-II 87
Figure 4-4 HASA Feasible Results Analysis of All Three Phases with Respect to Minimizing Each Objective per Iteration 88
Figure 4-5 HGA Feasible Results Analysis of All Three Phases with Respect to Minimizing Each Objective Per Iteration 89
Figure 4-6 NSGA-II Feasible Results per Iteration with Respect to Material Cost Minimization 90
Figure 4-7 NSGA-II Feasible Results per Iteration with Respect to System Mass Minimization 90
Figure 4-8 NSGA-II Feasible Results per Iteration with Respect to Displacement of Quasistatic Load P1 Minimization 90
Figure 4-9 100% Overlap Profile 95
Figure 4-10 100% Overlap – IIHS 95
Figure 4-11 50% Overlap Profile 95
Figure 4-12 50% Overlap – IIHS 95
Figure 4-13 30% Overlap Profile 95
Figure 4-14 30% Overlap – IIHS 95
Figure 4-15 Toyota Yaris 30% Overlap Impact with Side Support Structure Failure 97
Figure 4-16 Ford Taurus 30% Overlap Impact with Side Support Structure Failure 97
Figure 4-17 Group of Materials Optimized F9 Design System Mass and Cost 103
Figure 4-18 Group of Materials Optimized F9 Design Modified ECE R93 Point Load Measurements 104
Figure 4-19 NSGA-II Feasible Results per Iteration with Respect to Material Cost Minimization 106
Figure 4-20 NSGA-II Feasible Results per Iteration with Respect to System Mass Minimization 106
Figure 4-21 NSGA-II Feasible Results per Iteration with Respect to Displacement of Quasistatic Load P1 Minimization 106
Figure 4-22 100% Overlap Profile 109
Figure 4-23 100% Overlap – IIHS 109
Figure 4-24 50% Overlap Profile 109

Figure 4-25 50% Overlap – IIHS 109
Figure 4-26 30% Overlap Profile 109
Figure 4-27 30% Overlap – IIHS 109
Figure 4-28 100% Overlap Profile 110
Figure 4-29 100% Overlap – IIHS 110
Figure 4-30 50% Overlap Profile 110
Figure 4-31 50% Overlap – IIHS 110
Figure 4-32 30% Overlap Profile 110
Figure 4-33 30% Overlap – IIHS 110
Figure 4-34 Toyota Yaris Impacting the F9-2SDO at 30% Overlap 111
Figure 5-1 Toyota Yaris Impacting the Simplified Duel Spring FUPD 115
Figure 5-2 Experiment I & II Design Parameters – Side View of Chassis 115
Figure 5-3 Various Impact Section Height 116
Figure 5-4 Occupant Compartment Intrusion – 100% 117
Figure 5-5 Occupant Compartment Intrusion – 50% 117
Figure 5-6 Occupant Compartment Intrusion – 30% 117
Figure 5-7 Various Bottom Cure Angled Rigid Plates 119
Figure 5-8 Occupant Compartment Intrusion – 100% 120
Figure 5-9 Occupant Compartment Intrusion – 50% 120
Figure 5-10 Occupant Compartment Intrusion – 30% 120
Figure 5-11 Outer Curve Section Angle 121
Figure 5-12 Occupant Compartment Intrusion – 50% 122
Figure 5-13 Occupant Compartment Intrusion – 30% 122
Figure 5-14 Side Support Post 123
Figure 5-15 Side View of a Volvo VNL Chassis Rail (Permission from Volvo Group truck technology – North Carolina) 124
Figure 5-16 Overlap Side Support Placement to Chassis Angle Change 125
Figure 5-17 Occupant Compartment Intrusion – 50% 126
Figure 5-18 Occupant Compartment Intrusion – 30% 126
Figure 5-19 155 Degree - Top view 127
Figure 5-20 155 Degree - Back View 127

Figure 5-21 135 Degree - Top view 127
Figure 5-22 135 Degree - Back View 127
Figure 5-23 115 Degree - Top view 127
Figure 5-24 115 Degree - Back view 127
Figure 6-1 Heavy Braking Affects of a Vehicle - Side View 130
Figure 6-2 Velocity of the Toyota Yaris While Heavy Braking 132
Figure 6-3 Change of Ground Clearance Height of the Toyota Yaris While Heavy Braking 133
Figure 6-4 Velocity of the Tractor-Trailer While Heavy Braking 133
Figure 6-5 Change of Ground Clearance Height of the Tractor-Trailer While Heavy Braking 134
Figure 6-6 Longitudinal Acceleration of the Tractor-Trailer While Heavy Braking . 134
Figure 6-7 TruckSim Simulation and LS-DYNA Comparison of the Tractor-Trailer 136
Figure 6-8 CarSim Simulation and LS-DYNA Comparison of the Toyota Yaris 137
Figure 6-9 Heavy Braking of the Toyota Yaris vs. F9 FUPD Compatibility 137
Figure 6-10 Heavy Braking of the Toyota Yaris vs. F9 FUPD IIHS Intrusion 138
Figure 6-11 Heavy Braking Impact at 56 km/hr – 100% 140
Figure 6-12 Heavy Braking Impact at 64 km/hr – 100% 140
Figure 6-13 Heavy Braking Impact at 56 km/hr – 100% - IIHS 140
Figure 6-14 Heavy Braking Impact at 64 km/hr – 100% - IIHS 140
Figure 6-15 Tractor-Trailer Impacting the Side of a Volkswagen Passenger Vehicle [36] Photo: Kathleen O'Rourke 142
Figure 6-16 Structural B-Pillar (shown in Red) of a Toyota Yaris without Doors 142
Figure 6-17 Side Collision Testing Impact Approach Setups [38] 143
Figure 6-18 IIHS Side Impact Testing Guidelines 144
Figure 6-19 IIHS B-pillar to Longitudinal Centerline of Driver's Seat Rating [42] 144
Figure 6-20 IIHS Side Impact Test of a 2009 Toyota Yaris [44] 146
Figure 6-21 Toyota Yaris B-Pilar and Roof Cross Member 146
Figure 6-22 IIHS Side Impact Environment Setup 147
Figure 6-23 IIHS Evaluation Metric for B-Pilar Intrusion for the Toyota Yaris 147
Figure 6-24 IIHS B-Pilar Vertical Profiles - Intrusion Results 148

Figure 6-25 Post-Crash of the FEA Toyota Yaris – Correlating physical views seen in *Figure 6-20* 148
Figure 6-26 Impact Side Experiment Setup for FUPDs Testing 149
Figure 6-27 Top and Perspective View of Experiment Setup 150
Figure 6-28 IIHS B-Pilar Vertical Profiles - Intrusion Results..... 150
Figure 6-29 Without a FUPD Post-Crash – Top View 151
Figure 6-30 Without a FUPD – Driver Side View 151
Figure 6-31 Without FUPD – Angle View 151
Figure 6-32 F9 FUPD Post-Crash – Top View..... 151
Figure 6-33 F9 FUPD – Driver Side View 151
Figure 6-34 F9 FUPD – Angle View 151
Figure 6-35 Post-Collision of a Tractor-Trailer Rear-Ending a Passenger Vehicle Photograph Credited to Weld County Sheriff's Office [45]..... 154
Figure 6-36 Tractor-Trailer Rear Impact Toyota Corolla in Whitby Ontario, 2014 Photograph Credited to Cook Family 154
Figure 6-37 FMVSS 301R-02 – Barrier Crash Testing [46] 155
Figure 6-38 Overlap Coverage Toyota Yaris Rear Structure - Top View 157
Figure 6-39 Experiment Setup with Component VNL – Side View 157
Figure 6-40 Tractor-Trailer vs. Ford Taurus Rear Impact Setup..... 158
Figure 6-41 Metric for Evaluation Rear Impact Intrusion Results 158
Figure 6-42 Rear Occupant Compartment Evaluation Referenced to the Rear Passenger Seat Head Rest (Dark Red) – Top View of the Toyota Yaris (Top) and Ford Taurus (Bottom) 159
Figure 6-43 Experiment I Setup at 50% Overlap..... 159
Figure 6-44 Experiment I Setup at 50% Overlap – Top View..... 159
Figure 6-45 Yaris – Rear Impact – 100% Coverage (Head-on) 160
Figure 6-46 Yaris – Rear Impact – 50% Overlap 160
Figure 6-47 Taurus – Rear Impact – 100% Coverage (Head-on)..... 160
Figure 6-48 Taurus – Rear Impact – 50% Overlap..... 160
Figure 6-49 50% Overlap Rear Impact with a FUPDs – Ford Taurus..... 161
Figure 6-50 50% Overlap Rear Impact– Ford Taurus 161

LIST OF TABLES

Table 2-1 Measurement Reference Points in Referenced to Figure 2-9 51

Table 3-1 Impact Pressure Comparison 73

Table 4-1 Resulting Feasible Optimized Designs with Respect to Minimal Cost 91

Table 4-2 Benchmark and Optimal Designs Used for Dynamic Testing..... 91

Table 4-3 List of Materials and Mechanical Properties 102

Table 4-4 Benchmark and Optimal Designs Used for Dynamic Testing from Stage II Design Optimization 107

Table 6-1 Results of Impact Velocity and Change of Ground Clearance from Heavy Braking with a TTC of 1.1 seconds 135

Table 6-2 Intrusion Results..... 148

Table 6-3 Intrusion Results..... 150

ABBREVIATIONS

FUPD	Front Underride Protection Device
dsFUPD	Dual Stage Front Underride Protection Device
FEA	Finite Element Analysis
IIHS	Insurance Institute for Highway Safety
NCAC	National Crash Analysis Centre
ECE / UNECE	United Nations Economic Commission for Europe
NHTSA	National Highway Traffic Safety Administration
CVMSS	Canada Motor Vehicle Safety Standards
FVMSS	Federal Motor Vehicle Safety Standards
MOO	Multiobjective optimization
GA	Genetic Algorithm
ASA	Adaptive Simulated Annealing
LFOPC	Leap Frog Optimizer for Constrained Minimization
HGA	Hybrid Genetic Algorithm
HASA	Hybrid Adaptive Simulated Annealing
NSGA-II	Non-dominated Sorting Genetic Algorithm 2
SPEA-II	Strength Pareto Evolutionary Algorithm 2
PLT	Point Load Test
DP	Dual Phased
TRIP	Transformation-Induced Plasticity
HSS	High Strength Steel
CH	Cross Section Height
GC	Ground Clearance
TTC	Time to Collision / Time to Crash
ABS	Anti-lock Braking System
TS	TruckSim
CS	CarSim
LD	LS-DYNA

ACKNOWLEDGEMENTS

The author expresses great appreciation to AUTO21, and Volvo Group Truck Technology for their financial support throughout the project. Notably the team at Volvo Group Truck Technology Greensboro for their technical guidance, Rick Aveline and Steve Stratton.

Forever grateful for the support, encouragement, and guidance from Dr. Moustafa El-Gindy through this great opportunity.

Finally, I'm ever so thankful for the monumental love and support from my family and friends. For without them, I'd have nothing.

- Adapt, Fight & Conquer All

CHAPTER 1
INTRODUCTION

1.1 MOTIVATION

There are over 270 million passenger vehicles driven on North America roads every day with the expectation of getting to their destination safely; 23.5 million in Canada and 255.8 million in the United States [1, 2]. The advancements in vehicle safety technology have improved occupant survivability greatly over the past decades; from the introduction of seat belts to air bags, anti-locking braking systems (ABS) to collision avoidance systems. All of these advancements used in newer cars to reduce driver's likelihood of being in a collision while driving 100,000 miles from 30% in 2000 to 25% in 2008 year models. Even the survivability from a collision has improved from 82% to 79% over that 8-year span from safety advancements [3]. However, even with all the safety systems engineered into a vehicle, there is still a chance of an accident occurring and resulting in occupant injuries or even fatalities. A devastating and severe accident occurrence involves the impact between a heavy vehicle (ie. heavy truck, tractor-trailer, straight truck) and passenger vehicle, Figure 1-1. Heavy vehicles are often 20-30 times heavier than a passenger vehicle, and are taller which can cause contact incompatibilities between crash structures ground clearances. Consequently, in a collision the high momentum and taller height of the heavy vehicle miss contacts with the passenger vehicles, and allows the passenger vehicle to move underneath the heavy vehicle causing a state of underride.

Figure 1-1 Head-on Collision between a Passenger Vehicle and Tractor-Trailer [4]

Underride (also known as override) is an occurrence of incompatibility between vehicle structural members in a vehicle-to-vehicle collision, where one of the colliding vehicles becomes wedged and displaced beneath the structural members of the other vehicle. The most severe cases of underride are the head-on (front-to-front) collisions between a passenger vehicle and a heavy vehicle [5, 6, 7]. This incompatibility is primarily due to the chassis rails, or any structural absorption devices, not contacting the other vehicle's crash structure to absorb the impact of the collision. This is due to different ground clearance heights of the vehicles. Figure 1-2 displays a head-on collision where a passenger vehicle (in blue) underrides a tractor-trailer (red). The different ground clearances of the structural members, the height between the road and bottom of the chassis, are different which will allow the Yaris's chassis (Pink) to slide and wedge below the tractor-trailers (Green). Underride results in high levels of intrusion of the heavy vehicle into the compartment of the passenger's vehicle and safety cage.

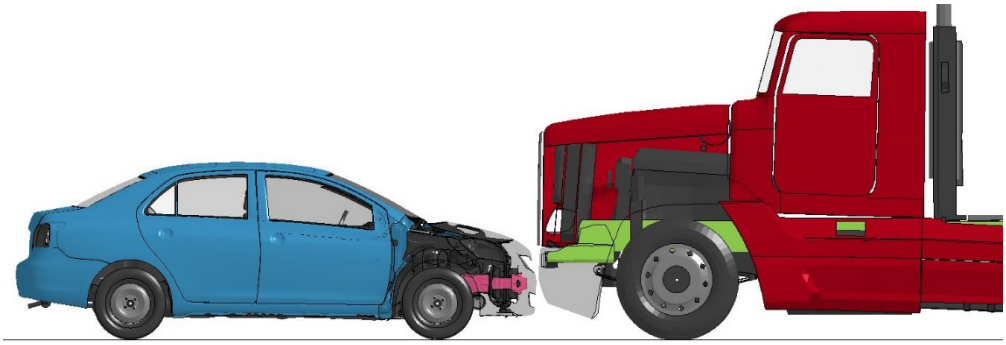

(a) Pre-Impact

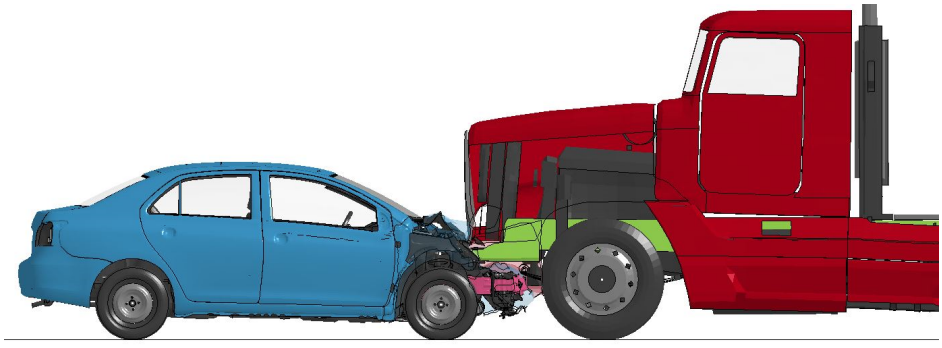

(b) Post-Impact

Figure 1-2 Front-Front Collision of the Toyota Yaris (Blue – Pink Chassis rail) Underriding a Tractor-trailer (Red – Green Chassis rail)

This incompatibility between structural members can be resolved with the addition of Front Underride Protection Devices (FUPDs) on to the heavy vehicle to limit underriding of smaller vehicles. In general, a FUPDs is a structural member attached to the front of the heavy vehicle's chassis to a lower ground clearance height and create a contact with the passenger car. This impact contact will allow a compatibility between both vehicles, allowing for energy to be absorbed and reducing intrusion into the occupant's compartment; effectively improving the crashworthiness of the heavy vehicle. Crashworthiness is the measurement of the ability of a structure to protect the occupant(s) in a collision and reduce fatalities/injuries.

Europe [8, 9] was the first to regulate and standardize the requirement of FUPDs on heavy vehicles, and has been adopted around the world, including Japan [10], Australia [11], and India [12]. Currently North America has not adopted or proposed FUPDs requirements due to criticism of underride protection devices performance, and the different style of tractor utilized by the North American transportation industry. This motivated the demand for investigation into the crashworthy benefits and design strategies of FUPDs for North American trucking industry.

Heavy trucks, tractor-trailers, and straight trucks are grouped into the term 'heavy vehicles', weighing 4,500 kg or more which makes them the largest and heaviest vehicles on the roads. Over 1.03 million heavy vehicles were registered for Canadian roads in 2014. Compared to the 21.7 million passenger vehicles, there were 21 passenger cars for every heavy vehicle registered in Canada. It is evident the trucking industry is growing by analyzing the decrease of the car-to-heavy-truck ratio from 2004: 27 passenger cars for every heavy vehicle [1]. However, the raw number of registered vehicles does not reflect the occurrence of passing by a heavy vehicle. On a daily average, heavy vehicles drive 2.5 times more than by passenger vehicles, as they travel far greater distances for longer periods at a time. This would entail that even though there are fewer trucks on the roads there is a high likelihood of encountering a truck and therefore a higher chance of a collision occurring [13]. These statistics do not count the heavy vehicles entering Canada from the USA, therefore the numbers may be higher.

Yet with the increasing growth of the trucking industry and safety technology improving, there is still an increasing trend in heavy vehicle collisions and deaths. The Insurance Institute for Highway Safety (IIHS) is a USA independent organization dedicated to setting vehicle safety guidelines and educating drivers on road collision and safety. The IIHS states that 1 in 10 highway deaths occurs in a collision involving a heavy vehicle [14]. In association with the Fatality Analysis Reporting Systems (FARS), the IIHS published the increasing trend deaths from collision with heavy vehicles since 2009 in the USA, Figure 1-3. Passenger vehicle occupants had a higher fatality rate than the occupant of the large truck. From Figure 1-3, there is an increasing trend of fatalities in recent years even though vehicles are becoming safer in collisions and include collision prevention technology. The USA's department of transportation concluded that the 89% of fatal head on collisions were caused by passenger vehicle driver, and the driver of the heavy vehicle was not at fault [15]. Conclusively there is still a great need for passive structural devices to enhance the crashworthiness and survivability of the passenger vehicle's occupants when crashing into a heavy vehicle.

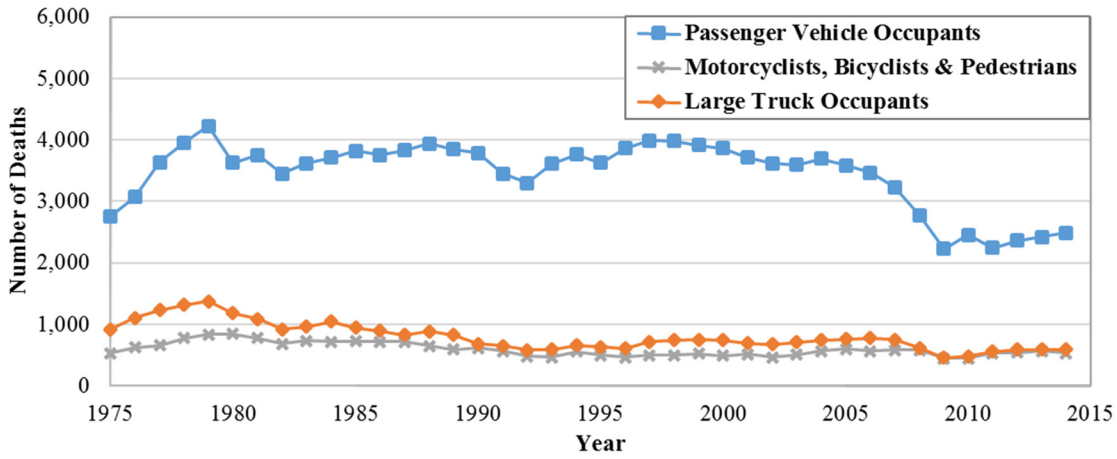

Figure 1-3 Deaths in Crashes Involving Large Trucks, 1975-2014 [14]

An in-depth report on fatalities and injuries from heavy vehicle collisions between 2001-2005 was released by Transport Canada. It concluded that collisions involving heavy vehicles resulted in 37% of all road fatalities, and only 11.5% injuries, Figure 1-4 [7]. Concluding the survival rate was lower when impacting a heavy truck compared to other vehicles. The report observed a rare and in-depth conclusion by evaluating the collision direction and type of heavy vehicle.

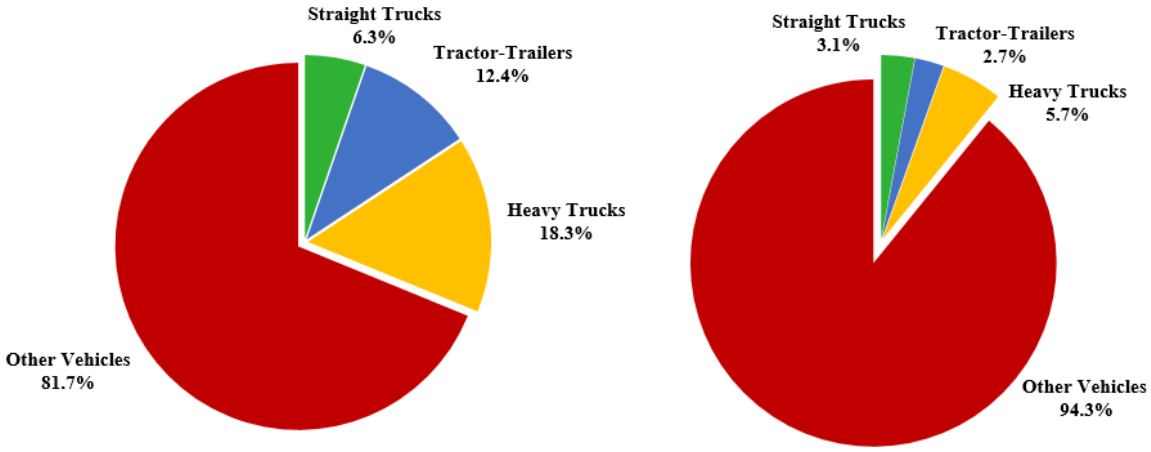

(a) Average Fatal Collision (b) Average Injury Related Collision

Figure 1-4 Overall Average Collision Statistic for Fatalities and Injuries in Canada Between 2001-2005 [7]

From the overall road collisions, tractor-trailers involved in head-on (2 vehicles – 2 directions or 2V2D) collisions with a passenger vehicle was the deadliest collision with the highest fatality rating of 32% and 5% resulted in only injuries; shown in Figure 1-5. Side impacts (2V1D or 2D) are impacts when either vehicle impacts the side of the other or the trailer. It had the second highest severity collision of heavy vehicle impacts with approximately 26% fatalities and 30% injuries. Rear impacts (2V1D) had the highest survival rating with 24% of injuries and 10% fatalities [7].

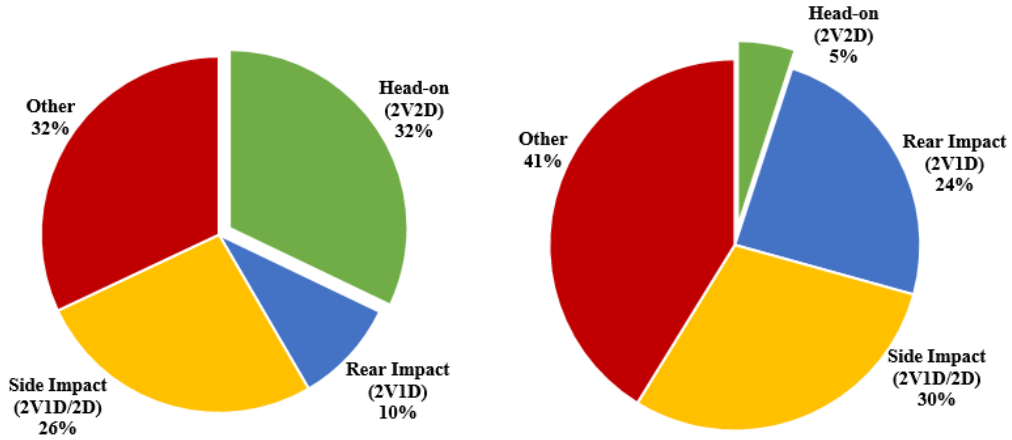

(a) Average Fatal Collision (b) Average Injury Related Collision

Figure 1-5 Tractor-Trailers: Average Collision Statistic for Fatalities and Injuries in Canada Between 2001-2005 [7]

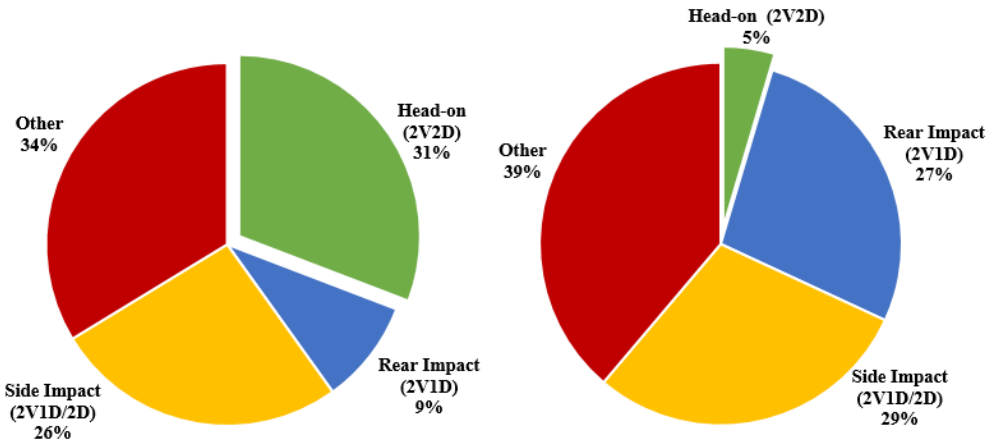

(a) Average Fatal Collision (b) Average Injury Related Collision

Figure 1-6 Heavy Trucks: Average Collision Statistic for Fatalities and Injuries in Canada Between 2001-2005 [7]

Heavy trucks concluded in simular precentages of fatalities and injuries as tractor-trailers for two vehicle collisions with headon collisions being the deadliest at 31% fatalities and 5% injuries, Figure 1-5.

There has not been an updated report from Transport Canada to show the current state of collisions involving heavy vehicles in such indepth review from 2005-2016. However, with IIHS's and USA's department of transportation concluding the increase in fatalities when heavy vehicles are involved in recent years (2009-2016). This greatly demonstrates the demand to develop and regulate superior safety standards where deficiencies exist in collision safety with heavy vehicles, primarily head-on collisions.

Enhancements to crashworthiness for vehicle to vehicle structural interactions in collisions is believed to be linked to the solidifying of proper design methodology [16, 5, 17]. This research was devoted to enlightening and developing the performance characteristics of FUPDs in head-on collisions with passenger vehicles to enhance occupant safety through design methodology. In addition, this work is to motivating the North America trucking industry to enhance collision safety of their fleets in hopes that every person of the roads arrives to their destination safely.

1.2 LITERATURE REVIEW

1.2.1 Variants of Tractor Styles

There is a very distinct variation of tractor design used in North America compared to the designs used in Europe. The conventional tractor (Figure 1-7-a) dominates the North American trucking fleets with Volvo truck, Mack trucks, etc. The European style of tractors (Figure 1-7-b), called cab-over engine tractors, are primarily used in Europe due to the contrast in vehicle length measurement standards, in an attempt to shorten the overall length of the tractor-trailer combination (Figure 1-8). Directive 96/53/EC conforms the tractor-trailer combination to limiting the total length to a maximum of 16.5 m, and the trailer length to a maximum of 13.6 m. Consequently, this only allows for the tractor to be 2.5m in length for the maximum trailer capacity [18]. The North American standards only limits the maximum length of the trailer allowing for a range of styles of conventional tractors [19]. Due to work's focus on North America, only FUPDs for conventional tractor's would be considered.

(a) Conventional Tractor (b) EU Cab-over engine Tractor

Figure 1-7 Tractor-trailer Variants [20]

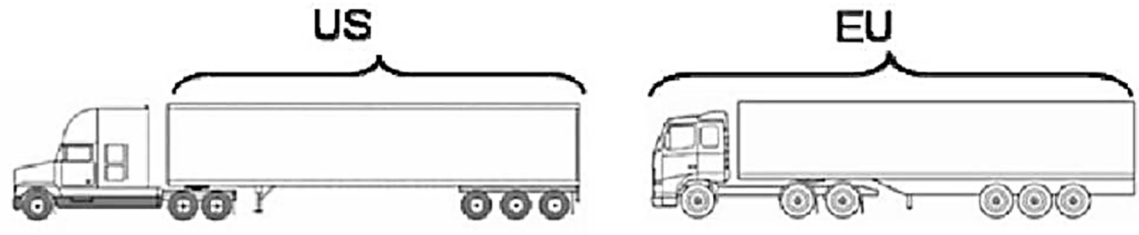

Figure 1-8 Conventional Tractor (North America) and Cab-over Engine Tractor (EU) Measurement Standards [21]

With the flexibility of design, North American conventional trucks are designed with various differences. Figure 1-9 displays the various front axle positions in conventional trucks with either Axle Forward (a) which is closer to the front of the tractor, or Axle Back (b) which is closer to the rear axle. From a vehicle dynamic prospective, the most important difference between set forward or set back is the allowable payload that can be hauled, farther apart truck axles (overall wheel base) increase the allowable carrying payload. However, due to limitations of payload capacities from bridge laws this configuration is limited. Set-back configurations allow for better turning radius, better visibility, and increased fuel economy due to the allowable design space to slope the hood [22]. Both styles are important in the design of FUPDs, however the axle back configuration will allow for more intrusion when impacted.

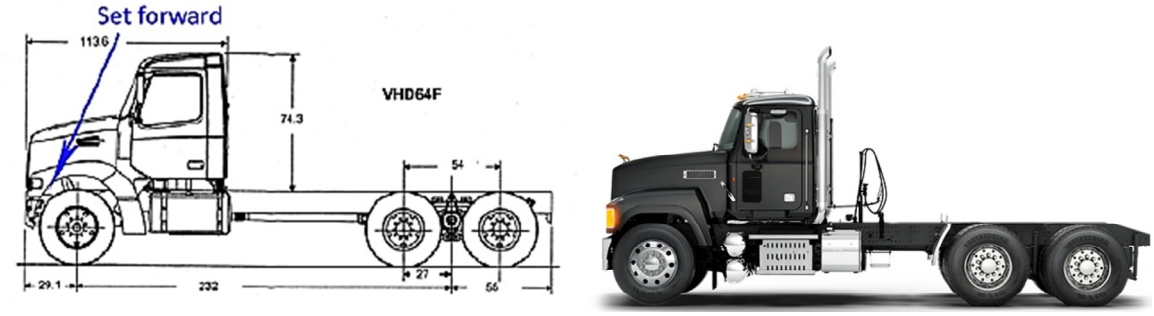

(a) Set Forward Front Axle Tractor Configuration

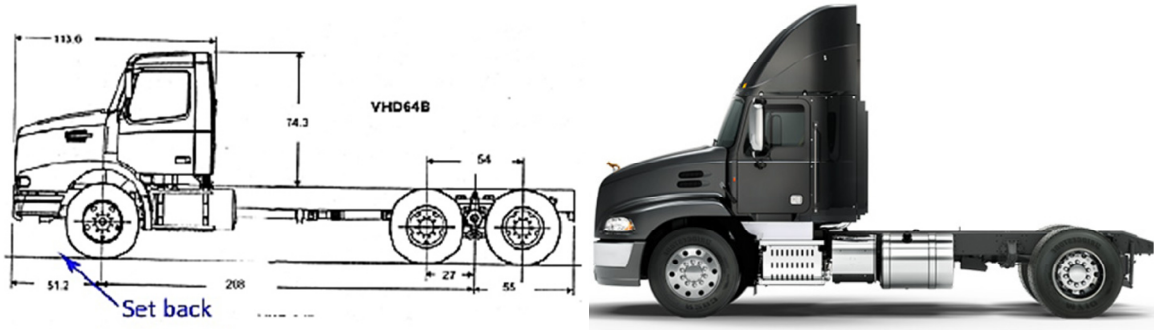

(b) Set Back Front Axle Tractor Configuration

Figure 1-9 Axel Position Variants in Conventional Tractors [23, 24]

Another geometric design difference in conventional tractors is the placement height of the front bumper (Figure 1-10); classified as above axle (a), below axle (b) and center of axle (c). As depicted, if the front bumpers height on the tractor is above the center of the axle it is deemed above axle. This also contributes to the available design space of a FUPDs.

(a) above axle (b) center of axle (c) below axle

Figure 1-10 Front Bumper Height Classification [23]

As the work is supported by Volvo Group Trucks Technology, the work only focuses on the development of a set back axle and center of axle bumper height configuration; specifically, a Volvo VNL series tractor.

1.2.2 Frontal Crash Testing

Passenger vehicles are regulated to frontal collision testing for crashworthiness and occupant safety before being allowed on the roads, which are governed differently between each country. Primarily the vehicle is given an impacting forward speed into a rigid wall/barrier or deformable barrier. A rigid wall or barrier is an immovable and non-deformable structure to which absorbs all applied energies, while allowing only the impacting object to deform. Fixed rigid barrier testing simulates a severe automotive collision [25]. In addition, some regulations require the impact of the vehicle at full width (100% overlap) or impacting only a percentage of a barrier causing a smaller overlap. Overlap impact is the percentage that the barrier covers the vehicle. The United States Department of Transportation's National Highway Traffic Safety Administration (NHTSA) regulates all automotive crash performance under Federal Motor Vehicle Safety Regulations (FMVSS). Canada's Department of Transportation regulates vehicle standards similarly to NHTSA under Canadian Motor Vehicle Safety Regulations (CMVSS). North American frontal crash standard (FMVSS 208\CMVSS 208) requires automotive manufactures to perform with a full wrap frontal collision tests at 56 km/hr to a rigid barrier to reviews only occupant injury/safety using a 50th percentile adult male test dummy. The vehicle is given an initial impact speed of 56 km/hr impacting at a rigid wall at 100%

overlap, Figure 1-11 [26, 27]. The forces of a single vehicle impacting the rigid wall are similar to the impact of two vehicles of the same weight just under the impact speed [28].

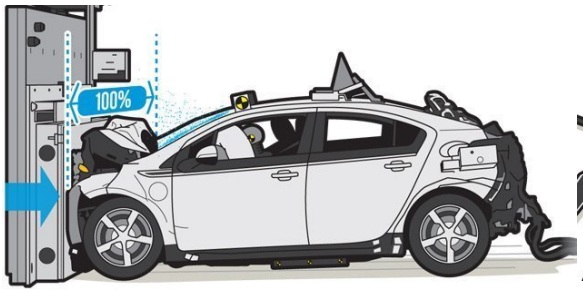

Figure 1-11 CMVSS/FMVSS 208 [29]

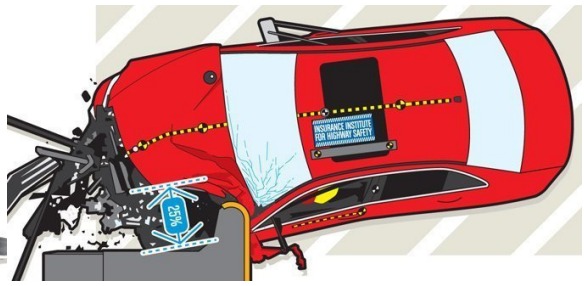

Figure 1-12 IIHS Small-Overlap Frontal Impact [29]

FMVSS\CMVSS regulations are a good step in the right direction for collision testing, however other occupant and vehicle safety organizations have criticised the regulations for being insufficient. Insurance Institute for Highway Safety (IIHS) is an independent, non-profit scientific and educational organization in the United States dedicated to a modern, scientific approach to identifying a full range of options for improving collision safety. The IIHS set a guideline for frontal testing with a different and severer approach than NHTSA by evaluating at different overlap conditions and higher speed. The vehicle test impacts a rigid barrier with a deformable aluminum honeycomb at 64 km/hr at a moderate overlap (40%) and small overlap (25%) configuration. The small overlap test simulates the impact of another vehicle or an object like a tree or utility pole when colliding with the front corner of a vehicle. IIHS's rating system evaluates from both occupant injury metrics form Hybrid III dummies and structural performance of the vehicle's structure/safety cage [28]. This standard is utilized by European Unions under Directive 96/79/EC under ECE R94 [30]. South Korea's Ministry of Land, Transport and Maritime Affairs (KNCAP) adopts both NHTSA and IIHS testing methods and regulated that both forms of testing to be passed; full wrap fontal collision at 56 km/hr and an offset frontal collision at 64 km/hr [31].

1.2.3 Current FUPD Regulations

There remains no regulation or standards for Front Underride Protection Devices for North American heavy vehicles, however the rest of the world has seen the need and demand for these protection devices.

In 2002, the Economic Commission for Europe (ECE) was the first to establish a standard for Front Underride Protection Devices for heavy vehicles to protect passenger vehicle occupants. Directed by requirement 2000/40/EC [8], ECE R93 regulates the details of FUPDs geometric limitations and performance requirements [9]. The regulation was adopted and regulated by Japan in 2007 [10], Australia in 2009 under ADR84/00 [11], and India under AIS069 in 2006 [12].

ECE R93 directs limitations of the geometric design of the FUPDs and the static loading conditions necessary to pass the regulation. Figure 1-13 illustrates various regulation requirements. The FUPDs geometrically must have a maximum ground clearance of 400mm, and a minimum frontal cross section height of 120mm. The strength performance of the FUPDs is evaluated through quasistatic point load testing, while mounted upon a tractor or equipped on a test bench. Three points along the FUPDs are separately applied with a quasistatic load, loading where inertial effects are negligible when applied, represented by P1, P2, and P3. Load points P1 and P3 are assigned 80kN (50% of permissible mass of the tractor-trailer), and P2 is assigned 160kN (100% of permissible mass of the tractor-trailer). The quasistatic load is longitudinally applied by a rigid ram for a minimum of 0.2 seconds. Post-loading, the FUPDs must not exceed 400mm of deformation measured from the front of the tractor. As well post-loading testing, the ground clearance height of the FUPDs must not exceed 450mm [9].

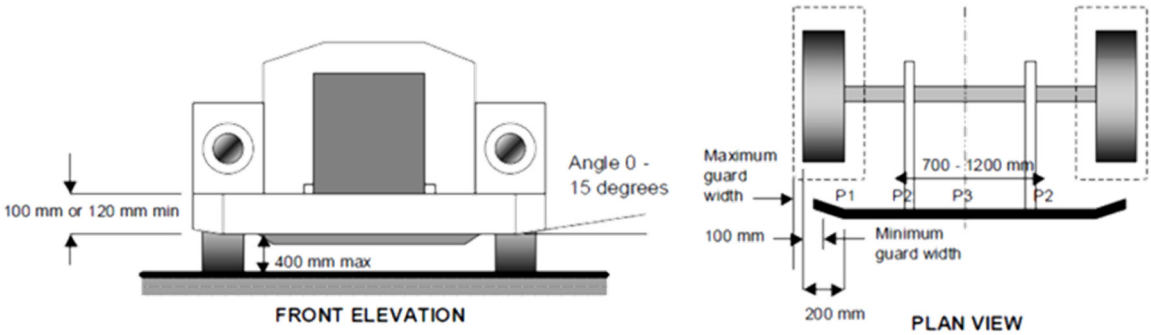

Figure 1-13 ECE R93 Geometry and Point Loading Testing [32]

India under AIS069 adopted ECE R93, however allows for a higher ground clearance of 450mm, and a post-loading ground clearance of 500mm [12].

However, there has been a growing concern and criticism from both academic and industrial leaders (Volvo Trucks/Mack Trucks, and Mercedes-Benz) on the inadequate

effectiveness of ECE R93. There has been a demand for higher strength stiffness and setting a minimal ground clearance height of the devices [5, 33]. Higher strength requirements of the FUPDs have been published, recommending the increase of point load magnitudes from P1 80kN to 400kN, P2 160kN to 300kN and P3 80kN to 200kN [32]. This would increase the stiffness of the device and increase overlap strength at P1. Loading conditions were criticized at lower magnitudes in other publications, which is discussed in working foundations section of this work. The ECE R93's allowable measured deformation of 400mm also has been shown to be inadequate, as concluded that most deformation measure between 50mm to 150mm [34]. There is obviously a need for a more in-depth and critical view into the loading conditions and geometric requirements.

1.2.4 Rear Underride Protection Devices

The only form of underride protection devices on heavy trucks in North America are Rear Underride Protection devices (RUPDs). RUPDs are structural members mounted on the rear end of the trailer, Figure 1-14, for when passenger vehicles impact the trailer (2V1D). Geometric and performance testing methods are regulated by CMVSS 223 in Canada [35], and FMVSS 223 in the United States [36]. Both regulations enhance the crashworthiness of the trailer and are in a good direction for being underride protection to North America. However, the regulations have been under severe criticism after the Insurance Institute for Highway Safety physical tested various North American RUPDs with impacting passenger vehicles to prove the extreme inadequacies and failures of the regulation (Figure 1-14) [37]. The IIHS tested stationary trailers with various RUPDs being impacted by a passenger vehicle at 56 km/hr with overlaps of 100%, 50% and 30%. This ignited pressure for the regulations to be revised by both countries [37, 38, 39].

Figure 1-14 RUPDs on a Manac Trailer [37]

Figure 1-15 Post-Impact of Passenger Vehicles and the Trailer Rear end a with a RUPD [37]

Similar to ECE R93 quasistatic loading, RUPDs tests require three sequential points load testing along the structure, Figure 1-16. Quasistatic point loads at P1 require a force of 50kN, 50kN at P2, and 100kN at P3 with the maximum allowable deformation under the load of 125mm. The Canadian regulation requires a secondary test involving the application of a full guard test of the RUPDs with a 350kN quasistatic load.

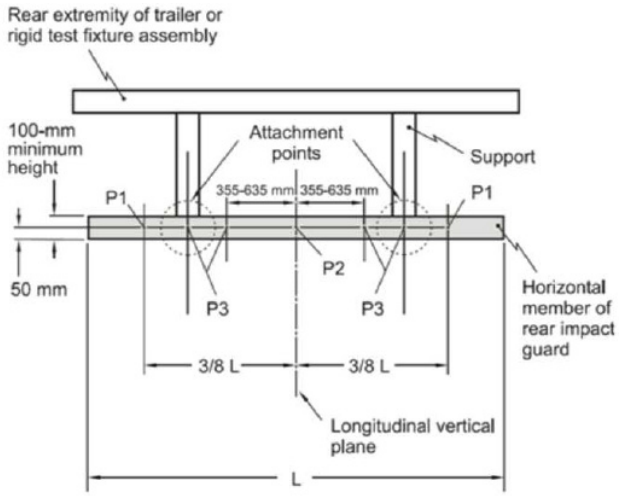

Figure 1-16 CMVSS 223 Loading Points for RUPDs [35]

1.3 WORKING FOUNDATION – METHODS FOR DESIGN AND TESTING

Front Underride Protection Devices have had various levels of publications contributing to the understanding and advancements of the crashworthiness of heavy vehicles. Previous to 2012, there has been some investigation into FUPDs development and research utilizing computational Finite Element Analysis (FEA) software LS-DYNA. Castellanos et al utilized FEA virtual environment as a method of testing FUPDs designs on a stationary tractor with an impacting Geo Metro car (900 kg). Published in the Int. J. Vehicle Systems Modelling and Testing Vol. 8, the simple FUPDs design utilized a horizontal tube and two holding brackets. Castellanos et al concluded and recommended the following foundations for the testing methods and FUPDs performance [6]:

- There could only be a 400mm max deformation.
- It is recommended that the FUPD absorbs 100 KJ of energy during static testing.
- Minimal occupant compartment intrusion at a crash speed of 64 km/hr.
- Shall not allow the passenger car deceleration (50ms longitudinal-direction average) greater than 30 g's at initial impact speed of 56 km/hr.
- ASI (Acceleration Severity Index) values should not exceed 3 at initial impact speed of 64 km/hr (limit for occupant survivability).

A 2010 publication utilized FEA methods with LS-DYNA for the investigation of FUPDs while utilizing a Ford Taurus. Krusper and Thomson propose energy absorbing components which were attached to rigid bars and using virtual spring models to contact a colliding passenger vehicle. The purpose of this type of testing was to conclude possibilities of accident mitigation through the tuning parameters of energy absorption stiffness [40].

From a design perspective, there was suggestion of designing a guard to generate deflection into the passenger vehicle outward and away from the tractor. However, the design was flawed due to the size of the device overhanging and the excessive design space needed [32].

Latest development in FUPDs for the North America conventional tractor trailers was published in a Master's thesis by Todd MacDonald in 2014, Front Underride Protection Devices: Methods for Design and Testing. MacDonald outlines various geometric parameters, modified regulations, testing methods, and design methodology. The foundation of the thesis takes on a three tier design methodology to developing a robust FUPD. The work utilizing finite element analysis (FEA) software, LS-DYNA, to experiment virtually and utilizes tools to engineer the designs in an optimal and feasible way [5]. MacDonald's thesis offers a foundation to this presented work with various conclusions being taken, reanalysed, changed, progressed, and/or solidified in this presented work; which is summarized in the following subsections.

1.3.1 Design Methodology

Tier 1 is a simplified experimental stage for preliminary geometry isolation using a FEA vehicle model to collide with a rigid surface. The simplified testing allows a starting point to analysing crash compatibility and underride from the passenger vehicle's perspective to give guidelines into the parameters of a FUPD. The rigid surface was constructed in two variations: rigid body and a dual spring FUPD (dsFUPD). The second tier implements conclusions from tier 1 in the development of a complete FUPD; a more realistic representation than a rigid body, with structural members, chassis contact, and with non-rigid material properties [5].

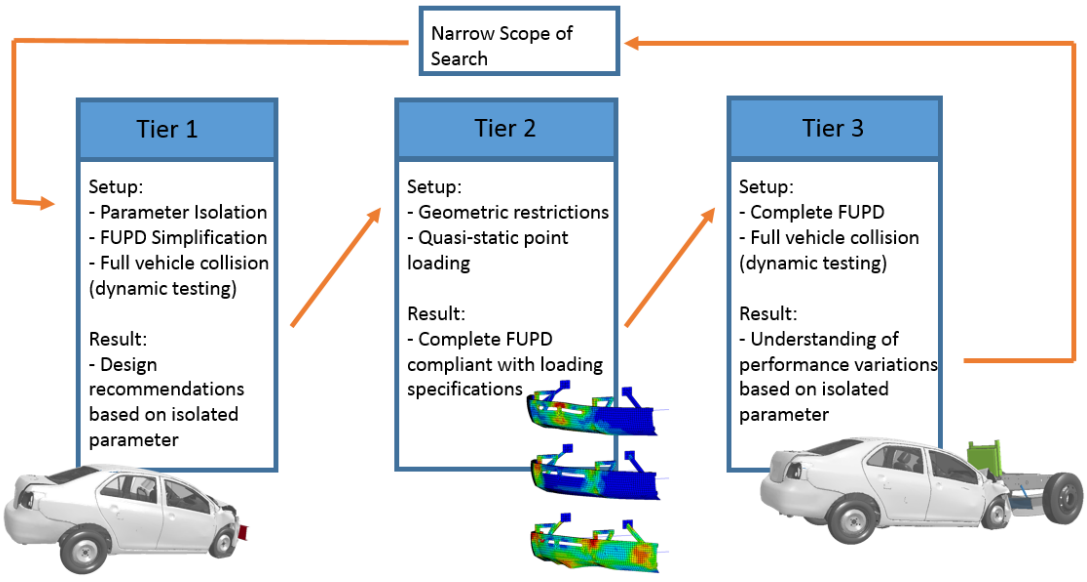

Figure 1-17 MacDonald's Three Tier Design Strategy [5]

Tier 2, driven by the results of tier 1, utilizes various tools to structuralize the design envelope, illustrated in Figure 1-18. Tier 2 first implements the geometric conclusions and design envelop into a geometric spacing to be analysed by a Topology Optimization and Shape Computation (TaSC) software [5]. Through LS-TaSC, topology supports the development of structures by defining load paths and reducing excess mass while sustaining structural integrity [41]. The resulting load paths are used as an aid for outlining rough geometry. The second phase of tier 2 structuralizes the FUPD from the rough geometry with deformable materials and member thicknesses in a computer aided design (CAD) software. At this stage optimization is implemented to ensure the device is not overdesigned via LS-OPT. The device is optimized for material thickness and support component shape to reduce physical mass and maintain structural strength. Optimization ensures the design is not overdesigned but remains effective. Both topology and optimization implements quasistatic load testing through rigid impactors at specific locations to comply with the desired regulation. In an implicit testing environment, quasistatic loading testing is a computationally fast process which allows for high number of simulations to be solved in a reasonable amount of time compared to dynamic testing with FEA vehicles [5].

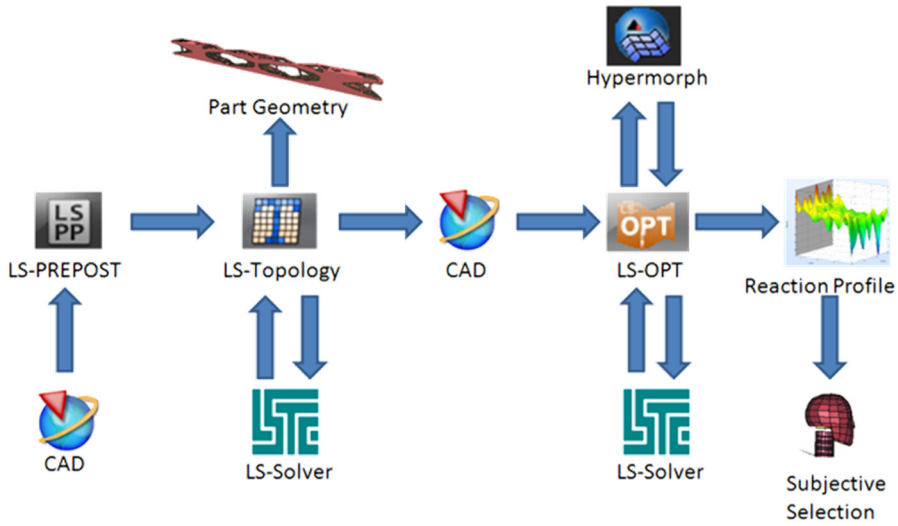

Figure 1-18 Tier 2: FUPD Design Map [5]

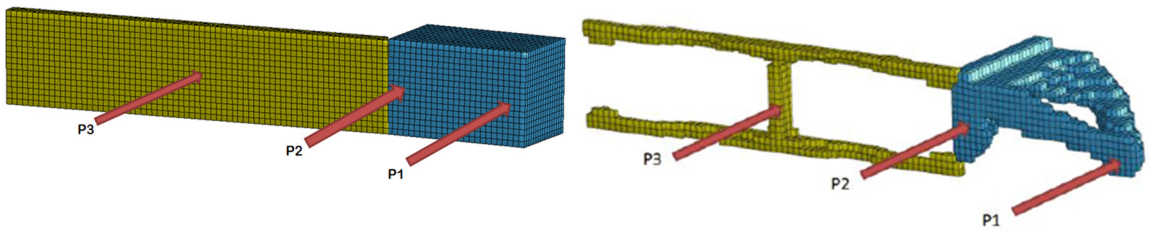

(a) Design Envelope (b) Final Load Path Iteration

Figure 1-19 Topology Optimization of a FUPD Design Envelope [5]

Tier two produces various FUPD designs that conforms to the desired loading condition to be subjected to the third tier. These designs are virtually experimented in a dynamic test with the use of valid FEA vehicle models to analysis the crashworthiness of the FUPD. The experiment was done in various scenarios and using two various FEA vehicles to collide into the FUPD which is attached to a component level Volvo VNL tractor model. The crashworthiness of the device was analysed by two performance evaluation metrics, crash absorption and Occupant Compartment Intrusion guidelines set by the IIHS [5]. From this design methodology various conclusions were determined.

1.3.2 Ground Clearance and Contact Section Height

Through virtual experiments using a rigid body and a passenger vehicle various conclusions were drawn, utilizing the tier 1 methodology. Investigations into ECE R93 geometric restrictions was focused while considering different collision scenarios at 100% and 50% overlap. Comparisons between the passenger vehicle and various ground clearances and two rigid bar heights were analysed. The ground clearance from the base of the rigid body was analysed from: 350mm, 400mm, 450mm, and 500mm, as well as a full rigid wall test. These ground clearances were tested with a 120mm and 240mm rigid bar [5].

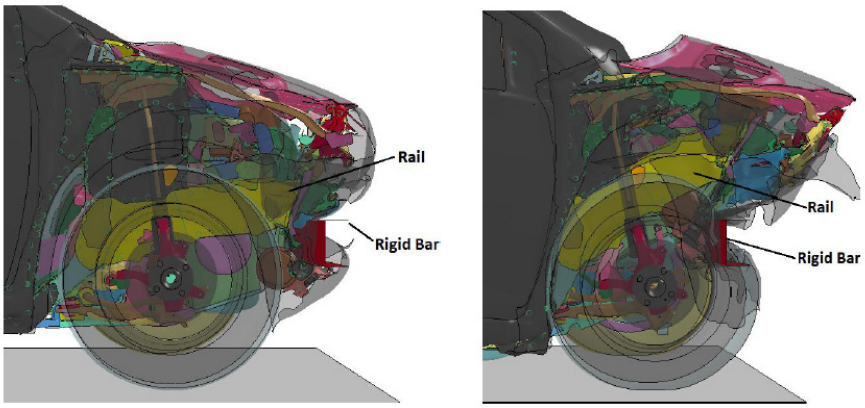

Figure 1-20 64km/h-100%-120mm with 350mm Ground Clearance at Time of Primary (Left) and Secondary (Right) Impact Force Peaks [5]

It was concluded that a ground clearance of 350mm and a 240mm rigid bar's crash compatibility was the most ideal and robust in at 64km/hr and 80km/hr. A rigid bar of 120mm height and 350mm ground clearance cause upward deflection of vehicle loading rails. Implementing anything above 400mm ground clearance proved to not stop the vehicle and allow for underride in overlap cases. Overlap coverage of 50% was influenced by both the engine and tyre contact forces. These results also were evaluated on a range of vehicles with different peak and average heights of force in an impact referenced from, Figure 1-21. National Highway Traffic Safety Administration (NHTSA) available physical crash test data supported the claim that the defined geometry would result in a better compatibility of impact height and impact surface [5].

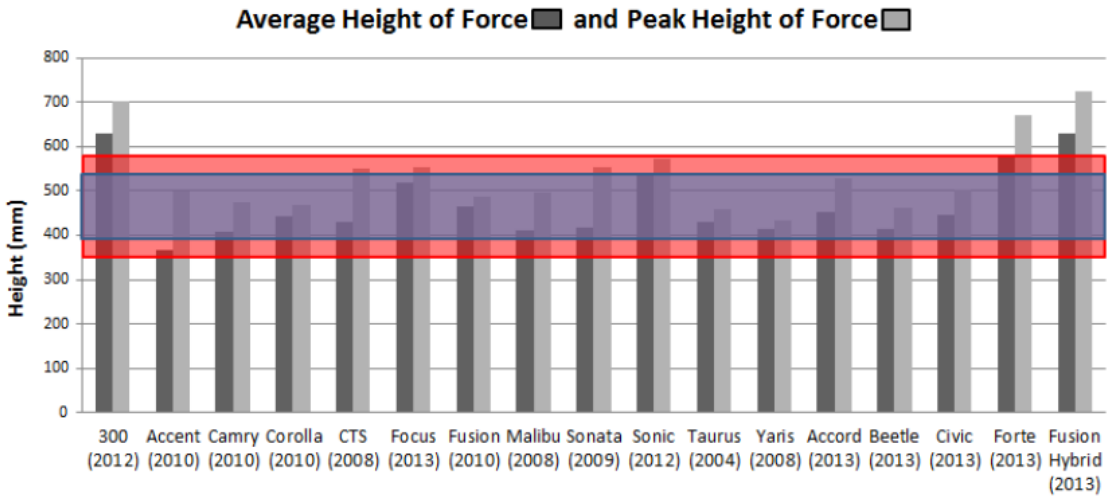

Figure 1-21 Force Height Comparison with ECE R93 (inner range - blue) and MacDonald (broad range - red) Recommended Geometry [5]

Concluding from the ground clearance and rigid bar heights, three varying FUPDs were created using tier 2 and optimized to pass ECE R93. After being placed on a simplified FUPD many conclusions were defined. Reduced ground clearance provides an increase in impact force within both cases, the relationship presented an opposite conclusion from the rigid bar test. The closer proximity of the tractor frame in contacting the passenger vehicle when ground clearance was reduced yields the increase in reaction force. Robust performance was appeared to increase across variations in ground clearance when the frontal structure height was set to 240mm. 50% overlap scenarios resulted in larger deformations. These designs proved that the ECE R93 failed to provide robust and safe FUPDs when overlaps are found. Furthermore, extended deformation values resulted, and demonstrated failure to provided sufficient support in stopping the vehicle [5].

The failure resides in the ECE R93 P1 point load of 80kN requirement being deemed insufficient [5].

1.3.3 Modified ECE R93

Resulting conclusions of failure from the ECE R93 to be robust in overlap conditions lead to developments in modifying the regulation. Two various FUPDs with varying lower tractor frame height ranges (600mm-650mm) were analyzed in dynamic collisions. The three FUPDs designs were optimized for section thickness using a single ultra-high strength steel while utilizing the ECE R93 quasistatic point load testing. The magnitudes of the point loads were changed from 80kN, 160kN, and 250kN to optimize various structural designs of the three FUPDs. Effectively as the point loads increased, the total mass of the FUPD increased, except for one design. Findings revealed the importance of considering dynamic testing with offset conditions. It was concluded that the ECE R93 quasistatic point load conditions should be increased to 160kN of force to strengthen/enforce end side supports. The work also restricts the resultant deformation to 100mm, from ECE R93 limit of 400mm [5].

1.3.4 Dual Spring System Testing Method

Due to computational timing, there was a need to simplify FUPDs testing environment and methods for simple geometric experiments to obtain preliminary results quicker. MacDonald developed a dual spring system testing method to analyze the frontal

impact area with the use of a rigid surface attached to springs, while being set up with the component level VNL (Figure 1-22). The spring were embedded with deformation characteristics represented ideal deformations in the longitudinal and vertical directions. The springs are mounted to the ideal nodal locations of structural members on to the component level VNL. The vertically direct spring acts as a hinging point with high stiffness. The representation of the expected deformation under collision cases of designed guards is embedded with the longitudinal spring. The spring's orientation reflects the device's tendency to deform longitudinally reward as well as upward in the direction of the tractor frame. This method of testing was found to fit into an ideal compatibility profile, Figure 1-23, and deemed reasonable to use for changing the rigid impact areas geometry [5].

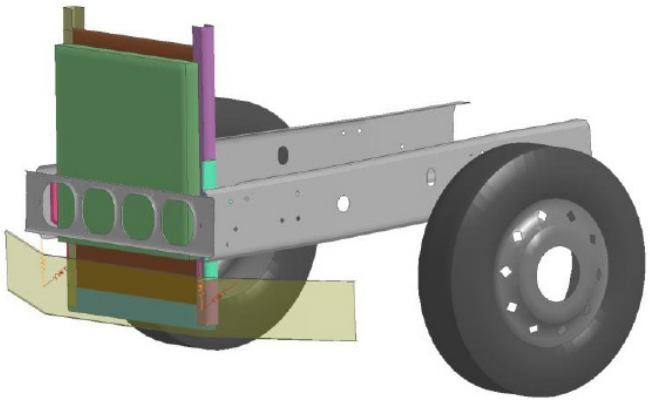

Figure 1-22 Simplified FUPD Constrained by Dual Spring System [5]

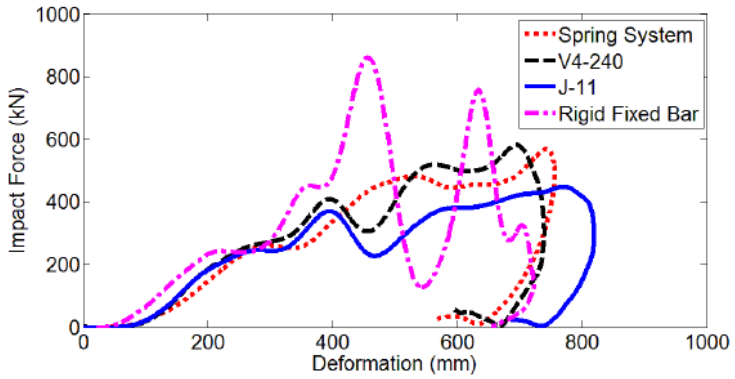

Figure 1-23 Compatibility Profile of Yaris 64km/hr – 100% Overlap: Justification of Utilizing Spring System Simplification [5]

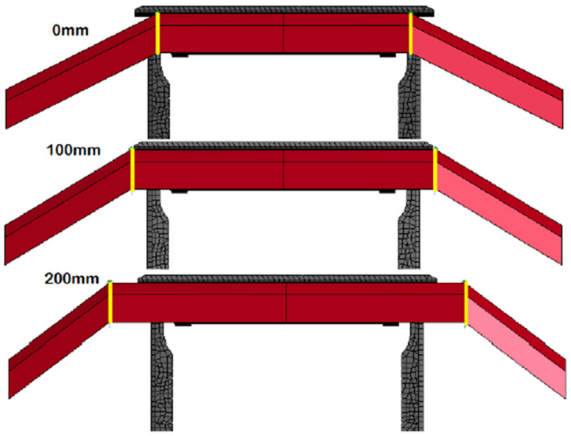

Figure 1-24 Concept 2 with Extension Variations: 0mm, 100mm and 200mm (Bottom View) [5]

From the duel spring testing, it was concluded that the extension of the front middle section of the FUPDs would likely to increase intrusion values in overlap cases. In addition, it was concluded that the extension should be closer to the chassis rail and then angle out towards the side of the tractor [5].

This method of testing frontal impact area proved to be useful when quickly iterating design parameters to develop more effective devices.

1.3.5 Dual Stage Front Underride Protection Device (dsFUPD)

Various FUPD designs were published in MacDonald's work for a Volvo VNL. From the conclusions of the duel spring testing methods, more sophisticated designs resulted from the research; the FUPD F8 (Figure 1-25) and dsFUPD F9 (Figure 1-26). The major difference between the two designs was that the dual stage Front Underride Protection Device (dsFUPD) utilized the tractor's radiator (shown in green and brown in Figure 1-25) and its energy absorption properties. The radiator was supported by FUPD structure behind it (seen in yellow in Figure 1-26) to allow passing of the modified ECE R93 requirements, and to allow support to the radiator in a collision. Both were optimized to reduce system mass and deformation from modified ECE R93 loading requirements by varying section thickness using a single high strength steel, and section area of the overlap side supports. The FUPDs F8 total mass was 30.67 kg, and the dsFUPD F9 was 41.74 kg.

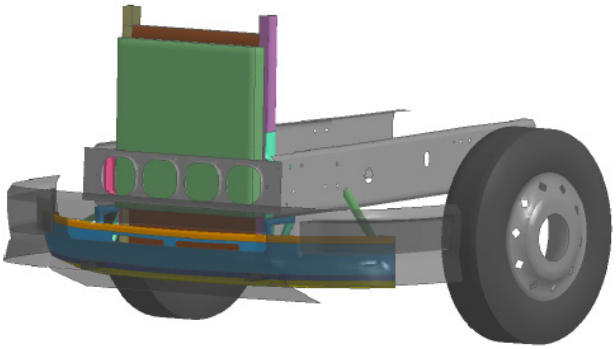

Figure 1-25 FUPD Model F8 [5]

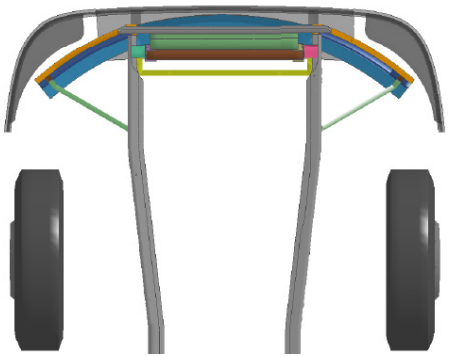

Figure 1-26 dsFUPD Model F9 [5]

The dsFUPD F9 concluded to reduce IIHS intrusion values in a 100% overlap testing and comparable compatibilities profiles from the collision, providing some insight to allowing the radiator to be introduced into the FUPDs domain [5].

1.3.6 Additional Consideration

Other collision scenarios were investigated in the publication to ensure the FUPD would perform robustly. Scenarios included angled collisions, and heavy braking.

1.3.6.1 Angled Collisions

Variations in alignments were experimented on to observe the robustness when the passenger vehicle impacted various types of FUPDs at an angle and offset. Experiments involved scenarios at 64 km/hr with offsets of 30% and an angled approach of 0, 15 and 30 degrees. Similar trends resulted from these offset collisions with an angle approach to the result of a direct impact (0 degrees angled approached) [5]. Therefore, concluding all experiments should be a direct approached collision.

1.3.6.2 Heavy Braking of the Passenger Vehicle

Heavy braking of the passenger vehicle was observed to analyse the robustness of the FUPDs as the passenger vehicle pitching may change the crashworthiness of the contact. Deceleration profiles of the wheels locking from an initial vehicle speed of 80 km/hr and 64 km/hr were validated in CarSim. Compared to the deceleration profiles from CarSim and LS-DYNA, both shared vary similar trends. Virtual collision experiments within LS-DYNA were simulated at identical closing speeds while the vehicle was; braked and pitched, braked and unpitched, unbraked and unpitched [5].

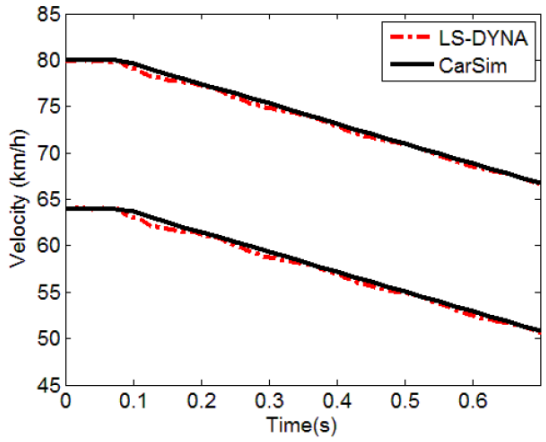

Figure 1-27 CarSim and LS-DYNA Deceleration Profiles (Wheels Locked) [5]

The passenger vehicle impacted only at a head-on (100% coverage) to the simplified testing of a rigid beam. Compatibility profiles at various closing speed (55km/hr, 60km/hr, 71km/hr and 78km/hr) resulted in insignificant differences of proper alignment of crashworthiness components between any of the different braking and pitching scenarios [5]. The tested closing speeds of the vehicle's front suspension experienced transient compression as impact occurs instantaneously.

The scenario was also experimented on a FUPD, (concept J11), to introduce a deformable structure. However, the results yielded similar responses to the simplified testing, as there were no significant variations in compatibility conclusions [5].

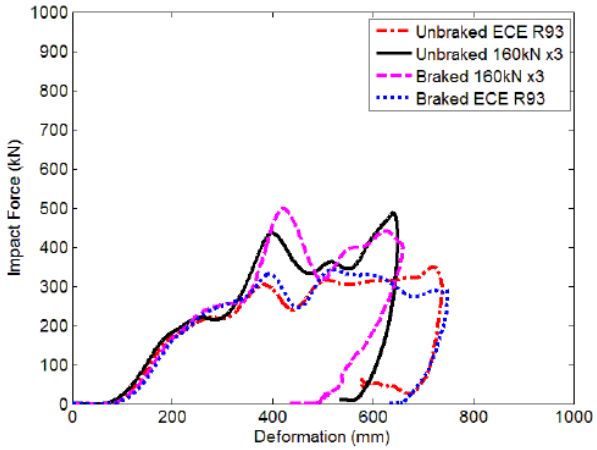

Figure 1-28 Yaris 55km/h vs J11 Concept FUPD Compatibility Profile

It was noted that the experiment relied on the assumption of the finite element passenger vehicle model reacting realistically to induce braking. As well, it was concluded that utilizing a dummy model, appropriate air bag and seatbelt, vehicle pitching might present variations in dummy injury criteria [5].

1.4 DEVELOPMENT SOFTWARE

1.4.1 LS DYNA

Livermore Software Technology Corporation virtual environment software LS-DYNA is a powerful highly nonlinear, transient dynamic finite element analysis program capable of simulating complex real world experiments and scenarios. Originating from DYNA3D, LS-DYNA was developed for the application of analysing the large deformations of structures from static and dynamics responses. It's highly nonlinear code allows for changing boundary conditions, analysis of large deformations, while using nonlinear materials. Explicit time integration is the main solution methodology for dynamic scenarios experiencing high load frequencies and transient dynamic events, i.e. high speed, short duration events with inertial forces. An implicit solver is another solution methodology available in LS-DYNA. Generally utilized for the application of static and quasistatic loading for structural analysis in which inertial effects are ignored. LS DYNA has tailored itself for the application in the automotive industry with the specialized tools and features including airbags, sensors, and seatbelts. A wide range of material behaviors are characterized through approximately one-hundred constitutive models and ten equations-of-state [42].

The application of the virtual environment is ideal for the desired approach to the development and testing approach of this research. The environment results in such an extensive study of an instantaneous impact and ability to study it is unparalleled to the physical realm. However, the accuracy and precision of results from the virtual environment of LS DYNA's solution and modelling techniques compared to the physical realm would need to be addressed. To experiment in the physical realm for its accuracy at such an in-depth approach would be astronomically expensive compared to the virtual approach. This is vindicated by utilizing extensively detailed computation models and

materials validated with physical testing. Additionally, LS-DYNA has been widely utilized in industry for crashworthiness and vehicle structural performance, including previous works on UPDs as mentioned [5, 6, 17, 40]. Conclusively, LS-DYNA virtual environment will provide the best and most cost effective approach to developing the devices, and study vehicle safety.

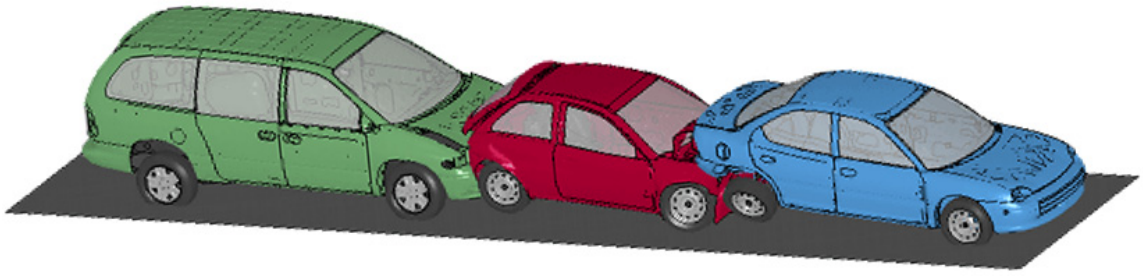

Figure 1-29 Visual Environment of LS-DYNA – Multiple Car Rear Impact [43]

1.4.2 LS-DYNA Tool Box - Topology, Shape and Size Optimization

With the utilization of LS-DYNA's FEA solving capabilities, Livermore Software Technology Corporation offers software modules for further analysis and design optimization. LS-TaSC and LS-OPT. Both modules plug-in to LS-DYNA's implicit and explicit solvers.

LS-TaSC is a Topology and Shape Computation tool plugs into LS-DYNA's to develop topology optimization utilized for optimization of structures in non-linear environments [41]. Refer to Figure 1-19 for an illustration. With dynamic loads and contact conditions, topology results in the development of a design envelope from the desired environment and available space for the structure/component. The desired available space was geometrically created and FEA meshed with small elements (2-5 mm) within the environment while surrounding/connecting to some structure(s). With the dynamic/quasistatic loading conditions contacting the design envelope, an optimizer attempts to reduce mass of the geometry through numerous iterations. The results yield the necessary mass to retain the load paths, while maintaining deformation parameters, to the connecting structure. From the Topology Optimization, results will only give an idea into the necessary structure for the design.

Livermore's LS-OPT is another plug-in for LS-DYNA which includes design optimization and probabilistic analysis. LS-OPT utilizes heuristic optimization methods for optimization of desired parameter to analyze the response targets [44]. Through various methods, the software will allow numerous simulations to respond to changing parameters and optimize the response. The methodologies of heuristic optimization and LS-OPT is discussed later in this chapter.

1.4.3 Mechanical Simulation Software - Vehicle Behavior Simulation

Mechanical Simulation Corporation provides advance software for simulating vehicle dynamic behaviors of automobiles with CarSim and heavy vehicles in TruckSim. The software allows for accurate and realistic vehicle dynamic results from a maneuverer in a very quick computational time [45]. CarSim and TruckSim was primarily used to observe dynamic characteristics of the vehicles as FEA models may not behave the same dynamically. The software is not capable of structural analysis or vehicle to vehicle collision analysis.

1.5 OPTIMIZATION TECHNIQUES

Within the LS-DYNA tool-box of plug-in software, there are optimization tools to aid in the benefit of the research contents optimization. Optimization is a complex and controversial field of study when applying to various problems. For this research, the optimization techniques and methods are bound to only the available techniques and algorithms from LS-DYNA's LS-OPT. The following literature will help in the aid of understanding the details of optimization theory.

1.5.1 Metaheuristics Optimization

Metaheuristics optimization techniques are a flexible group of trial and error based algorithms that can be used to generate a Pareto optimal front of solutions. Metaheuristic algorithms are general purpose techniques and can be used to solve almost any optimization problem. Most metaheuristic algorithms are nature-inspired and are comprised of two major components: they are stochastic and involve natural selection. Expected solutions are usually acceptable and most of the time converge to the optimal solution. Metaheuristic

algorithms are more appropriate for a complex optimization problem, such as the FUPDs structural optimization, where there are many interconnected variables and complex objective functions [46].

1.5.2 Optimization Strategies

1.5.2.1 Direct Simulation

Direct simulation optimization is a computationally expensive process but highly accurate optimization strategy in which the software directly solves for the optimal points [47]. There is no approximation error when using direct optimization as only simulated results are used to find optimal values. However, this will increase computation time with the increase in simulation runs [44].

1.5.2.2 Metamodel Optimization

Instead of directly optimizing the design, Metamodel-based optimization strategies create and optimize an approximate model, called the metamodel, to find the optimal design. The metamodel can be used to find the Pareto optimal front for multiple objective solutions in a simple and computationally inexpensive manner. Metamodel strategies use various techniques in creating the model, such as Genetic Algorithms and Simulated Annealing.

There are three strategies for automating the metamodel based optimization: Single Iteration, Sequential Strategy, and Sequential with Domain Reduction. Single Iteration is a strategy in which sampling points are done only once, which is not ideal. Sequential Strategy samples data sequentially with small number of points chosen for each iteration and multiple iterations. The advantage of Sequential Strategy is its stopping condition, as it will exit the optimization when the meta-models or optimum points have sufficient accuracy. The third strategy uses the same approach as Sequential Strategy with the addition of Domain Reduction to reduce the size of the search space sub-region. However, Sequential Strategy with Domain Reduction has been deemed unsuitable for multiobjective optimization. Using a Sequential Strategy should only be used with fixed parameters [44].

1.5.3 Optimization Algorithm Methods

1.5.3.1 Genetic Algorithm (GA)

A subclass of Evolutionary Algorithms (EA), Genetic Algorithms (GA) are a nature inspired search heuristic that simulates Darwin's theory of survival of the fittest philosophy. GA bases on the principles of natural evolution and the notion of competition. Natural genetic elements are used to drive the search procedure of the process, which is reproduction, crossover, and mutation [48]. Computational based GAs develop a population based solution to discover the solution space in an effort to converge to fittest values.

Two variations of GAs for direct optimization were used in the research; Elitist Non-Dominated Sorting Genetic Algorithm II (NSGA-II) and Strength Pareto Evolutionary Algorithm II (SPEA-II). NSGA-II, developed by Prof. Kalyanmoy Deb, tries to converge to a Pareto optimal front and then it spreads solutions to obtain diversity on the Pareto optimal front [49]. NSGA-II can also be applied in metamodel optimization. The SPEA-II strength approach has proven to outperform NSGA-II non-dominated solution of higher dimension objective spaces in multiobjective optimization problems [50].

Advantages & Disadvantages

Genetic Algorithms are suitable for computing complex optimization problems as they are flexible in handling most types of objective functions. Whether it is time-dependent, linear/non-linear, continuous/discrete, or contains random noise, GAs can produce useful results. Parallelism is also an important advantage as the algorithm pursues multiple solutions in parallel. Each individual is a different solution to the optimization problem. Populations are made up of multiple individuals therefore, many solutions are being evaluated simultaneously with each passing generation [46].

Although quite powerful, genetic algorithms are computationally expensive as they need a great number of generations to be effective. It is also difficult to determine when to terminate a genetic algorithm. Specifying a maximum number of generations has become a widely accepted practice [46].

Multi-Objective Evolutionary Algorithms

Defining the objective function in a multi-objective problem is quite complicated. There are multiple approaches to determining which particular solution is better and which objectives should carry more weight during the selection of the fittest individuals. The two genetic/evolutionary algorithms used in this project, NSGA-II and SPEA-II, both use a Pareto dominance-based approach.

Pareto dominance-based approaches introduce objective weighting when determining the fitness of each individual. This type of evaluation allows for the comparison of solutions with respect to one another. The main advantage of this approach is that there is no need to convert a multi-objective problem into a single objective. Dominance based systems accomplish this naturally. Since they evaluate all solutions based on a single dominance criterion, the problem is transformed into a single objective function. This technique ensures that there is no bias towards one objective over another [46].

Elitist Non-Dominated Sorting Genetic Algorithm II (NSGA-II)

NSGA-II converges to a Pareto front with each generation and consequently tries to obtain solutions that are evenly distributed along the front. First the algorithm generates the offspring population through crossover and mutation. The parent and offspring populations are then evaluated using the Pareto dominance ranking. The individuals with the lowest ranks (i.e. the most dominant of the parent and offspring populations) are considered for carrying over into the next generation, Figure 1-30. The crowding distances between individuals (distance an individual is away from the next closest individuals) is also calculated [44].

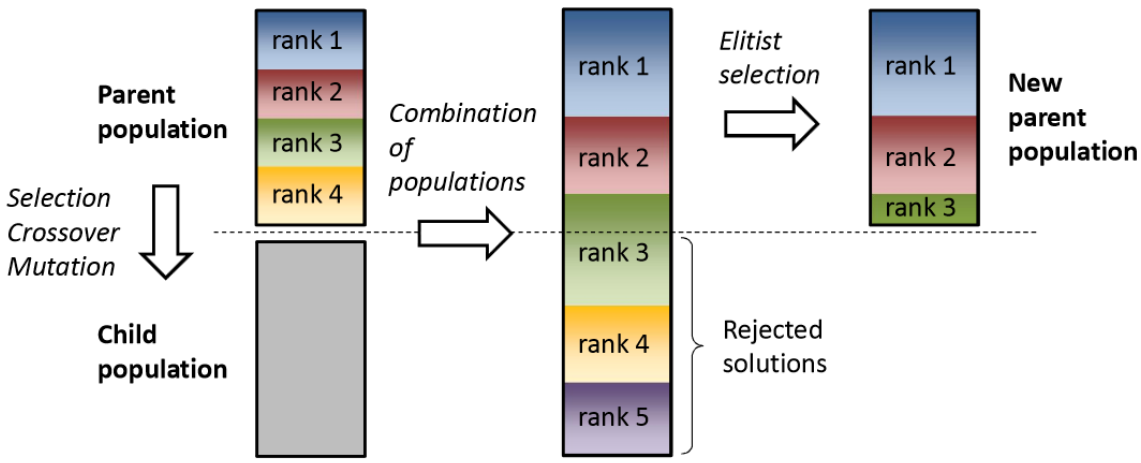

Figure 1-30 Elitism Procedure in NSGA-II [47]

Individuals who have the same rank are then placed in priority order using their crowding distance value. Individuals who are furthest from their neighbors are placed higher in the priority list. This evaluation continues to lower and lower ranks until enough individuals have been selected to satisfy the next generation's population size [44].

Strength Pareto Evolutionary Algorithm II (SPEA-II)

SPEA-II is very similar to NSGA-II with a subtle difference. The algorithm maintains a secondary archive of a finite number of individuals. This archive contains all the non-dominated individuals from all previous generations. Once the archive capacity has been reached a crowding distance comparison is used to compute which individuals to keep and which to discard [50].

SPEA-II uses the offspring of the current generation and the archive of non-dominated individuals when creating the next generation. Fitness is determined through the use of dominance rank and dominance count techniques described above. Each individual is compared to the offspring population as well as the archive in order to determine which individuals to carry over to the next generation [50].

With higher dimensional objectives, SPEA-II provides a better spread of solutions on the Pareto optimal front than NSGA-II [50].

1.5.3.2 Adaptive Simulated Annealing (ASA)

Simulated Annealing (SA) is a global stochastic optimization algorithm that mimics the nature of the heating and cooling of metals to obtain a stronger crystalline structure, otherwise known as metallurgical annealing process. SA employs an algorithm in which its search initializes with a high temperature state and cooling slowly in efforts to search for the lowest energy state, the global minima of the optimization problem [44].

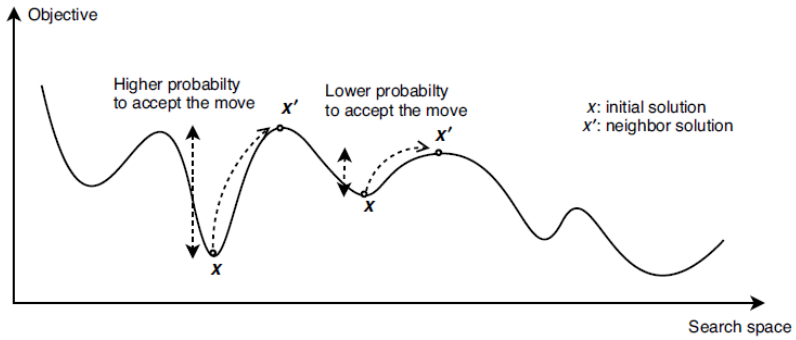

Figure 1-31 Simulate Annealing Probability & Local Minima [51]

New points are sampled and accepted during the course of the process using a probabilistic criterion to improve the probability of that inferior points are not accepted, while updating the temperature. Once the temperature has fallen substantially, the search terminates. Then the system will be re-annealed to focus in the regions with potential improvements by updating the annealing time associated with parameters and the energy function. There are two critical parameters that influence the performance of SA algorithms; the transition probability and the cooling schedule. The transition probability will determine the probability of accepting unsuitable solutions [44].

$$\boldsymbol{p = e^{-\frac{\Delta E}{k_B T}} > random\ number} \qquad \textbf{1-1}$$

'kB' is the Boltzmann constant and is most often given a value of 1. 'T' is the temperature for the particular cooling stage. 'ΔE' is the change in the objective function's value between states. Analyzing equation 1.1, the choice of the initial temperature is critical. For a particular 'ΔE', if 'T' goes to infinity then the probability of accepting an unsuitable solution will result in 1 or 100%. If 'T' results to 0 then for a given 'ΔE', 'p' will also result in 0. This implies that only better solutions are accepted resulting in the algorithm getting trapped in a local minimum [44]. Additionally, for a given temperature,

the lower the increase of the objective function, the higher the probability of accepting the new unsuitable solution [51].

There are many ways to control the cooling schedule, which presents a trade-off between computation time and the quality of the solutions. There are many different methods used to modify the temperature of the cooling schedule, which can be linear, geometric, logarithmic or adaptive. The one that concerns this project is the adaptive method used in adaptive simulated annealing (ASA) [51].

With SA, the ability to be effective in wide variety of hard optimization problems, however it can become trapped within basins, global minimum or deep local minimums. However, a multi-start strategy can negate these problems with this type of line search optimization algorithms [51].

1.5.3.3 Hybrid Algorithms with Leap Frog Optimizer for Constrained Minimization

Both Genetic Algorithm and Adaptive Simulated Annealing are designed to find the global optimal solution, however they have the disadvantage of identifying the correct stopping criterion. It is a computationally intensive approach when running an algorithm sufficiently long enough to ensure the global optimal solution. LS-OPT provides an improvement to this computational expensive approach by providing both algorithms with a hybrid algorithm format, HGA and HASA. The speed of obtaining the global optimum is enhanced by hybridizing the global optimizer with local gradient based optimization method; the Leapfrog Optimizer for Constrained Minimization (LFOPC). The global optimizers obtain the basin of the global optimum quickly, while the gradient based optimization methods refine the optimal solution very quickly with favorable solutions initially. Conclusively, LS-OPT uses the global optimizers GA and ASA as a global optimizer to obtain good starting solution followed by a single LFOPC run to converge the local optimum faster [44].

1.5.4 Metamodeling Techniques

Only three of LS-OPT's more sophisticated metamodeling techniques with point selection space filling technique was to be explored in this work: Feedforward Neural Network (FNN), Radial Basis Function Network (RBF), and Kriging.

Feedforward Neural Network (FFN) is a division of artificial neural network with the implementation of sigmoid basis functions. FFN is a multilayered neural network that models the relationships between a set of input variables and an output variable in the form of numerical units, which are connected to the neurons. Between input and output network layers, there are hidden layer(s) of inter-neurons. These layers are connected by strengths (weights) and biases, which are learnt from training data from the optimization algorithm. The learning phase is contributed by the input neurons in the form of design parameters and associated outputs (responses/objectives). The solver is learning in an effort to steer the network parameters towards minimizing a distance measured. Model computed data distance is measured by the mean square error (MSE) [44].

FFN and RBF methods are similar, except for their choice for basic functions, and solution approaches. FFN uses linear evaluation of the weights and biases. Radial Basis Function Network (RBF) allows the regression processes to be split between layers while analyzing layers in a non-linear fashion. RBF commonly uses Hardy's multi-quadric and the Gaussian basis function [44].

Originally used for approximating true ore grade based on sampling, Kriging metamodeling is a special case of an RBF combined with an additional lower order polynomial and uses Gaussian correlation functions and Gaussian Basis functions:

$$y(x) = f(x) + Z(x) \qquad \textbf{1-2}$$

Where the function *f(x)* is the known polynomial while Z is the stochastic component. Where *Z(x)* may be calculated to associate with the Gaussian correlation function to estimate the response. These estimations are compared to the actual response [44].

1.6 CRASHWORTHY MATERIALS

Crashworthiness is the objective of sacrificing a structure for the safety of its occupants. The structure is designed to fail, but fail in a controlled manner. This control of failure is built into the design through its material selection. In the modern design of vehicle structures, vehicle weight reduction and heightened safety standards have become important criteria. The main component into ensuring that these two criteria are balanced is to optimize the materials built into the design. The automotive industry has focused on utilizing aluminum alloys, magnesium alloys and modern forms of steels. For the heavy vehicle industry, front underride protection devices are built with aluminum alloys for the reduction in weight due to abide to front axle weight requirements. Though, with innovative and modern forms of steels, the balance between weight reduction and improved crash safety can be met from there increased formability, and high mechanical strength properties (yielding, and strain hardening) [52]. These high strength steels with the ability to reduce weight prove to be strong competition towards aluminum, magnesium alloys and plastics for automotive applications [53].

Modern Steels can be broken down into three metallurgical designation classes, seen in Figure 1-32; low-strength steels (LSS), conventional High Strength Steels (HSS), Advanced High-Strength Steels (AHSS) [53].

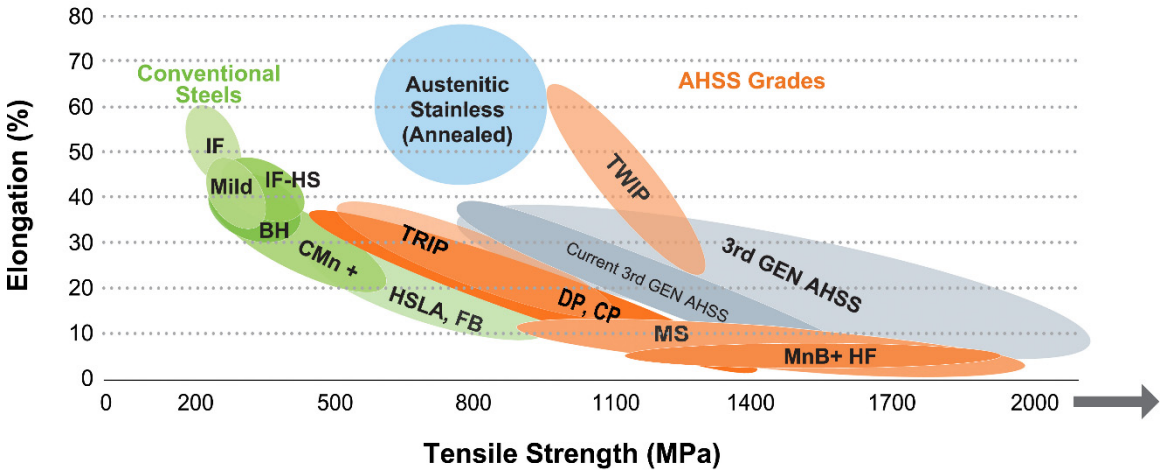

Figure 1-32 Metallurgical Designation Range of Steel Alloys Grades [52]

AHSS have improved crash worthiness properties compared to HSS and LSS [54, 55, 56]. AHSS include various types with very different metallurgical properties: Dual Phase (DP), Complex-Phase (CP), Ferritic-Bainitic (FB), Martensitic (MS or MART), Transformation-Induced Plasticity (TRIP), Hot-Formed (HF), and Twinning-Induced Plasticity (TWIP). Within small and tight design areas in the passenger compartment (such as the A and B-pillar), structural elements rely on extremely high-strength steels for the extreme high yielding strength for anti-intrusion into the comportment, such as Martensitic and boron-based Press Hardened Steels (PHS) [53, 56].

The crashworthiness of the FUPDs needs to be rigid enough to prevent underriding balanced with FUPD deformation to absorb energy and reduce intrusion into the passenger vehicle. Constructing the FUPD with extremely high-strength steels may be too rigid and effect this imbalance by only allowing the passenger vehicle to deform. Dual phase (DP), twinning induced plasticity (TWIP) steels, and Transformation-Induced Plasticity (TRIP) have been well utilized in automotive structures for their potential energy absorption and controlling plastic deformations [55, 56]. DP steels are multiphase materials with a ferrite matrix microstructure containing a hard martensitic second phase in the form of islands. Compared to HSLA steels with similar yield strengths, DP steels have continuous yielding behaviors, lower yield/tensile strength ratios, higher strain hardening rates at low strain and higher levels of uniform and total elongation characteristics. The high strain hardening characteristics (n value), especially at the beginning of plastic deformation, presents desirable properties for controlling impact energies. Notably, DP steels are welded with all conventional welding methods [53]. Transformation-Induced Plasticity (TRIP) consist of a microstructure of a primary matrix of ferrite with austenite embedded with varying hard phases with martensite and bainite present. The retained austenite found in TRIP progressively transforms to martensite with increasing strain. This effect causes an increase in the strain hardening rate at higher strain levels and progress as strain persists. TRIP has a lower initial strain hardening rate compared to DP. However, DP initially high strain hardening rate begins to diminish as the strain progresses [56]. The materials prove to hold good characteristics of both work hardening and bake hardening to significantly improve the energy absorption due to the flow stress increase [53].

1.7 CLOSING REMARKS

The aim and objectives of this work was to build upon previous research and directives from the industry partner to further the design methodology, and understandings of crashworthiness of Front Underride Protection Devices. In order to remain relevant in terms of application and design, the project was to utilize the most recent passenger vehicles and tractor-trailer finite element models. The work primarily focused on transportation tractors (Volvo VNL series). A set of well-defined tasks have been performed and are outlined below:

- Verify and enhance the criticism of existing regulation requirements and published recommendations with increase criticism for occupant intrusion. Investigate and enhance the understandings of ECE R93 point load magnitudes. Enhance the understandings of small overlap collisions, correlating to ECE R93 P1 loading conditions.
- Develop advanced approach to optimization techniques to satisfy industrial targets of cost effectiveness.
- Enhance the application of steel materials for crashworthiness for the FUPD.
- Experiment with various FUPDs geometry configuration to recommend limitations on to prevent underriding.
- Investigate other collision scenarios in which the FUPDs performance may come into question.

CHAPTER 2
TESTING METHODS & EVALUATION METRICS

This work experiments through various cases for the development of underride protection devices completely through virtual testing environment of finite element analysis (FEA). The FEA virtual testing environments are developed with valid physics to replicate the physical realm. 'Environment' refers to the computational software and code in which the experiment is implemented in, and to be computationally solved. The virtual environment can be visually displayed. Using FEA environments provide a cost effective approach to destructive testing (so called physical testing or in-field testing), especially of vehicle to vehicle collision and FUPD development testing, which would need astronomical funding. Furthermore, there are open source and publically available FEA vehicle models that have a high degree of detail and accuracy which was used for testing and allow this research to be possible at a low cost. The major cost to utilizing advanced FEA methods is the hardware demand as the solvers demand relatively high computational power, however it is only a small percentage of the cost compared to crashing a $150,000 USD tractor.

The philosophy to the work uses a three tier design methodology to understand, build and enhance different components of the FUPD, Figure 2-1. Its primary objective is to ensures computational effectiveness, design enrichment, and meeting industrial targets while progressing the development. In addition, evaluate and conclude on the ECE R93 regulation and published conclusions to ensure overall FUPDs performance is adequate for passenger vehicle safety. The original design methodology for underride protection devices was established in previous works, see Section 1.3.1 for full details. In summary tier 1 is a simplified experimental stage for preliminary geometry isolation using FEA vehicle model to collide with a rigid surface. There are two various experiments for this tier: utilizing a rigid body (ie. wall or bar), and a dual spring FUPD (dsFUPD).

Tier 2, driven by the results of tier 1, utilizes various tools to structuralize the design envelope, Figure 2-2. Tier 2 first implements the geometric conclusions and design envelop

into a geometric spacing to be analyzed through LS-TaSC topology. The FEA design envelop is subjected to quasistatic point load testing environment (P.L.T.), Section 2.2.2. From the results from topology, the FUPD structure is remodeled in computer aided design (CAD) software and FEA meshed. Next the structure is given valid deformable materials and member thickness in the FEA environment to be optimized with LS-OPT. In an implicit testing environment, quasistatic loading testing is a computationally fast which allows for high number of simulations to be solved in a reasonable amount of time compared to dynamic testing with FEA vehicles. This stage of the tier required investigation to increasing computational effectiveness by building and refining the optimization process from previous developments. The need to optimize for more materials and cost was needed to benefit industrial targets and enhance FUPD performance.

With a fully developed and optimized FUPD design, tier 3 implements an explicit testing environment with a valid FEA vehicle model. The experiments are completed in various scenarios and using two various FEA vehicles to collide into the FUPD which is mounted to a component level Volvo VNL tractor model. The crashworthiness of the device was analyzed by two performance evaluation metrics, crash absorption and Occupant Compartment Intrusion guidelines set by the IIHS. From this design methodology various conclusions were determined.

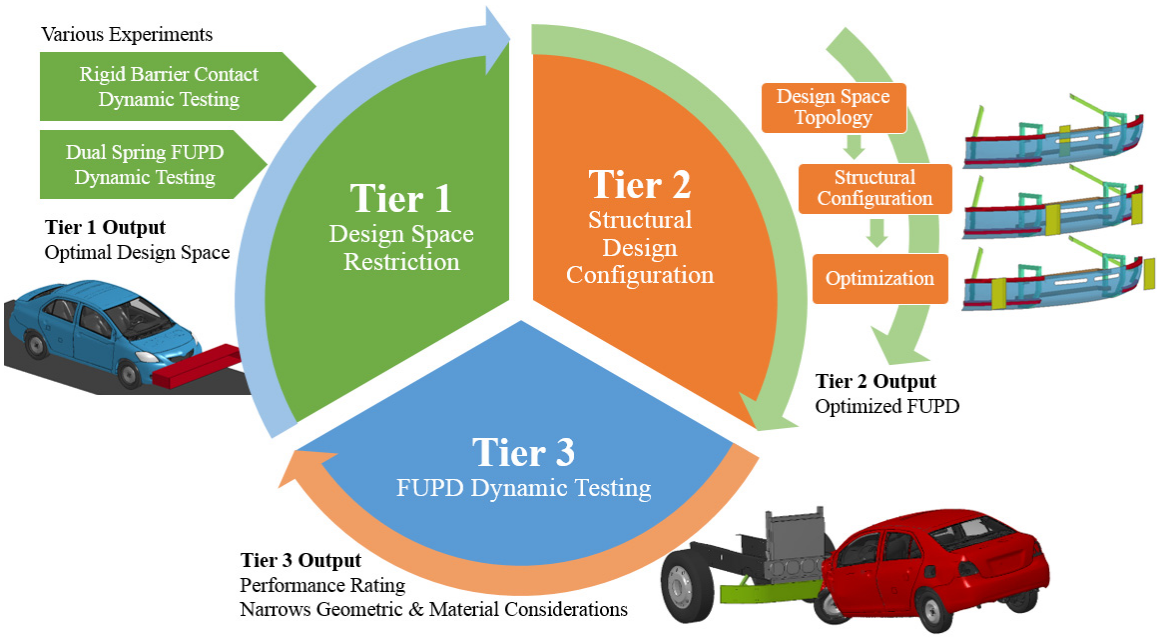

Figure 2-1 Design Methodology Structure

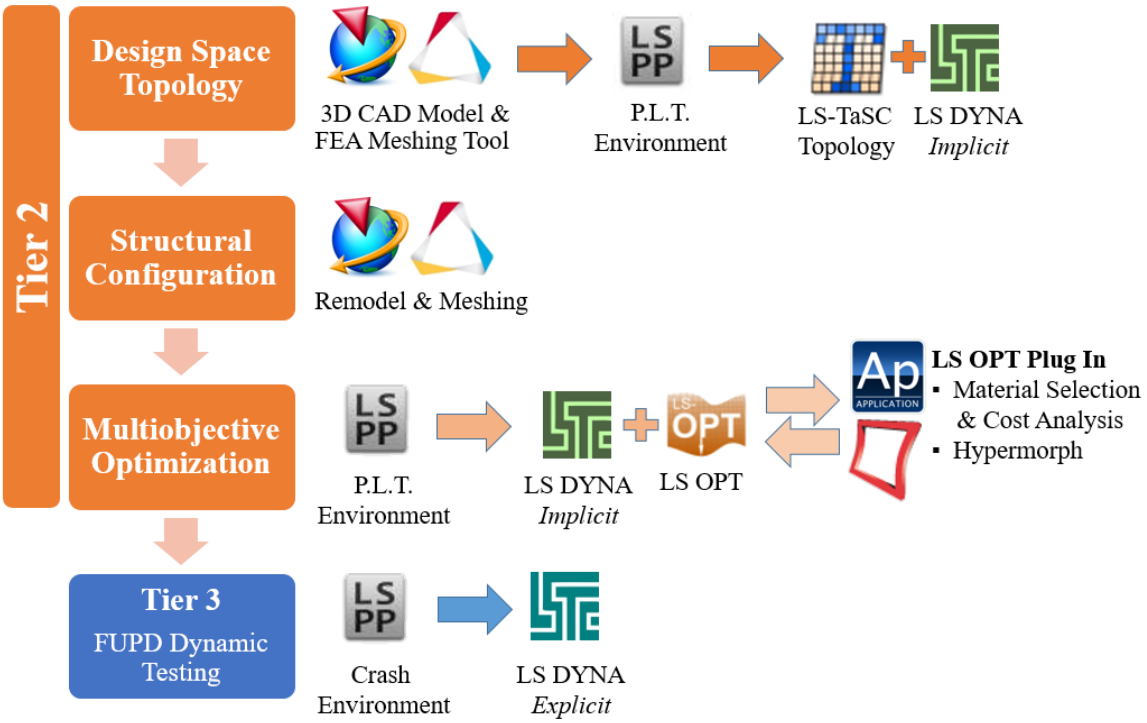

Figure 2-2 Tier 2 and 3 – In detailed Process Map

2.1 FINITE ELEMENT ANALYSIS VEHICLE MODELS

2.1.1 Passenger Vehicle Models

The National Crash Analysis Center (NCAC) developed and publicly released various full Finite Element Analysis vehicle models for educational purposes for the study of crashworthiness. NCAC's collaborative effort with Federal Highway Administration (FHWA), National Highway Traffic Safety Administration (NHTSA), and the George Washington University (GWU) developed valid models from physical testing. These highly sophisticated models are an irreplaceable resource for the research which solidifies the results and conclusions. The in-depth extent into the work would not be capable without their generosity. Due to the 2+ years development time of a full FEA model there is only a limited number of vehicles. The 2010 Toyota Yaris and 2001 Ford Taurus were upon the newest and accurate models that had been released. Both were validated at a closing speed of 64km/hr [19].

The US Department of Transportation Federal Highway Administration established testing roadside safety hardware regulations, documented through the Manual for Assessing Safety Hardware 2009 (MASH). It sets forth new testing evaluation techniques for the crash testing of safety hardware devices for the use on the Nation Highway System (NHS). A guideline of vehicle classes based on recommended properties (ie. Vehicle Mass, Dimensions, etc.) is established [52].

The NCAC developed a complete finite element model of the 2010 Toyota Yaris Sedan in accordance with MASH (Figure 2-3). The Toyota Yaris is a 4 door compact sedan with a 1.5L V4 engine and a weight of 1271 kg [53, 54], deeming a MASH classification of a 1100C vehicle (small car) [52]. Three physical front crash tests were used for the validation of the FEA models, include National Highway Traffic Safety Administration (NHTSA) test 6221 and test 5677, as well as IIHS test CEF0610. NHTSA test 6221 and 5677 (Figure 2-4) a full wrap frontal crash test against a load cell wall in accordance to CMVSS 208, with vehicle closing speed of 56 km/hr. IIHS moderate-overlap frontal impact test CEF0610 collided the Toyota Yaris at a closing speed of 64 km/hr [54].

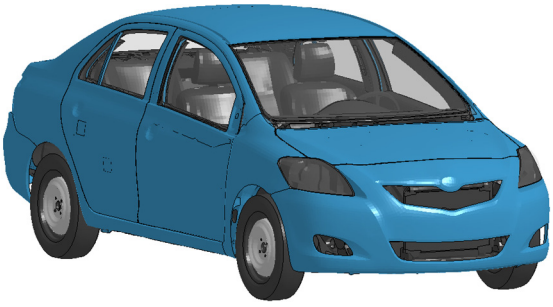

Figure 2-3 2010 Toyota Yaris FEA model provided by NCAC

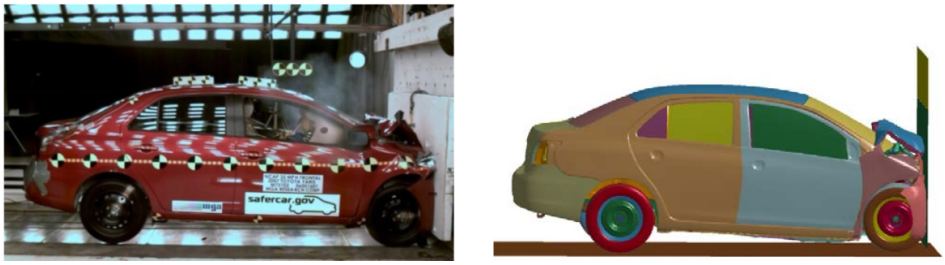

Figure 2-4 Impact Comparison of the Toyota Yaris in NCAP Test 5677 and simulation [55]

A 2001 Ford Taurus was also developed by NCAC, Figure 2-5. The Taurus is a 4 door mid-size sedan with a 3.0L V6 engine weighing 1777 kg, classifying it as 1500A

(intermediate car) [52, 55]. Validation of the model incorporated NHTSA test 4776 in accordance to CMVSS 208 at 56 km/hr, and IIHS test CF00010 moderate-overlap frontal impact test at 64 km/hr [55].

Figure 2-5 2001 Ford Taurus FEA model provided by NCAC

2.1.2 Tractor-Trailer Models

2.1.2.1 Full Tractor-Trailer Model

The work also utilizes a full finite element tractor-trailer model of a Freightliner FLD120 tractor. It was developed through the collaborative efforts of Battelle Memorial Institute (BMI), the Oak Ridge National Laboratory (ORNL) and the University of Tennessee at Knoxville (UTK). The physical crash validation of the FEA model was conducted by the tractor colliding with a concrete roadside barrier, a common testing method for tractors (Figure 2-6). The model is a set back front axle, day cab tractor model with a 194in wheelbase attached to a 45ft long trailer, with the combined weight of 23,127 kg [56]. The model does not contain a front underride protection device and is mainly utilized for benchmarking purposes. The most common and generally accepted method of testing with the tractor-trailer is holding the tractor stationary and initiating a closing speed of the passenger vehicle [5, 6, 17, 40].

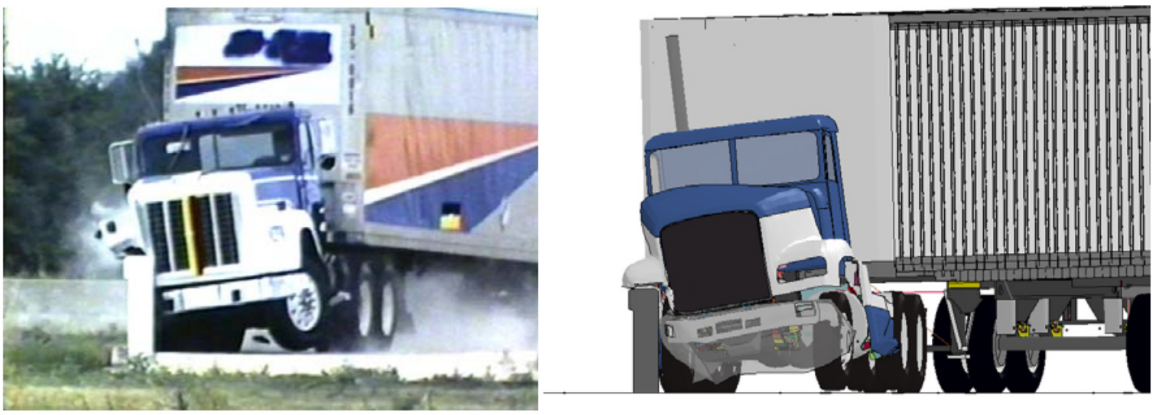

Figure 2-6 NTRCI Tractor-trailer Validation with a Roadside Barrier

2.1.2.2 Component Level VNL Tractor Model

Within the virtual environment for dynamic collision testing, a structural level tractor model was created to only resemble the necessary components for the frontal crash compatibility. Ideally a full vehicle model would be used for all analysis, but for computational expense a simplified approach is needed. The structurally focused component level models has been previously validated for the development and testing of FUPDs [5, 6]. In addition, with the projects support from Volvo Group Trucks Technology, a tractor model was developed to reflect the geometric structure of Volvo's VNL series tractor (Figure 2-7). The developed model conforms both FUPDs geometric restrictions and corresponding interactions associated with components located at the front of a tractor. NTRCI model lead to the material type and section thickness of the radiator, radiator mounts, bumper and frame components for the VNL model. The fixed tractor wheels and tyre are placed in the environment for possible interactions with a colliding passenger vehicle rather than their influence throughout the collision [5].

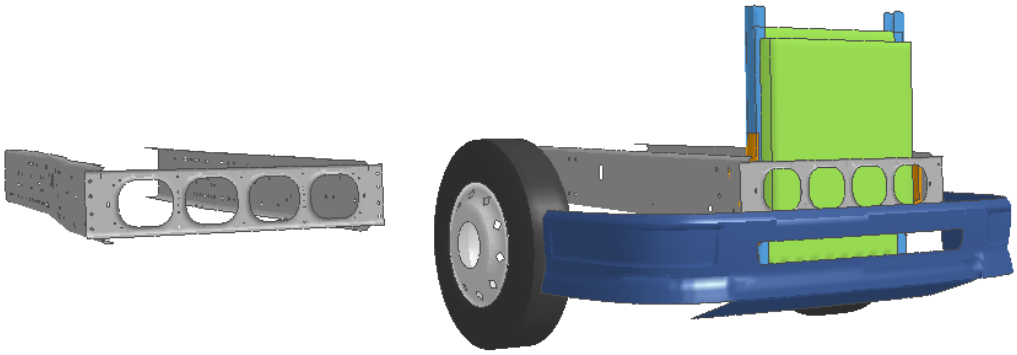

Figure 2-7 Primary (left) and Secondary (right) Component Level VNL Tractor Models [5]

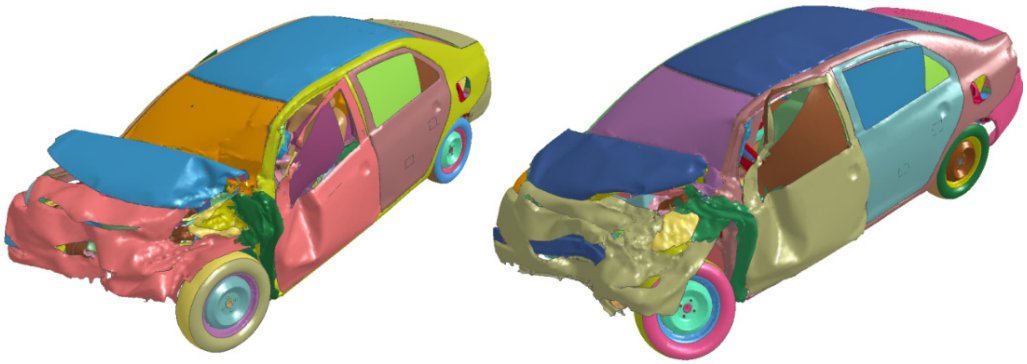

Figure 2-8 Comparisons of Collisions Involving Toyota Yaris with Closing Speed of 64km/h and 50% Overlap versus the Primary Component Level VNL Tractor (left) and complete NTRCI Tractor-Trailer Model (right) [5]

2.1.2.3 Dual Stage FUPD F9 Model

Developed at the University of Ontario Institute of Technology, the duel stage front underride protection device (dsFUPD) F9 design was developed for the Volvo VNL [5]. It was constructed from a single high strength, low alloy (HSLA) steel with a total mass of 41.74 kg. It was optimized through Hybrid Adaptive Simulated Annealing (HASA) for the variables of material thickness and cross section area of the members for the objective of reducing mass and deformation. After fine tuning and enhancing the finite element model, the dsFUPD F9 was used in this work to investigate topics for improving the design methodology, and better understanding of the performance of FUPDs in general.

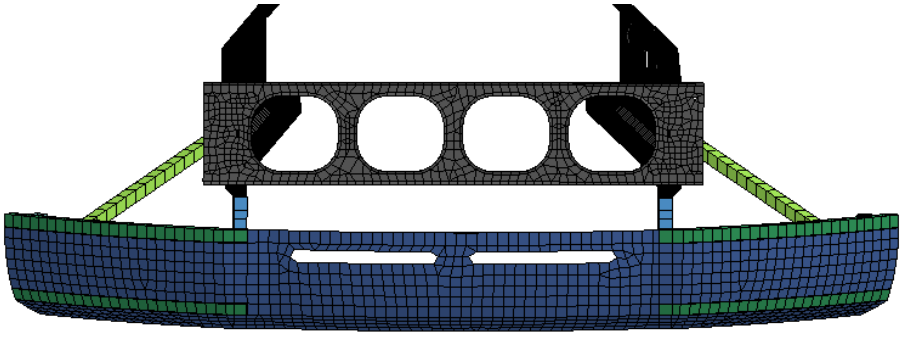

Figure 2-9 dsFUPD F9 model

2.2 VIRTUAL ENVIRONMENT SETUP

2.2.1 FEA Solver Environments

There are two various testing environments in which FEA models can be solved in; Implicit and Explicit. Explicit time integration is the main solution methodology to solving the finite element code for analyzing large deformation events in a small time frame. Implicit transient analysis solvers are ideally used for static, quasi-static, and dynamic problems with a low frequency content; when desired environments neglect inertia forces. An important factor between the two solvers is the duration of solve time and output results as it can affect development time. The advantage of using implicit analysis is for the speed in which it can solve compared to explicit integration, 100 to 1000 times faster. Increasing computational speed to from hours in explicit to minutes when using implicit solvers. However, a major issue with implicit solvers is the computational cost per step is unknown since the speed depends on the convergence behavior of the equilibrium iterations. The time step controls most of the computational timing and is an important factor between the two solvers. Implicit transient analysis time steps are independent to the model in the environment are set to the user's desire, which is generally serval orders of magnitude larger than explicit time. Explicit analysis time step is dependent on the environment and must be less than the Courrant time step (time it takes for a sound wave to travel across an element). The smallest size and densest element will control the time step and increase computational time [42]. Computational time also depends on the hardware the solvers are being completed on. Within this work couple of various hardware systems were used, and will be depicted within the chapter if required. These factors are important to note to ensuring models, environments, testing methods are created effectively and optimally.

To ensure accurate and valid collision experiments, the main solver method is based on explicit time integration. However, to increase development speed, implicit analysis would be used for testing FUPDs when applying ECE R93 quasistatic loading conditions. For full details on the theory, physics and formulation of the LS-DYNA solvers, please review the LS-DYNA Theory Manual (http://www.lstc.com/download/manuals) [42]. Within this study, full Newton Method is used for implicit solutions. Implicit analysis is

also very ideal for optimization procedures as large number of models would need to be solved simultaneously. For reference, Belytschko-Tsay Element formulation was utilized in majority of the work's models. Penetration of elements was resolved for more accurate contacts between impacting element models by using soft constraint formulation.

2.2.2 Quasistatic Point Load Experiment

The impact experiments using the finite element vehicle models are computationally expensive, especially if the full tractor-trailer is used. For development and quick insight into the performance of the FUPDs design, a quasistatic point load experiment is used. This form of testing ensures the FUPD passed the desired standards in a quick manner. As the nature of the experiment is quasistatic, neglecting inertia forces, implicit solvers are used. This allows for a quick solve time, between 2 mins - 5 mins compared to 8+ hours real time for the full dynamic experiment. This is in reference to the hardware used for the work, more powerful hardware can reduce the real time dramatically but present the same trends.

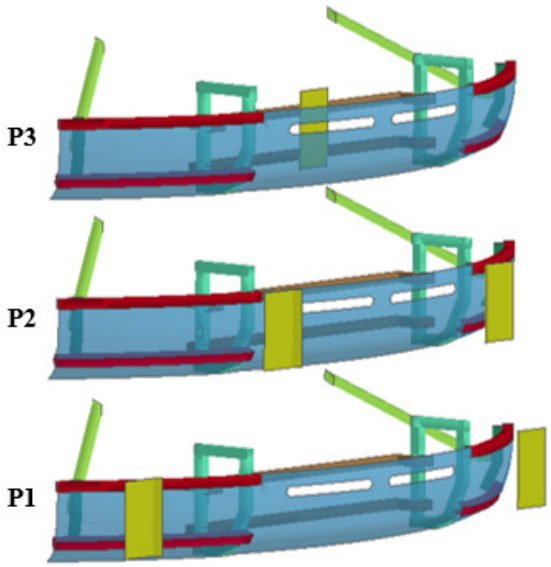

Figure 2-10 Quasistatic Loading Environment

Tier 2 of the FUPD design methodology utilizes this setup for topology experiments and structural performance the Modified ECE R93 testing environment, unless specified. The environment simultaneously loads the protection device model with quasistatic loads in 3 locations to observe the resultant deformation, Figure 2-10. The experiment applies the loading of 160kN quasistatic loads, and is limited to less than 100mm of deformation

to be acceptable in the modified ECE R93 regulation. Subsequent work in the project has proven it is a concrete testing method for optimization and robust performance testing.

2.2.3 Dynamic Collision Experiments

Dynamic collisions between a passenger vehicle and the FUPD provided a superior method to analyzing the performance of FUPDs structural design. The experiment utilizes the passenger vehicles environment impacting the desired entity. Tier 1 utilizes dynamic collisions with rigid bodies. While tier 3 utilizes the FUPD mounted onto the component level VNL in dynamic collisions. For each case of experiments conducted in this work the desired setup is explained. Normally a passenger vehicle was set to a closing speed of 64 km/hr at a desired overlap for a testing duration of 0.2 seconds. To ensure the vehicle was accurately experimented on, the vehicle was normally the impacting entity and was always relative impact to a static object (unless otherwise specified). This was to ensure the accuracy of the finite element model is not diminished, as the models were always validated in reference to a static object.

The overlap coverage was always in respect to the area overlapping the passenger vehicle, Figure 2-11. For 50% and 30% overlap, the impacting entity was shifted to only cover the area of the driver side of the passenger vehicle. Head-on collisions are deemed 100% overlap, it resembles the direct impact of the tractor-trailer and passenger vehicle. The 50% and 30% overlap reflects the vehicle slightly diverting into the other lane. In addition, 50% overlap help reflect the ECE R93 P2 location and 40% P1 location.

Figure 2-11 Overlap Coverage with Respect to the Passanger Vehicle

Within tier 1, the component level VNL with dual springs was used in place of the structural members of the FUPDs, Figure 2-12. Instead a rigid surface with a simple geometric area is used to defined the impact area, in which will help define geometric parameters of the front of the FUPD. The springs are embedded with ideal longitudinal and horizontal deformations characteristics from results of developed FUPDs. In the present work, the characteristics were tuned for more accurate representation. This method of tier 1 testing was only to benefit the development of deformable FUPDs. The experiments follow the same procedure as the deformable FUPDs process.

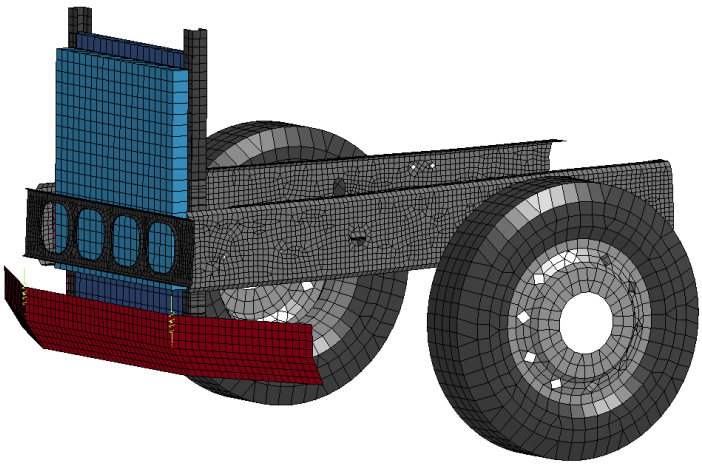

Figure 2-12 Simplified FUPD (in red) Constrained by Dual Spring System

2.3 EVALUATION METRICS

2.3.1 Compatibility Profile of the Collision

Evaluation for structural performance and impact performance between vehicles is critical to the understanding and development of underride protection devices. An appropriate evaluation criteria was needed to gauge the performance of the impact while observing the impact stiffness and energy absorption management. Depicted in other works for underride protection devices and collision studies, the compatibility profile of the collision illustrates the progression in time of the total impact force and the relative displacement of the vehicle. If there is a compatibility between objects contacting causing deformation, the displacement is deemed to be relative deformation. This evaluation metric is primary for explicit dynamic collision experiments. Results provide the understanding of the interactions and how the FUPDs distributes the energy. Relatively, the working/absorbed energy (area under the curve / integral of force vs. deformation) from the impacting vehicle will remain constant, therefore for design purposes this working energy needs to be balanced; higher impact forces in which transfers to the passenger vehicle for a lower deformation of the FUPDs or lower impact forces but higher deformation which can transfer to higher intrusion values.

For visual understanding, Figure 2-13 illustrates the compatibility profile of the experiment with the passenger vehicle. Marked in Figure 2-13 as (1), the usual first stage of the impact is the initial contact between the entities, followed by the impact forces of the vehicles chassis rails (2). The largest or second peak in impact forces is due to the inertial forces and contact with the engine and engine mount (3). The last stage of the impact is when the vehicle rebounds off the impacting entity and moves in the opposite (negative) direction (4). For small overlap impacts, the vehicle impacts and deflects off the entity, and continues to travel in the positive direction.

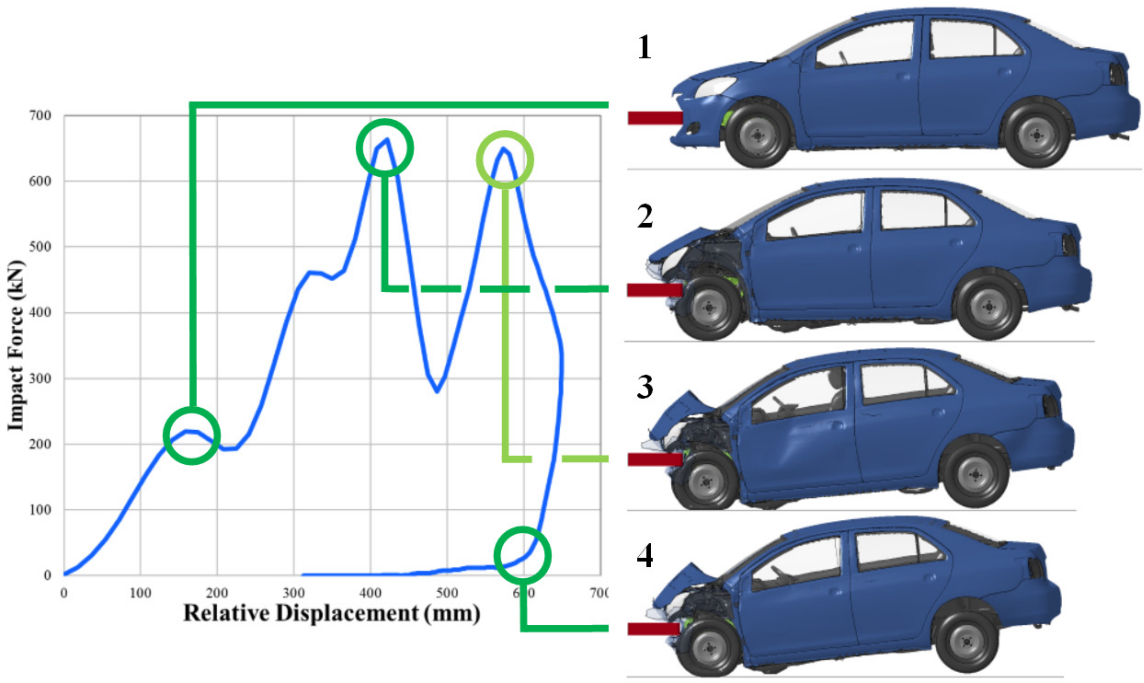

Figure 2-13 Impact Force vs. Relative Displacement/Deformation

2.3.2 Contour of Interface Resultant Forces

Contact impact force data between two entities can be visually displayed on the models. The visualization of interface resultant forces provide insight of the local forces are being applied onto the entities. Within the work, the models would be displayed in resultant sections and refer to the compatibility profile at its relative displacement/deformation. This is exemplified in Figure 2-14.

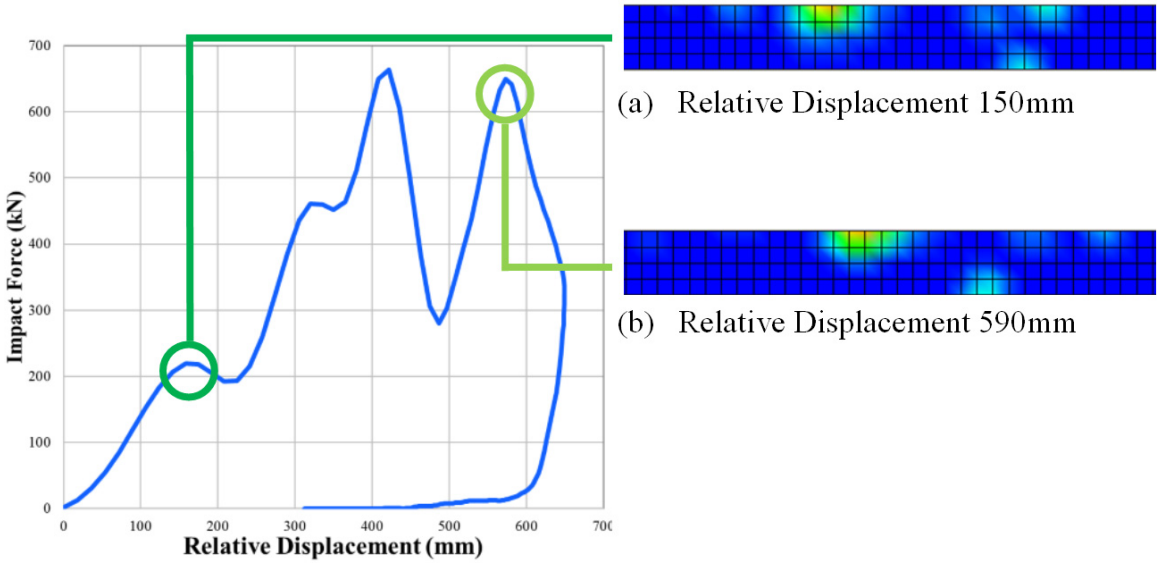

Figure 2-14 Impact Forces Relation to Visual Contour Force Displace

2.3.3 Insurance Institute for Highway Safety - Rating Occupant Compartment Intrusion

Quantifying structural performance from a collision was needed to refine results and approach evaluations in a more sensitive method. The Insurance Institute for Highway Safety (IIHS) methods for Occupant Compartment Intrusion aids in the quantifying crashworthiness performance for the structural integrity and occupant safety. IIHS guidelines for the measurement of Occupant Compartment Intrusion for moderate overlap frontal collisions evaluates intrusion into the driver's safety cage at 8 locations, Figure 2-15. The measurements used represent the residual movement and deformation changes pre/post-collision at seven points on the vehicles interior and the closing distance between the A- and B-pillars is the ideal behind the structural ratings.

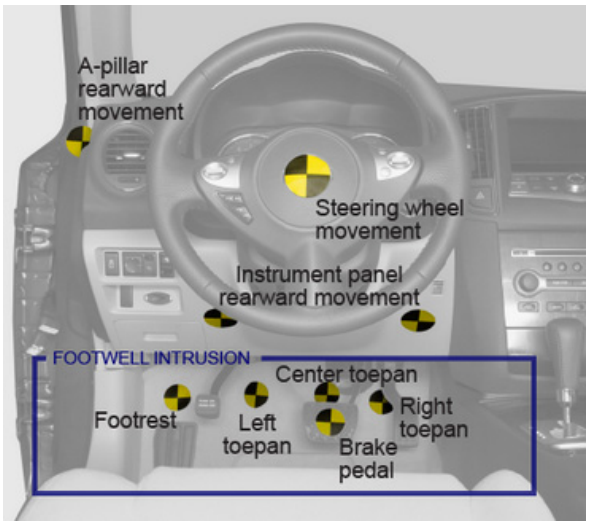

Figure 2-15 IIHS Intrusion Measuring Reference Points [28]

Two of the interior measurement points are located on the lower instrument panel, in front of the driver's knees; four points are in the foot-well area, three across the toe-pan and one on the driver's outboard footrest; the last measured point is on the brake pedal. The pre- and post-collision locations of these points are measured with respect to a coordinate system originating on the driver door striker. The measured movement of the interior seven points is adjusted to reflect movement toward the driver seat [52]. For the FEA model, the movement towards to the driver seat is represented by the locations of its attachment to the vehicle floor, expect for the A- To B-pillar closure [53].

The structural rating is based on comparison of intrusion measurements with guidelines. The X-Y-Z vector resultant movements of the toe-pan, footrest, and brake pedal points are used for comparison with the rating guidelines. Only the rearward movement (X) of the instrument panel is compared with the guidelines. Figure 2-16 displays the ranges for these measurements and associated structural ratings in which results are plotted on. Vehicle models with all intrusion measurements falling in the area labeled good will receive a good structural rating if no additional observations lead to a downgraded rating. It is important to note that some patterns of deformation are less desirable regardless of its intrusion measurements. If this observation is made, the structural rating will be modified to reflect this result [52]. For better reflection of the characteristics of an underride collision, a slight modification to the A-pillar intrusion point measurement was set forth instead of the door.

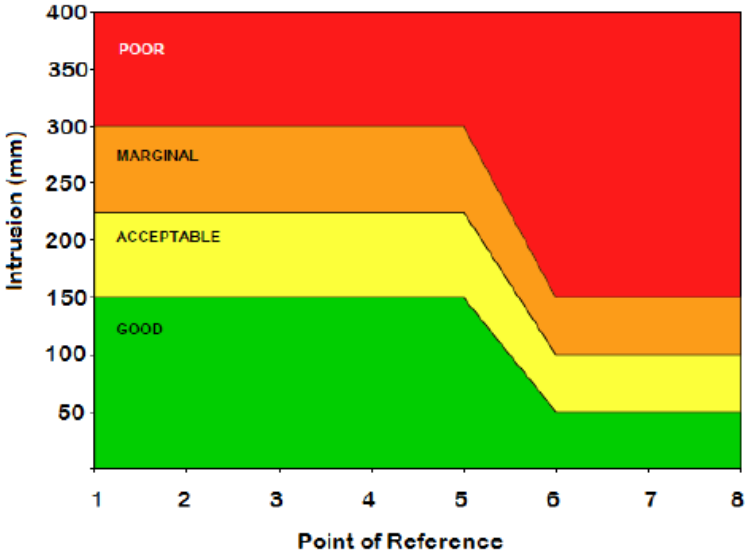

Figure 2-16 IIHS Guidelines for Rating Occupant Compartment Intrusion [52]

Table 2-1 Measurement Reference Points in Referenced to Figure 2-16

Reference Number	Measured Position in Vehicle
1	Footrest
2	Left toepan
3	Center toepan
4	Right toepan
5	Brake pedal
6	Left instrument panel
7	Right instrument panel
8	Door or A-Pillar (Modified Case)

For application of the NCAC finite element models for the IIHS rating system, the validation testing results were gaged to the FEA results. The Toyota Yaris IIHS values resulted from the FEA test were in an acceptable range for most of the reference points, Figure 2-17. The exception was the brake pedal, reference point 5, as it had an approximately 100mm increase from the FEA model compared to the crash test CEF0610. This was the result of the finite model not containing a brake pedal. Most of the differences between the physical and FEA results were due to most reference points are on the floor of the vehicle. The Ford Taurus results comparable to the Toyota Yaris, with results in an acceptable range, except for the brake pedal, Figure 2-18. Reference points 6 to 8 are also slightly higher, however follow the same trend.

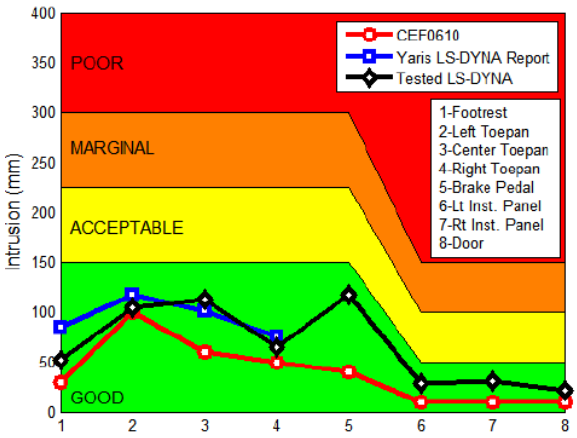

Figure 2-17 Toyota Yaris IIHS test comparisons [17]

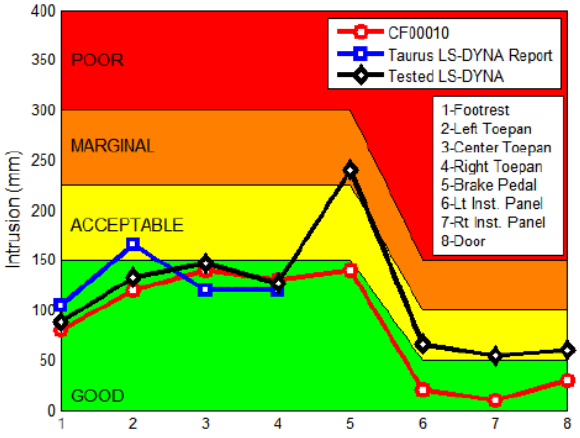

Figure 2-18 Ford Taurus IIHS test comparisons [17]

2.4 INITIAL ENVIRONMENT CONDITIONS CONSIDERATION

The environment conditions for all experiments remain bounded to the validation conditions of the vehicles. The NCAC FEA vehicle environment (including the model) were validated with physical testing standards involving the passenger vehicle colliding and a specific impactor. Closing velocities of the validation were set to 56 km/hr to 64 km/hr for the specific validation frontal impact testing. However, the validation was set to impacting full walls or on deformable contact, which can present some challenges when experimenting with other applications. Furthermore, to maintain the accuracy and validity

the vehicles, environments are utilized. For application, models such as the FUPD and VNL model are embedded into the vehicles environment. The vehicle closing velocities are kept in range of 56 km/hr to 64 km/hr for frontal impacts. The exception to maintaining vehicle's highest validity is presented and discussed in Chapter 6.2 SIDE IMPACT OF PASSENGER VEHICLE and 6.3 REAR IMPACT OF PASSENGAR VEHICLE. Chapter 6.2 extends beyond the validation zone published by NCAC, however section presents validation from physical testing and FEA testing to solidify its results. While, Chapter 6.3, extended beyond the validation zone, the quantitative results can be concluded as trends in FUPD performance but do not apply to design considerations.

CHAPTER 3
GEOMETRIC PARAMETERS & LOADING CONDITIONS

The first steps to ensuring that underride does not occur is to ensure the impact contact between structural members of both vehicles can be compactable. The geometric parameters of ground clearance and cross section height of the front underride protection device can ensure passenger vehicles can be compatible. This chapter investigates, verifies, and builds upon current ECE regulations and prior publications set/modified parameters through tier I dynamic testing method. In addition, the quasistatic loading conditions are evaluated upon from a dynamic impact perspective from the contact force contours. The chapter consists of two experiments to verify and conclude on geometric parameters of ground clearance and impact contact area, and the modified ECE R93; The first was to replicate previous publication results by utilizing a rigid bar to define geometric parameters for the FUPD. The second was to ensure the application is applicable to FUPD designs built from the conclusions.

3.1 VIRTUAL EXPERIMENT I – DYNAMIC IMPACT WITH A RIGID BAR

The European regulation for FUPDs under ECE R93 outlines the current limitations of the maximum ground clearance to 400mm (450mm in India - AIS069) and the section height of the FUPD cross-member should be no larger than 120 mm. As illustrated in Figure 3-1, the ground clearance is the distance between the ground/road and the lowest part of the FUPD, and the cross section height is the vertical height to the impacted structure. The ground clearance is important to define and limit as a higher clearance may influence underriding of the passenger vehicle due to the miss-contact interaction of the FUPD. However, lowering the ground clearance may cause an ineffective compatibility of the impact contact as the passenger vehicle's structure over rides the device. The cross section height is the impact area in which the FUPDs should be designed around to ensure

the contact area is large enough to absorb the impact, and enough height to be compatible with impact heights from other vehicles.

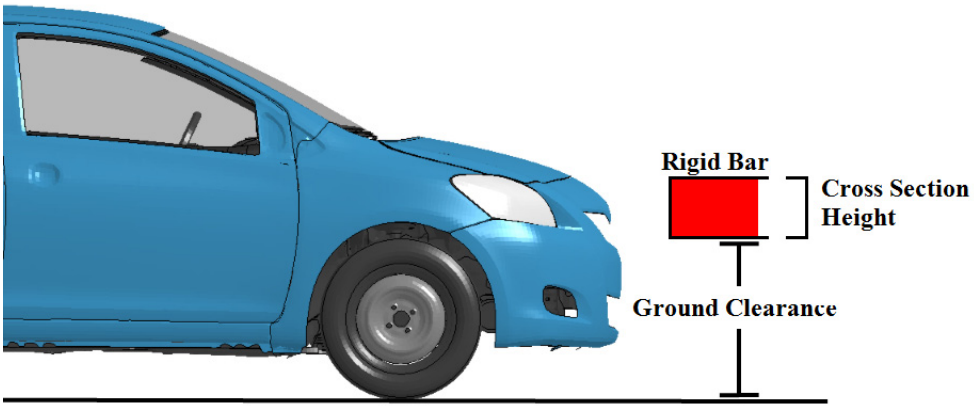

Figure 3-1 Vertical Measurements

As described in Chapter 1.3.2, a prior publication concluded the geometric parameters for an optimal compatible collision considered of a cross section height should be no less than 240mm at a ground clearance between 350-400mm. The publication experimented with only a FEA Toyota Yaris impacting a rigid beam at various ground clearances and two different cross section heights at 64 km/hr. Conclusions were only analyzed from compatibility profiles of the collisions (section 2.3.1). In addition, the impact contact heights of various passenger vehicles on the roads in North America were compared with the concluded height of a FUPD would be compatible for a major of vehicles Figure 1-21. However, the experiment lacks more critical metric to analyze from IIHS compartment intrusion to ensure compartment safety. In addition, small overlap (30% overlap) considerations are not evaluated, as well as the localization of the forces.

In addition to geometric parameters, ECE R93 directs a quasistatic point load testing at various points along the front of a FUPDs. Prior publications experimented and proposed modifications to the ECE R93 quasistatic loading conditions, descripted in Chapter 1.3.3. It was concluded to increase P1 and P3 quasistatic point loads from 80kN to 160kN from the performance of various optimized FUPDs in dynamic testing with the Toyota Yaris. The various FUPD designs were optimized with different loading conditions. This form of an experiment methodology was cumbersome as increasing the force magnitudes would only increase material thickness of each part of the FUPD, and effectively increase its

strength stiffness. However, it does not effectively defend the increase in force magnitudes as impact forces from the vehicle may not be centralized at the ECE R93 reference points. This opened the investigation into the analysis of impact force magnitudes and location of the localized forces to compare to regulations.

From the foundations, ECE R93 P2 point load is gauged to 160kN which is noted to be 100% of the permissible mass of the tractor-trailer. ECE P1 and P3 point loads magnitude of 80kN (50% of the mass) [9, 32]. This notion draws the connection that a FUPD should be designed with an applied stiffness for absorption is based on the vehicle weight. The regulation leads to the conclusions that the testing methodology is geared to full width impacts and not considering overlap scenarios. In addition, for overlap conditions at P1, it suggests that the impact stiffness should only be half. These ideals may be contradictory to the state of the energy management of the impact.

From a 1999 publication, the 100% overlap / full width impact provides the maximum energy absorption by the structural parts, in other words 100% impact stiffness. However, with the 50% overlap, the vehicle stiffness relies on of the one chassis rail and part of the engine for energy absorption. Concluding only 50% of the impact energies are regularly available from the full width impact. If the vehicle was designed for a full width impact, then the vehicle's energy absorption would only absorb 50%, relying on the passenger's compartment to absorb the other 50%. In addition, the impact forces and deceleration levels are approximately 2.5 times higher. This results into higher intrusions into the passenger compartment [66]. This concludes that the impact from the vehicle would be higher in an overlap. However, the publication may not reflect the more modern vehicles, such as the 2010 Toyota Yaris. In addition, the 1999 conclusions may be considered irrelevant as the results are far older than the MASH rules that test vehicles should be no more than 6 model years of age to be analyzed [58].

Therefore, it was set to analyze and conclude if the applied forces from the Toyota Yaris at different overlaps to reflect the conclusions from the 1999 publication, and the point load loading trend of the ECE R93 regulation.

The compatibility profiles of the collisions, impact force vs deformation, results are also the total overall impact forces between the contacts, not the localized areas. Dynamic

experiments with the rigid bar and the impacting vehicle can result in localized contact forces to observe the critical areas within the impact contact. Segment resultant interface forces can be visually output through contours in the FEA mesh of the rigid bar, Figure 3-2. The goal of the investigation of the visualization is to observe exactly where the forces are being applied, and by what magnitude. To help the visualization, the point load placements from ECE R93 are shown.

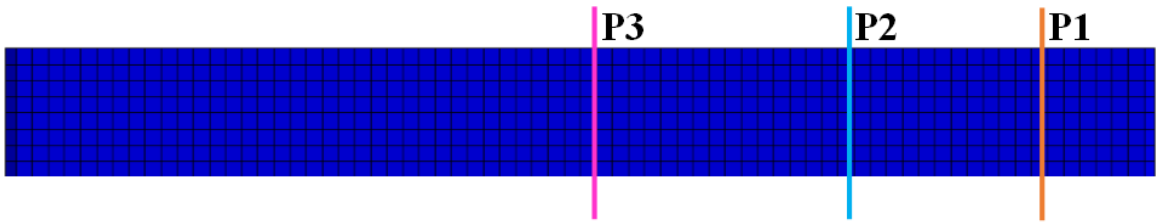

Figure 3-2 Rigid Bar Front Profile with ECE R93 Point Load Placements

In summary, with improvements to the FEA vehicle models and evaluation metrics, there was a need to verify, build, and enhance previous conclusions for geometric parameters, and ECE R93 load magnitudes. The introduction of IIHS intrusion metrics would enhance conclusions concerning to occupant safety through dynamic collisions with a rigid bar for geometric parameters. Being more critical to small over lap conditions by evaluating at an overlap of 30% would broaden the study. While experimenting with dynamic collisions for geometric parameters, the impact contact forces would be evaluated to review the ECE R93 loading conditions in a more solidified manner.

3.1.1 Virtual Experiment I – Setup

The Toyota Yaris and Ford Taurus were set to 64 km/hr closing speed to the immoveable and rigid bar. The rigid bar was set to two different cross section heights, noted as CW, of 120mm and 240mm. As well, the ground clearance, noted as GC, was varied at 300mm, 350mm, 400mm, 450mm, and 500mm. To ensure a robust analysis every iteration was observed at the three different overlaps (Head-on, 50% and 30% coverage). The rigid bar is immoveable in space and not deformable. This evaluation only takes the perspective of the compatibility of the passenger vehicle since any structural stiffness from the tractor-trailer would be above the heights testing. Three sets of results are obtained from each case; Collision Compatibility Profiles, IIHS intrusion for compartment intrusion,

and Impact Force Contour. Impact Force Contours visually show where the largest forces from the vehicle onto the rigid bar. Note only contours are critical points during the duration of the impact are shown. For contrast, a full wall test at all three overlaps was also conducted for both vehicles closing speeds at 64 km/hr into a rigid wall.

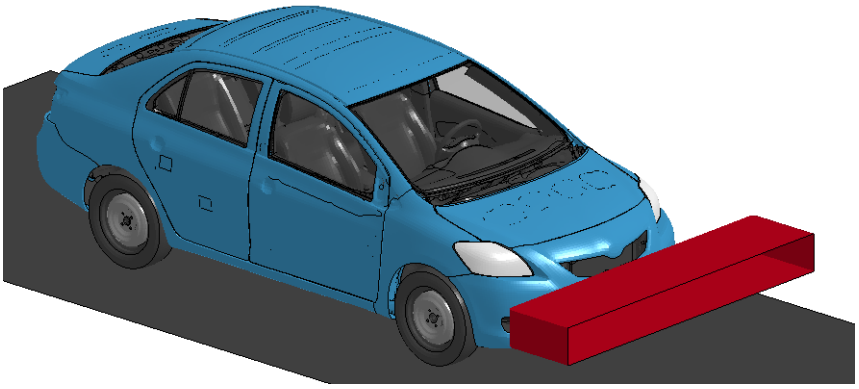

Figure 3-3 Experiment Setup –Head-On 100% Coverage

3.1.2 Virtual Experiment I – Results

The resulting figures follow the naming convention of:

Vehicle – Overlap – Rigid Bar Cross Section Height (CH)

3.1.2.1 Results I – Collision Compatibility Profiles – Toyota Yaris

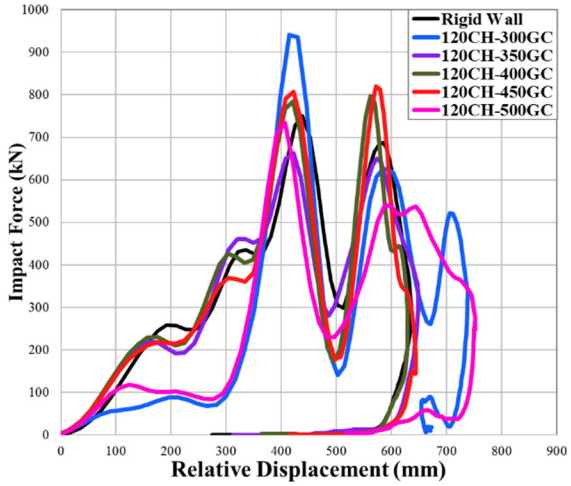

Figure 3-4 Yaris – 100% – 120CH

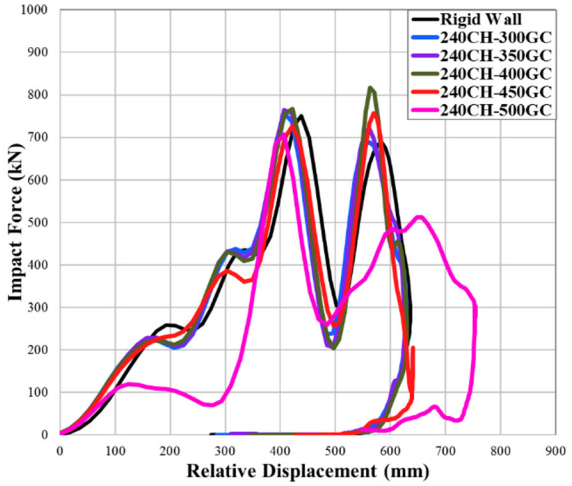

Figure 3-5 Yaris – 100% – 240CH

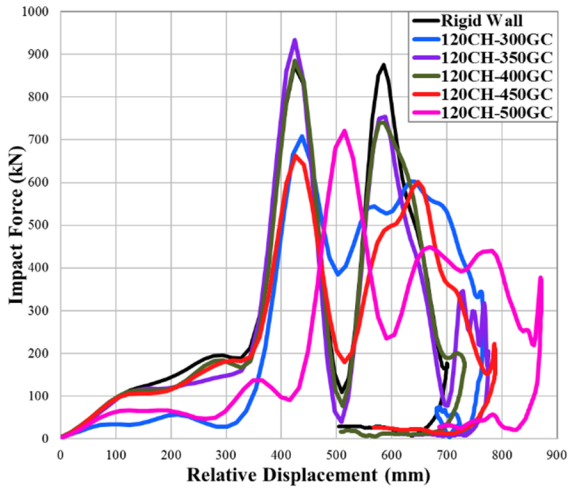

Figure 3-6 Yaris – 50% – 120CH

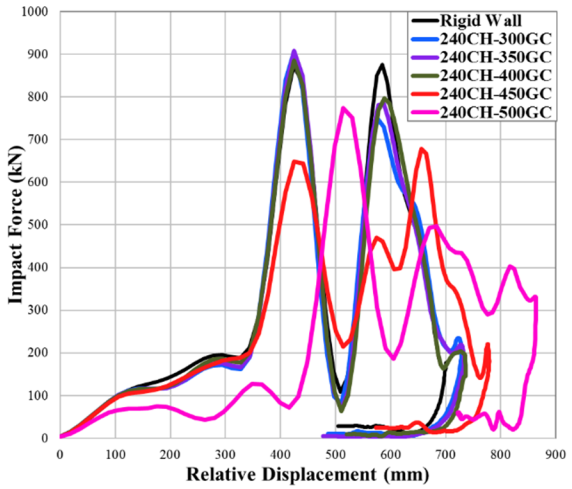

Figure 3-7 Yaris – 50% – 240CH

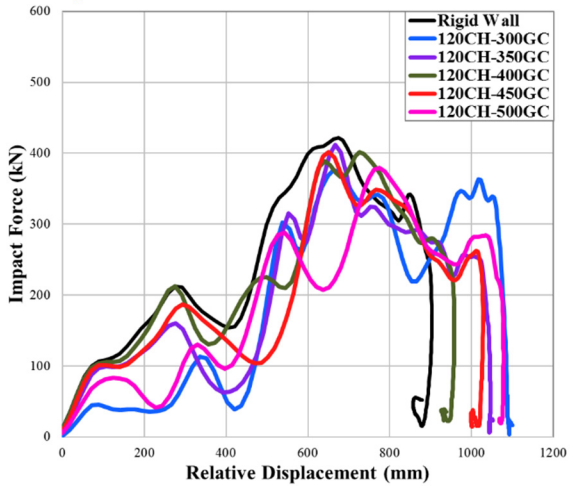

Figure 3-8 Yaris – 30% – 120CH

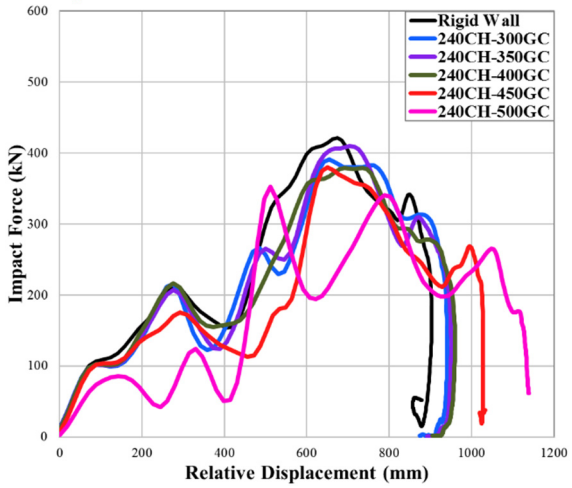

Figure 3-9 Yaris – 30% – 240CH

3.1.2.2 Results I – Collision Compatibility Profiles – Ford Taurus

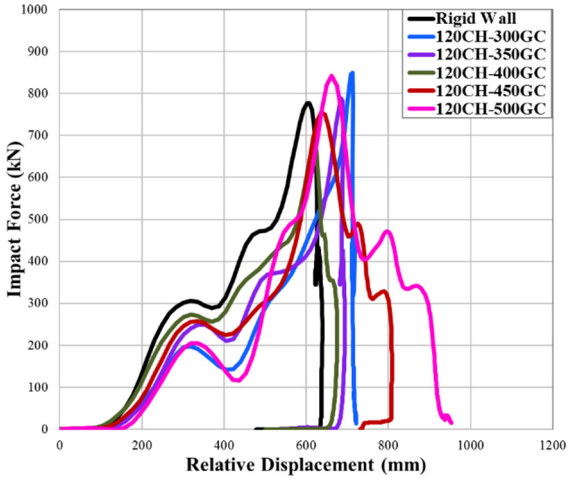

Figure 3-10 Taurus – 100% – 120CH

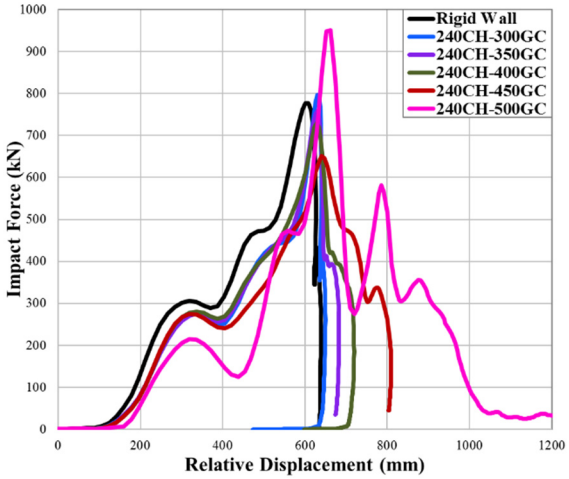

Figure 3-11 Taurus – 100% – 240CH

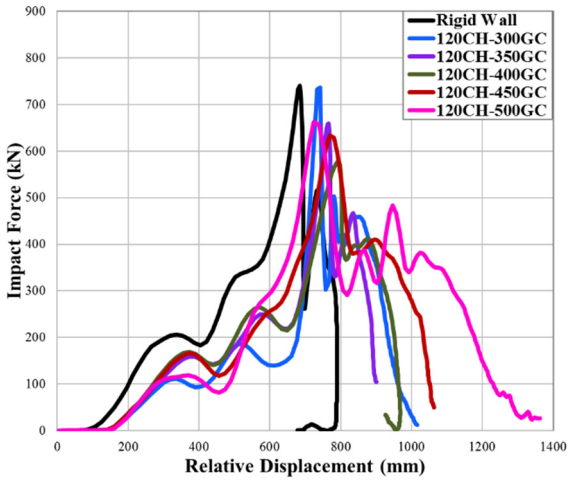

Figure 3-12 Taurus – 50% – 120CH

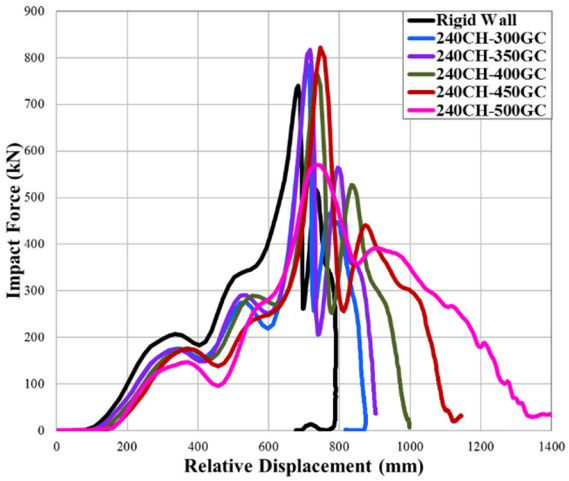

Figure 3-13 Taurus – 50% – 240CH

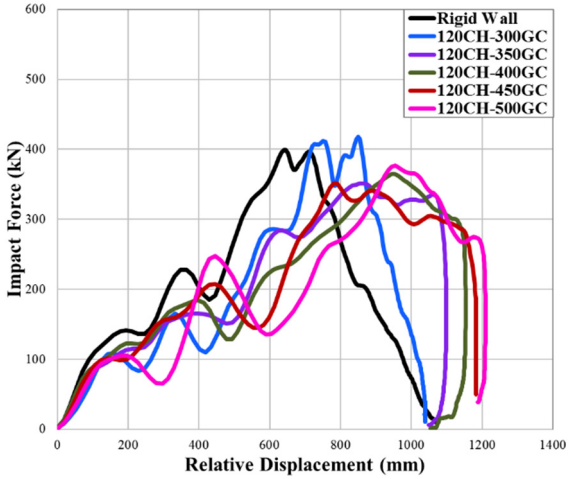

Figure 3-14 Taurus – 30% – 120CH

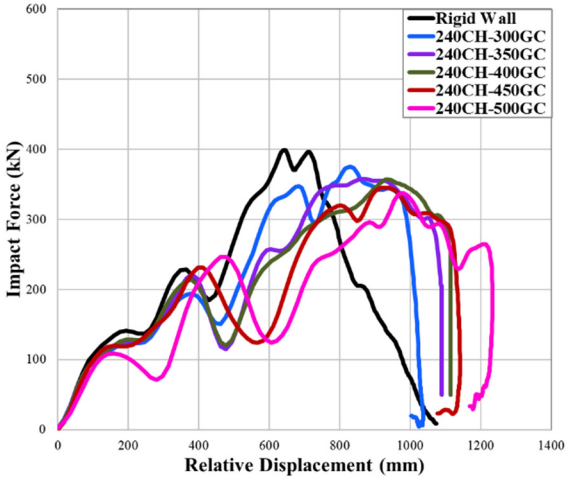

Figure 3-15 Taurus – 30% – 240CH

3.1.2.3 Results II – IIHS Intrusion Matrices – Toyota Yaris

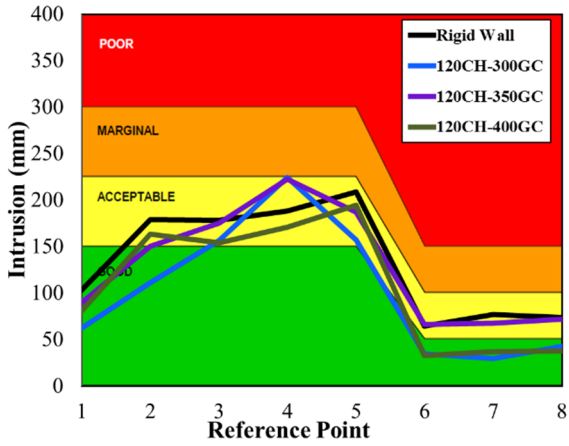

Figure 3-16 Yaris – 100% – 120CH

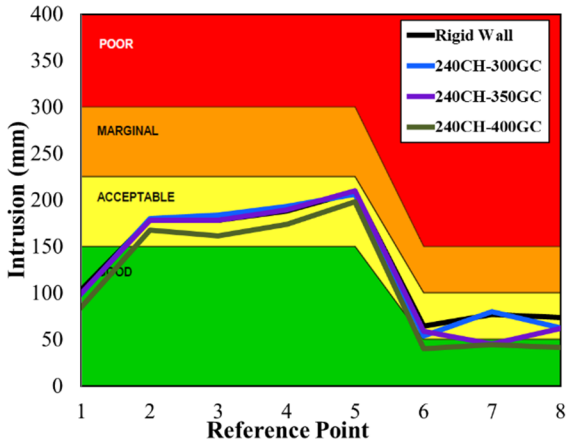

Figure 3-17 Yaris – 100% - 240CH

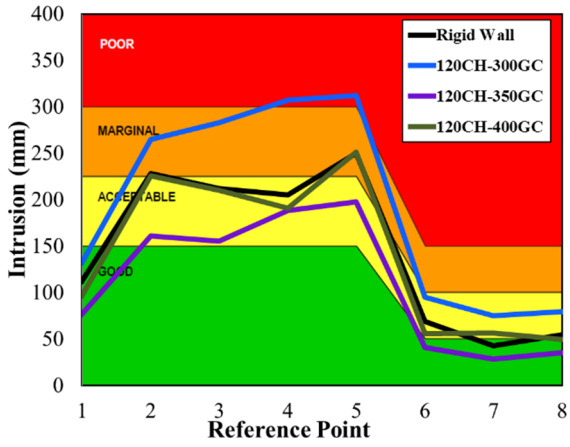

Figure 3-18 Yaris – 50% – 120CH

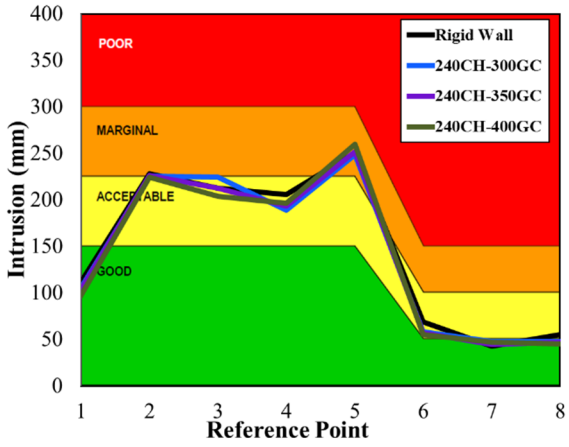

Figure 3-19 Yaris – 50% – 240CH

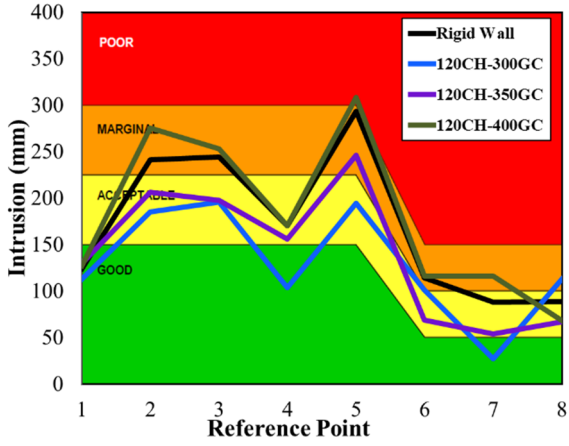

Figure 3-20 Yaris – 30% – 120CH

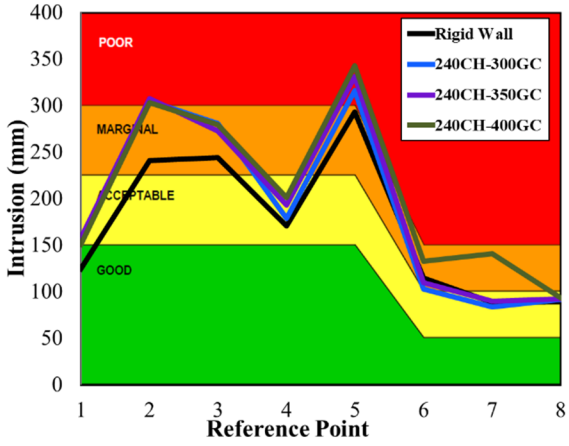

Figure 3-21 Yaris – 30% – 240CH

3.1.2.4 Results II – IIHS Intrusion Matrices – Ford Taurus

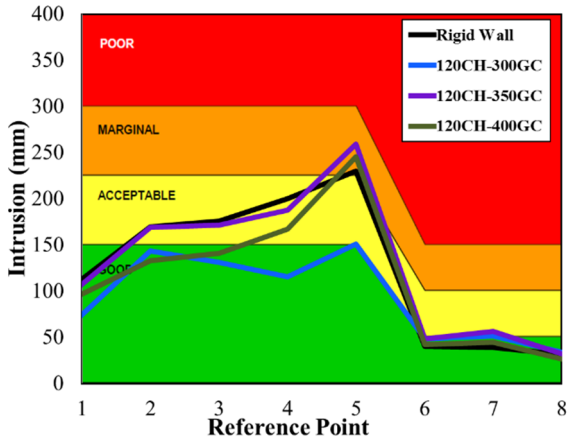

Figure 3-22 Taurus – 100% – 120CH

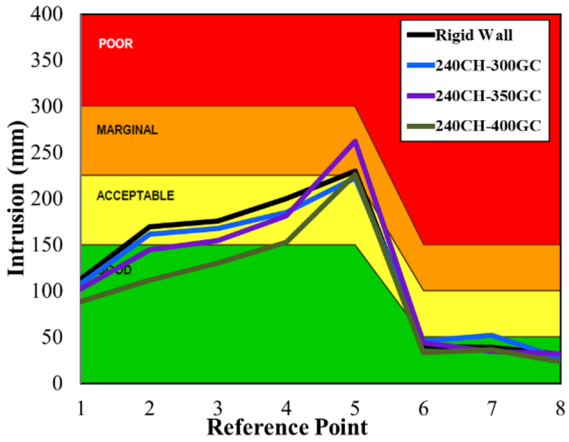

Figure 3-23 Taurus – 100% – 240CH

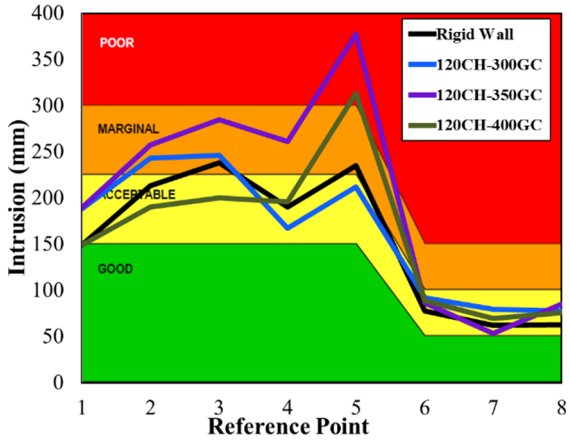

Figure 3-24 Taurus – 50% – 120CH

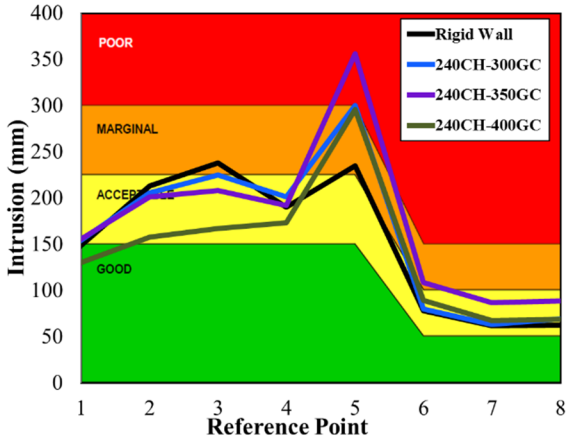

Figure 3-25 Taurus – 50% – 240CH

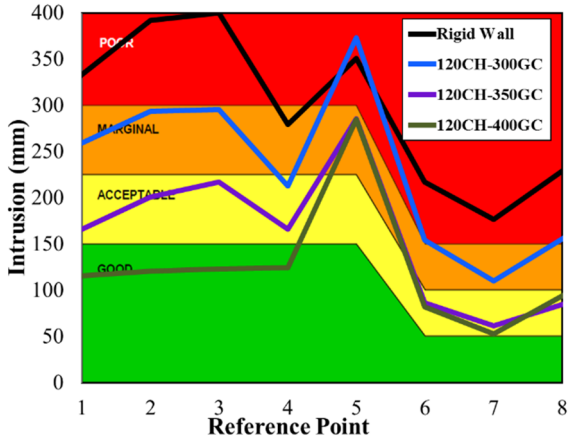

Figure 3-26 Taurus – 30% – 120CH

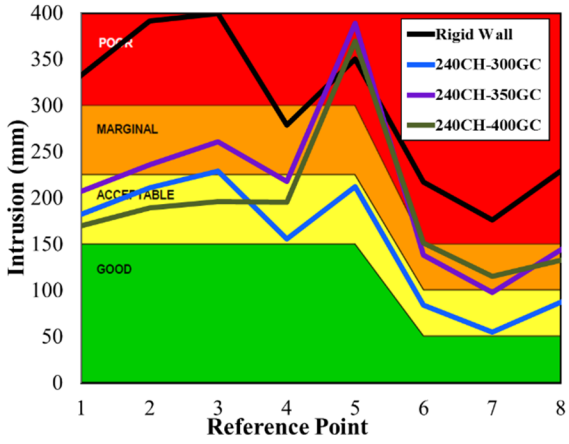

Figure 3-27 Taurus – 30% – 240CH

3.1.2.5 Results III – Impact Force Contour – Toyota Yaris

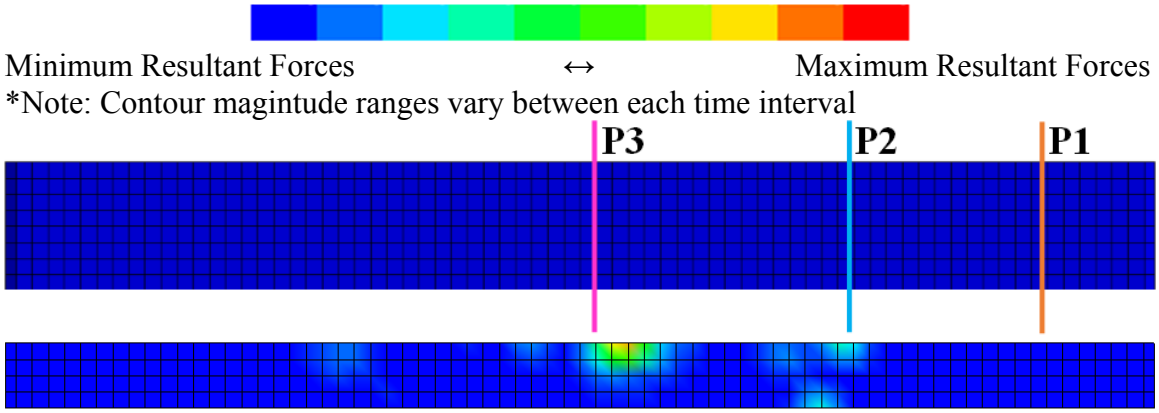

(a) Relative Displacement 425mm – Max impact force

(b) 600mm – second peak impact force

Figure 3-28 100% Overlap for 120mm Height at 350mm Ground Clearance

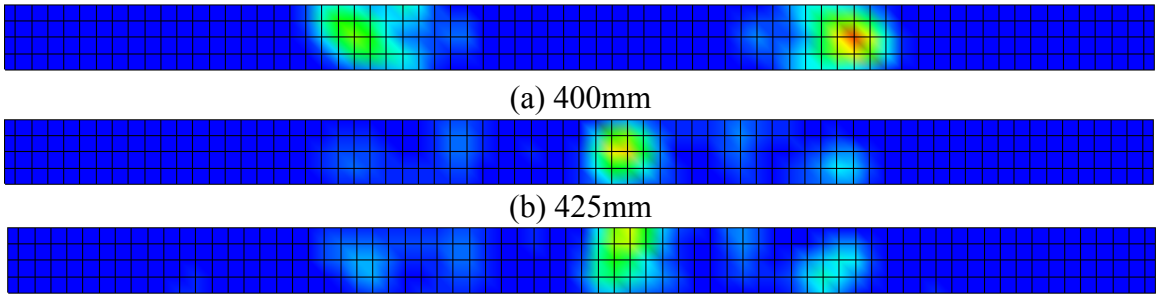

(a) 400mm

(b) 425mm

(c) 560mm

Figure 3-29 100% Overlap for 120mm Height at 400mm Ground Clearance

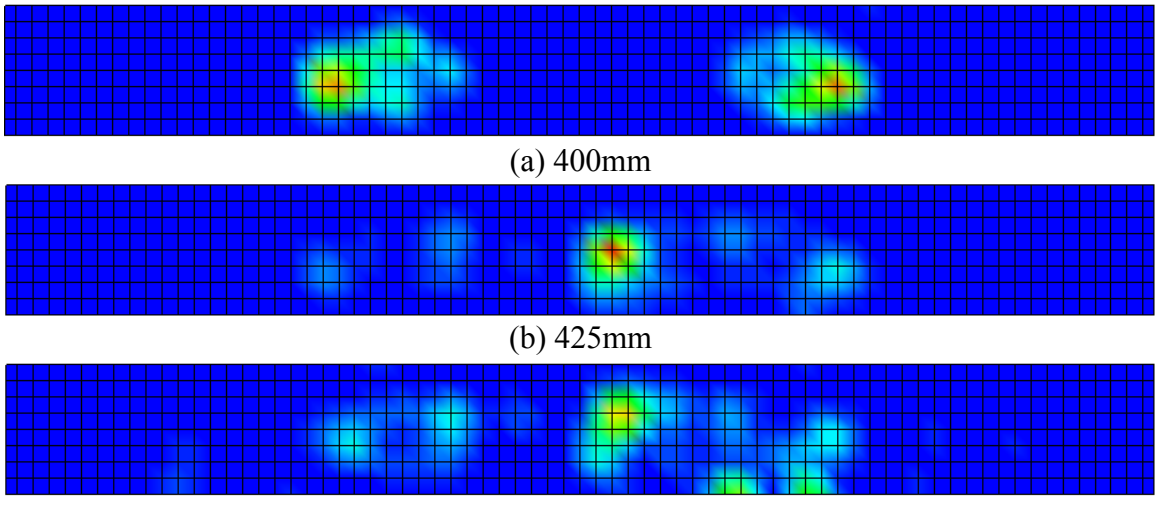

(a) 400mm

(b) 425mm

(c) 560mm

Figure 3-30 100% Overlap for 240mm Height at 350mm Ground Clearance

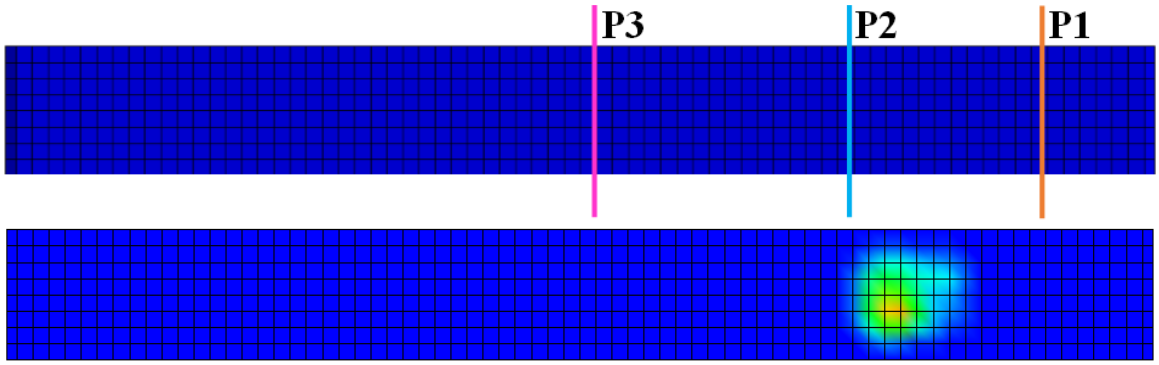

(a) 400mm

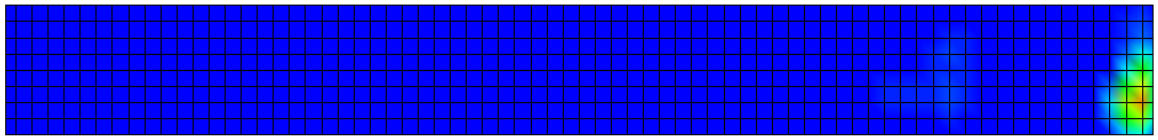

(b) 425mm

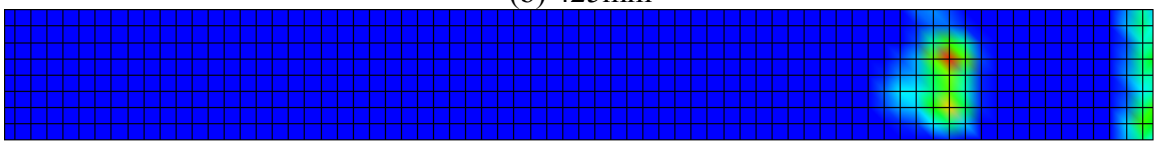

(c) 580mm

Figure 3-31 50% Overlap for 240mm Height at 350mm Ground Clearance

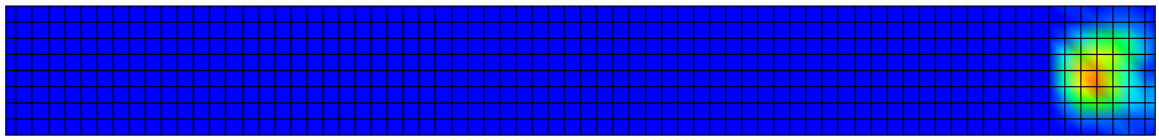

(a) 425mm

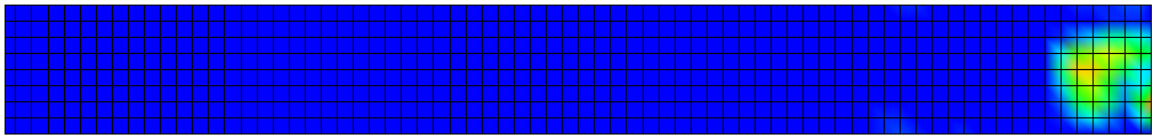

(b) 625mm

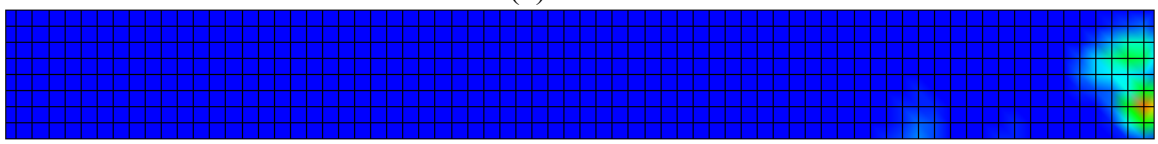

(c) 850mm

Figure 3-32 30% Overlap for 240mm Height at 350mm Ground Clearance

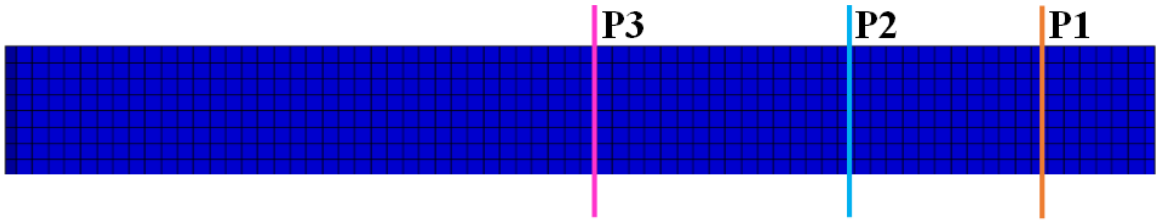

(a) 400mm

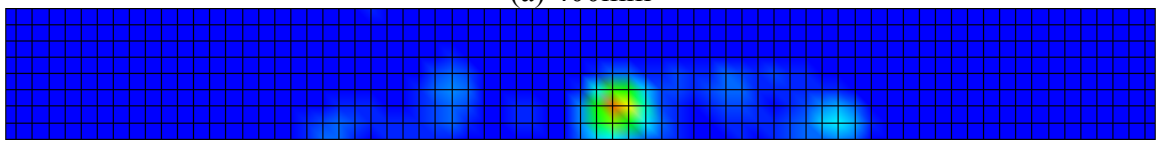

(b) 425mm

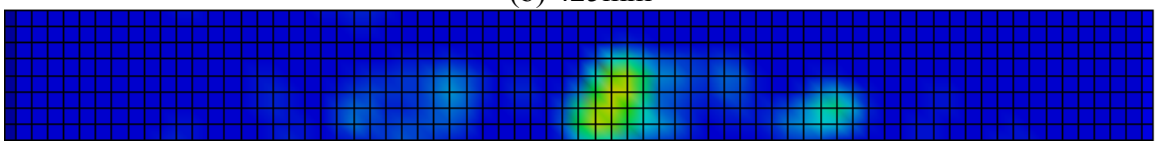

(c) 560mm

Figure 3-33 100% Overlap for 240mm Height at 400mm Ground Clearance

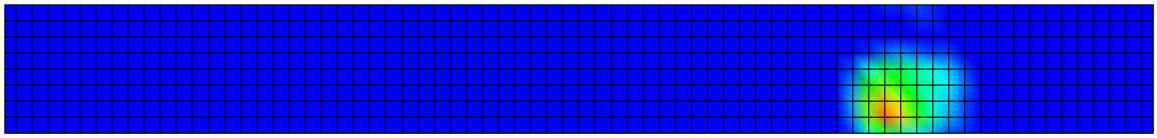

(a) 400mm

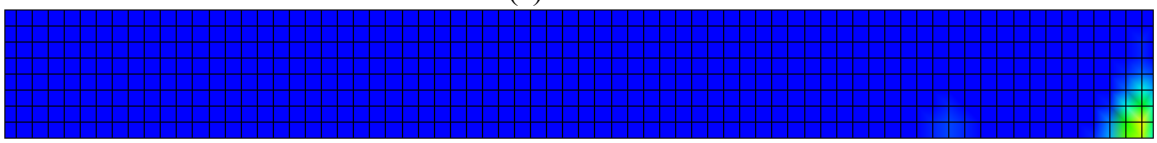

(b) 425mm

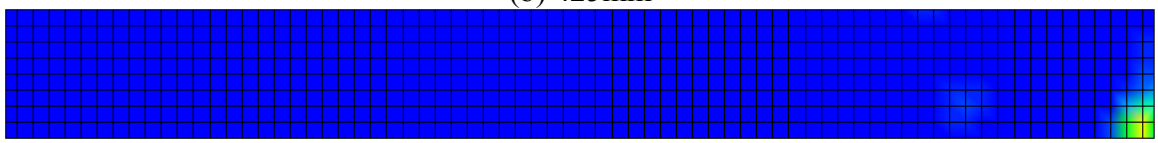

(c) 580mm

Figure 3-34 50% Overlap for 240mm Height at 400mm Ground Clearance

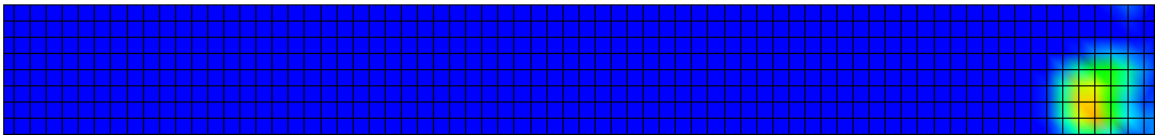

(a) 425mm

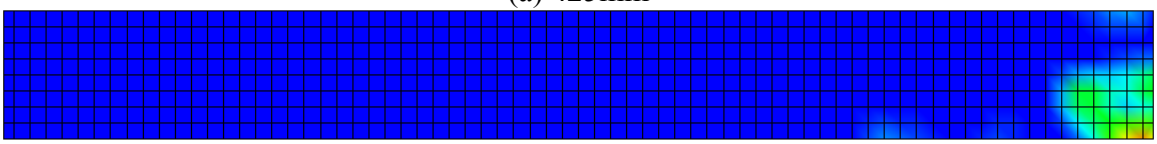

(b) 625mm

Figure 3-35 30% Overlap for 240mm Height at 400mm Ground Clearance

3.1.2.6 Results III – Impact Force Contour – Ford Taurus

All Contours can be found in the appendix as only the critical contour's discussed are presented here.

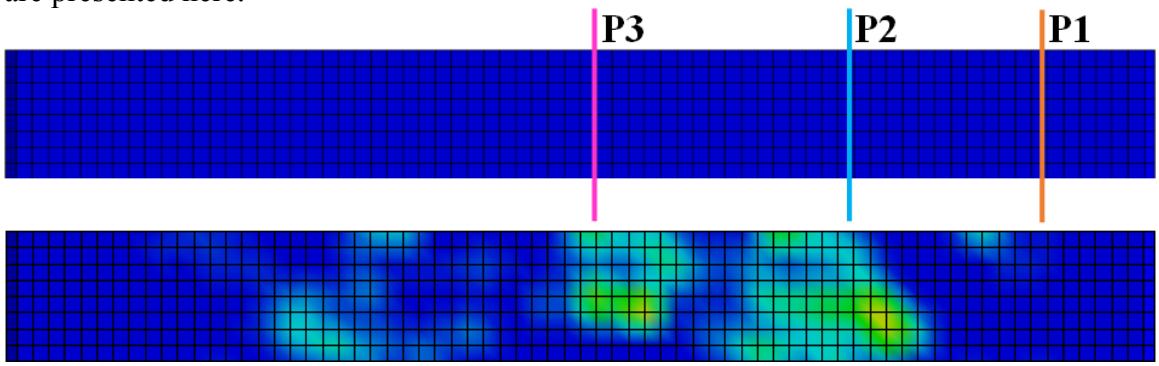

(a) 610mm

Figure 3-36 100% Overlap for 240mm Height at 350mm Ground Clearance

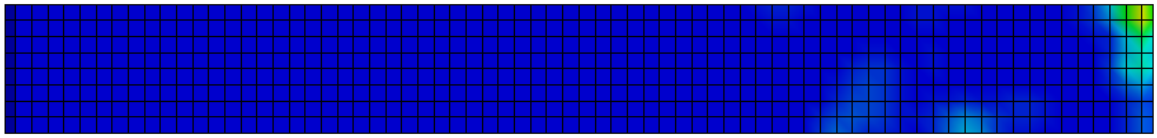

(a) 650mm

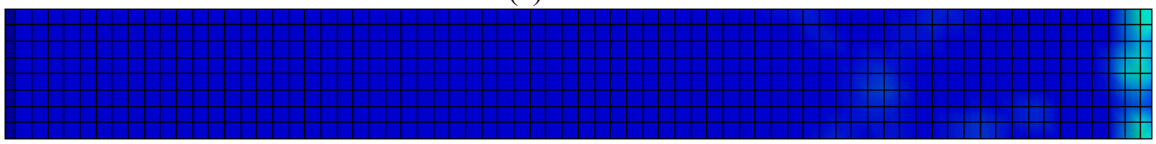

(b) 800mm

Figure 3-37 50% Overlap for 240mm Height at 350mm Ground Clearance

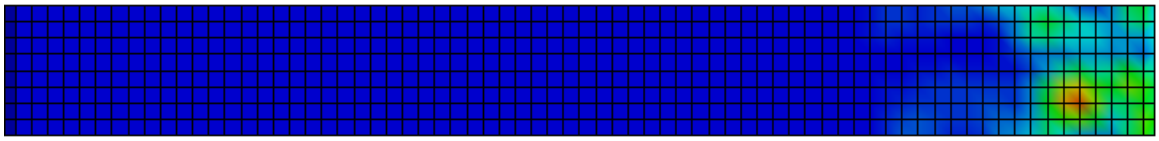

(a) 800mm

Figure 3-38 30% Overlap for 240mm Height at 350mm Ground Clearance

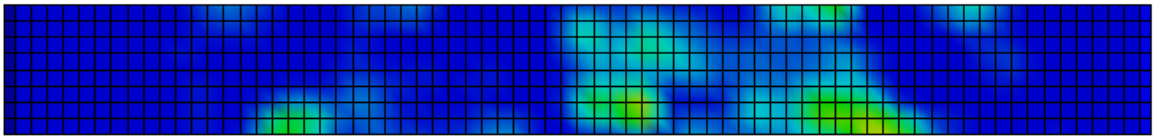

(a) 610mm

Figure 3-39 100% Overlap for 240mm Height at 400mm Ground Clearance

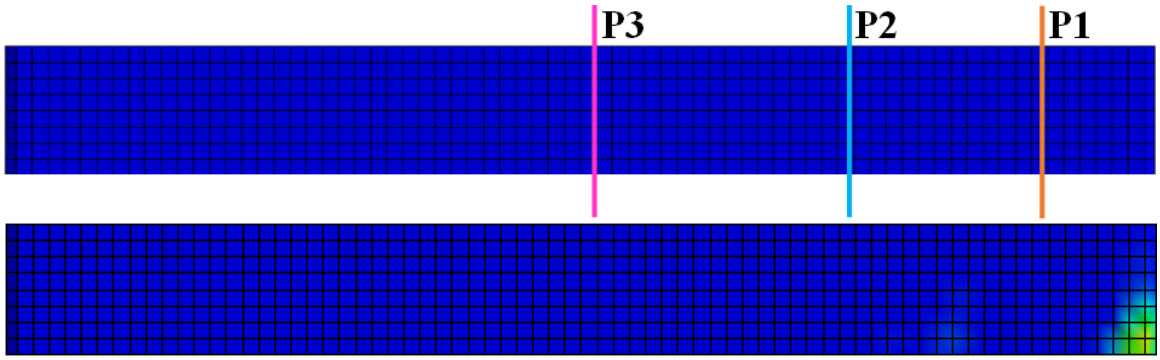

(a) 650mm

(b) 800mm

Figure 3-40 50% Overlap for 240mm Height at 400mm Ground Clearance

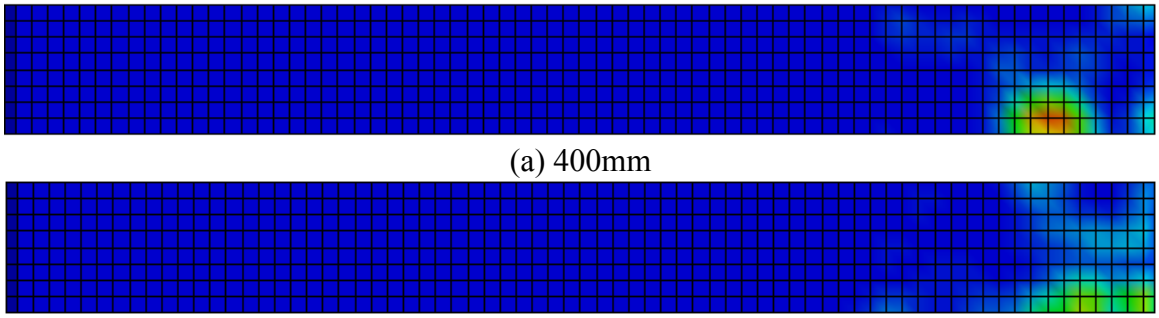

(a) 400mm

(b) 900mm

Figure 3-41 30% Overlap for 240mm Height at 400mm Ground Clearance

3.2 GROUND CLEARANCE AND CROSS SECTION HEIGHT

The experiment evaluated the ground clearance and contact section height utilized both Toyota Yaris and the Ford Taurus. Compatibility profiles, IIHS intrusion metrics, and impact force contours were presented between Figure 3-4 and Figure 3-41. For the vehicle impact visuals, the vehicles are colored blue, the chassis structural member of the vehicle is colored green, and the rigid bar is red.

First conclusions from the data determines that the ground clearance of 500mm will result in underride of both passenger vehicles and is recommended to not be used for the FUPD. This definitive conclusion is illustrated in Figure 3-42 as the green chassis wedges underneath the rigid bar.

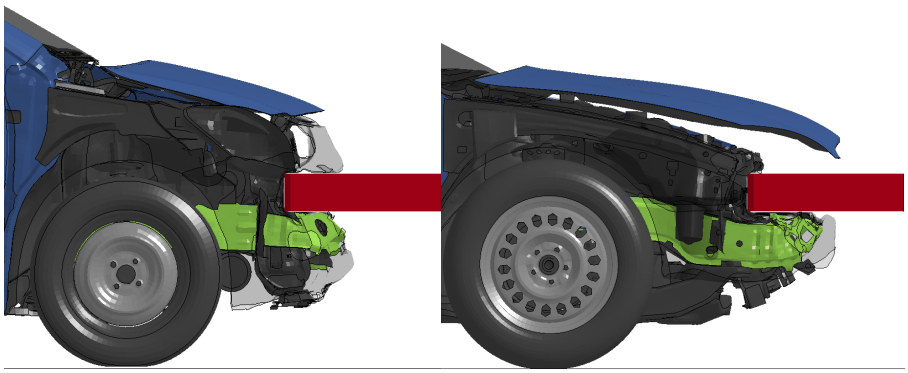

(a) Toyota Yaris (b) Ford Taurus

Figure 3-42 120mm Cross Section Height – 500mm Ground Clearance

For 100% overlap and 120mm cross section height; The first to note is that a the 120mm cross section height with any ground clearance below 350mm is not recommended as both vehicles override the rigid bar, Figure 3-43. A 300mm ground clearance allowed the Toyota Yaris to override the rigid bar causing little deformation into the vehicle without any compatibility between the rigid bar and front structural members, seen in the compatibility profiles. This ineffectiveness can be seen with the Ford Taurus as well. The tyres of the vehicles were the only effective energy absorber. This ineffectiveness will result in a poor design of the FUPD as its desired to ensure there is compatibility between structural members.

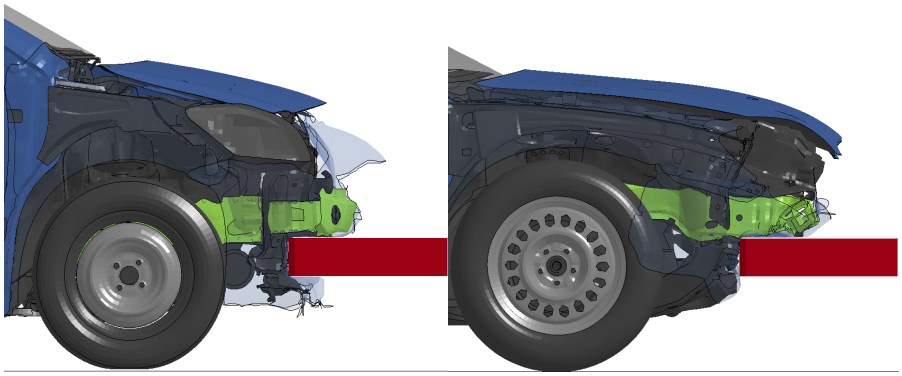

(a) Toyota Yaris (b) Ford Taurus

Figure 3-43 120mm Cross Section Height – 300mm Ground Clearance

The 450mm ground clearance, as regulated by India as the minimum ground clearance, also resulted in allowing an unfavorable amount of relative displacement for both impacting vehicles and cross section heights. The 450mm ground clearances proves to be too high to be create a ‘good’ compatibility with the Ford Taurus. 350mm and 400mm ground clearances concluded to be the most effective for a 120mm cross section with both

interacting similar to the rigid wall providing enough compatibility. The IIHS results were very similar for the Ford Taurus between 350mm and 400mm, however the 400mm ground clearance showed improved results in reference points 6 to 8. However, from Figure 3-43 it can show that both vehicles structural members (in green) start to slide above the rigid bar causing effective energy absorption of the members. This ineffectiveness can be seen as well in Figure 3-28 (a) and (b) as the peak impact forces are not fully contained. Figure 3-29, shows even with the increase of ground clearance height in which 'centers' the impact forces can cause issues when being impacted by passenger vehicles with higher ground clearance.

For 100% overlap and 240mm cross section height, the results show good enhancement over the 120mm cross section; first to note the IIHS values for both 350mm and 400mm ground clearances improve over the 120mm. The compatibility profile of the collision with the 240mm cross section also concluded with improved results for ground clearances for 300mm, 350mm, and 400mm. The 300mm and 350mm ground clearance compatibility were slightly better over the 400mm in the collision profiles for the Ford Taurus. However, the IIHS values for 400mm showed the more favorable results over other ground clearances at 100% overlap. From the visuals Figure 3-30 and Figure 3-44, the 350mm ground clearances provide a more 'centered' impact for both vehicles and containing the impact energy's compared to the 400mm ground clearance Figure 3-33 and Figure 3-45.

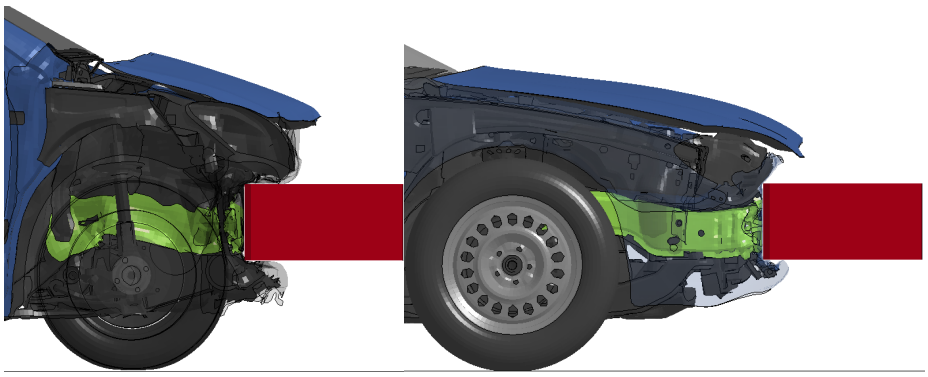

(a) Toyota Yaris (b) Ford Taurus

Figure 3-44 240mm Cross Section Height – 350mm Ground Clearance

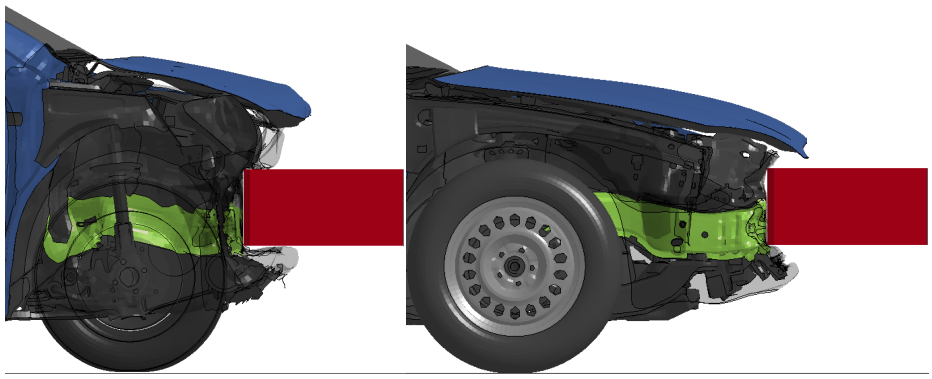

(a) Toyota Yaris (b) Ford Taurus

Figure 3-45 240mm Cross Section Height – 400mm Ground Clearance

The 50% overlap data presented similar trend of conclusions from the 100% overlap. For 50% overlap and 120mm cross section height; 300mm, 450mm, and 500mm ground clearance compatibility profiles present unfavourable results compared to 350mm and 450mm. For the Ford Taurus, 300mm ground clearance also showed little rebound as deformation continues to the end of the results. Conversely, the Toyota Yaris, the 400mm ground clearance stopped deformation before 350mm. Yet from the IIHS intrusion results, the 350mm ground clearance preformed the best for the Toyota Yaris compared to 400mm ground clearance slightly higher. The Ford Taurus, the critical reference points 6, 7, and 8 resulted almost exact values for all three ground clearances.

For 50% overlap and 240mm cross section height; For the Toyota Yaris the compatibility profiles were very similar results for 300mm, 350mm and 400mm. However, for the Ford Taurus, the 300mm preformed better than 350mm and 400mm ground clearances. Though, the IIHS intrusion values for the Ford Taurus presented the 400mm ground clearance more favourable. While the IIHS intrusion results for the Yaris were the very similar for all three ground clearances.

For the small overlap of 30% and 120mm cross section height; the ground clearance of 400mm resulted to stop the Toyota Yaris with the minimum deformation, while the 350mm ground clearance controlled the impact and stopped for the Ford Taurus. The 300mm ground clearance showed to continuously deform the Ford Taurus through the impact. From the IIHS results the 350mm showed a more desirable clearance as the critical reference points 6, 7, and 8 were more acceptable.

For 30% overlap and 240mm cross section height; the compatibility profiles for the Toyota Yaris were very similar for 300mm, 350mm, and 400mm. However, the IIHS values were very similar, except that the 400mm ground clearance was higher for reference points 6 and 7. For the Ford Taurus, the 300mm compatibility profile showed the least deformation. 350mm, and 400mm ground clearances also showed higher IIHS values compared to the 300mm ground clearance.

Strong conclusions can be stated for the geometric parameters of ground clearance and cross section height for the desired FUPD to induce effective compatibility by resembling a 'wall' to stop underride. Both Ford Taurus and Toyota Yaris were experimented with for each case, however the Toyota Yaris can be viewed to be more sensitive and important due to its lower ground clearance. The ground clearance of 350mm and 400mm resulted in 'good' compatibility collision profiles for both cross section heights when either vehicle impacted. The IIHS results also trended the same result for the recommendation of the FUPDs a minimum ground clearance height of between 350mm and 400mm. In addition, the cross section height should be minimally 240mm to ensure all impact forces are contained and transferred into the FUPD. It is also recommended that the 450mm ground clearance, as regulated by India, be reduced to ECE regulation of 400mm maximum ground clearance. These results agree with the previous study.

3.3 IMPACT FORCES & LOADING CONDITIONS

With the data and conclusions from the experiment of the Toyota Yaris impacting the rigid bar, conclusions of the localized impact forces can be drawn. Experiment cases of 240mm cross section height to the 350mm ground clearance height will be mainly focused on as it the cases covered most of the impact area. The Toyota Yaris compatibility profile for 240mm cross section height and 350mm ground clearance is seen in Figure 3-46. The compatibility profiles correlate with the visual contours.

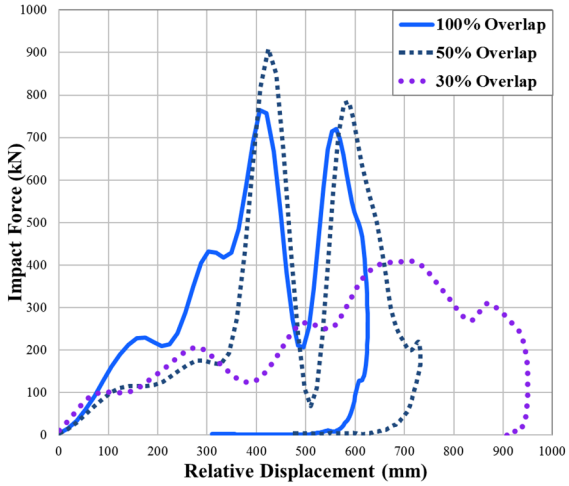

Figure 3-46 Toyota Yaris Impact to the Rigid Bar Compatibility Profile for 240mm Height at 350mm Ground Clearance

In Figure 3-30 for the 100% overlap shows the progression of the impact from (a) to (c). Figure 3-30 (a) depicts the impact forces at 400mm relative displacement, prior to the first impact peaks Figure 3-46. The impact forces are from the Toyota Yaris chassis structural rails in which centeralize around the locations of ECE P2. Both Left and right impact areas contribute to the total impact forces. As the rigid bar progress the intrustion, the force than translates to the center of the rigid bar due to the inertial impact from the engine. These forces centerize at P1 when the relative displacement reachs 425mm (first peak), seen in Figure 3-30 (b). The second impact peak at 550mm displacement can be seen in Figure 3-30 (c), it is the impact forces of the tyres and the engine. The Ford Taurus presents the same progression force impact, however the results from the contours are not as definitive as the the Toyota Yaris, Figure 3-36.

The 50% overlap shows a progression of impact forces in Figure 3-46**,** and visual contours in Figure 3-31(a) to (c). The Toyota Yaris's chassis rails induced the force onto the rigid bar at the location between P2 and P3, seen in Figure 3-31(a). The impact force than translates towards P3 and to the end of the rigid bar as the inertial forces of the engine are induced, Figure 3-31(b). The last illistrates the impact of the wheel on to the rigid bar Figure 3-31(c). Compared to the 100% overlap, the impact force of the chassis rail induced the same area and relatively the same amount of force.

For the small overlap impact of 30%, Figure 3-46 and visual contours in Figure 3-32(a) to (c). For the overlap the relative displace shows the vehicle impacting and piviting around the edge of the rigid bar. Majority of the impact was absorbed by the tyre, primarly after the 650mm relative displacement mark, producing a large impact pressure area.

Table 3-1 Impact Pressure Comparison

Overlap Case	Figure	Relative Displacement (mm)	Peak Force (kN)	Area of Force (cm^2)	Impact Pressure (MPa)	Percentage Difference of Max Pressure
100%	Figure 3-30(a)	400	24	162	1.48	22%
	Figure 3-30(b)	425	50	171	2.92	44%
	Figure 3-30(c)	550	28	180	1.55	24%
50%	Figure 3-31(a)	400	20	297	0.67	10%
	Figure 3-31(b)	425	113	171	6.59 (max)	**100%**
	Figure 3-31(c)	580	74	144	6.30	96%
30%	Figure 3-32(a)	500	16	324	0.48	7%
	Figure 3-32(c)	700	35	261	1.34	20%

These impact contours were analyzed from the impact pressure at notable points in time from Figure 3-30 to Figure 3-32 and shown in Table 3-1. The worst case forces (max force) from the impact was applied to the area to result in impact pressure. The max impact pressure was then used to benchmark the rest of the of the results. For 100% overlap seen in Figure 3-30(a), the impact pressure only represents the right contour in the figure, which is developed by the left chassis rail (passenger side). The left rail produces the max impact pressure onto the rigid bar, and used to evaluate the overlap impact pressure. From Table 3-1, the impact pressure from the 50% overlap presents the max impact pressure which is influenced by the engines inertia impact, Figure 3-31(b). While the impact from the tyre presents slightly lower magnitude of impact in Figure 3-31(c). Compared to the impact of 100% overlap, the 50% overlap impacted the rigid beam by a magnitude of 2.3 times. Figure 3-30(b), presents the impact at ECE R93 P3 location (center point of the FUPD). From the impact pressure, it is a magnitude of 2 times higher than most impacts at P2. Conclusively, the great impact pressures are found between P2 and P3 or the edge of the rigid bar at magnitudes equal to or greater than any at 100% overlap.

These results correlate with the 1999 publication stating that the impact forces and deceleration levels are approximately 2.5 times higher [66]. The 2010 Toyota Yaris's frontal structural stiffness would cause higher impact pressure/force onto the contact at overlap cases. The effects of the higher impacts can be also seen in the intrusion values as the 50% and 30% overlaps (Figure 3-19 and Figure 3-21) increase in magnitude over the 100% overlap. These conclusions relate back to the necessary FUPD structural stiffness in which needs to be created to insure the impact does not cause failure and underride. The ECE R93 deemed that the overlap point load P1 be 80kN. Through from the impact pressure shown in overlaps, that magnitude should be at least twice as much to 160kN to insure the necessary stiffness strength. ECE R93 P1 should also be considered to be increased as the area is induced by a high impact pressure in a 100% overlap.

Conclusively, the structural stiffness of the FUPD should be designed with strength for all overlap conditions. To ensure the FUPD structural stiffness is compactable with the impacting forces, P1 is recommended to be increased at or above 160kN.

3.4 VIRTUAL EXPERIMENT II – VERIFYING RESULTS ON A DEFORMABLE FUPD

The rigid bar provides an ideal 'wall' experiment to observe the desired geometry parameters, and localization of contact forces. However, the energy management of the impact may reflect differently when a deformable FUPD is impacted by a passenger vehicle compared to the rigid bar. Experiment II investigated the impact forces and energy management from a deformable FUPDs to solidify modifications to ECE R93. The geometry recommendations of 350mm ground clearance and 240mm cross section area are designed with the dsFUPD F9. The F9 was also optimized using the modified ECE R93 with all point load magnitudes at 160kN.

3.4.1 Virtual Experiment II – Setup

The dsFUPD F9, made with a single high strength steel, was mounted on the component level VNL model and experiment on with the ideals of tier III, dynamic testing.

Both Toyota Yaris and Ford Taurus were set to impact the dsFUPD F9 at 64 km/hr at three overlaps (100%, 50% and 30%).

3.4.2 Virtual Experiment II – Results

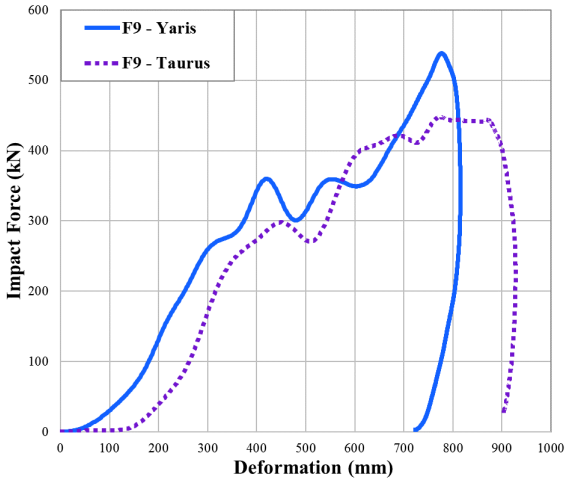

Figure 3-47 100% Overlap – F9

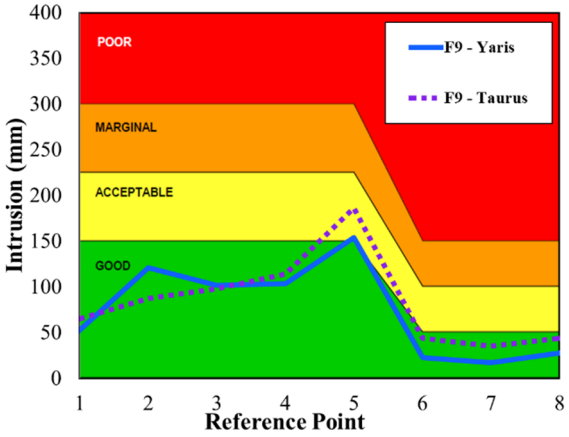

Figure 3-48 100% Overlap – F9 – IIHS

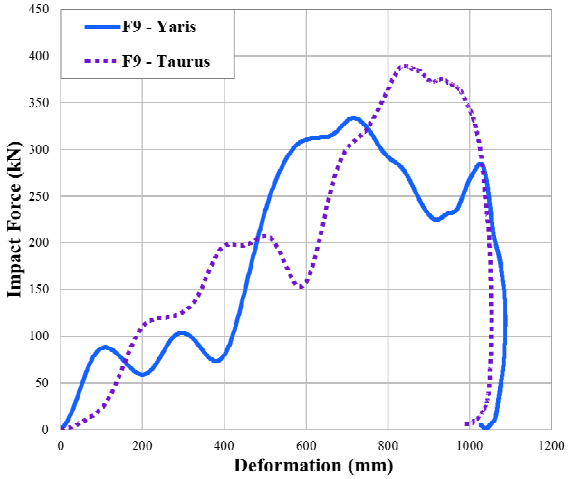

Figure 3-49 50% Overlap – F9

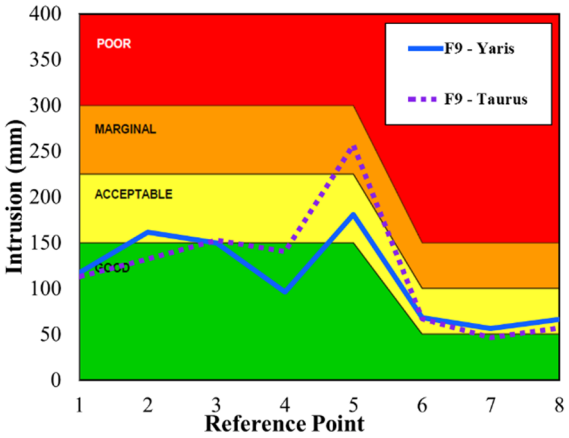

Figure 3-50 50% Overlap – F9 – IIHS

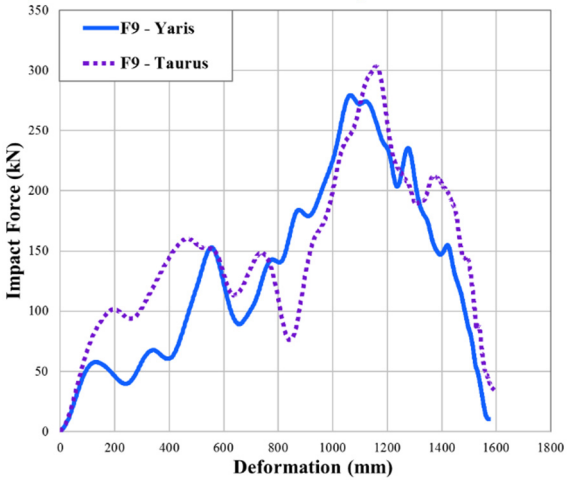

Figure 3-51 30% Overlap - F9

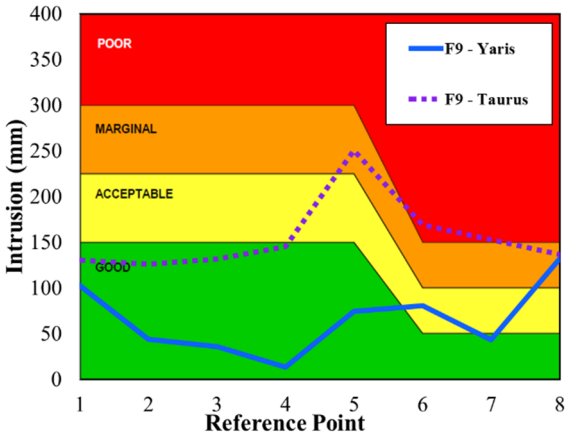

Figure 3-52 30% Overlap – F9 – IIHS

3.4.2.1 Results III – Impact Force Contour – Toyota Yaris

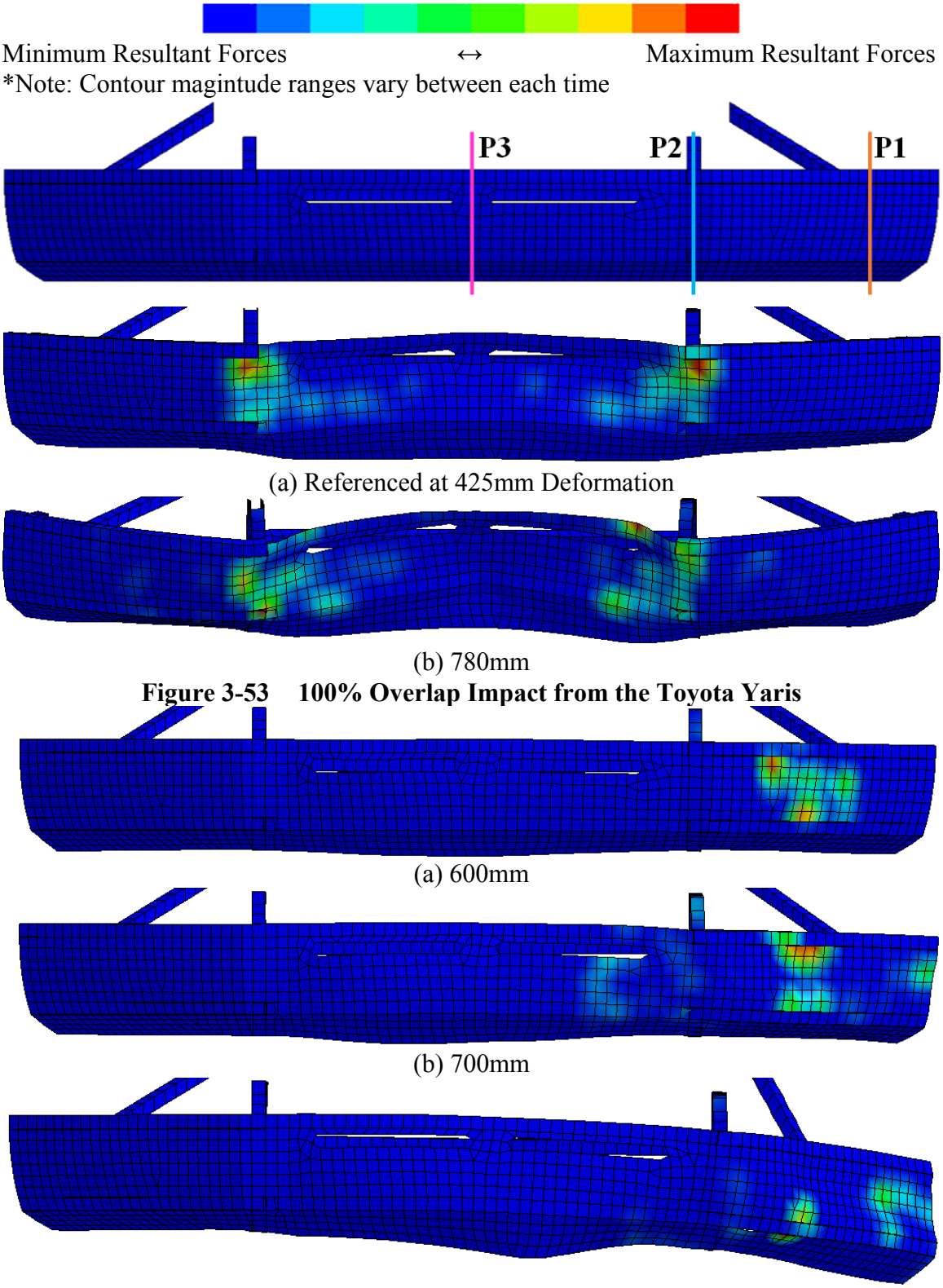

(a) Referenced at 425mm Deformation

(b) 780mm

Figure 3-53 100% Overlap Impact from the Toyota Yaris

(a) 600mm

(b) 700mm

(c) 1050mm

Figure 3-54 50% Overlap Impact from the Toyota Yaris

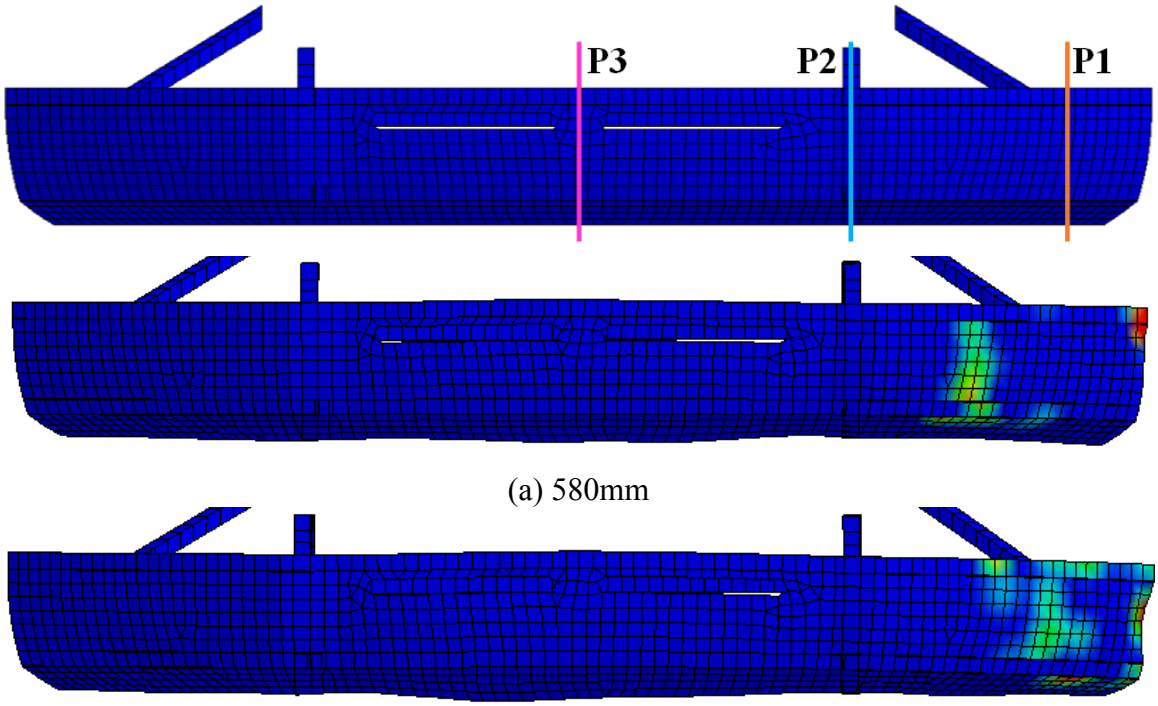

(a) 580mm

(b) 1100mm

Figure 3-55 30% Overlap Impact from the Toyota Yaris

3.4.3 Virtual Experiment II – Conclusions

The 100% overlap, the F9 FUPD model preformed ideally by preventing underride while resulting with low compartment intrusion magnitudes (Figure 3-48). The energy up to the max impact force was absorbed by the structural members of the passenger vehicle and the FUPD, seen in Figure 3-47. The final amount of impact energy absorbed by the contact between the tyre and the FUPDs. By design, the main areas of contact energy absorption of the impact pressures are localized the ECE R93 P2 location, which holds for the full duration of the impact. A majority of the energy was absorbed into the radiator of the tractor.

The 50% overlap was the point of main concern, when comparing the localization of impact forces. The peak forces were applied between P2 and P1, though closer to P1 as seen in Figure 3-54(a). The locations of the impact force areas were constant through the impact duration, with the addition of forces applying to the edge of the FUPD, Figure 3-54(b) and (c).

From the 50% overlap conclusions, the same trend of impact pressure locations was found for the 30% overlap Figure 3-55 (a) and (b). The peak forces were applied to the edge of the FUPD.

In conclusion, the impact pressure locations prove to be heavily applied to the P2 location in the 100% overlap. For overlaps less than 50%, the ECE R93 P1 location resulted in being critical in withstanding the impact forces. The structural stiffness of the FUPD should be constant across the full width. That is, if the P2 location would be defined by an impact stiffness of 160kN (100% tractor weight), then the overlap location P1 should be also defined with the same or more stiffness withstanding 160kN instead of 80kN (50% tractor weight). This recommendation would aid greatly in the prevention of underride for overlap cases.

3.5 CHAPTER SUMMARY

Within this chapter, the design methodology tier I - design space restrictions were implemented to verify the geometric parameters of the front underride protection device to ensure 'good' compatibility with a passenger vehicle. Experiments utilized two passenger vehicles impacting a rigid bar with varying parameters with closing speeds of 64 km/hr at three overlaps. Compatibility profiles of the impact and IIHS occupant compartment intrusion metrics aided in the conclusions. The results verify recommendations that the FUPD should have a ground clearance of 350-400mm. Any ground clearance of above 400mm can result in underride from the passenger vehicle's structure members, while a ground clearance less than 300mm can induce override of the passenger vehicle. It is also recommended that the cross section height of the FUPD should be no less than 240mm.

In addition to the chapter, the experiments yielded the visual localization of impact forces to correlate and conclude on ECE R93 regulation loading conditions. ECE R93 loading conditions suggest for a direct head-on impact by regulating the FUPD to be constructed with a higher stiffness towards at the center of the tractor (P2) with a magnitude of 160kN (100% of the tractor weight). While regulating a lower stiffness on the outer side of the FUPD 80kN (P1 - 50% weight). However, it was concluded higher impacts at

overlap conditions (less than 50% overlap) as the structural energy absorption of the passenger vehicle was lower. Therefore, the FUPD would need a higher structural stiffness. It was recommended that the ECE R93 P1 be increased to 160kN or more. These conclusions were applied to a deformable FUPD (model F9) to verify results.

CHAPTER 4
DESIGN OPTIMIZATION METHODOLOGY & CRASHWORTHY MATERIALS

The introduction of a front underride protection device may cause the front axle weight to approach or exceed the maximum allowable weight, which is a critical problem to allowing the tractor on the roads. Therefore, the lightest possible design may be more favourable, but with lightweight material the costs are expected to increase greatly. In addition, light weight materials may need more design area than heavier materials to be able to manage the impact forces. However, all of these affect the over all cost of the FUPDs and the balance of insuring the cost is effective. It is a complex problem in which the designer needs to balance. Optimization methods for the structural design are an important tool to obtaining an desired design to meet desired targets. The importance only escalates more when complex designs contribute to industrial design targets and needs for crashworthy, light weight, and cost effective products. This complexity was optimized through a Multiobjective Optimization approach.

Within this work, there was a need to further exploration into alternative optimization methods and approach for design. Previous approaches to optimization only minimized for FUPD deformations and mass with varying member thicknesses [5]. The main focus of this work was to investigate improvements in the optimization function by including material cost as an objective in the optimization function with various materials. This was to meet industrial requirements for reducing costs, system mass, and improve crash worthiness. The other focus was to evaluate an effective method to approach heuristic optimization of FUPDs to effectively result in optimal designs. In addition, there was a need to determine various sets of materials that would be ideal for FUPDs to insure effective structural crash stiffness for developing the lightest designs. Within this chapter, a design optimization methodology is set fourth.

4.1 DESIGN OPTIMIZATION METHODOLOGY

The work utilizes Livermore's LS-OPT for the heuristic optimization methods of the FUPD's design. Limited to LS OPT optimization algorithms, two strategies were used:

a) Direct simulation optimization using a Pareto optimal frontier.

b) Metamodel-based optimization.

Direct simulation optimization allows for the use of Genetic Algorithms (GA), NSGA-II and SPEA-II. Metamodel-based optimization allows for Genetic Algorithm NSGA-II and Adaptive Simulated Annealing (ASA) optimization algorithms. Metamodel algorithms also have hybrid forms with the use of leapfrog optimization. Within the metamodel-based optimization three metamodel sampling techniques was be observed to view the preferred optimization method. A modified ECE R93 quasistatic loading testing method in the LS–DYNA environment was utilized in the optimization process for its computational speed and accurate results.

Proposed designs were tested using a dynamic experiment method by colliding two different vehicle types in three collision scenarios into a simplified Volvo VNL model with the attached FUPD F9 model. The performance of each design was evaluated through compatibility profiles and passenger vehicle compartment intrusion.

With increasing objective targets from industrial requirements, designers are forced to rely on sophisticated multi-objective metaheuristics methods. Multi-objective optimization reflects the trade-offs among objectives in a set of solutions since there is no true single optimal design with respects to all objectives, defined as a Pareto optimal solution. A Pareto optimal front is created when solutions that can no longer minimize one objective without worsening the result of another objective [46].

Within this research LS-OPT, a standalone design optimization and probabilistic analysis package, is used. LS-OPT has two optimization strategies available, which are direct optimization and metamodel optimization. Within these two branches there exist multiple algorithms that can be used, as shown in Figure 4-1.

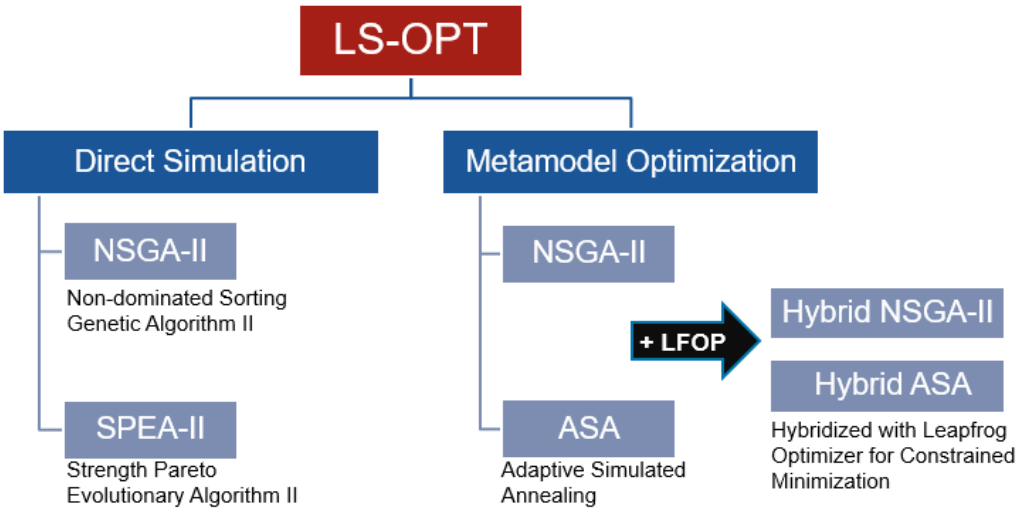

Figure 4-1 Optimization Selection Path

Optimization can explore a given problem in a global approach, where the fully range of the function is explored, or a local approach in which the optimization is limited to a set range or bound [46, 48]. Two main global metaheuristic optimization algorithm methods can be selected, Genetic algorithm and adaptive simulated annealing, as well as hybrid forms with an integrated local optimization algorithm method, Leapfrog Optimizer for Constrained Minimization (LFOPC). LS-OPT also provides different metamodel techniques for exploration to improve optimal solutions.

4.2 MULTIOBJECTIVE OPTIMIZATION APPROACH TO DEVELOPING FUPDs

The FUPD F9 design was utilized in this work to be enhanced through optimization. The original F9 design was optimized for material thickness and cross section for each member to reduce system mass and deformations. The design only utilized a single high strength steel. While the use of various materials remained unexplored [5]. It was also necessary at this point in the work to enhance on the industrial objective targets of the feasibility of the design cost when optimizing FUPDs.

LS-OPT allows for accessibility into optimization of model parameters, more specifically material and thickness parameters. Multi-objective optimization of these two

(2) types of parameters for minimizing system mass and deformation had been the focus thus far in the development of FUPDs. Though to improve on industrial targets, optimization for product cost and material selection becomes more critical to objectify. However, LS-OPT is not tooled to meet the needs of design cost analyses for optimization of the model. Nevertheless, this disconnect was solved by creating an application to allow an objective response, which deploys and scavenges data to allow for a response data point. Output data from LS-OPT operations is captured by the application and analyses of specific data to produce a response to LSOPT for the material cost of the model. The final product of the application outputs the material cost of the model via a simple equation for each part:

$$\sum \boldsymbol{Cost} * \boldsymbol{Mass} \qquad \textbf{4-1}$$

A set of ferrous and non-ferrous materials with a large range of yield strengths and costs was implemented into the current work's optimization variables to allow for each member. This will allow individual members to be optimized for material type and thickness. Material selection should be a more focused topic and the selection should be refined, but as the concept stands it was comprised of a large range of materials with yield strengths that vary from, 500MPa to 1.2GPa, as it was needed to review the performance of the optimization. Material costs per weight were applied in finding the material cost per part of the FUPD. Material cost did not include the manufacturing costs, and not within the scope of this work. However, the material costs are based on the cost of a produced sheet of material.

4.2.1 OPTIMIZATION TESTING ENVIRONMENT

LS-OPT executes a set of LS-DYNA solving environments with varying designs simulated with the modified ECE R93 testing environment. Each design must withstand the 160kN quasistatic loads, and was limited to less than 100mm of deformation to be passable as a design.

The testing environment simultaneously loads the protection device model with quasistatic loads in three locations to observe the resultant deformation, described in section 2.2.2. The advantage to the model is that it was computationally inexpensive to simulate compared to testing with full finite element vehicle models. Optimization as

complex as the FUPDs with full vehicle models would take months on the accessible hardware.

4.2.2 EXPERIMENT I – OPTIMIZATION APPORACH

The variables and objectives for the multi-objective optimization problem for FUPDs were progressively looked at within this work to analyze the progression, if any, on how the optimization function *f* can improve.

$$\boldsymbol{f(Variables) = \min(objectives)} \quad \textbf{4-2}$$

The first stage of the optimization exploration sought to improve and build on the optimization function. Each phase built off the previous phase to observed improvements.

Phase 1 only used material thickness variables for optimization using a constant expensive high yield strength material while objectively minimizing system mass and all three quasistatic point load displacement ($\Delta X_{P1,}\Delta X_{P2,}\Delta X_{P3}$). This method was utilized in the original development of the dsFUPD with published results. The previous published results will be the benchmark for the current work's designs. Described as Phase 1, equation 4-3 shows the optimization function problem.

Phase 1:

$$\boldsymbol{f(Thickness) = \min(\Delta X_{P1}, \Delta X_{P2}, \Delta X_{P3}, Mass)} \quad \textbf{4-3}$$

The second phase variance replaces the constant material with the set of materials as a variable, equation 4-4.

Phase 2:

$$\boldsymbol{f(Thickness, Material) = \min(\Delta X_{P1}, \Delta X_{P2}, \Delta X_{P3}, Mass)} \quad \textbf{4-4}$$

The third phase employment material cost as an objective with the various material types and thicknesses, while minimizing system mass and quasistatic point load deformation.

***Phase* 3**:

$$\boldsymbol{f(Thickness, Material) = \min(\Delta X_{P1}, \Delta X_{P2}, \Delta X_{P3}, Mass, Cost)} \quad \textbf{4-5}$$

The three phase exploration, equation 4-5, was implemented in direct optimization with NSGA-II and SPEA-II, and within metamodel optimization with GA (NSGA-II algorithm), ASA, and hybrid forms, HGA and HASA (seen in Figure 4-1). LS-OPT

parameter setup was chosen to conform to previous practices within the work and used defaulted parameters. All direct optimization experiments employed a practical approach with a population size of 30 with 100 generations/iterations. Metamodel implementation used RBF with a space filling point selection for 30 iterations and 30 simulation points per iteration. As the research progressed and optimal solutions raised, the work explored into different techniques and toolbox parameter changes. RBF Metamodel technique was primarily used, but FFN and Kriging were to be explored.

The optimal method for optimization needed to result with an accurate range of minimal solutions, i.e. strong Pareto front. Optimal design configurations are deemed feasible if the design passes the modified ECE R30 regulation, which then are able to prove its crash worthiness in dynamic testing, experiment II. The appropriate method for optimization should be computational effective and provide a relative number of feasible results. Designs should be within the range of a system mass of 30kg to 40kg and show minimal deformation at all points.

4.2.2.1 Virtual Experiment I – Results

The following displays the results from optimization which applies all three phases and optimization methods. CPU timing pre iteration for the optimization process, excludes FUPD model simulation, to compare the added processing time while using metamodeling techniques. 3D illustration into the feasible results of all 3 objectives from the phase 3 optimization problem, which also gives a visual view of how objective hierarchy issues can arise. Metamodeling results of all three phases are also displayed for HASA and HGA. Direct optimization results of NSGA-II are also illustrated to show differences in phases 2 and 3. The final portion of tabulations show the final optimal design points for each optimization method and phases with respect to minimizing material cost.

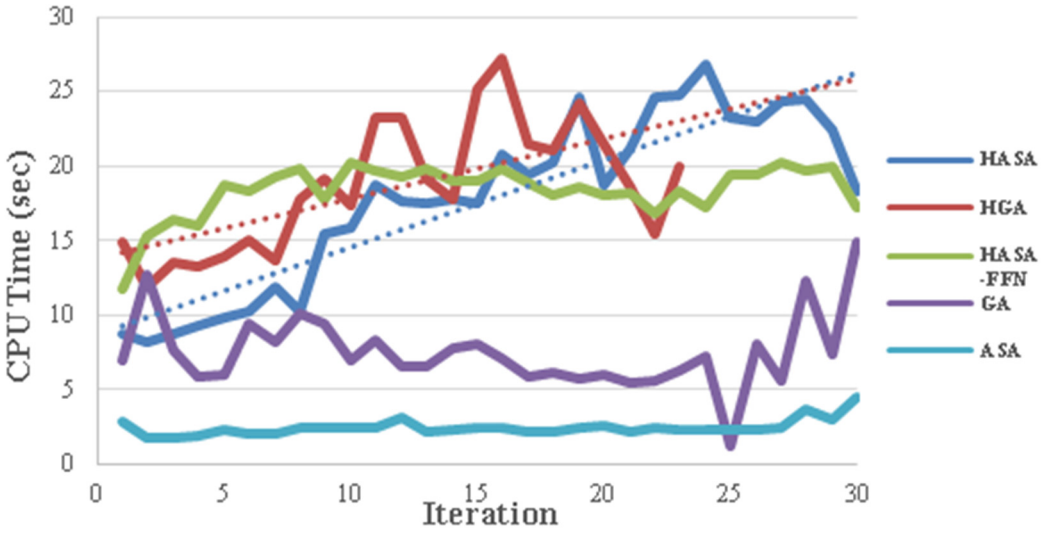

Figure 4-2 Computational Results of Phase 3 Optimization Solving CPU time.

Note this does not include LS DYNA model solve time, only the optimization re. The optimization section was executed on the same Intel 4 core computer.

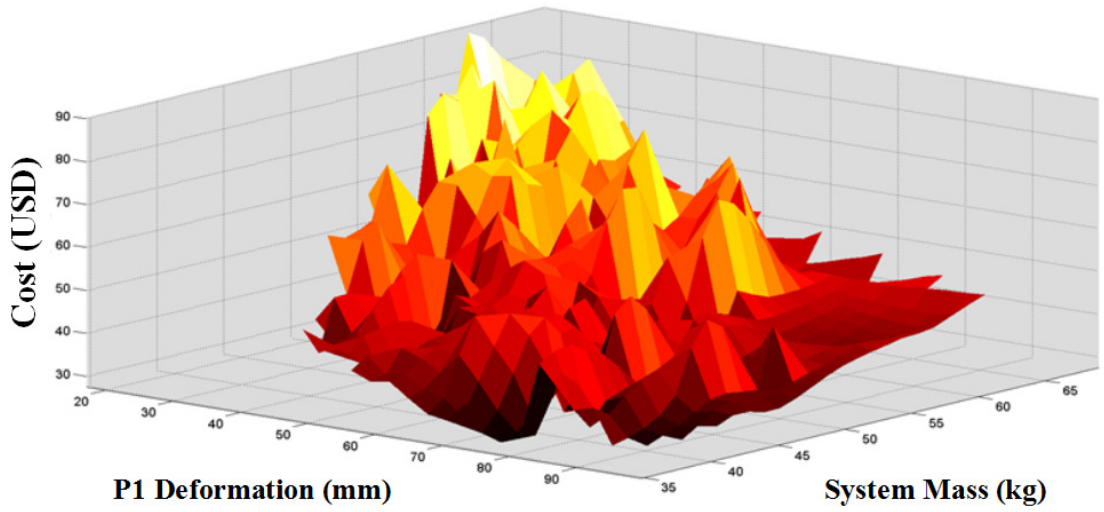

Figure 4-3 Feasible Results from Phase 3 NSGA-II

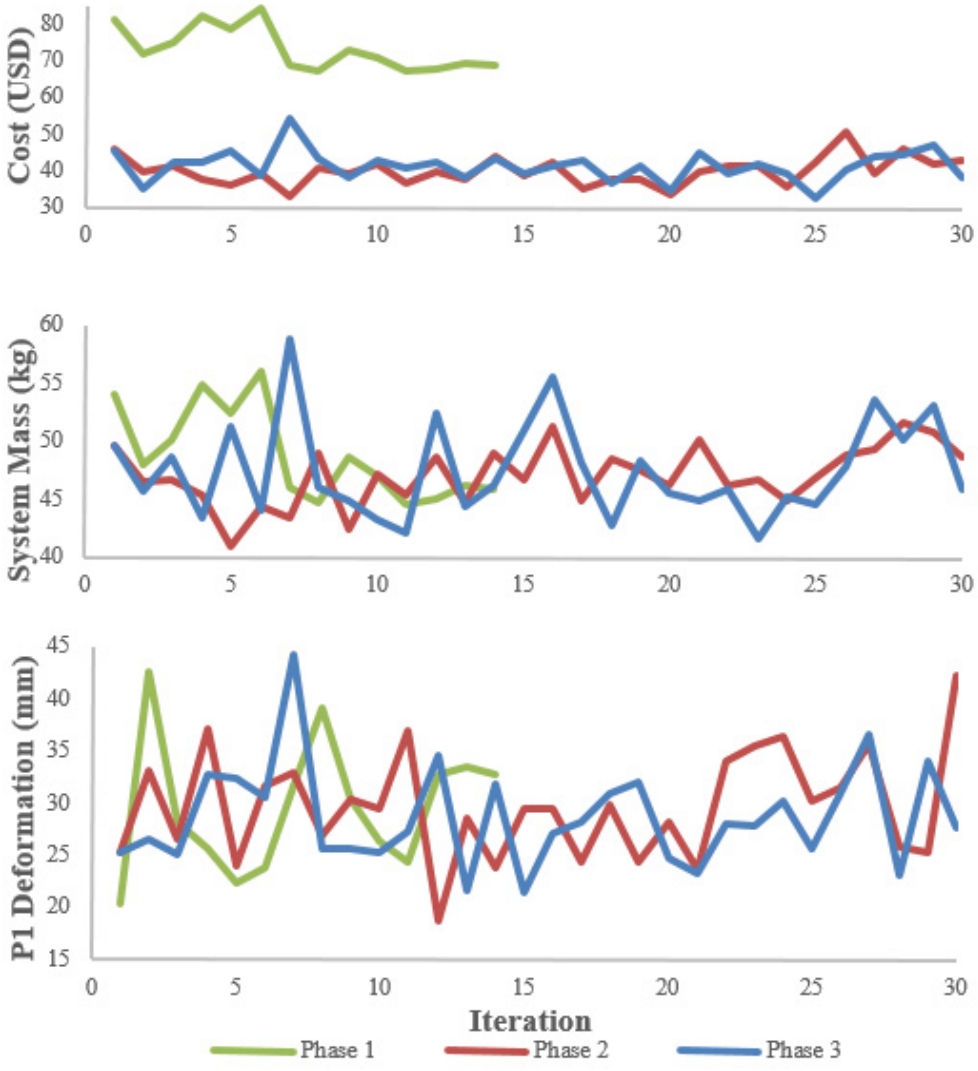

Figure 4-4 HASA Feasible Results Analysis of All Three Phases with Respect to Minimizing Each Objective per Iteration

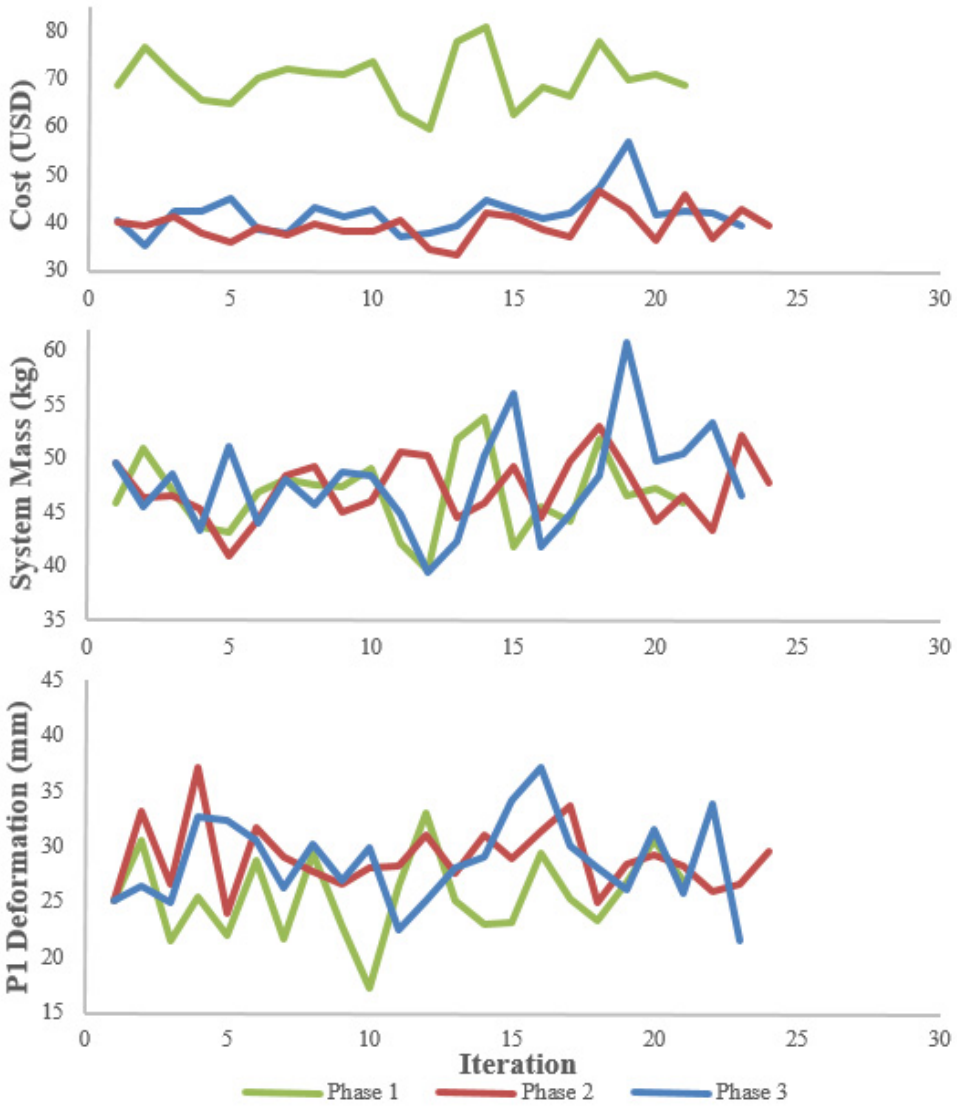

Figure 4-5 HGA Feasible Results Analysis of All Three Phases with Respect to Minimizing Each Objective per Iteration

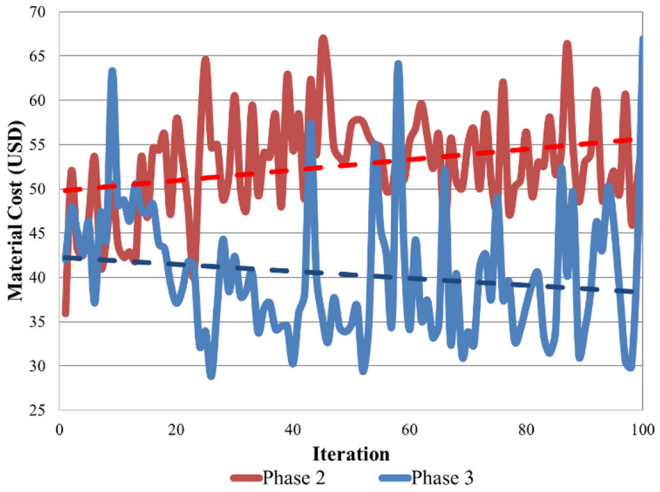

Figure 4-6 NSGA-II Feasible Results per Iteration with Respect to Material Cost Minimization

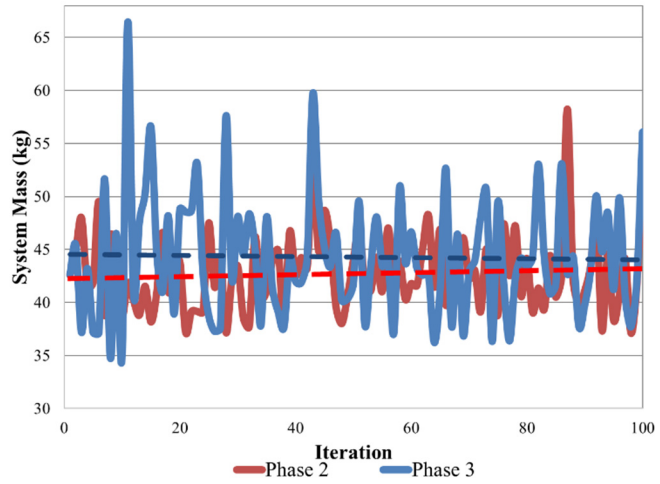

Figure 4-7 NSGA-II Feasible Results per Iteration with Respect to System Mass Minimization

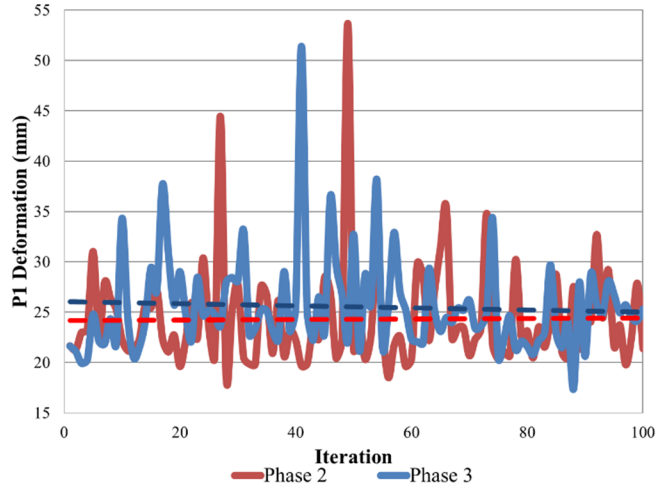

Figure 4-8 NSGA-II Feasible Results per Iteration with Respect to Displacement of Quasistatic Load P1 Minimization

Table 4-1 Resulting Feasible Optimized Designs with Respect to Minimal Cost

Optimization Algorithm		Mass (kg)	Cost (USD)	Quasistatic Load Displacement (mm)		
				P1	P2	P3
Original F9	Phase 1	41.76	66.82	27.00	8.22	43.17
HGA	Phase 2	45.63	35.31	96.46	17.79	97.08
	Optimal Point*	49.77	37.19	36.19	18.71	86.87
	Phase 3	44.94	33.51	51.06	83.00	96.22
HASA	Phase 2	44.54	32.66	87.26	2.91	95.71
	Phase 3	43.38	33.17	68.79	4.32	72.96
	Optimal Point*	46.95	34.59	40.76	18.37	89.50
SPEA	Phase 2	39.61	59.41	37.04	0.79	84.25
	Phase 3	42.88	29.55	92.73	0.86	86.99
NSGA	Phase 2	42.58	35.91	78.43	37.36	85.57
	Phase 3	37.25	28.82	88.35	11.94	99.11
	Optimal Point*	42.3	32.77	37.1	16.9	76.46

*Optimal point was taken with respect to all objectives

Table 4-2 Benchmark and Optimal Designs Used for Dynamic Testing

Optimization Algorithm		Mass (kg)	Cost (USD)	Quasistatic Load Displacement (mm)		
				P1	P2	P3
F9	Phase 1	41.76	66.82	27.00	8.22	43.17
F9-OPT	NSGA Phase 3	42.3	32.77	37.1	16.9	76.46
Difference		0.54	34.05 (50.96%)	10	8.68	56.46

4.2.2.2 Virtual Experiment I – Discussion & Conclusions

Both direct and metamodeling optimization proved to be viable options for multi-objective optimization in all 3 phases. Metamodeling methods were computational inexpensive processes that utilizes cost optimization, phase 3, to obtain small gains over just material optimization, phase 2 (Figure 4-4 and Figure 4-5). HGA and HASA both resulted in similar samples of optimal points, and higher percentage of feasible results over there non LFOPC hybrid forms, ASA and GA. HASA took 8452.0 CPU seconds after 30 iterations with 30.08% feasible points. Where HGA took 428.75 CPU seconds, on the same hardware, after 23 iterations with 34.72% of the points being feasible. However, when only

in need of just material thickness to minimize system mass and deformation (phase 1), HASA with RBF was the most suitable for the single variable line search. HASA with RBF completed within 14 iterations, 4 less than its base form ASA and 7 less than HGA, with similar results. Metamodeling techniques was explored with phase 3 optimization function in HASA and HGA, which showed comparable results. HASA with FFN or Kriging metamodeling techniques proved to take the full set of 30 iterations with no improvement to the results. The techniques only increased the optimization time. It should be noted that Kriging was not applied to Figure 4-2, as it resulted to be very computationally expensive. In total HASA-Kriging took 30 iterations in 1.04E+05 CPU seconds (5 CPU hours), compare to HASA 534.8 CPU seconds and HGA 428.85 CPU seconds.

An optimization problem arises as an increase in objectives are introduced into the optimization function. Objective hierarchy problems arise when observing the results for an ideal optimal design, as observed in Figure 4-3. The issue was how to sort feasible designs, which passed modified ECE R93, and filter out the ideal optimal designs. From a production point of view, cost would hold more importance over system mass, as a given range of 30-50kg is acceptable, but should be minimized. However, minimizing cost should not take importance over minimizing deformation from the quasistatic loadings, especially at P1, to not affect the crash worthiness of the device. Conclusively, observations of the results found ideal optimal designs by minimizing the material cost, having a relatively close system mass to 40kgs or less, while not sacrificing large increases of P1 deformation. Quasistatic point load P1 deformation ideally should be less than 50mm to ensure a more rigid overlap impact. Using this philosophy, the selection seen in Table 4-1 with phase 3 HASA obtained a better ideal design over phase 2 HGA. Phase 3 and 2 HASA found better and more ideal optimal results than HGA. Conclusively, HASA was more computational expensive than HGA, but HASA obtained more accurate and ideal design results and would be a more ideal method for metamodeling optimization.

The ideal optimal design philosophy was more important when analyzing direct optimization, where large amount and spread of data points was obtained at the cost of computational time. Phase 3 NSGA-II finished in 147150 CPU seconds, 57% slower compared to phase 3 HASA-RBF 8452.0 CPU seconds, on similar hardware. This was due

to direct optimization methods set to solving for 100 iterations, with no stopping conditions. Furthermore, for direct optimization the data needed to provide greater accuracy in minimizing the objectives over the longer iteration span to be computationally effective compared to metamodeling. Figure 4-6, Figure 4-7, and Figure 4-8 displays the effectiveness of minimizing primarily each objective for phase 2 and 3. For all three figures, the trends (dotted line) show a minimizing slope (decreasing trend) as the optimization progresses for phase 3 compared to the increasing trend of phase 2. Figure 4-6 shows great improvement optimizing for material cost of the device as an objective (phase 3) can result in over just phase 2. Phase 3 NSGA-II presented 7 ideal optimal designs below HASA design at an ideal optimal of $34.59. Phase 2 NSGA-II would not result in any ideal optimal designs below $40, with only 2 resulting feasible designs. SPEA-II did not have sufficient ideal designs below $40 as well for both phase 3 and 2. SPEA-II presented a greatly lesser value of feasible data point over 100 iterations compared to NSGA-II. Phase 2 SPEA-II had a feasible percentage of 20.76% and a phase 3 of 14.43% compared to phase 2 NSGA-II of 42.77% and phase 3 of 36.77% feasible data points. SPEA-II resulted with too large of a spread and not enough refined feasible results. Phase 3 NSGA-II proved to greatly minimize all three objectives while providing a good selection of feasible designs and a range of ideal designs. Direct optimization with NSGA-II resulted with 13.0% feasible results below $40 compared to 6.7% from metamodeling HASA. Though both proved to have the same percentage of ideal design results of 25% below $40 with NSGA-II with 26:97 ideal to feasible results, and HASA 3:12. Furthermore, NSGA-II provided an ideal optimal point, Table 4-1, 4.62kg lighter, $1.82 cheaper, and 3.66mm less deformation then phase 3 HASA's optimal design.

Conclusively, NSGA-II with material cost optimization (phase 3) provided the most ideal optimal results compared to the other methods. HASA should be used to explore the general limitations of the device with respect to material thickness of one material. It's suggested that phase 1 HASA-RBF to be used first to test if each separate material is viable to be used in the design, i.e. some materials below 500MPa yield strength showed poor crashworthy results when being implemented into the FUPD. Verifying material selection through optimization a single material will ensure that it is strong enough to support a collection of materials to optimize with. A good sum of feasible results should be obtained

within a computationally quick manner to ensure longer processes are effective. Once a collection of materials is obtained, general exploration can be executed with HASA-RBF.

Furthermore, the ideal optimal design should use the more accurate and effective approach to optimizing FUPD designs by using Direct simulation optimization with NSGA-II and material cost optimization (phase 3).

4.2.3 Virtual Experiment II – Dynamic Collision Testing

With the ideal optimized design, the crash worthiness of the device must be ensured through dynamic testing to be deemed an optimal design. For this section of Experiment II, the optimal design from Experiment I was taken and tested with the Toyota Yaris and Ford Taurus finite element models.

4.2.3.1 Virtual Experiment II – Setup

The crash worthiness of the ideal optimal design was then tested and compared to the original FUPD F9 design which was optimized using phase 1 HASA, both compared in Table 4-2. The FUPD F9 was mounted onto a simplified VNL frame and experimented with the passenger vehicle having a closing speed of 64km/hr. A robust approach to dynamic testing was taken to ensure quality of the design with the use of two vehicle models, the lighter and lower impact Toyota Yaris and the heavier Ford Taurus. Three overlap collision scenarios were tested; 100%, 50%, and 30%. Insurance Institute for Highway Safety occupant compartment intrusion analysis and compatibility profiles are used to conclude the collision performance.

4.2.3.2 Virtual Experiment II – Results

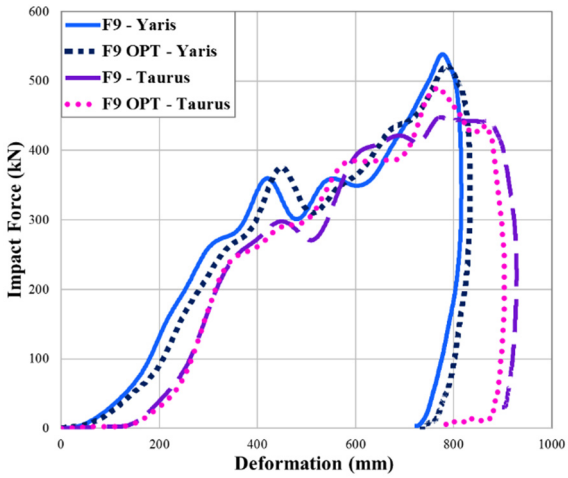

Figure 4-9 100% Overlap Profile

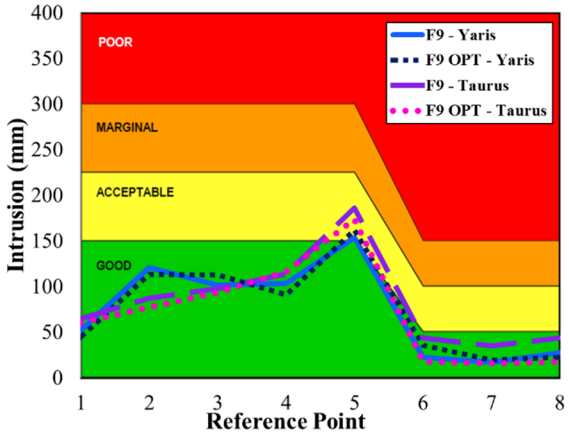

Figure 4-10 100% Overlap – IIHS

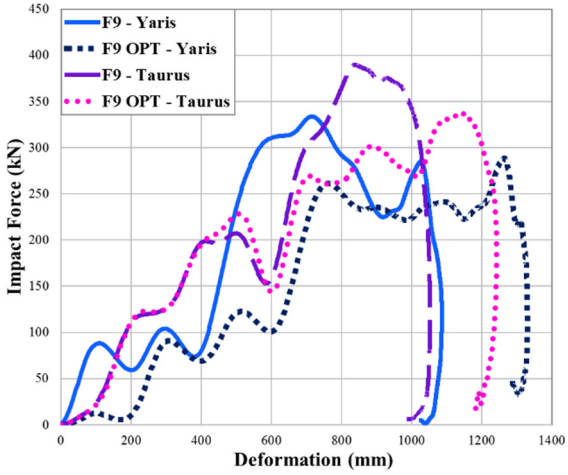

Figure 4-11 50% Overlap Profile

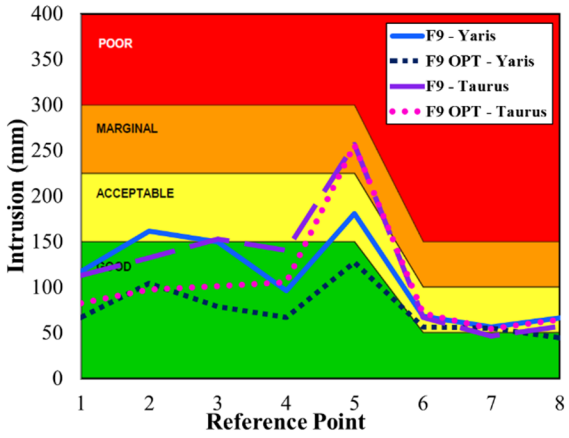

Figure 4-12 50% Overlap – IIHS

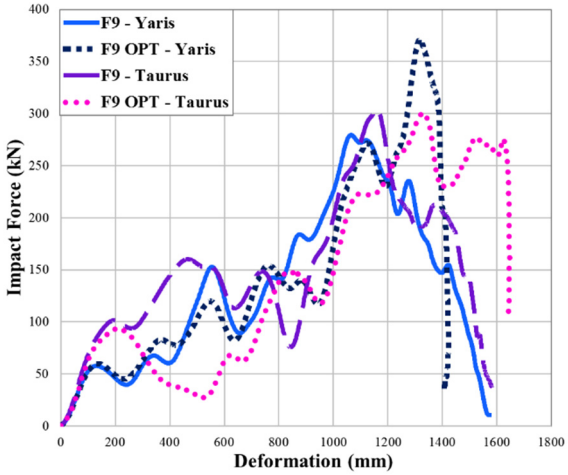

Figure 4-13 30% Overlap Profile

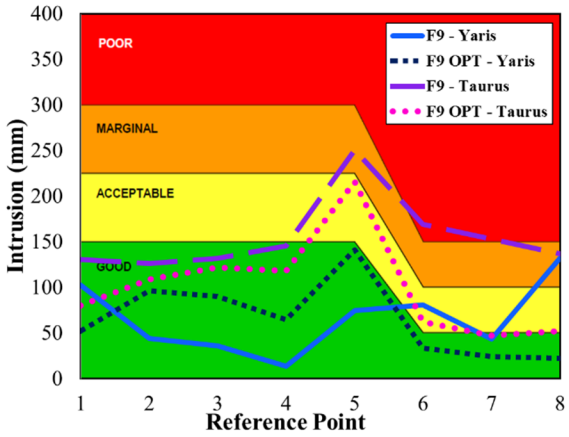

Figure 4-14 30% Overlap – IIHS

4.2.3.3 Virtual Experiment I – Discussion & Conclusions

Figure 4-9 to Figure 4-14 compares the crash worthiness results of the original FUPD F9 and the optimized FUPD F9, denoted by F9-OPT. This analysis only compares the original to the OPT, and does not analyze the design decisions other than the material aspects.

From Figure 4-9 and Figure 4-10, both vehicle impacts in the 100% overlap scenario preformed similarly. F9-OPT showed a slight increase in deformation compared to the stiffer F9. However, the IIHS values for both are the equivalent within the 'good' range, Figure 4-10. Conversely, 50% overlaps show an great improvement of the F9-OPT's compartment intrusion values over the original F9 configuration, Figure 4-12. However, with the relatively weaker materials used in the F9-OPT design, it can be seen in Figure 4-11 that the energy absorption effects of the material help reduce impact forces compared to the more rigid materials used in the F9. The F9-OPT was able to reduce peak impact forces by approximately 80kN on the Toyota Yaris, resulting in a reasonable increase in relative deformation. The F9-OPT showed greater improvement to the Ford Taurus's IIHS values, while allowing for a lesser impact peak for an increase in relative deformation. From Figure 4-13, the 30% overlap shows some misrepresentation as the vehicles slides along the FUPD and passes the tyre, displaying a high deformation but a rapidly decline in impact force. The F9-OPT once again had the benefit of absorbing more energy through the material while mitigating the increase in compartment intrusion. The 30% overlap occupant compartment intrusion, Figure 4-14, concludes the improvements of intrusion values from F9-OPT, especial for A-Pilar intrusion values. shows similar results between to designs while being within the "good" range. However, even the visuals observe a different failure that the data miss represent Figure 4-15 and Figure 4-16. The 30% overlap the side support structure of the F9-OPT (shown in green) proves to be too weak and fails to withstand the impact of the vehicles. This allows the passenger vehicle to impact and bend the FUPD around the chassis mount, and the vehicle impact the tractor's tyre. Even though the F9-OPT P1 passed the modified regulation requirements, failures do happen. This is why the dynamic testing is important to conduct. Improvements to the material and/or thickness increase for the side support structure can improve the small overlap stiffness, as the original F9 did.

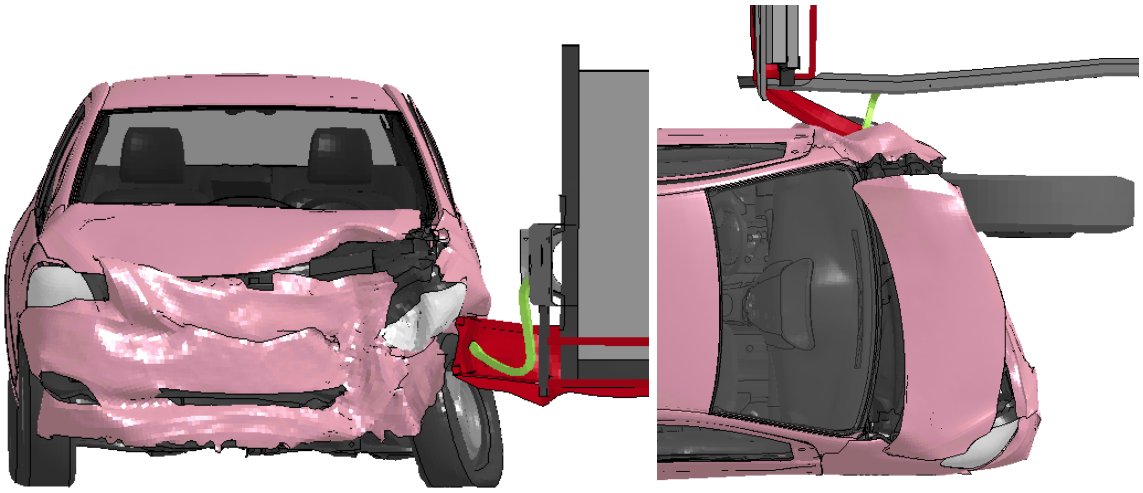

(a) Rear View (b) Top View

Figure 4-15 Toyota Yaris 30% Overlap Impact with Side Support Structure Failure

Figure 4-16 Ford Taurus 30% Overlap Impact with Side Support Structure Failure

Overall the F9-OPT preforms as good as the original F9 design for the 100% and 50% overlaps, proving that the ideal optimal design was feasible and effective. However, material selection should be enhanced to insure that the side support structure is not optimized with weak materials.

4.2.4 Design Optimization Methodology Conclusions

Within the first section of this chapter, multi-objective optimization methods and function improvements was explored in ordered to find a computational effective and accurate approach that would provide optimal FUPDs design. The published dsFUPD F9 design for a Volvo VNL series tractor trailer was optimized into a F9-OPT design. The optimization process deemed to include material variables for the design and include material cost into the optimization function to better suit the needs of the industry. While advancing the simple optimization function of system mass and deformation objectives with varying material thickness, an effective method was found.

After optimal design was selected in this work, dynamic testing was used to evaluate the crash worthiness through impact compatibility profiles and IIHS occupant compartment intrusion measurements. From the NSGA-II ideal optimal design, F9-OPT, dynamic testing resulted in similar performances. However, improvements for 30% overlap collision scenarios is needed to ensure designs do not weaken and intrude results into marginal or poor intrusion values.

A two stage design optimization methodology was set out to improve the overall FUPD development. Direct simulation optimization method using NSGA-II proved to enhance optimization with material cost as a minimizing objective with deformation and system mass with varying part material and thicknesses. NSGA-II also proved to give a large sample of feasible and optimal solutions compared to other methods. It is recommended that if material selection is needed to be explored, a simple optimization functions would be good enough. Optimizing for system mass and deformation with a single material with varying material thickness values should use HASA with RBF. Once a selection of materials is set, designers should implement the them into the NSGA-II material cost optimization to obtain an enhance result of ideal optimized designs. In summary:

2 Stage Design Optimization Methodology

Stage I: Single Material Consideration

- Metamodeling with Hybrid ASA for fast exploration
- Single Material Optimization (Phase 1)

$$\boldsymbol{f(Thickness) = \min(\Delta X_{P1}, \Delta X_{P2}, \Delta X_{P3}, Mass)}$$

- Used to build a group of materials selection for Stage II

Stage II: Material Collection Optimization

- Direct Simulation Strategy with NSGA-II Algorithm
- Cost Optimization (Phase 3)

$$\boldsymbol{f(Thickness, Material) = \min(\Delta X_{P1}, \Delta X_{P2}, \Delta X_{P3}, Mass, Cost)}$$

- Final Optimized Design Configuration

The next section to this work explores material selection to improve energy absorption and cost effectiveness.

4.3 CRASHWORTHY MATERIALS

This section sets forth the exploration of crashworthy materials to build front underride protection devices. The exploration of materials furthers the understanding of useable materials to enhance the crashworthiness, reduce system mass and material cost. Currently, most European and Australian FUPDs are constructed of aluminum for its light weight qualities, which is relatively expensive compared to steel [67, 68]. However, with aluminum's lower yield strengths and strain hardening properties relative to steel, it may not be the ideal material to aid for crashworthiness of a tractor. To increase strength for the aluminum material, thicker members are needed resulting in a bulky design in a location where design space is limited. The other category of materials to consider are steel alloy materials. Steels have high strength mechanical properties reducing material thickness, and therefore the need for design space, while providing higher stiffness. However, steel is a dense material (density of 7.83kg/m^3), nearly 3x higher than aluminum (density of 2.82 kg/m^3). Conclusively, steel presents issues of being desirable due to heavy designs, especially when the critical weight of the front axle of the tractor is being approached or exceeding. However, seen in the previous section of the chapter, 40kg weight was the ideal weight for passing the ECE R93 modified and dynamic for the FUPD F9 model. Therefore, the work needed to investigate into superior materials for crashworthiness to reduce overall system mass.

As mentioned before, past publications utilized a single high strength steel with no variations or investigations. The previous section only utilized a small sample group of 10 materials between 500MPa to 1.2GPa yield strength. The small sample was used only to progress and determine an optimization methodology and to not further the complexity of the optimization methods, in which this chapter focused on the finite details of material section. A broad assortment of materials was utilized for experimentation to analyze the range of mechanical properties, seen in Table 4-3.

Various types include High Strength Low Alloy (HSLA), Dual Phase Steels (DP), Triple Phase Steels (TRIP), Martensite (M), Aluminum, High Strength Steel (HSS), and Structural Steel (SS). The material mechanical properties utilized in this work are valid

material data from material manufactures and reliable resources [69, 70, 55, 71]. The material costs were obtained from North American and European manufactures, and reflect the costs from January 2015. The material cost used may not reflect the true cost as it is influenced by mass production and manufacturing costs, in which could be incorporated into the optimization cost analysis easily. However, for this work the cost of a finite sheet of material was used, and then calculated to cost (USD) per weight (metric tonne). The strain hardening exponent was calculated from the obtained log-log stress strain curves utilized in the experiments. Obtaining valid material properties proved difficult due to the need of stress strain data, this would limit the number and diversity of used materials.

This section of the chapter investigates the application of steel materials for the F9 FUPD design while utilizing the outlined 2 stage optimization design methodology. From the 2 stage design optimization methodology, stage I single material consideration filters out the worthy materials that can be used for the design to develop a group of crashworthy materials that would be viable to be implemented. Once the group of assorted materials had been established, the group of materials were used to optimize the FUPDs in stage 2.

4.3.1 Optimization Stage I – Single Material Consideration

Stage I of the optimization utilizes single material optimization to filter the worthy materials with the use of Metamodeling with Hybrid ASA for fast exploration for Phase 1 Optimization. Only material thickness would be optimized for the objective of point load deformation and system mass (Equation 4.4). The FUPD F9 model was utilized while being optimized with the modified ECE quasistatic point load testing environment. Only one material was optimized at a time for 30 iterations of Hybrid ASA. The optimal design for the material should pass the modified ECE R93 requirements and be no more than 100mm of deformation.

Table 4-3 lists the materials that were investigated. A total of 28 materials with yield strength ranging between 241MPa to 1200 MPa were assembled; 28 steel variants.

Table 4-3 List of Materials and Mechanical Properties

Material Name	Yield Strength (MPa)	Ultimate Tensile Strength (MPa)	Strain Hardening Exponent (-)	Material Cost (USD$ per metric tonne)
ASTM A569 Carbon Steel [69]	241	338	0.11	600.00
DP500 [55]	310	528	0.14	1013.30
HSLA Grade 50 SAE950X [69]	340	450	0.13	1045.00
DOCOL 600 DP [70]	350	600	0.17	1014.13
HSLA350 [55]	412	468	0.21	826.73
TRIP600 [55]	414	697	0.20	1276.00
SAE 1040 Hot Rolled Steel Alloy [69]	415	675	0.17	800.00
HSS 590-CR [55]	431	593	0.18	850.00
SAE 1045 Hot Rolled Steel Alloy [69]	443	581	0.12	771.62
DOCOL 800 DP [70]	500	800	0.18	1058.22
DOGAL 800 DP [70]	500	800	0.16	1102.31
TRIP780CR [55]	505	793	0.26	1386.00
Steel Wrought 4620 [69]	507	853	0.22	738.55
ASTM A653 Grade 80 [69]	550	862	0.21	850.00
HSLA Grade 80 / SAE980X [69]	557	690	0.16	1166.00
DOGAL 600 DP [70]	600	600	0.16	1058.22
Steel Wrought 1030 [69]	609	1061	0.12	738.55
DOGAL 800 DPX [70]	620	800	0.14	1124.36
DOCOL 1000 DP [70]	700	1000	0.17	1102.31
DOCOL 1000 DPZE [70]	700	1000	0.17	1543.24
DOCOL 900 M [70]	700	900	0.11	1080.27
Steel Carbon A514 [69]	775	1006	0.17	705.48
SAE 4340 Hot Rolled Steel Alloy [69]	855	1325	0.18	1102.31
DP 980 [55]	907	1037	0.13	1399.94
DOCOL 1200 M [70]	950	1200	0.20	1179.47
Steel Wrought 4140 [69]	960	1410	0.11	992.08
DOCOL 1300 M [70]	1030	1300	0.18	1201.52
DOCOL 1500 M [70]	1200	1500	0.15	1245.61

4.3.1.1 Stage I Optimization – Results

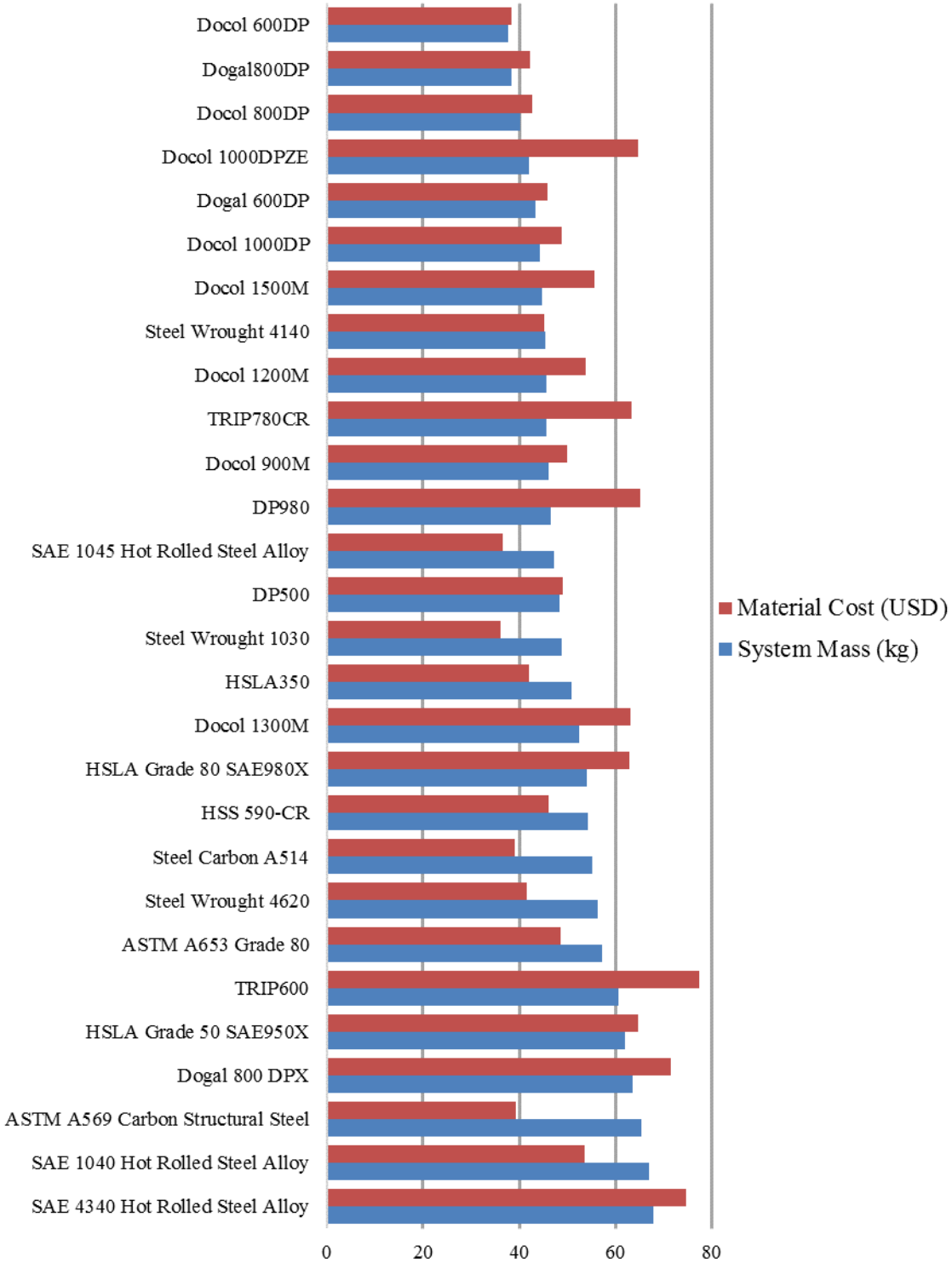

Figure 4-17 Group of Materials Optimized F9 Design System Mass and Cost

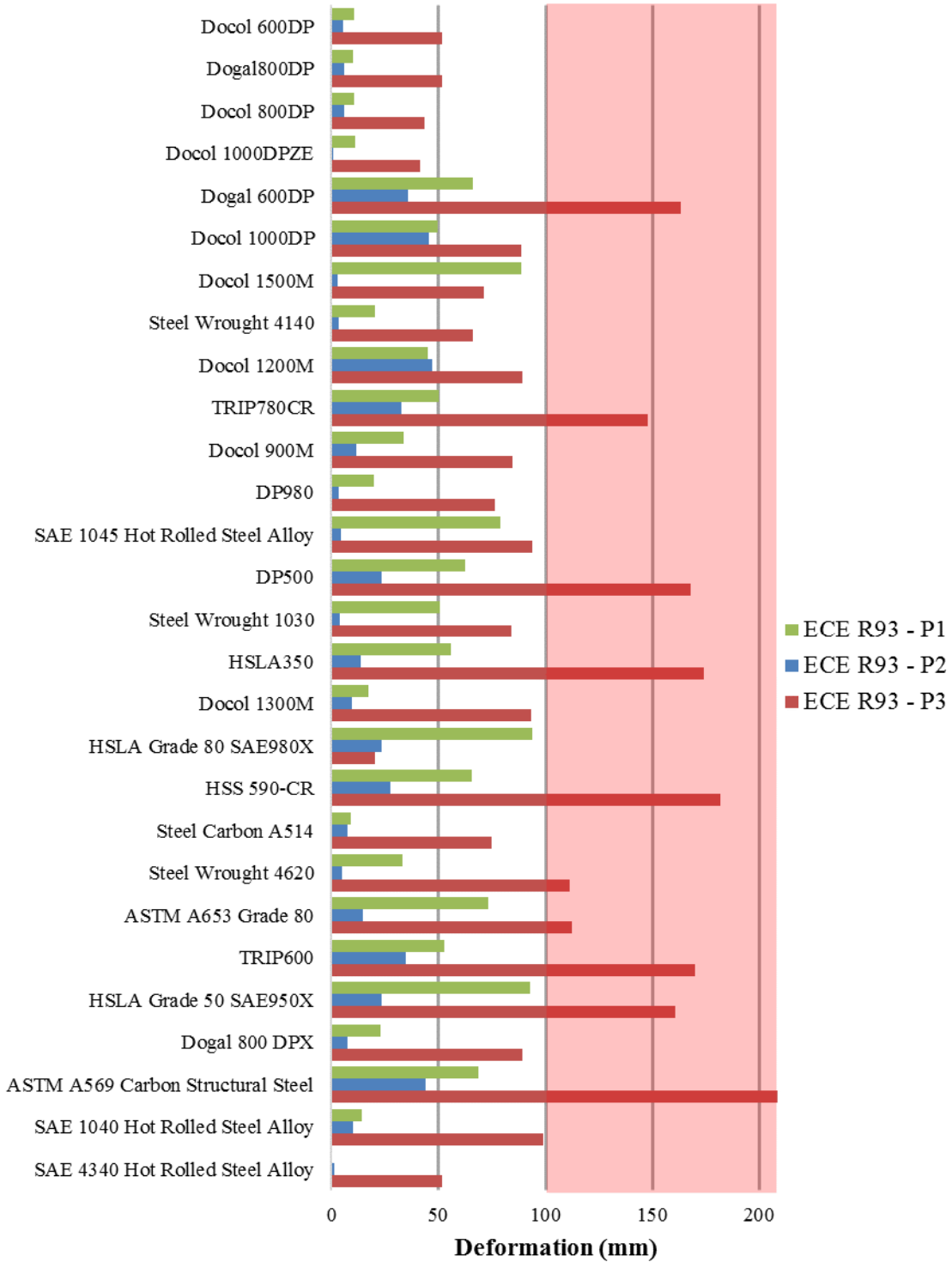

Figure 4-18 Group of Materials Optimized F9 Design Modified ECE R93 Point Load Measurements

4.3.1.2 Stage I Optimization – Discussion & Conclusions

The 28 materials yield strength ranges between 241MPa to 1200 MPa were individually optimized for the F9 FUPDs design to establish a collection of materials for the stage II optimization. Figure 4-17 presents the optimal design for each material for cost and system mass, listed from the lowest to highest weight. Figure 4-18 is listed in the same order, but shows the deformation performance from the modified ECE R93 testing. Ten of the materials prove to fail the modified testing standards by deformation more than 100mm, and will not be considered to be added into the collection of optimal materials. Notably the TRIP steels all fail to withstand the requirements within a good range, which was considered to be viable for crashworthiness (section 1.6). Dual phased (DP) steels ranked higher compared to most of the other materials used. Only 5 of the materials were able to weigh around 40kg, with 1 failing the P3 requirements (Dogal 600DP). The most rigid design was formed with SAE 4340 HR Steel with little P1 and P2 deformation, however the system mass and cost was exceedingly high with a weight of 67kg. SAE 4340 would still be utilized for the collection of materials but is not desired to be utilized singularly for FUPDs.

4.3.2 Stage II Optimization – Material Collection Optimization

With the established collection of materials, stage II was implemented to assemble the different materials in efforts to lower cost, system mass, and maintain optimal performance. Phase 3 Direct Simulation Strategy with NSGA-II Algorithm method was utilized (Equation 4-6) for 100 iterations. The optimization performance would be analyzed to ensure the method progressed in optimizing for the three objectives.

The optimal design was then selected and verified through dynamic testing to ensure the design was truly optimal for implementation. The optimal design was compared to the original F9, and F9-OPT to conclude on performance, cost, and weight.

4.3.2.1 Stage II Optimization – Results

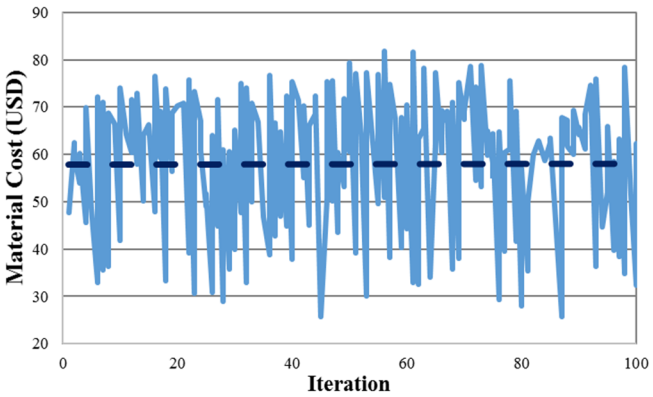

Figure 4-19 NSGA-II Feasible Results per Iteration with Respect to Material Cost Minimization

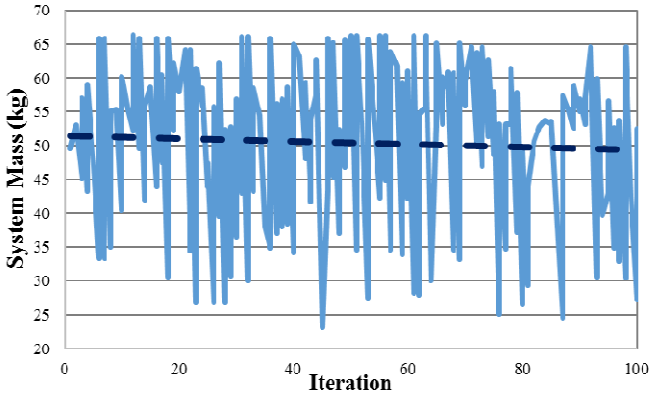

Figure 4-20 NSGA-II Feasible Results per Iteration with Respect to System Mass Minimization

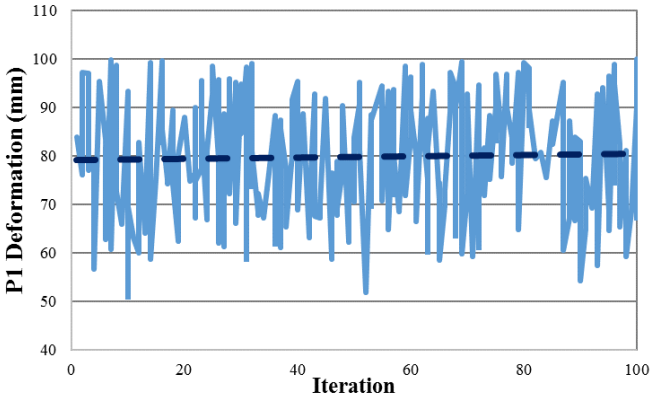

Figure 4-21 NSGA-II Feasible Results per Iteration with Respect to Displacement of Quasistatic Load P1 Minimization

Table 4-4 Benchmark and Optimal Designs Used for Dynamic Testing from Stage II Design Optimization

Optimized Designs	Mass (kg)	Cost (USD)	Displacement (mm)			Reduction from F9-2SDO	
			P1	P2	P3	Mass	Cost
F9	41.76	66.82	27.00	8.22	43.17	44.7%	59.89%
F9-OPT	42.3	32.77	37.1	16.9	76.46	45.4%	18.2%
F9-2SDO	23.1	26.80	91.75	12.6	93.71		

4.3.2.2 Stage II – Discussion & Conclusions

The optimization method of using NSGA-II for phase 3 function proved to work efficiently. Material Cost (Figure 4-19) and P1 displacement minimization (Figure 4-21) illustrated a slight increase in optimal cost points as iterations progressed. More importantly, system mass trends progressively lowered as the iterations progressed.

The resulting optimal design proved to show great improvements over the previous designs, seen in Table 4-4. Named, F9-2SDO (2 stage design optimization) resulted in a 44.7% reduction in mass to 23.1 kg, compared to the other designs. The design's weight would be competitive to aluminum FUPD weights. The cost of the design was also very reasonable, however with the unknown manufacturing costs, the true design cost would be higher. Interestingly, the F9 was optimized with all 28 materials, however the F9-2SDO optimized to only consisting of DP materials. All member thicknesses also are within the range of available manufacturing thicknesses. Conclusively, the F9-2SDO results from optimization proved to be a more optimal result.

4.3.3 Design Verification – Dynamic Collision Testing

With the F9-2SDO design, the crash worthiness of the device must be confirmed through dynamic testing to be deemed an optimal design. For this section of Experiment II, the optimal design from Experiment I was taken and tested with the Toyota Yaris and Ford Taurus finite element models.

4.3.3.1 Design Verification – Setup

The dsFUPD F9-2SDO was mounted onto a simplified VNL frame and experimented with the two passenger vehicles with a closing speed of 64km/hr. Three overlap collision scenarios were tested; 100%, 50%, and 30%. IIHS occupant compartment intrusion analysis and compatibility profiles are used to conclude the collision performance.

4.3.3.2 Design Verification – Toyota Yaris

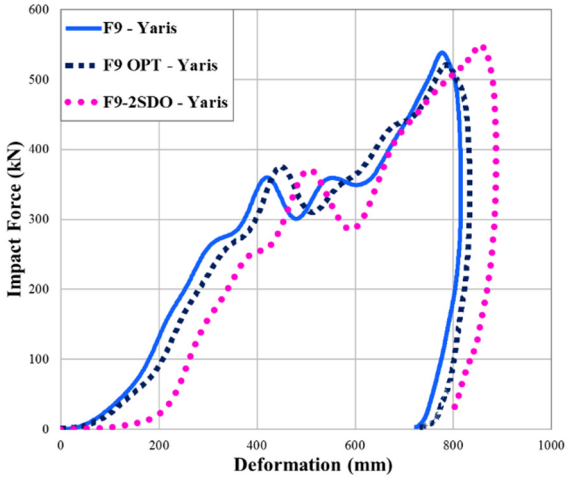

Figure 4-22 100% Overlap Profile

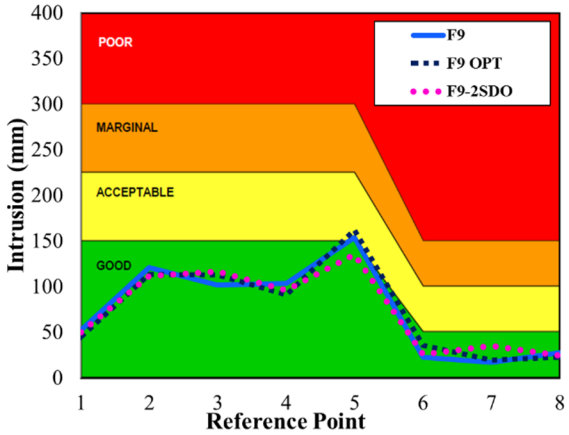

Figure 4-23 100% Overlap – IIHS

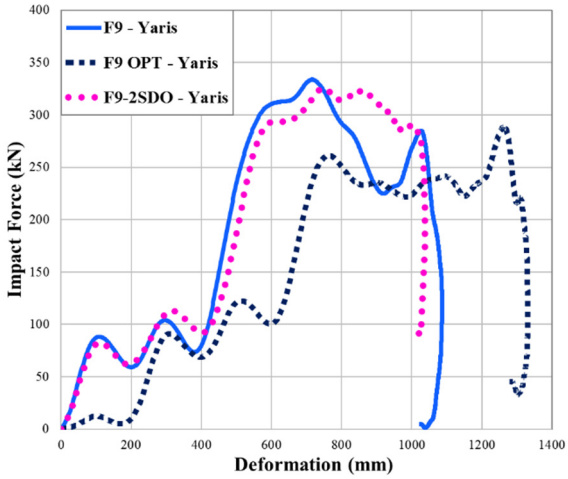

Figure 4-24 50% Overlap Profile

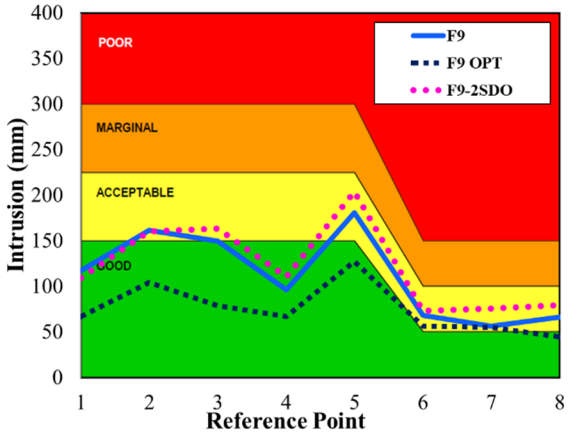

Figure 4-25 50% Overlap – IIHS

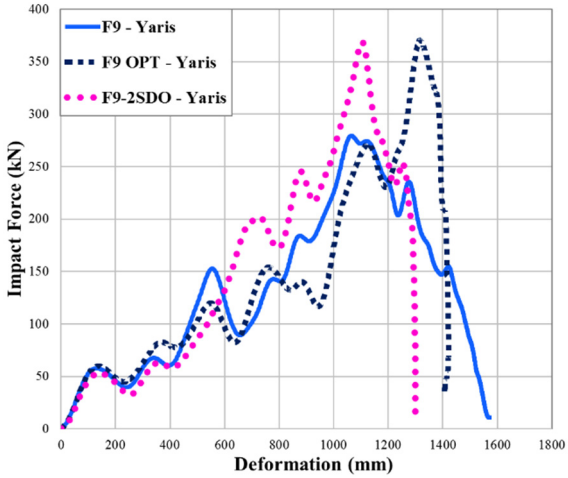

Figure 4-26 30% Overlap Profile

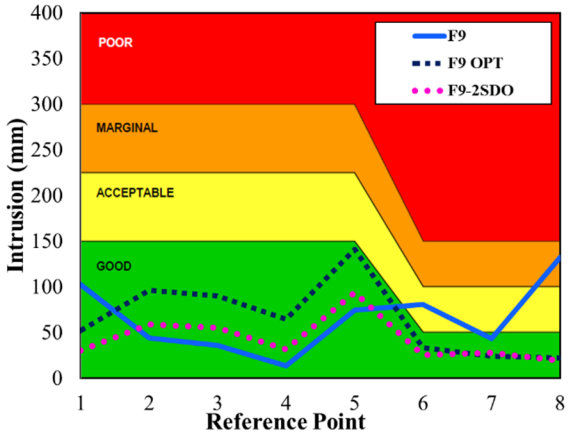

Figure 4-27 30% Overlap – IIHS

4.3.3.3 Design Verification – Ford Taurus

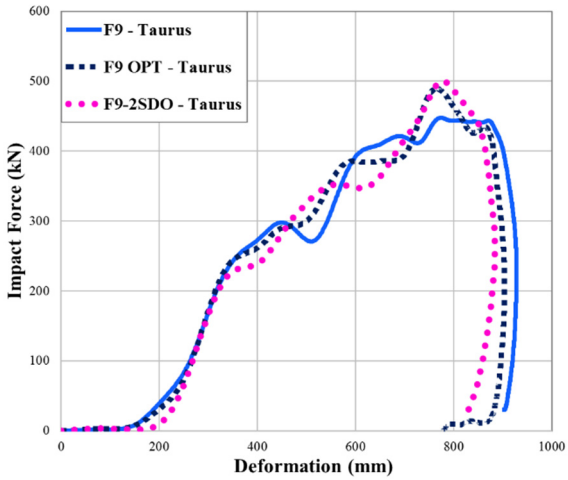

Figure 4-28 100% Overlap Profile

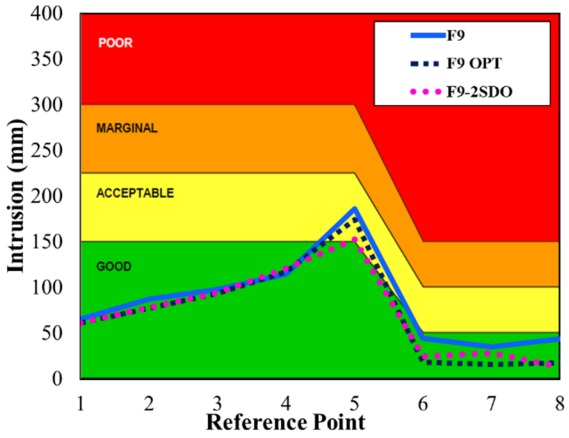

Figure 4-29 100% Overlap – IIHS

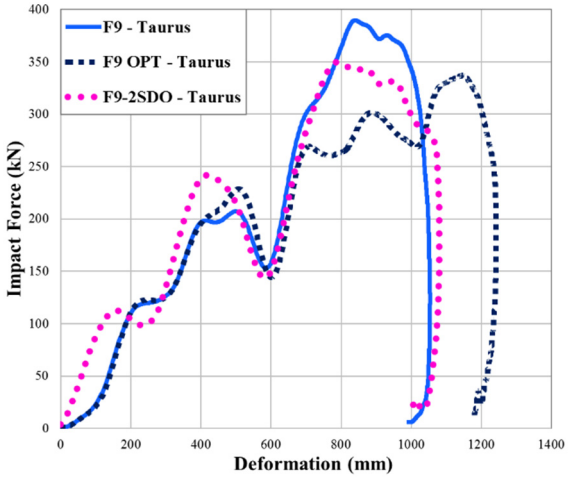

Figure 4-30 50% Overlap Profile

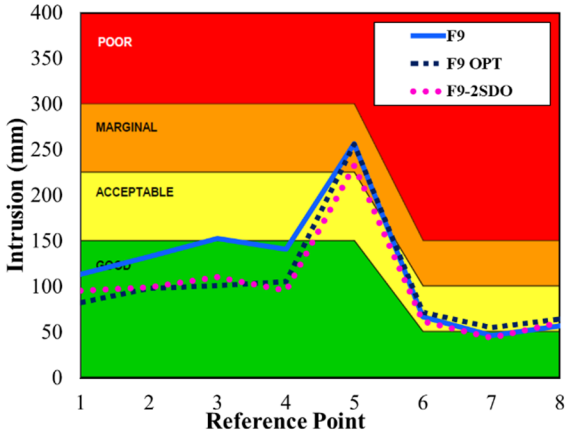

Figure 4-31 50% Overlap – IIHS

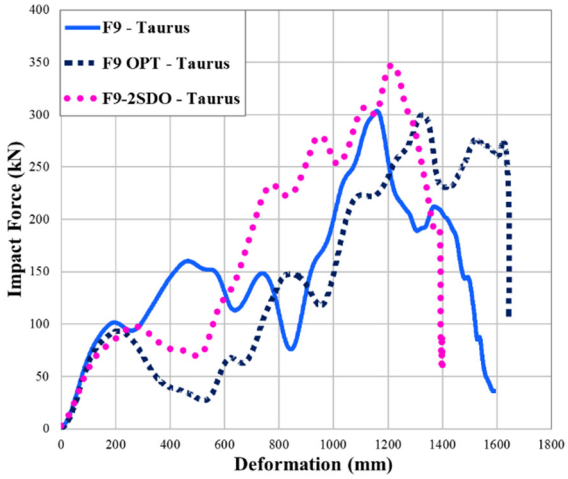

Figure 4-32 30% Overlap Profile

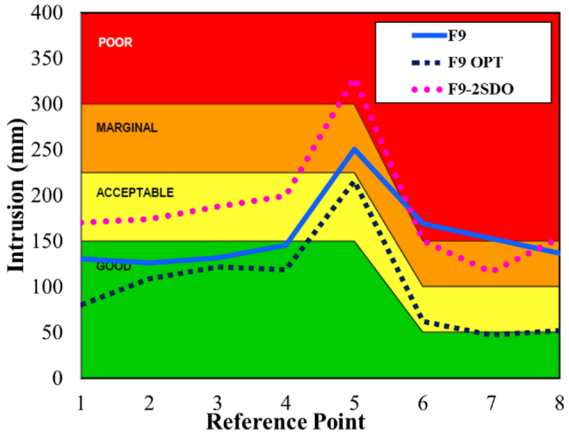

Figure 4-33 30% Overlap – IIHS

4.3.3.4 Design Verification – Discussion & Conclusions

The optimized design F9-2SDO from Stage II Optimization needed to be verified through dynamic testing with the Toyota Yaris and Ford Taurus. Conclusively the design passed provided a compatible impact which ensured good energy absorption, lower intrusion and prevented underride. Figure 4-22 to Figure 4-27, illustrates the impact results from the Toyota Yaris, while Figure 4-28 to Figure 4-33 show the Ford Taurus results. The majority of the results showed comparable performances between the F9-2SDO and the stiffer F9, while reducing intrusion values. The overlap impacts improved greatly over the F9-OPT with the implementation of superior material selection, as the F9-2SDO side structural member does not fail from both impacts (Figure 4-34). The increase in stiffness, resulted in higher intrusion values into the Ford Taurus impact at 30% overlap, Figure 4-33.

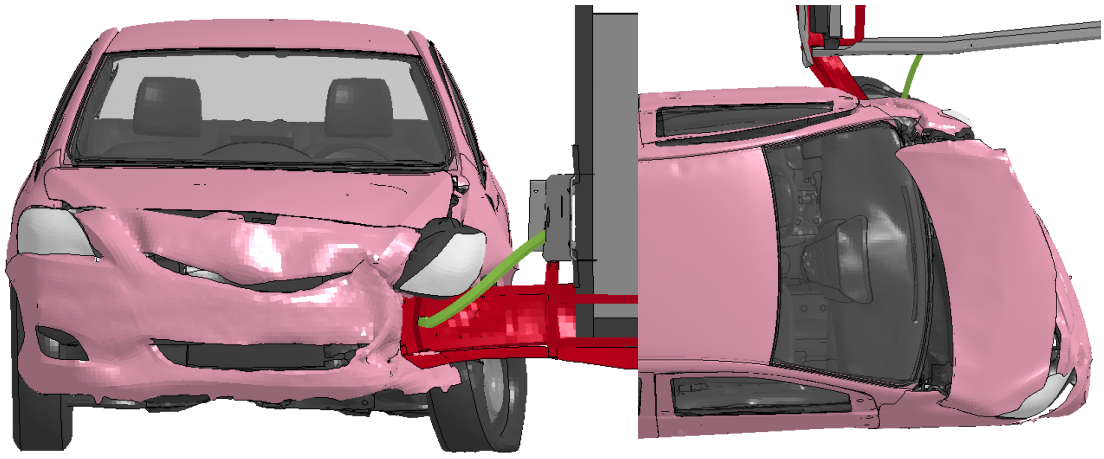

(a) Front View (b) Top View

Figure 4-34 Toyota Yaris Impacting the F9-2SDO at 30% Overlap

4.3.4 Crashworthy Materials Conclusions

The application of crashworthy materials for front underride protection devices was investigated in this section of the chapter. An assortment of valid materials from manufacturers were used for the optimization of the F9 dsFUPD design. The selection of materials ranged from low-strength steels (LSS), conventional High Strength Steels (HSS), and Advanced High-Strength Steels (AHSS). The optimization utilized the established 2 stage design optimization method. The first stage refined a collection of materials by ensuring the material should be used singularly in an optimized design. The second stage

used the passing collection of materials to be optimized together to assemble a FUPD design that would be lightweight, cost effective and crashworthy. The resultant optimal design needed to pass dynamic testing to solidify its optimal design stance.

4.4 CHAPTER SUMMARY

Within this chapter, multiobjective optimization methods and function improvements was explored in ordered to find a computational effective and accurate approach that would provide optimal FUPDs design. The published dsFUPD F9 design for a Volvo VNL series tractor trailer was optimized. The optimization process deemed to include material variables for the design and included material cost into the optimization function to better suit the needs of the industry. While advancing the simple optimization function of system mass and deformation objectives with varying material thickness, an effective method was found. Direct simulation optimization method using NSGA-II proved to enhance optimization with material cost as a minimizing objective with deformation and system mass with varying part material and thicknesses. NSGA-II also proved to give a large sample of feasible and optimal solutions compared to other methods.

The first section concluded on a 2 Stage Design Optimization Methodology. If material selection is needed to be explored, a simple optimization function would be sufficient. Optimizing for system mass and deformation with a single material with varying material thickness values should use HASA with RBF. Once a collection of materials was set, designers should implement them into the NSGA-II material cost optimization to obtain an enhance result of ideal optimized designs. In summary:

2 Stage Design Optimization Methodology

Stage I: Single Material Consideration

- Metamodeling with Hybrid ASA for fast exploration
- Single Material Optimization (Phase 1)

  $$\boldsymbol{f(Thickness) = \min(\Delta X_{P1}, \Delta X_{P2}, \Delta X_{P3}, Mass)}$$
- Used to build a group of materials selection for Stage II

Stage II: Material Collection Optimization

- Direct Simulation Strategy with NSGA-II Algorithm
- Cost Optimization (Phase 3)

$$\boldsymbol{f(Thickness, Material)} = \mathbf{min}(\Delta \boldsymbol{X_{P1}}, \Delta \boldsymbol{X_{P2}}, \Delta \boldsymbol{X_{P3}}, \boldsymbol{Mass}, \boldsymbol{Cost})$$

- Final Optimized Design Configuration

After the optimal design was selected in this work, dynamic testing was used to evaluate the crashworthiness through impact compatibility profiles and IIHS occupant compartment intrusion measurements. From the NSGA-II ideal optimal design, F9-OPT, dynamic testing resulted in similar performances. However, improvements for 30% overlap collision scenarios is required to ensure designs do not weaken and intrude resulting in marginal or poor intrusion values.

With the failure in performance of the F9-OPT for 30% overlap and the need for superior material selection, the 2 Stage Design Optimization Methodology was implemented. With the focus on automotive steels, 28 materials were selected to build a collection of worthy materials concluding from stage I. The collection of worthy materials was then applied to stage II to assemble the varying materials into the design in efforts of reducing mass, cost, and maintain deformations. The crashworthy performance of the final optimized design was proved through dynamic testing. Conclusively the final optimized design maintained the crashworthy performance of a more rigid material at 45% of the weight.

CHAPTER 5
DESIGN FOR ENHANCED CRASHWORTHINESS COMPATIBILITY

Optimization of a design is a continuous effort to ensure that every aspect of the design is configured to a peak performance. At this stage of the research, the aspect of geometry configuration was needed to ensure the front underride protection device is designed optimally and perform robustly. There are many variables that the FUPD that needs to considered in the design space for a North American conventional tractor; for example, the aerodynamic geometry of the front bumper which dictates the curvatures of the FUPDs. As well, other vehicle components may conflict with ideal placements of the FUPDs structural members. Limitation on design parameters of the FUPDs would help refine and optimize the design space for the lower cab area. Within this chapter, various geometry parameters were experimented to analyze the change in performance of the frontal impact area. The vertical contact section height, curved base angle, and curved end angles are parameters in which the tractor's bumper will either need to govern or conformed to. This is to ensure the impacting vehicle does not underride more due to the steepness in angle. These parameters utilized the tier 1 design methodology of the Dual Spring Component Level VNL model with an attached frontal contact plate (Figure 5-1 shown in red). Since the only the geometric front contact is only to be considered, the duel springs would be the most time effective approach. The last geometric experiment observes the placement angle of the side structure support, in which is critical to small overlap collisions. The results would effectively support the defining of an optimal and robust design space envelope for the FUPD that would prevent underride, and improve occupant safety. The parameters were evaluated on the IIHS occupant intrusion, and performance of not allowing the passenger vehicle to underride. Utilizing tier 1 design methodology, the duel spring FUPD testing on the component level FUPD was primarily used for the geometric investigation. Dynamic testing with the deformable F9 design was utilized for side support investigation.

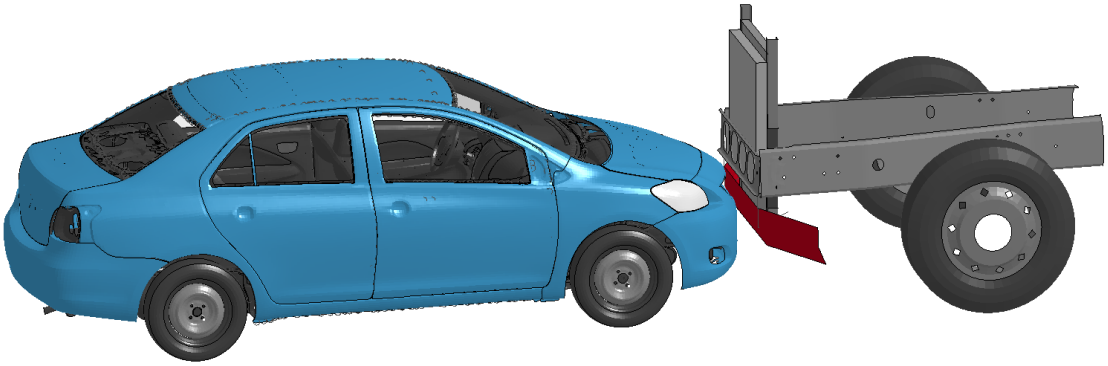

Figure 5-1 Toyota Yaris Impacting the Simplified Duel Spring FUPD

5.1 VIRTUAL EXPERIMENT I – IMPACT VERTICAL SECTION HEIGHT

The vertical impact section height is an important geometric parameter to consider in developing the shape of the contact structure of the FUPDs. Typically, there is an aerodynamic plastic bumper in front of the FUPDs with an angled curve, which needs to be taken in account. This curve can potentially allow the impacting vehicle to slide under the FUPDs and cause underride. Experiment I and II takes in consideration in the curve angle and when to start the curve to insure the compatibility was not affected, Figure 5-2.

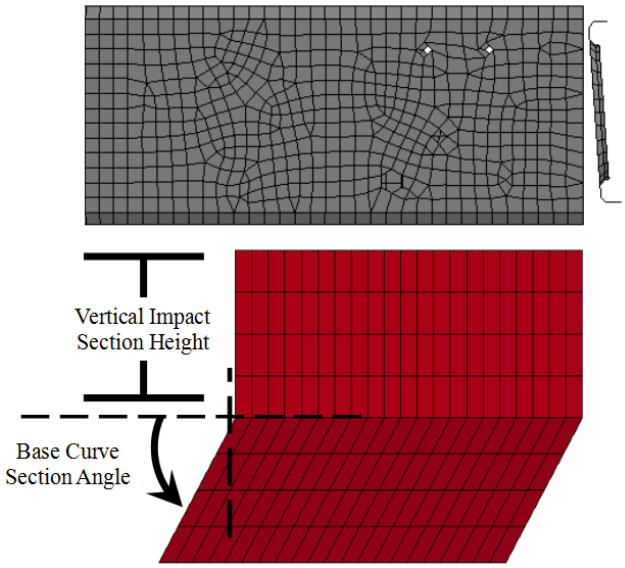

Figure 5-2 Experiment I & II Design Parameters – Side View of Chassis

5.1.1 Virtual Experiment I – Setup

This experiment utilized the duel spring FUPD testing method with a rigid impact plate to analyze geometry. The Toyota Yaris impacted the component level VNL at 64 km/hr for 100%, 50% and 30% overlap cases. Only the height of the vertical section of the impactor was varied, while the protruding back angle was constant. Vertical height sections of 60mm, 120mm, 180mm, and full height 240mm was used, measured from the top of the impact plate, Figure 5-3.

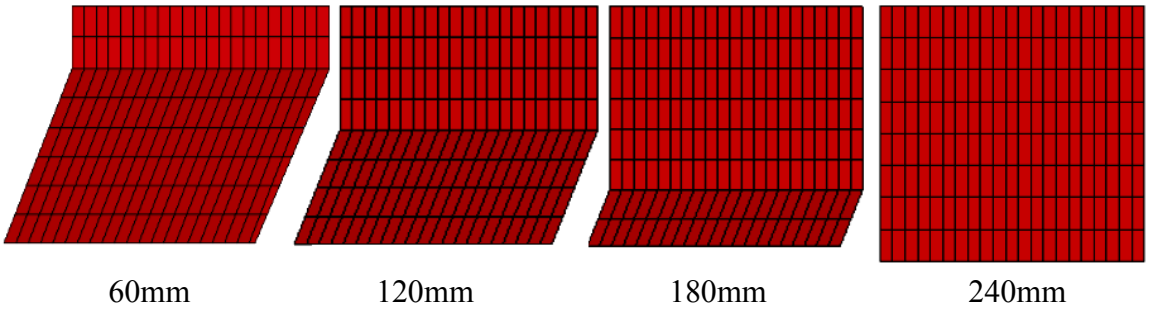

Figure 5-3 Various Impact Section Height

5.1.2 Virtual Experiment I – Results

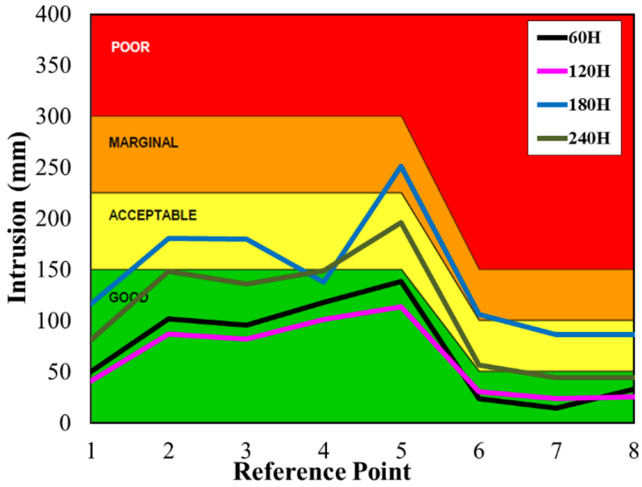

Figure 5-4 Occupant Compartment Intrusion – 100%

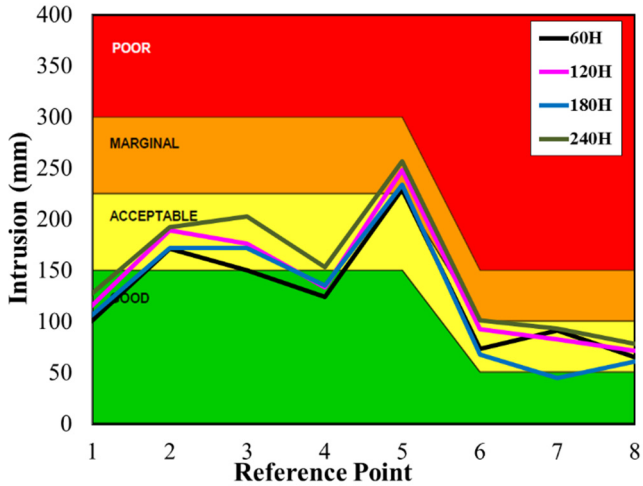

Figure 5-5 Occupant Compartment Intrusion – 50%

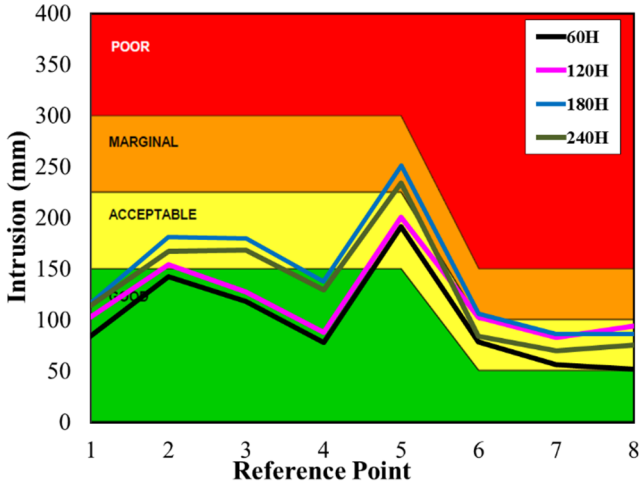

Figure 5-6 Occupant Compartment Intrusion – 30%

5.1.3 Virtual Experiment I – Discussion & Conclusions

The 120mm vertical impact section height proved to be more favourable in the direction 100% overlap, Figure 5-4. The 60mm section height also provides lower intrusion magnitudes. However, for the moderate overlap cases of 50%, seen in Figure 5-5, conclude similar results between all four section heights. Notably, the 180mm section height provides a lower intrusion into the more sensitive IIHS reference points 6, 7, and 8. Figure 5-6 illustrates the small overlap case, 120mm and 60mm section heights show 'good' to 'acceptable' ranges. As the impact section height increased to being fully vertical from the top to the base of the FUPD, the intrusion and increases the contact starts to follow the vehicle to slide further into the cab area. In addition, without at least a vertical section, the passenger vehicle may not result in "good" crumpling as the angle backwards may slide the structural members down wards towards the ground and cause underride.

Conclusively, its recommended that the vertical impact section height be fully vertical for at least half of the frontal contact face before curving for aerodynamic design.

5.2 VIRTUAL EXPERIMENT II – BASE CURVE SECTION ANGLE

Experiment II investigated the curve angle of the base section of the impact plate while maintaining a constant vertical impact section height, Figure 5-2. The base curve is critical for the design of the FUPD to ensure underride is not induced due to the small angle of curvature. In addition, the aerodynamic of the front bumpers geometry may dictate the curvature of the FUPD, as the bumper may be developed before hand. If the development of the FUPDs is completed concurrently with the full lower cab section, the design of the FUPDs should be considered before the bumper.

5.2.1 Virtual Experiment II – Setup

This experiment utilized the duel spring FUPD testing method with a rigid impact plate to analysis geometry. The Toyota Yaris impacted the component level VNL at 64 km/hr for 100%, 50% and 30% overlap cases. The base curve section angle was varied to

15, 30, 45, and 60 degrees, Figure 5-7. The impact plate maintained the ground clearance of 350mm.

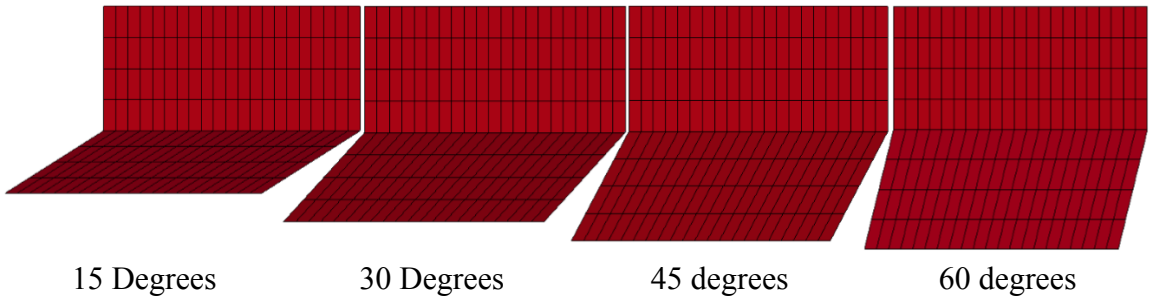

Figure 5-7 Various Bottom Cure Angled Rigid Plates

5.2.2 Virtual Experiment II – Results

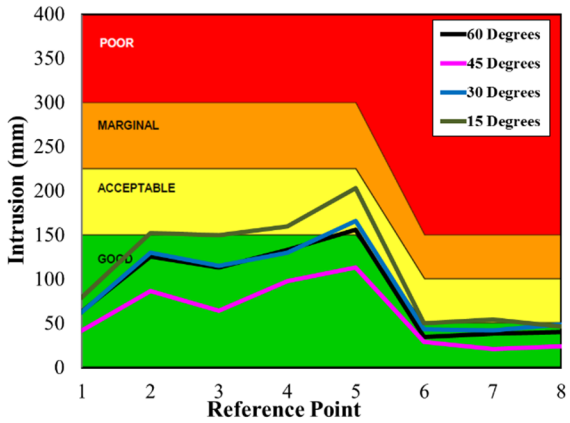

Figure 5-8 Occupant Compartment Intrusion – 100%

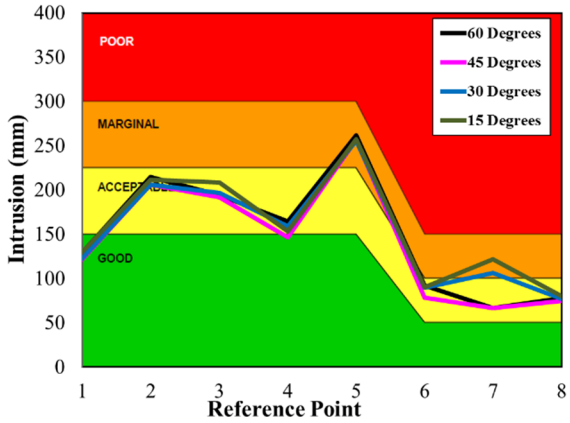

Figure 5-9 Occupant Compartment Intrusion – 50%

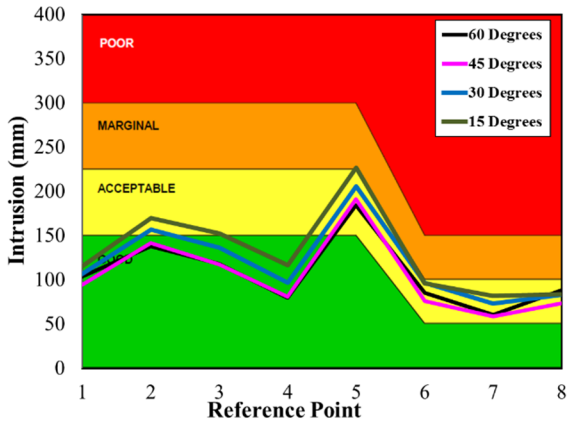

Figure 5-10 Occupant Compartment Intrusion – 30%

5.2.3 Virtual Experiment II – Discussion & Conclusions

From the IIHS occupant compartment intrusions, the 50% and 30% overlaps show similar results for all degrees of base section curve angle, seen in Figure 5-9 and Figure 5-10. The 60 and 45 degree angles show an improved impact contact. Figure 5-8 illustrates the 100% overlap case in which the 45-degree angle proves to be the most favourable base section curve angle as the intrusion levels are lower. The base curve angle resulted in being important for the impact contact with the passenger vehicles tyres. While the vertical height section allowed for a 'good' compatibility with the structural members of the passenger vehicle. The four different degrees did not show influence of underride due to the angle. This leads to the conclusion that as long as frontal impact area has a ground clearance of 350mm with an overall vertical height coverage of 240mm, the angle will not influence any underride. It is recommended that the base section curve angle remains near 45 degrees.

5.3 VIRTUAL EXPERIMENT III – OUTER CURVE SECTION ANGLE

Experiment III, focused on the outer curvature of FUPDs in which is also affected due to the aerodynamic shape of the North American conventional tractor's bumper. The outer curve section angle influences the impact of overlap cases and how the colliding vehicle is managed. The angle can influence the vehicle to impact and diverted off the FUPD or allow the FUPD to absorb the impact and 'catch' the colliding vehicle by absorbing the full impact.

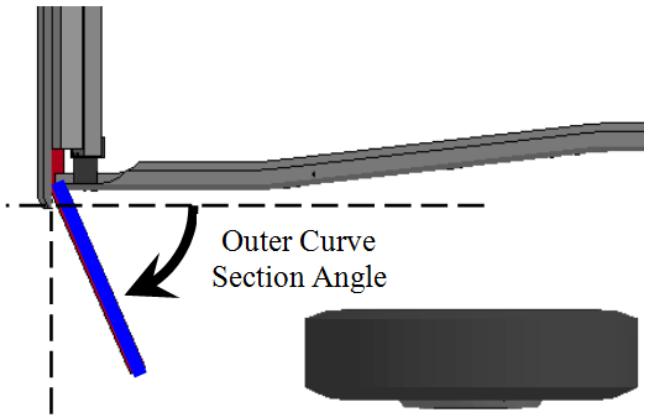

Figure 5-11 Outer Curve Section Angle

5.3.1 Virtual Experiment III – Setup

This experiment utilized the duel spring FUPD testing method with a rigid impact plate to analyze geometry. The Toyota Yaris impacted the component level VNL at 64 km/hr for 50% and 30% overlap cases. The 100% overlap case would not apply to the outer curvature. The curve angle away from the chassis was investigated at 12, 24, 36 and 48 degrees, Figure 5-11. The length of the impact plate was adjusted for each angle to ensure the length complies with the regulated length to the tyre by ECE R93.

5.3.2 Virtual Experiment III – Results

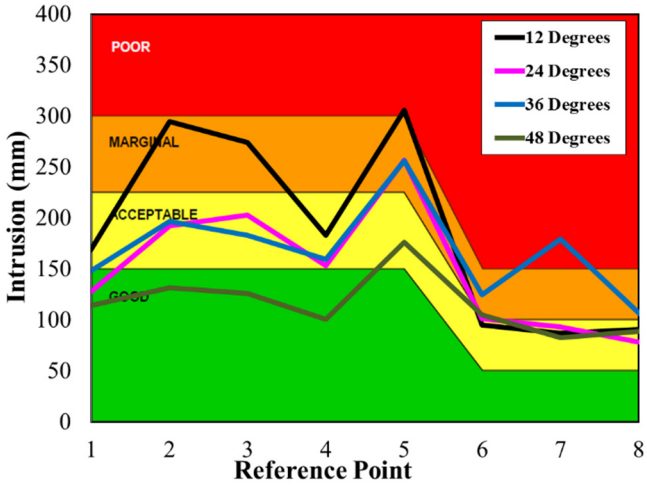

Figure 5-12 Occupant Compartment Intrusion – 50%

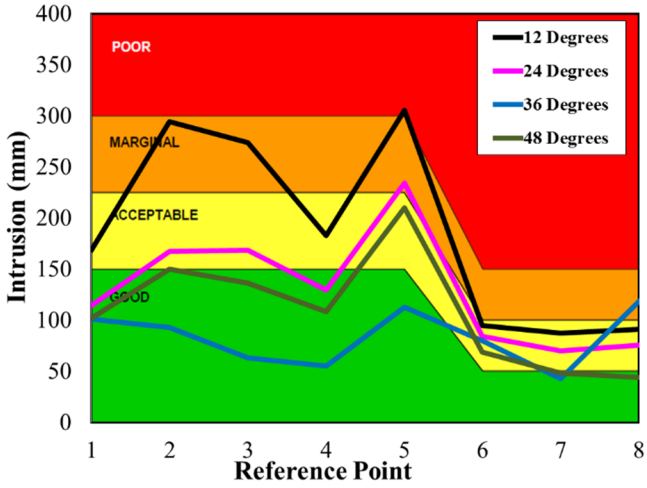

Figure 5-13 Occupant Compartment Intrusion – 30%

5.3.3 Virtual Experiment III – Discussion & Conclusions

From the IIHS occupant compartment intrusion metrics, Figure 5-12 and Figure 5-13, the outer curvatures between 36 and 48-degrees is more favourable. The 48-degree curve showed improved results between the two overlap cases. However, for the more sensitive IIHS reference points for the instrument panels and a pillar (6, 7, and 8), the cases show some indifferences. This was primarily due to the vehicle either being caught by the FUPD, causing deformation and therefore intrusion, or the vehicle would slide off and diverts passed the tractor tyre. Its recommended that the outer curvature be designed between 36 to 48 degrees from the chassis.

5.4 VIRTUAL EXPERIMENT IV – SIDE OVERLAP SUPPORT

The final set of geometry configuration experiments for the of the FUPDs focused on the side support structure. The importance of the side support structure is to absorb all the impact energy from any overlap collisions less than ~40%, in which there is only the front tyre to stop the incoming vehicle. In addition, the side support stabilizes and protects the passenger vehicles from underriding when the vehicle overlaps only one chassis rail of the tractor-trailer. Previous chapters concluded that the ECE R93 P3 location should be designed to resist the same impact as one of the chassis rails, 160 kN point load force. However, the side structure can be optimized to pass the modified ECE R93, yet can fail dramatically in dynamic tests, as seen in CHAPTER 4. The structure is a critical component in which needs to have an optimal configuration in which leads to this case of experimentation.

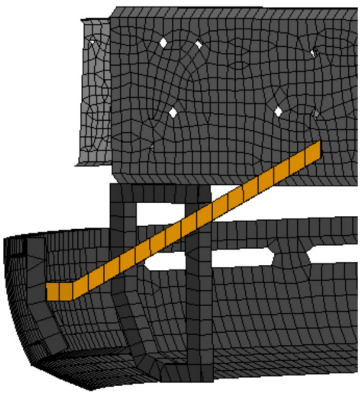

Figure 5-14 Side Support Post

The side support structure conflicts with current tractor-trailers arrangement of components along the chassis rail. The experiments would help direct a better platform configuration when implementing the FUPDs and to ensure that the energy absorption is effective without conflicting in current or future arrangements along the chassis rails.

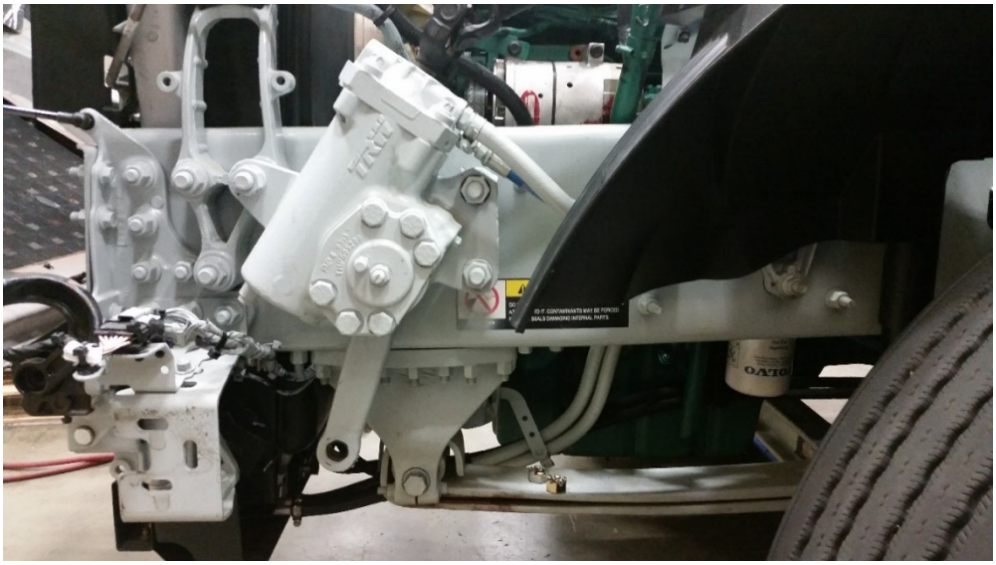

Figure 5-15 Side View of a Volvo VNL Chassis Rail (Permission from Volvo Group truck technology – North Carolina)

5.4.1 Virtual Experiment IV – Setup

To experiment on configuration of the side support attachment, the rigid F9 FUPD was utlized to dynamicly test at 50% and 30% overlap with the impact velocity of the Toyota Yaris at 64 km/hr. Five varous obtuse angles of the side support attachment to the chassis was experimented on between 115° to 155°. To ensure that variable angle of the side post was equally observed for energy absorption, the structure was not shortened/elongated to connect to the chassis rail. If the length of the structure was changed it would affect the amount of energy absorption from the change of mass of the structure, which would not be affected when comparing just the contact angle. Therefore, the length had to be constant. In addition, to simulate a rigid rail connection of the structure the end of it was constrained in all directions. Figure 5-16 illistrates the various angles of the structure that was experimented. The IIHS metrics for occupant compartant intrusion was utlized to observe the intrusion values. The observations from FEA analsysis of effective

plastic deformation would also serve to aid in concluding the preformance of the side impact support.

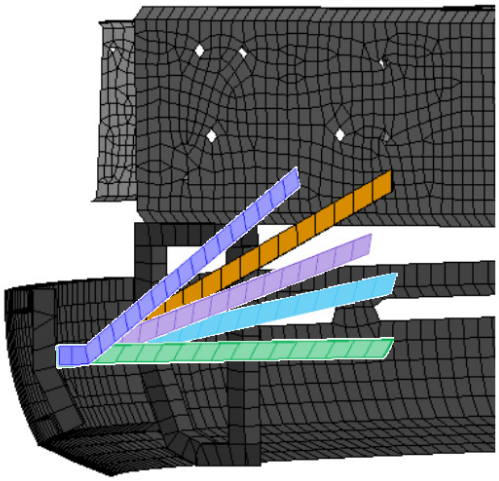

Figure 5-16 Overlap Side Support Placement to Chassis Angle Change

5.4.2 Virtual Experiment IV – Results I: IIHS Occupant Compartment Intrusion

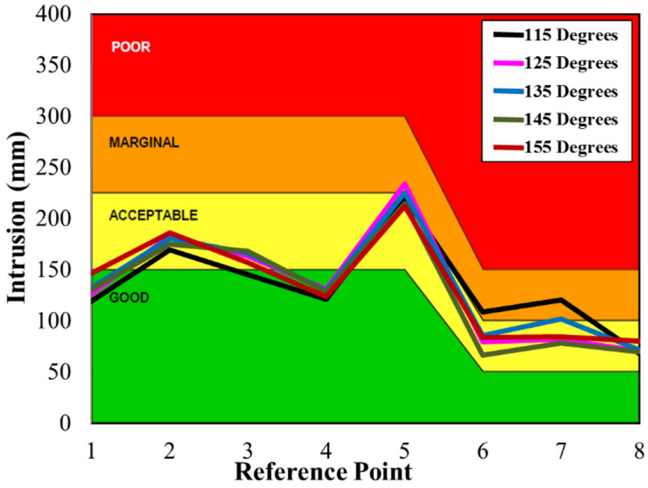

Figure 5-17 Occupant Compartment Intrusion – 50%

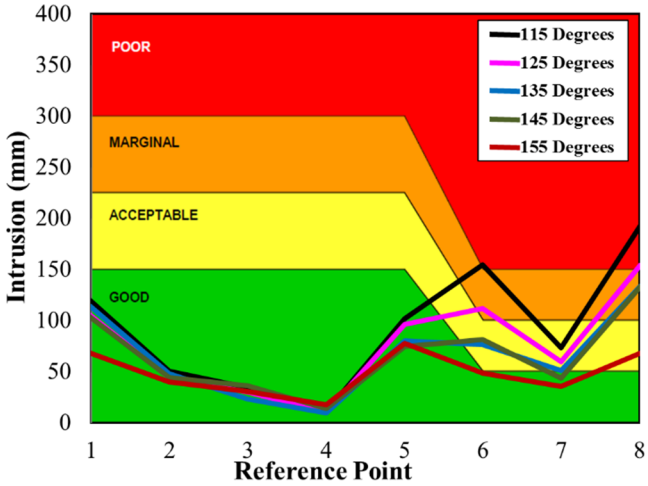

Figure 5-18 Occupant Compartment Intrusion – 30%

5.4.3 Virtual Experiment IV – Results II – 30% Overlap: Plastic Strain

The following figures show the plastic deformation of the side support structure from a 30% overlap collision at the peak impact (right before the vehicle rebounds).

Minimum Effective Plastic Strain ↔ Maximum Effective Plastic Strain

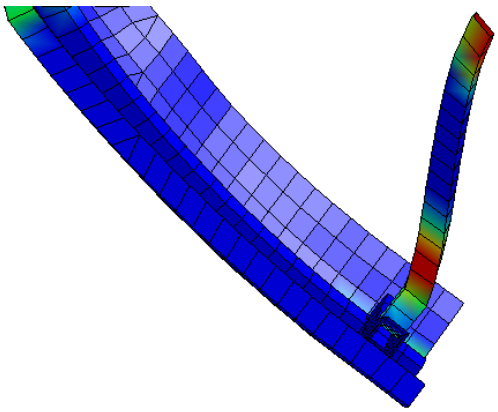

Figure 5-19 155 Degree - Top view

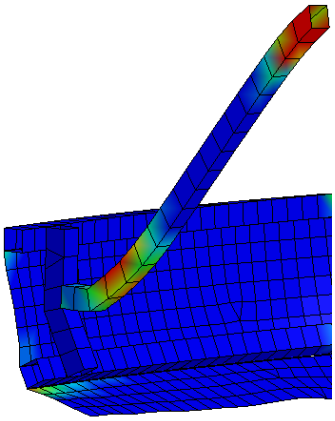

Figure 5-20 155 Degree - Back View

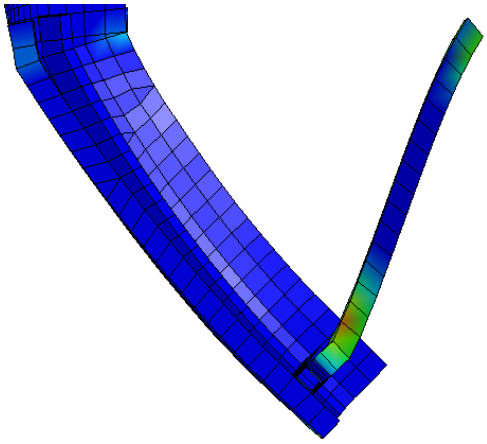

Figure 5-21 135 Degree - Top view

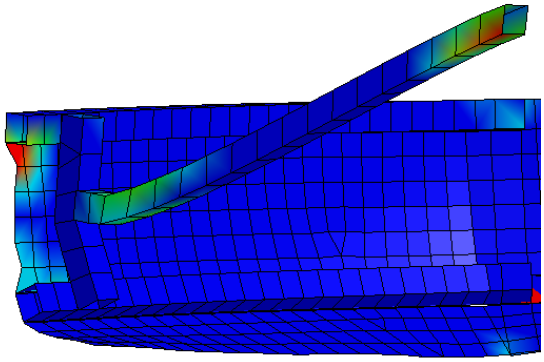

Figure 5-22 135 Degree - Back View

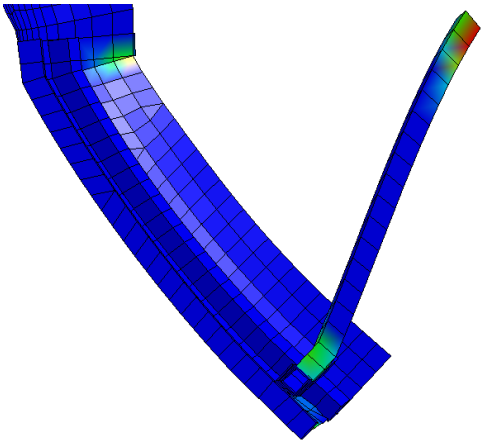

Figure 5-23 115 Degree - Top view

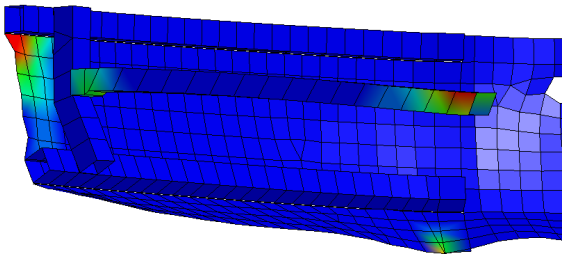

Figure 5-24 115 Degree - Back view

5.4.4 Virtual Experiment IV – Discussion & Conclusions

The 50% overlap IIHS metrics for compartment intrusion seen in Figure 5-17 illustrate similar intrusion results for all degrees, with the expectation of the reference points at the left (6) and right (7) instrument panel. The structure at 115 degrees and 135 degrees show marginally higher intrusion values. The side support structure resulted in only helping to stabilize the vehicle from rotating around the impacting chassis rail and portion of the FUPDs.

For the 30% overlap scenarios allowed for the side support to absorb the full impact of the vehicle. Figure 5-18 illustrates the IIHS metrics for compartment intrusion for 30% overlap collisions and presented a logical trend in results from the change of angles. The notion that the FUPDs side support was more rigid if it caused more intrusion into the vehicle is apparent when observing the results from the IIHS and FEA plastic deformation figures. The results concluded in a trend of reducing and leveling of the angle would increase intrusion values, therefore the structure remained more rigid and absorbed energy more effectively. Figure 5-19 to Figure 5-24 visually presents the FEA of the plastic deformation from the impact before the vehicle rebounded or slid off of the FUPDs, peak deformation and impact. From the figures, the trend shows that the increase in angle, therefore connection height to the chassis rail, would cause more bending and plastic deformation to the side structure during an impact. It would be more effective to ensure that the configuration of the side support be lower along the chassis, connecting to the bottom of the rail or other placement. An ideal location would be on the leaf spring mount, just below the chassis, Figure 5-15. The leaf spring mount is also incredibly rigid and able to with stand very high forces, concluding an ideal mounting location.

Conclusively, its recommended that there should be a side support structural member connected at a more level angle in reference to the FUPD. The angle is recommended to be between 135 to 115 degrees from the FUPD mounting to the chassis or leaf spring mount.

5.5 CHAPTER SUMMARY

Within this chapter the geometric configuration for front underride protection devices frontal impact area was investigated. Tier 1 design methodology for design was utilized with dynamic testing of the Toyota Yaris. Three of the four virtual experiments investigated with the duel springs environment while configuring the impact plate area for a desired parameter. The fourth experiment observed the placement of the attachment for side support structural member of the FUPDs.

The following was recommended from the experiments:

- The vertical impact section height be fully vertical for at least half of the frontal contact face before curving for aerodynamic design.
- The base curvature of the FUPD should be relatively near 45 degrees from the vertical section height.
- The outer curvature should be designed between 36 to 48 degrees from the chassis to promote “good” compatibility of overlap collisions.
- The side support structural member should be mounted lower to the chassis or on the leaf spring mount for improved strength of the member.

CHAPTER 6
ADDITIONAL CONSIDERATIONS FOR FUPDs PERFORMANCE

With the focus of this research on the development of front underride protection devices for head-on collisions, it was worth considering other various collisions that will likely happen. The chapter is devoted to investigating three various scenarios to consider for crashworthiness of the FUPDs. The first scenario that was investigated was heavy braking before the impact. Heavy braking causes the vehicle to dive/pitch and lower the front end of the vehicle in which may cause compatibility issues in the impact. The last two studies observed the side and rear impact from the front of the tractor-trailer to passenger vehicle was analysed to see if the FUPDs crashworthiness performance was affected and if it would improve occupant safety.

6.1 HEAVY BRAKING AND PITCHING

In a pre-collision scenario, the drivers of both vehicles are presumed to apply a large force onto the brake pedal to reduce speed and veer out of the colliding vehicle in hopes of preventing a collision or limiting damage. When the driver applies the break, the weight transfers to the front of the vehicle, compressing the suspension, and causing the front end of the vehicle to angle downwards to the ground, ie. dive. Pitching causes the vehicle's frontal structure to lower, causing a reduction in ground clearance. This change of ground clearance may cause performance issues with the FUPD to be compatible with the colliding vehicle.

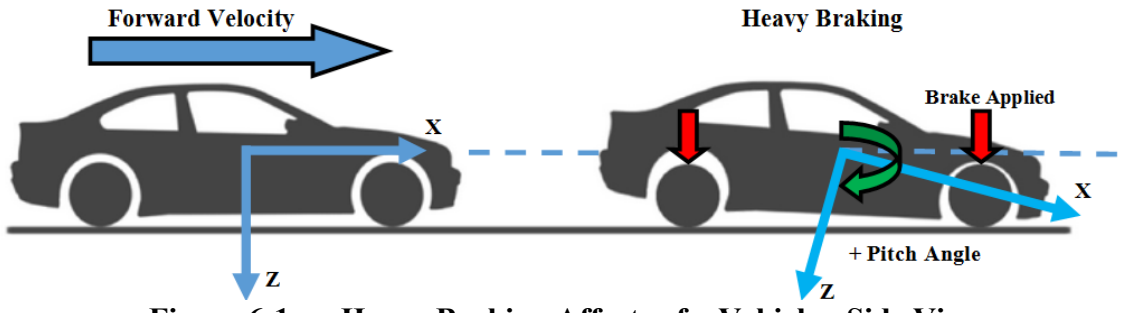

Figure 6-1 Heavy Braking Affects of a Vehicle - Side View

There has been a previous studied on FUPDs performance in a heavy braking scenario, mentioned in Section 1.3.6.2, which the passenger vehicle was only considered to brake and pitch. There was a gap in this topic as there had no consideration of the tractor-trailer pitching [5]. This is highly unlikely that the event of a pre-collision that only the passenger vehicle would only brake, however possibility is there as much as if the tractor-trailer would only brake or both would. This section extends the topic of heavy braking and pitching effects to take in account of all three scenarios: only the passenger vehicle (previously done), only the tractor-trailer, and then both heavy braking.

An important factor to take into account when setting up this problem was to knowing the closing impact velocity and pitch angle from heavy braking. This impact speed is relative to the initial velocity before braking, and duration of time before the imminent collision. To determine the closing impact speed and pitch angle, the time to collision (TTC) was assumed. TTC is the time duration of declaration from the activation of the brakes until the impact. TTC can be subjective as it can be affected by various factors; changes between age, driving experience, pre braking speed, driving conditions, etc. For heavy braking cases, studies have concluded that a TTC of 1.5 seconds or less is considered a critical impact that will cause occupant injury or fatality. Furthermore, it was concluded that the worst case time to collision while heavy braking is 1.1 second [72, 73].

The following experiment utilized the TTC to obtain impact velocities and pitch angle from heavy braking to observe and conclude on the FUPDs performance in a dynamic collision.

6.1.1 Virtual Experiment I – Impact Velocity and Pitch Angle

The first experiment into analyzing the performance of the FUPDs in a heavy braking and pitching event was to obtain accurate impact velocities and pitching angles. With the use of TruckSim and CarSim, explained in section 1.4.3, the characteristics of the Tractor-Trailer and Toyota Yaris were utilized to simulate the dynamic performance of the vehicles in a heavy braking scenario. This verification was to observe if the FEA models were accurately performing the heavy braking maneuver. Past publications concluded that the CarSim model can be accurately represented in LS-DYNA for the heavy braking with initial velocity at both 64 km/hr and 80 km/hr for only the Toyota Yaris [5]. However, there

has been no conclusions into the heavy braking effects from the tractor-trailer prospective in regards to FUPDs performance. Velocities and pitch angles of the chassis from heavy braking are both obtained and compared to the FEA models behavior in LS-DYNA.

6.1.1.1 Virtual Experiment I – Setup

Experiment I simulated heavy braking at initial velocity of 64 km/hr and 80 km/hr, this range was desired to ensure the LS-DYNA models would maintain the validity range. Heavy braking was simulated in TruckSim and CarSim by applying a max braking force to simulate a driver applying a large load onto the brake pedal. Within LS-DYNA environment, all wheels are locked (non-ABS event) from rotation after a small period of time, due to the lack of sophisticated braking systems in the FEA model. Both ABS and non-ABS configurations were both observed over a range of impact speeds which would be more likely for modern passenger vehicles.

6.1.1.2 Virtual Experiment I – Results

Legend Guideline: Software – Speed – ABS/No ABS

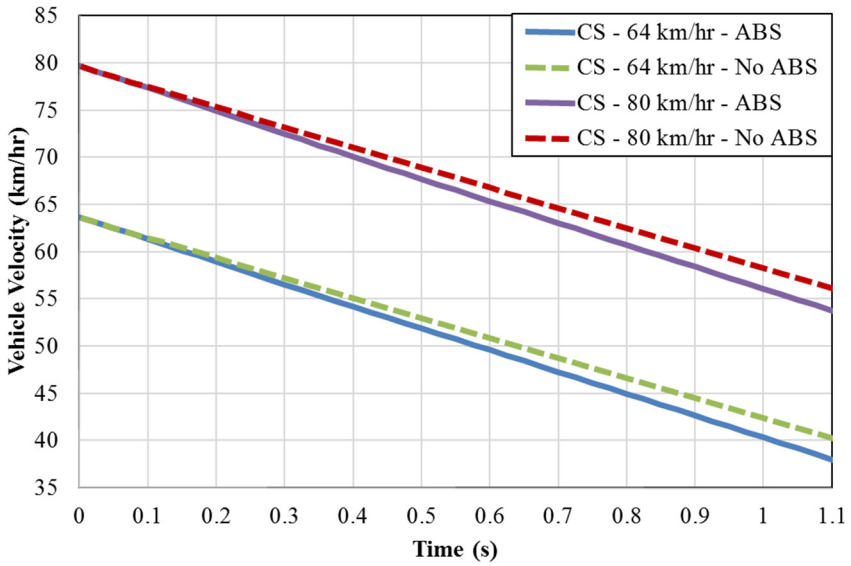

Figure 6-2 Velocity of the Toyota Yaris While Heavy Braking

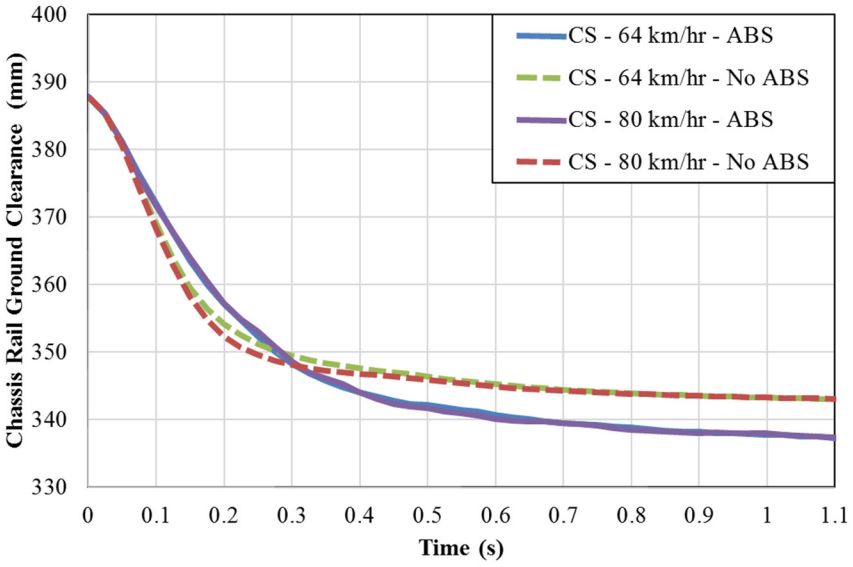

Figure 6-3 Change of Ground Clearance Height of the Toyota Yaris While Heavy Braking

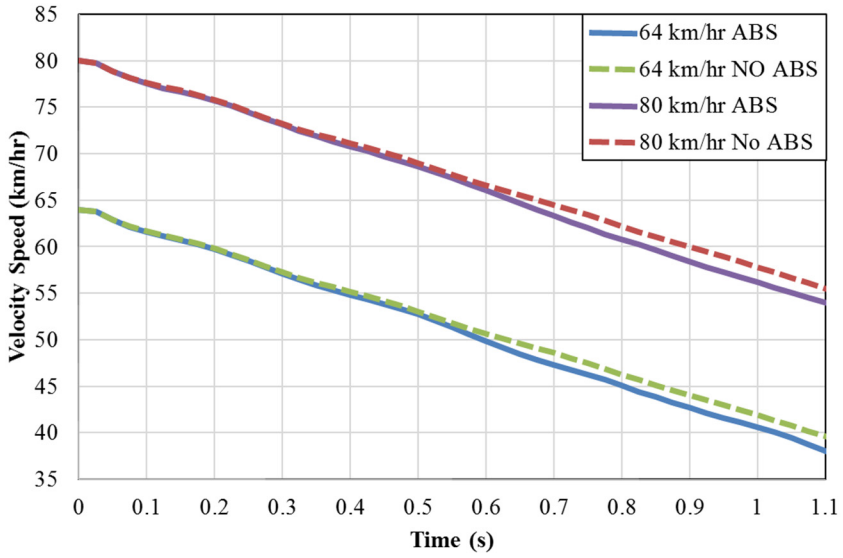

Figure 6-4 Velocity of the Tractor-Trailer While Heavy Braking

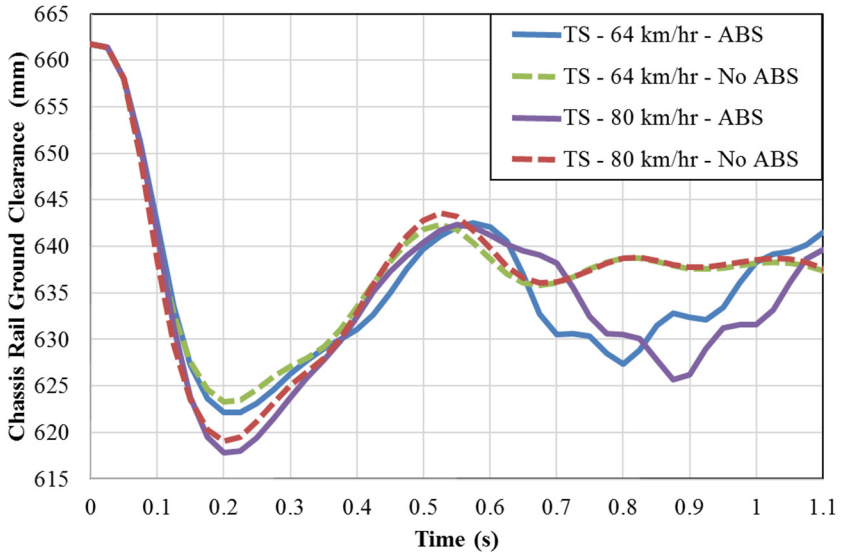

Figure 6-5 Change of Ground Clearance Height of the Tractor-Trailer While Heavy Braking

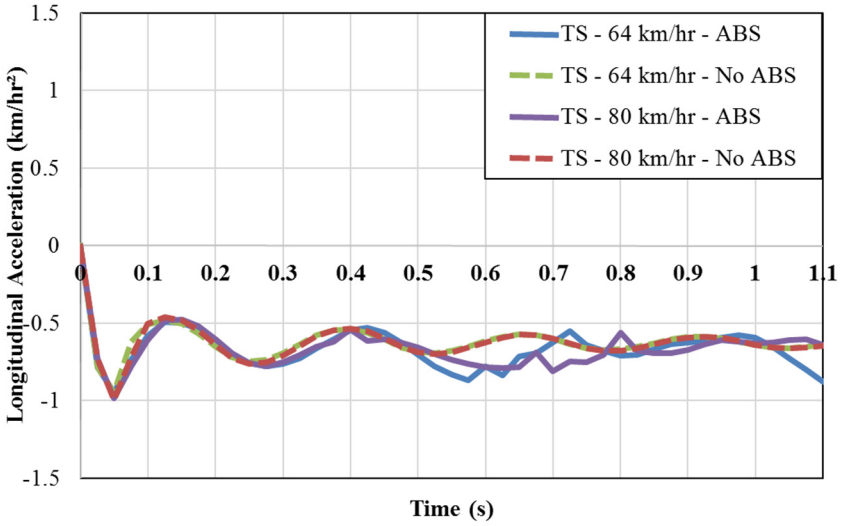

Figure 6-6 Longitudinal Acceleration of the Tractor-Trailer While Heavy Braking

6.1.1.3 Virtual Experiment I – Discussion & Conclusions

Figure 6-2 and Figure 6-3, illustrates the vehicle performance from heavy braking from CarSim of the Toyota Yaris. For the evaluation of the time of impact at 1.1 seconds, the Toyota Yaris's initial velocity of 64 km/hr had an impacting velocity of 40 km/hr with ABS and 41 km/hr without ABS. The Toyota Yaris's initial velocity of 80 km/hr had an impacting velocity of 54 km/hr with ABS and 56 km/hr without ABS. The pitching angle

of the chassis stabilized to 1.6° with ABS at 1.1 sec and 1.8° without ABS for both initial velocities. The change in ground clearance of the chassis towards the ground was affected by the pitch by 54mm with ABS, and 48mm without ABS.

For the tractor-trailer, Figure 6-4 and Figure 6-5 illustrates the results from TruckSim and the results of an impact at the TTC of 1.1 seconds. The impact velocity was found to be 54 km/hr from heavy braking from 80 km/hr and 37 km/hr from 64 km/hr. For both initial velocities, the tractor-trailer's chassis pitch stabilizes to 0.2° causing a change in ground clearance of 10mm towards the ground.

Table 6-1 Results of Impact Velocity and Change of Ground Clearance from Heavy Braking with a TTC of 1.1 seconds

	Initial Velocity	Impact Velocity	Change in Ground Clearance
Toyota Yaris	64 km/hr	40 km/hr (ABS) 41 km/hr (Without ABS)	-54 mm (ABS) -48 mm (Without)
	80 km/hr	54 km/hr (ABS) 56 km/hr (Without ABS)	
Tractor-Trailer	64 km/hr	37 km/hr	-10 mm
	80 km/hr	54 km/hr	

6.1.2 Virtual Experiment II – Heavy Braking Dynamic Collision

With the conclusions of Experiment I, dynamic collision environments were developed in LS-DYNA to experiment the performance of the FUPDs during heavy braking events.

Heavy braking of the Toyota Yaris without ABS was simulated by applying zero rotation to the vehicle's tyres after a short time. This method was the only valid method in simulating heavy braking as the FEA models do not have comprehensive braking systems. Therefore, the models can not accurately simulate air brakes of the tractor trailer or an ABS system of the Toyota Yaris. Previous research utilized the same method of applying a braking affect and resulted in a good correlation between CarSim and LS-DYNA [5].

Experiment II was devoted in observing if there was good correlation in vehicle behaviour between TruckSim and LS-DYNA for heavy braking, and to observe the collision.

6.1.2.1 Virtual Experiment II - Setup

The environments were developed for the Toyota Yaris to start at an initial speed of 64 km/hr and 80 km/hr, then apply a heavy brake from a far distance to impact head-on to the component level VNL with the single high strength steel F9 FUPDs. Next, the tractor-trailer was staged in the same manner of heavy braking and impact the stationary Toyota Yaris head-on without applied brakes.

6.1.2.2 Virtual Experiment II – Results

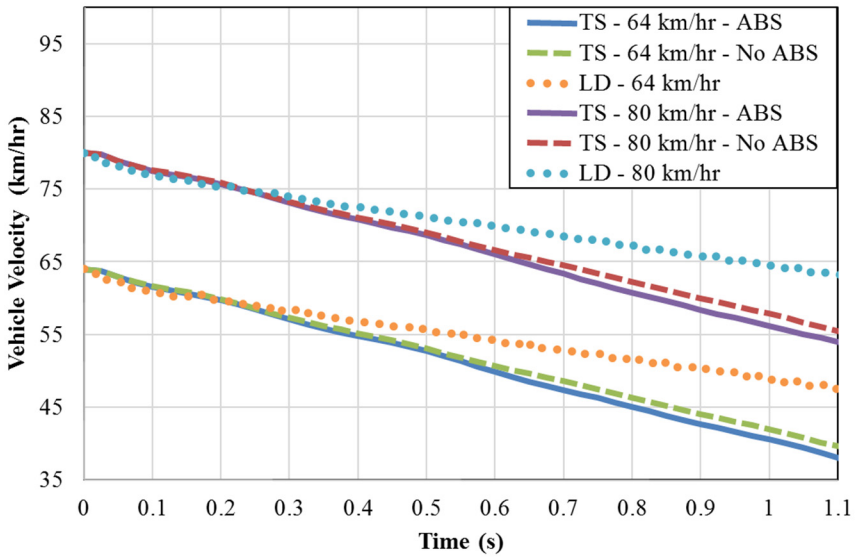

Figure 6-7 TruckSim Simulation and LS-DYNA Comparison of the Tractor-Trailer

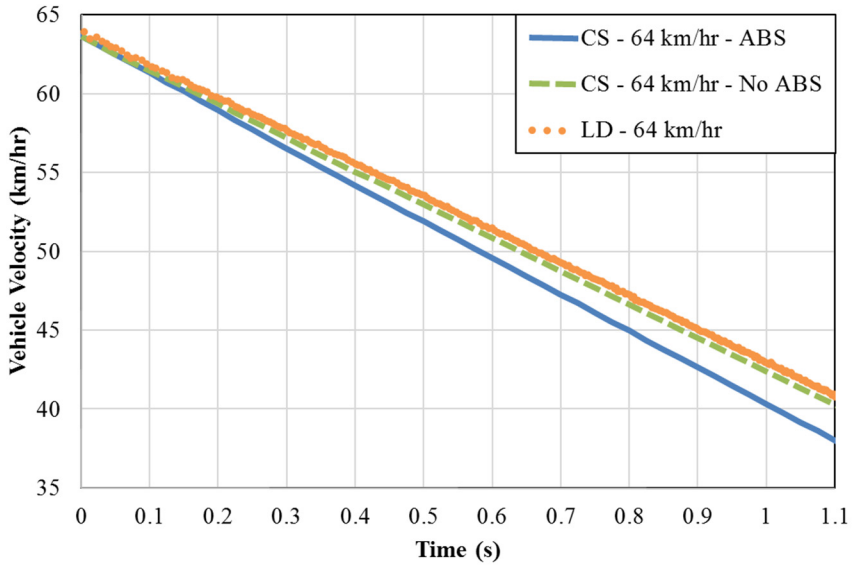

Figure 6-8 CarSim Simulation and LS-DYNA Comparison of the Toyota Yaris

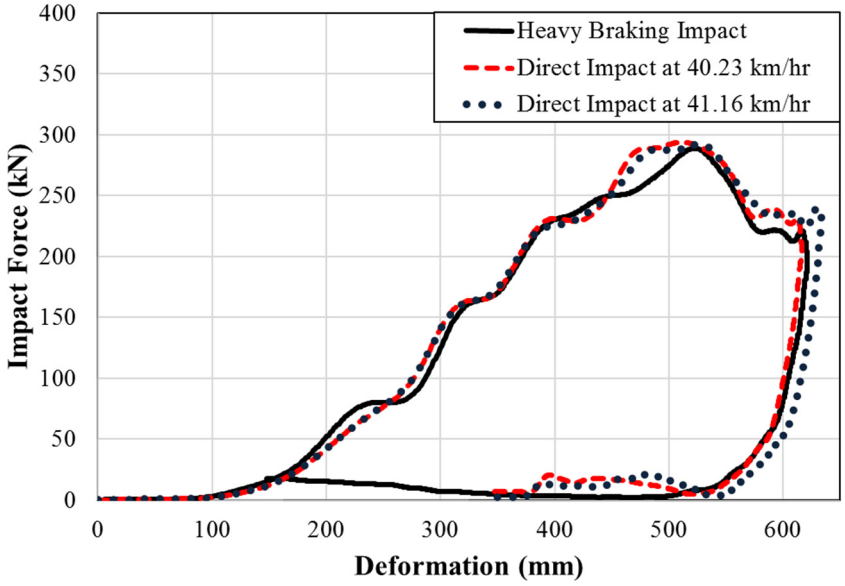

Figure 6-9 Heavy Braking of the Toyota Yaris vs. F9 FUPD Compatibility

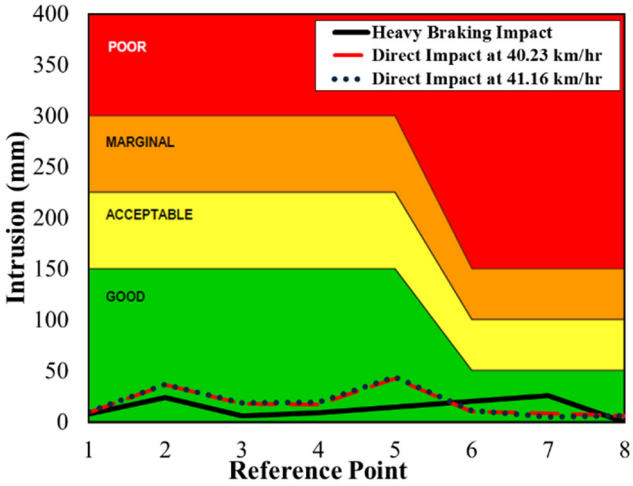

Figure 6-10 Heavy Braking of the Toyota Yaris vs. F9 FUPD IIHS Intrusion

6.1.2.3 Virtual Experiment II – Discussion & Conclusions

The experiment concluded various results and lead to analyzing a better direction for experimentation.

First, the tractor-trailer did not accomplish an accurate representation of the deceleration from heavy braking. Additionally, the FEA model did not pitch as an effect to the heavy braking, and the computational time for the experiment was extremely expensive and not feasible for experimentation on the author's computational power. Conclusively the tractor-trailer FEA model could not be accurately represented a heavy braking scenario.

The heavy braking results of the Toyota Yaris was accurately represented the declaration and impacting the FUPDs in the event, as previous research concluded. In addition, the Toyota Yaris's chassis does not pitch when heavy braking. This however can be effectively resolved by applying the pitch angle to the chassis of the FEA model from the results of Experiment I.

Another issue with this experiment was that it was computationally expensive. The LS-DYNA solver is meant for transient experiments and not long duration events. It should not need to have the vehicle starting at a far distance and heavy braking to analyze the impact at the desired velocity. To prove this, the results from the full heavy braking impact experiment (1.5 second duration) was compared to the standard dynamic experiment setup

(0.2 second duration - explained in section 2.2.3) at the impacting velocities found at 1.1 seconds from Experiment I (section 6.1.1.2). The initial 64 km/hr impacting velocities of 40.23 km/hr (with ABS) and 41.16 km/hr (without ABS) from Figure 6-2 were utilized. Figure 6-9 and Figure 6-10 shows the results and proved to correlate closely between all impacts. Conclusively, it is more computationally effective if the environment is setup at the impact instant utilizing the data (closing speed and pitch) from CarSim/TruckSim.

6.1.3 Virtual Experiment III – Heavy Braking Dynamic Collision

From the conclusions of Experiment I and II, the heavy braking dynamic collision environments were created to accurately simulate various heavy braking scenarios. In a collision it's plausible that both vehicles will apply the brakes before the impact. However, it is as plausible that only one vehicle will apply the brakes, or neither will.

6.1.3.1 Virtual Experiment III - Setup

This experiment section evaluated the different cases: No pitching from either vehicle, pitching of just the Toyota Yaris, pitching of just the tractor-trailer, and pitching of both vehicles. These cases were experimented on with an initial velocity of 80 km/hr with an impact velocity of 56 km/hr. As well, a second set of experiments that were observed at the impacting speed of 64 km/hr. A 64 km/hr impact velocity was determined through CarSim to be an initial velocity of 89 km/hr and a pitch of 0.2° for a non-ABS Toyota Yaris.

These events would be impacting the component level VNL with the rigid F9 FUPDs in only a head-on scenario (100% overlap).

6.1.3.2 Virtual Experiment III – Results

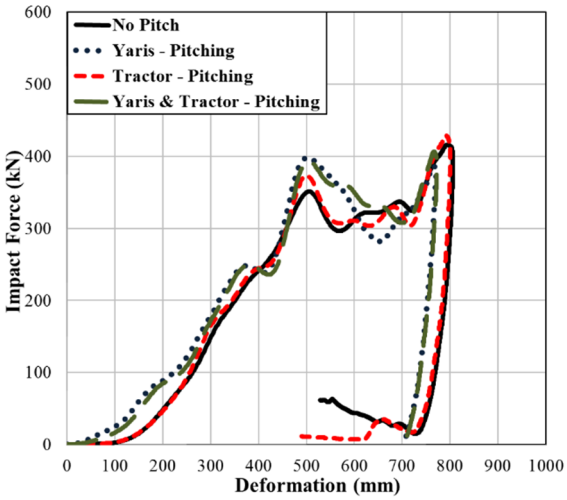

Figure 6-11 Heavy Braking Impact at 56 km/hr – 100%

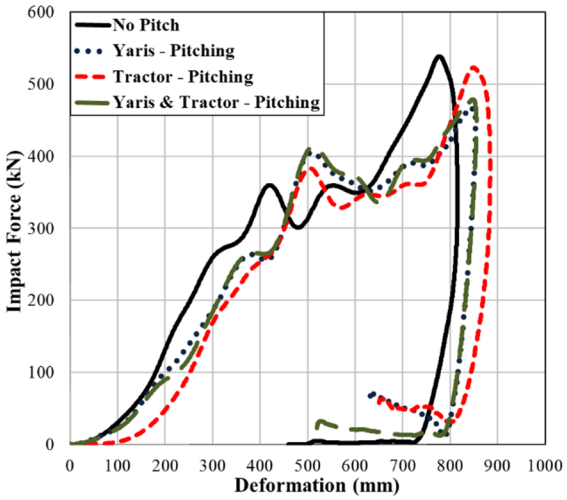

Figure 6-12 Heavy Braking Impact at 64 km/hr – 100%

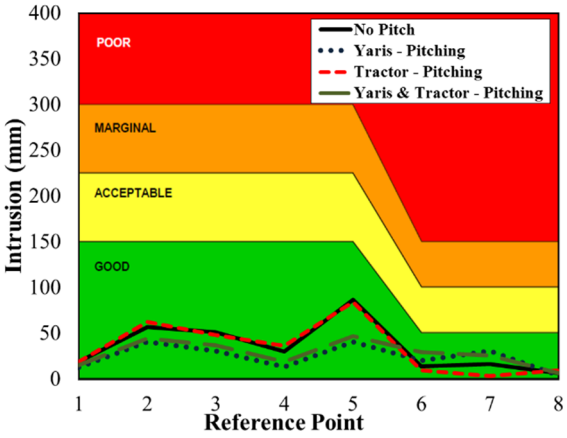

Figure 6-13 Heavy Braking Impact at 56 km/hr – 100% - IIHS

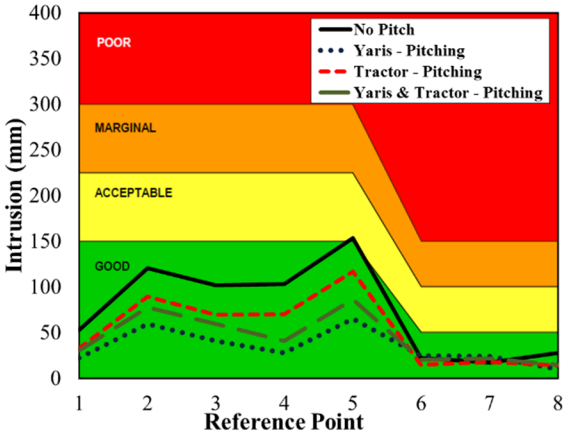

Figure 6-14 Heavy Braking Impact at 64 km/hr – 100% - IIHS

6.1.3.3 Virtual Experiment III – Discussion & Conclusions

The impact velocity of 56 km/hr, Figure 6-11 and Figure 6-13, illustrate a minor change in the impact compatibility between all four scenarios. Results show a correlation that the pitching of just the Toyota Yaris is the same at if both were to pitch. This is due to that the fact that the pitching of tractor-trailer only causes the chassis to change clearance by 8mm towards the ground. This 8mm does not cause issues with the FUPDs performance during a pitching event. Furthermore, when the tractor-trailer only pitches the event causes the same compatibility and intrusion levels as if neither vehicles were to pitch.

Results of the impacting velocity of 64 km/hr, shown in Figure 6-12 and Figure 6-14, illustrate a similar conclusion from the 56 km/hr impact. The compatibility profile of the impact for if only the Toyota Yaris pitched and if both vehicles were to pitch was almost identical. Yet the pitching of both vehicles presented a small increase in IIHS intrusion values between reference points 1-5. When the tractor-trailer would only pitch during the impact, the compatibility presented a higher deformation than if there was no pitching between both vehicles, however the IIHS results were lower.

Conclusively, the pitching effects from heavy braking does not cause any performance issues of the FUPDs. The event of both vehicles not heavy braking and pitching is a severer impact than if either or both would. Therefore, research should not focus on this matter.

6.1.4 Section Discussion

This section focused on the collision compatibility between the passenger vehicle impacting a tractor-trailer when either or both braked heavy causing a pitch angle on the chassis and impact absorption structures. The time to collision for a severe impact was assumed is to be 1.1 second and is utilized to find impacting velocities and chassis pitch angles through Trucksim and CarSim. These results were reproduced in a LS-DYNA simulation and proved that the Toyota Yaris can accurately represent heavy braking without ABS. However, the tractor-trailer failed to correlate results with TruckSim due to the lack of modeling detail of the brake system. As well, a full heavy braking experiment setup was extremely computational expensive and not effective when the solver was built to analyze from any desired velocity. The rigid F9 FUPDs was utilized for head-on impacts with the Toyota Yaris. Four difference cases of heavy braking and pitching were experimented on; when it (the tractor-trailer) would pitch, when just the Toyota Yaris would pitch, when both would, and when either would pitch. The cases presented results that were similar and did not present any failures and did not affect the compatibility of the FUPDs. It was concluded that the pitching effects from heavy braking does not cause the FUPDs to preform ineffectively. The event of both vehicles not heavily braking and pitching is a more severe impact than if either or both would. Research direction should not focus on this matter.

6.2 SIDE IMPACT OF PASSENGER VEHICLE

As research progresses the understanding that front underride protection device improves collision and occupant safety in frontal impacts is obvious, which bares the question if it improves collision and/or if the FUPDs performance holds in other impact scenarios. Side impacts (2D2V) impacts (Figure 6-15) contributed to approximately 13% of fatalities and 8.7% of injuries with tractor-trailers in Canada between 2001 and 2005 [7]. Often called a t-bone or broadside accidents, the event is when one vehicle impacts the lateral side of another. Furthermore, this section will focus on the front of tractor-trailer impacting the side passenger in which the FUPDs would be significant in the scenario.

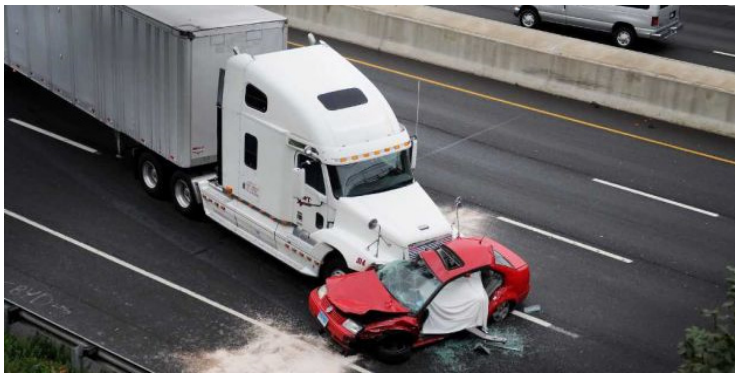

Figure 6-15 Tractor-Trailer Impacting the Side of a Volkswagen Passenger Vehicle [74] Photo: Kathleen O'Rourke

Unlike the frontal end of a vehicle with large amount of design space for impact energy absorption, the structural design of the side of a passenger vehicle does not have enough area to absorb the impact energies effectively. Side protection relies mostly on the B-pillar (Figure 6-16) and side airbags to ensure the safety of the passenger.

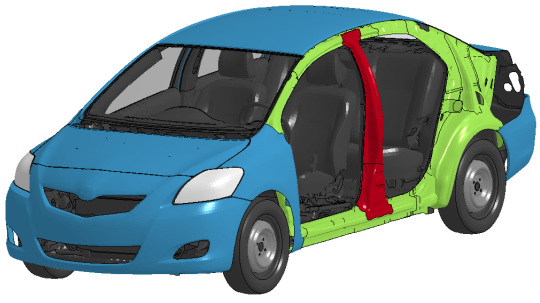

Figure 6-16 Structural B-Pillar (shown in Red) of a Toyota Yaris without Doors

The global vehicle safety analysis organizations, USA's National Highway Traffic Safety Administration (NHTSA), Economic Commission for Europe (ECE), and the Insurance Institute for Highway Safety (IIHS), have variations on side impact testing of vehicles (Figure 6-17). NHTSA's, a division of the USA department of transportation, evaluates side impact testing from the Federal Motor Vehicle Safety Standard (FMVSS 214D) Side Impact Protection Dynamic Performance Requirement. The standard tries to replicates a 1,370 kg (3,015 pound) vehicle impacting the driver side of another at 62 km/hr (38.5 mph) at an intersection. The dynamic testing utilizes a motionless vehicle (in neutral and without applied brakes) being impacted by a moving cart at 54 km/hr (33.5 mph). The cart consists of a moving deformable barrier (MDB) and honeycomb barrier face weighing 1,361 kg (3000 pound) with an impacting ground clearance of 279 mm when mounted on the test cart. The cart impacts the test vehicle at a 27° angle approach, which forms an angle of 63° with the longitudinal centerline of the test vehicle. The evaluation of the standard only relies on crash test dummies results and not structural performance [75].

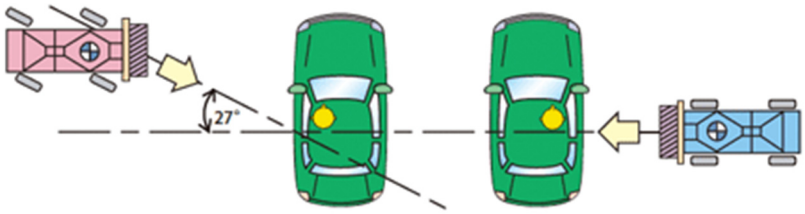

(a) FMVSS 214D (b) IIHS & ECE R95

Figure 6-17 Side Collision Testing Impact Approach Setups [76]

The Economic Commission for Europe (ECE) regulation for The Protection of the Occupants in the Event of Lateral Collision ECE R95 is widely adopted by many countries; EU, Japan, Australia, etc [76]. ECE R95 conducts a collision experiment similar to FMVSS utilizing a cart with a moving deformable barrier and honeycomb barrier face weighing 950 kg (2,100 pound) with an impacting ground clearance of ground clearance of 300 mm when mounted on the test cart. The dynamic testing utilizes a motionless vehicle (in neutral and without applied brakes) being impacted by a moving cart at 50 km/hr (31 mph). The approach of the impact is done at 90° to the impacting vehicle at the B-Pilar location. ECE R95 also does not evaluate the structural performance of the vehicle, but utilizes crash test dummies [77].

Insurance Institute for Highway Safety (IIHS), side impact guideline's testing procedure is similar to ECE R95 but with a heavier cart and considers the structural performance (Figure 6-18). The cart consists of a moving deformable barrier and honeycomb barrier face weighing 1,500 kg (3,300 pound) with an impacting ground clearance of 379 mm when mounted on the test cart. The cart impacts the test vehicle at a right angle approach of 90° to simulate a typical-height SUV or truck. IIHS evaluates the impact performance through crash test dummies results as well as structural performance of the B-Pilar. The test vehicle's structural performance is analyzed by measuring the intrusion into the occupant compartment around the B-pillar, Figure 6-19. The intrusion is gauged by the centerline of the driver's seat Figure 6-19 (b). Charts gauging the intrusion by negative numbers indicate the amount by which the crush stopped short of the seat centerline [78].

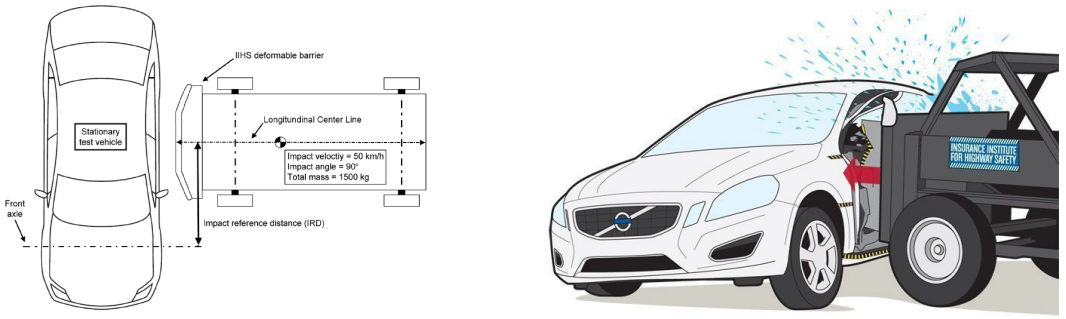

(a) IIHS Side Impact Top View [78] (b) IIHS Sled impacting a Volvo [29]

Figure 6-18 IIHS Side Impact Testing Guidelines

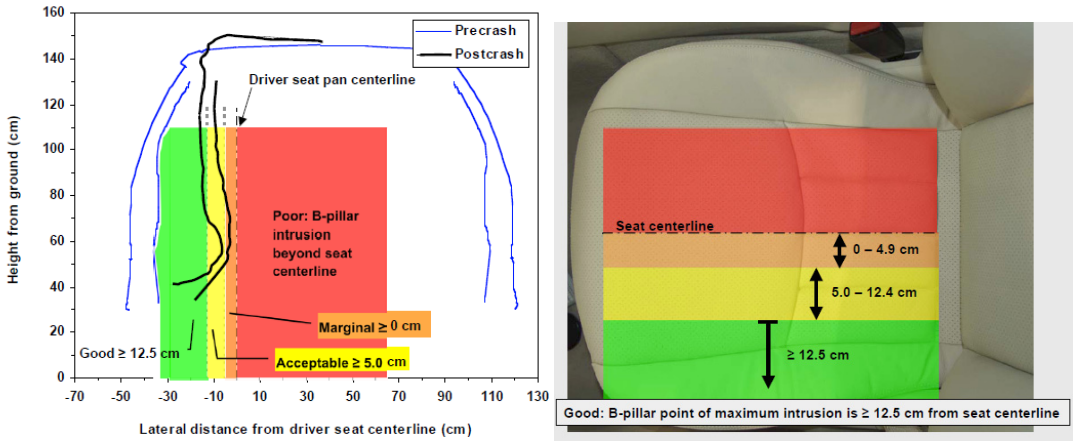

Figure 6-19 IIHS B-pillar to Longitudinal Centerline of Driver's Seat Rating [79]

Taking into consideration of all three side crash testing methodologies from FVMSS, ECE, and IIHS the testing from the IIHS is a more severe impact and higher

standard. IIHS's methodology will also evaluates the structural performance rather than just relying on dummy behaviour, which was out of scope for the research. Furthermore, it was chosen to utilize IIHS testing due to its structural analysis and available testing results.

To begin experimentation on the FEA model of the Toyota Yaris, the structural side of the vehicle needed to be validation for side collision with physical results. The model had only been validated for frontal collisions between 40-64 km/hr and there has been no research or reference to side impact testing of the model at the time of this publication. The National Crash Analysis Centre, creator and developer of the FEA vehicle model and validation, published a technical summary update of the development and validation of the Yaris model in November 2011 stating it would be in future works. Yet there has not been an update published [80]. However, all materials, geometry, and dynamics are still valid within the vehicle for up to its valid impact velocities. Therefore, to be able to conclude on the subject, the model should be validated with available physical testing results. Validation would only be done structurally and no with the research into the behaviour of crash test dummies, which should be done for accuracy when crash test dummies are more superior. After validation of being able to use the Toyota Yaris FEA model for side impact, testing of the FUPDs performance was concluded.

6.2.1 Virtual Experiment I - Structurally Validating the Toyota Yaris for IIHS Side Impact Crashworthiness Evaluation

The first goal of this section was to create a valid vurtial enviorment to experiment with the Toyota Yaris and FUPDs models. The IIHS release physical testing results for the Toyota Yaris 4-door sedan for side impact testing in which measured of occupant compartment intrusion on driver side. Testing reports CES0638 and CES0639 conclude intrusion measurements of the B-pillar to longitudinal centerline of the driver's seat was -10.5 cm and -9.5 cm, respectively [59]. This data was very useful to gauging the structural accuracy of the FEA model. The physical magnitudes show a marginal difference of 1cm between two physical tests which can be viewed as an error of ±1cm. For evaluation purposes between the physical and FEA results, a range between -9cm to -11cm of B-Pillar intrusion would be considered an acceptable range of accuracy.

Figure 6-20 IIHS Side Impact Test of a 2009 Toyota Yaris [59]

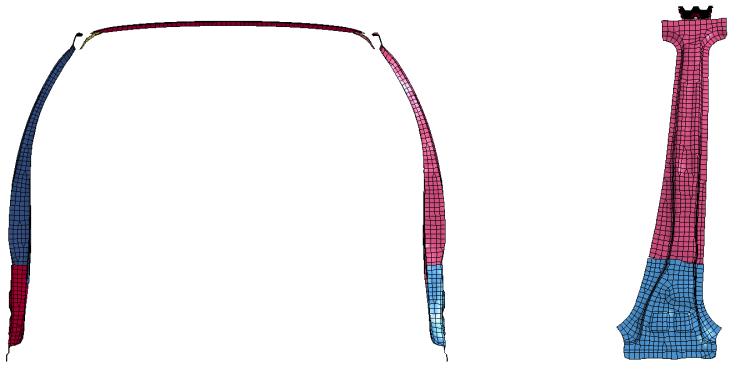

(a) Front View (b) Lateral View

Figure 6-21 Toyota Yaris B-Pilar and Roof Cross Member

These physical results can be used to validate the side impact while utlizing a valid IIHS Movable Deformable Barrier cart FEA model. LSTC released validated side impact barrier models (LSTC.IIHS_SHELL_BARRIER.150302 V3.0) for IIHS side impact testing which was utilized in this section.

6.2.1.1 Virtual Experiment I - Setup

Utilizing the Yaris's environment, the FEA IIHS cart was setup in the environment to comply with testing the IIHS experiment test setup, Figure 6-22 and Figure 6-23.

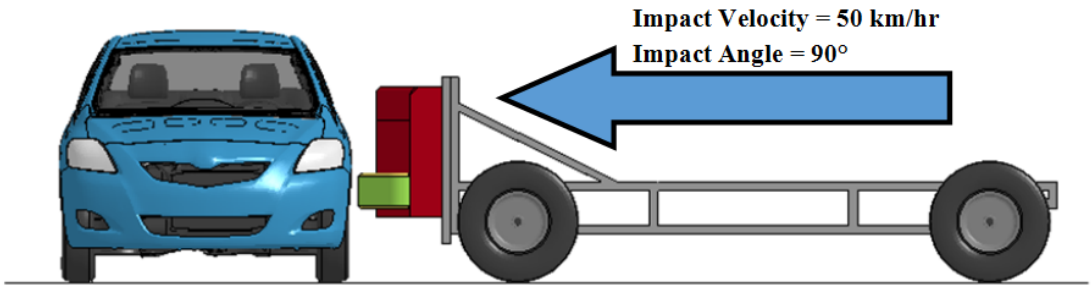

Figure 6-22 IIHS Side Impact Environment Setup

The IIHS cart was set to an impact speed of 50km/hr impacting the driver's side of the Toyota Yaris at a 90° angle centered to the B-pillar. The evaluation of the experiment utilizes the IIHS guidelines for determining the structural intrusion of the B-pillar (Figure 6-21) by using measurements from the centerline of the driver's seat, shown in Figure 6-23.

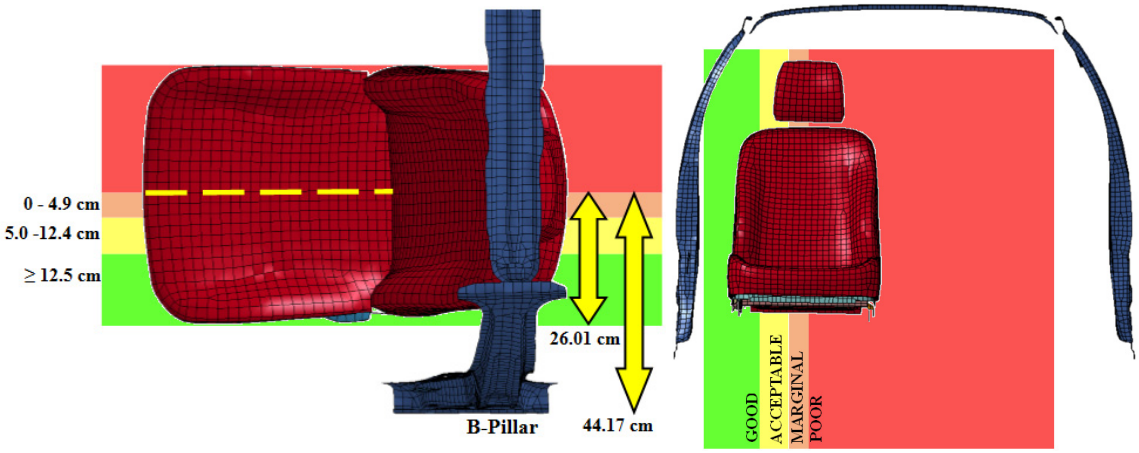

Figure 6-23 IIHS Evaluation Metric for B-Pilar Intrusion for the Toyota Yaris

6.2.1.2 Virtual Experiment I - Results

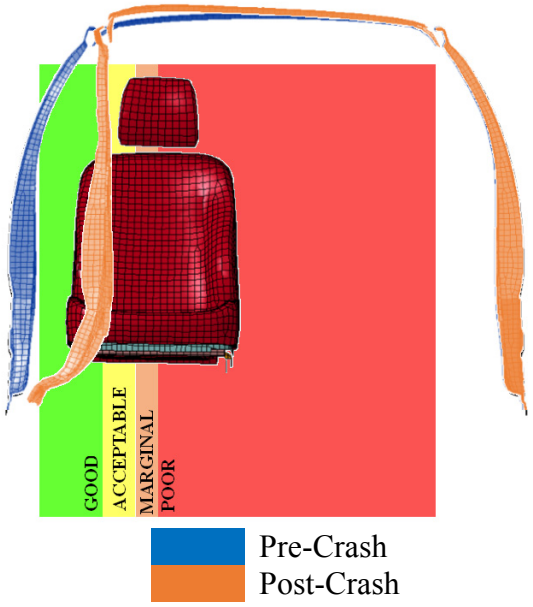

Table 6-2 Intrusion Results

	B-pillar to longitudinal centerline of driver's seat (cm)
CES0638	-10.5
CES0639	-9.5
FEA Test	-10.7

Figure 6-24 IIHS B-Pilar Vertical Profiles - Intrusion Results

Figure 6-25 Post-Crash of the FEA Toyota Yaris

6.2.1.3 Discussion & Conclusions

The FEA results from the IIHS side impact experiment of Toyota Yaris were in an acceptable accuracy range with resulting B-Pillar intrusion of -10.7cm seen in Figure 6-24. The FEA visual results seen in Figure 6-25, concluded in a similar results to the physical images in Figure 6-20 with similar deformations of the doors and B-pillar. Conclusively the results show that the structure should be valid to use for side impact experimentation. Further validation of the FEA model may be needed with the use of FEA crash test dummies to ensure the dynamic forces are accurate.

6.2.2 Virtual Experiment II – Dynamics Side Impact Crashworthiness of the FUPDs

Conclusions from the previous section proved that the FEA model of the Toyota Yaris was suitable for side impact testing with an acceptable result with respect to physical results. The next stage of this part of the research was to evaluate the performance of FUPDs. The experiment utilizes the rigid F9 FUPDs and the Component Level VNL Tractor Model to evaluation the intrusion into the lateral side of the passenger vehicle.

6.2.2.1 Virtual Experiment II - Setup

As stated in section 2.1.2.2, the front impact of the component level presents an acceptable representation of the impact from the full tractor-trailer FEA model. The component VNL was a static structure and would not be converted into a moveable structure, like the IIHS cart from the previous section. Reconstruction of the component VNL to apply the valid momentum to impact the Toyota Yaris would be very time consuming and may cause some invalided results. Furthermore, utilizing the momentum of Toyota Yaris through a lateral velocity into the VNL can represent a relatively impact into the structure to observe performance trends of FUPDs.

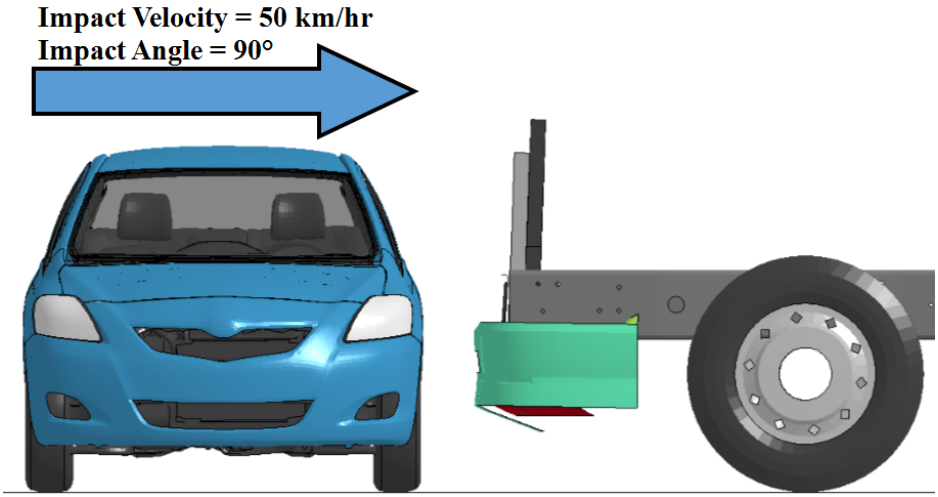

Figure 6-26 Impact Side Experiment Setup for FUPDs Testing

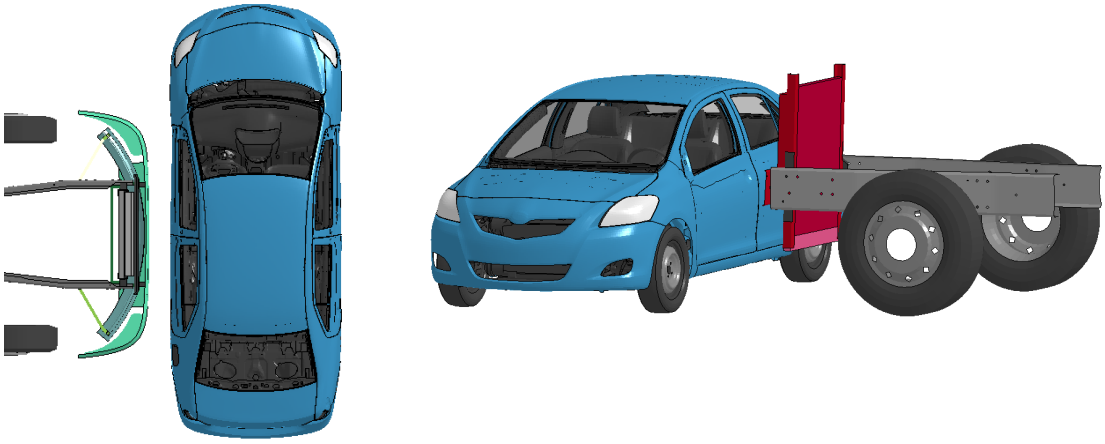

Figure 6-27 Top and Perspective View of Experiment Setup

The Toyota Yaris was positioned at 90° to the Component Level VNL Tractor Model, with and without a FUPDs attached, on the drive lateral side and initialized with a velocity of 50 km/hr directed to the model. (Figure 6-26 and Figure 6-27) The results of the experiment will be evaluated in the same matter of the IIHS Evaluation Metric for B-Pilar Intrusion, Figure 6-23.

6.2.2.2 Virtual Experiment II - Results

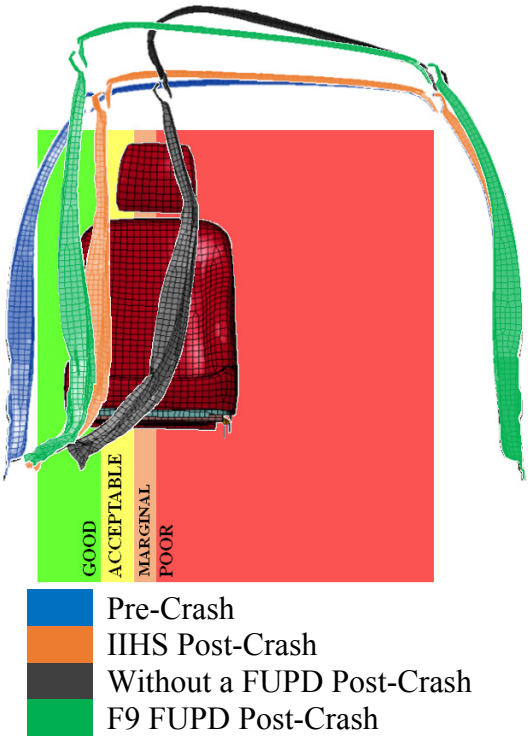

Table 6-3 Intrusion Results

Experiment	B-pillar to longitudinal centerline of driver's seat (cm)
Pre-Crash	-
IIHS	-10.7
Without a FUPD	+14.2
F9 FUPDs	-16.9

Figure 6-28 IIHS B-Pilar Vertical Profiles - Intrusion Results

Post-Crash Images from the FEA environment.

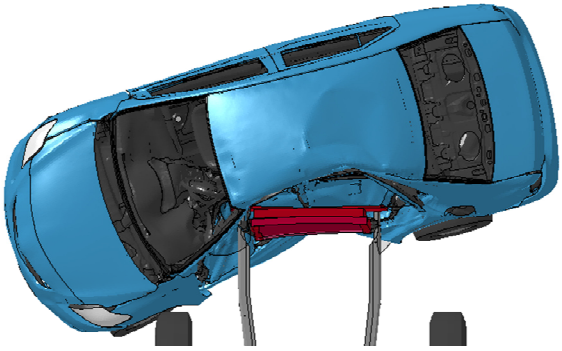

Figure 6-29 Without a FUPD Post-Crash – Top View

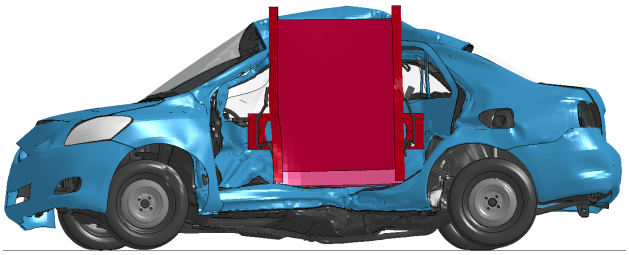

Figure 6-30 Without a FUPD – Driver Side View

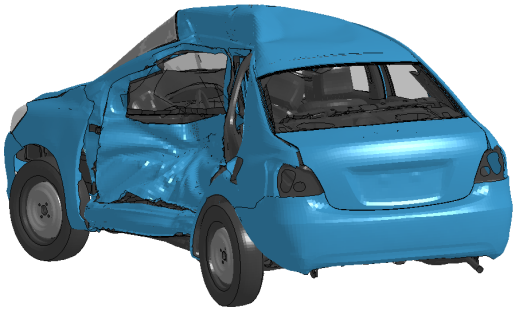

Figure 6-31 Without FUPD – Angle View

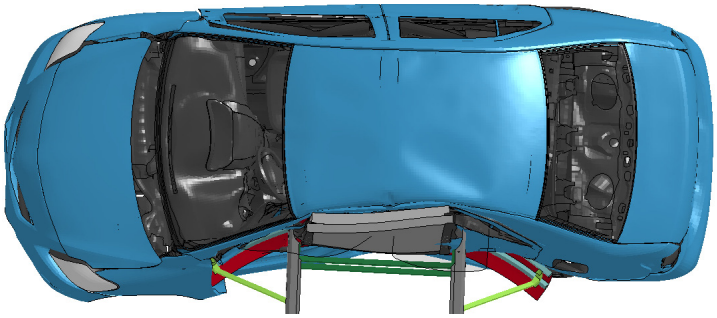

Figure 6-32 F9 FUPD Post-Crash – Top View

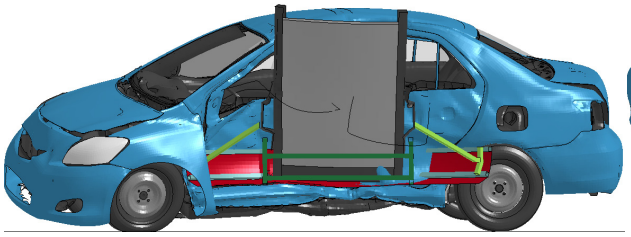

Figure 6-33 F9 FUPD – Driver Side View

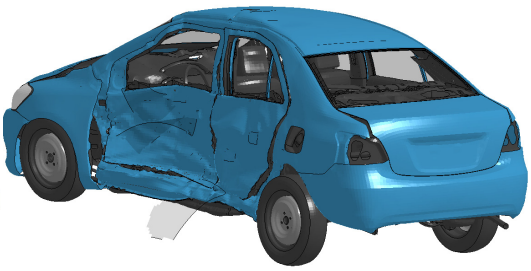

Figure 6-34 F9 FUPD – Angle View

6.2.2.3 Virtual Experiment II - Discussion & Conclusions

IIHS's guideline B-Pillar Vertical Profiles intrusion metrics, Figure 6-28 and Table 6-3, were used to evaluate the performance of the FUPDs crashworthiness in a side impact. When comparing the results, it should be noted that the IIHS validation experiment was setup with a different dynamic procedure compared to the FUPDs experiment and only shown for a reference in Figure 6-28. Furthermore, results from component level testing is within the same range of the IIHS results/physical results. The main evaluation is more for the trend of the performance of the FUPD.

Results showed that the VNL with the FUPDs attached dramatically improved the intrusion compared to without a FUPD by 31.1cm of the B-pillar intrusion across the driver's seat, which is more than half the width of the seat. Visuals from Figure 6-29 to Figure 6-34 display a lot of the reasoning for the improvement. One reasoning of the improved intrusion is the length and area the FUPDs provides to allow contact with one or both of the wheels. With the FUPDs the radiator is the main impact contact impacting the doors and B-Pillar. The impact height of the event was also lowered with the FUPDs allowing the impact to contract the stronger/wider area of the B-Pillar. For the same reasoning, the FUPDs does improve the compatibility and intrusion levels than the IIHS test results when using the cart.

6.2.3 Section Discussion

Within this section, the crashworthiness of a tractor-trailer with and without a FUPDs was evaluated during a side impact scenario. Side impacts (2D2V) impacts involving tractor-trailers are the second highest fatality rate collision event in Canada between 2001 and 2005 [7]. The FEA Toyota Yaris model was first validated from available physical data to ensure that the event can be experimented on due to the lack of verification from the developers and other researchers. The validation utilized the IIHS's side impact testing methodologies and evaluated using B-Pillar vertical profiles for intrusion. From comparing physical test data and validated FEA IIHS side impact cart, the experiment concluded that the Yaris was valid to use for B-Pillar intrusion in an acceptable range.

The second stage to this section was to evaluate the component level VNL with and without a FUPDs to analyze the performance in a side impact. Toyota Yaris impacted the VNL at a 90° angle from the driver side at 50km/hr. The experiments concluded that the FUPDs spread of structure and lower impact height allowed to improve side impact greatly.

Conclusively, the performance of the FUPDs proved to improve crashworthiness of a tractor-trailer impacting the lateral side of a passenger vehicle.

6.3 REAR IMPACT OF PASSENGAR VEHICLE

From the notions that a tractor-trailer with a FUPDs improves crashworthiness and occupant safety of the passenger vehicle in both front and side impacts, the next direction would be to analysis the rear impact of the passenger vehicle (2DV1). This section is devoted to observing rear end impacts of passenger vehicles from a tractor-trailer.

Figure 6-35 Post-Collision of a Tractor-Trailer Rear-Ending a Passenger Vehicle Photograph Credited to Weld County Sheriff's Office [81]

A Canadian study from 2001-2005 showed that rear impact (2V1D) impacts cause 9.3% of fatalities and 27.3% injuries from tractor-trailer impacts. The report, as stated before, does not suggest if the impact was from the tractor-trailer to the rear of the passenger vehicle or vice-versa, only the fact it the tractor-trailer was involved. Furthermore, this scenario had the highest survival rate compared to front and side impacts as seen in Figure 6-36 [7].

Figure 6-36 Tractor-Trailer Rear Impact Toyota Corolla in Whitby Ontario, 2014 Photograph Credited to Cook Family

Unlike side impacts and frontal collision testing of passenger vehicles, global vehicle safety analysis organizations are lacking in rear end impact regulations or

guidelines. The USA's NHTSA regulates a rear impact test of the passenger vehicle to ensure the protection of the fuel tank through FMVSS 301R-02 – Barrier Crash; Fuel System Integrity (2008 updated). The regulation importance is directed to reducing fatalities and injuries occurring from fires that result from fuel spillage during and after motor vehicle crashes. The testing utilizes an impact cart configured with a moving deformable barrier (MDB) and honeycomb barrier face weighing 1,361 kg (3000 lbs), the same as the FMVSS 214D for side impact. The cart is setup to impact the stationary test vehicle's rear side at 80 km/hr with 70% overlap, seen in Figure 6-37. The post-crash evaluation of the test only records the amount of fuel lost from the impact and does not take any account into occupant safety from the intrusion [82].

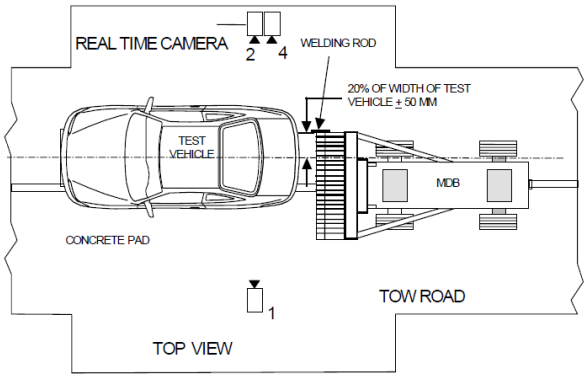

Figure 6-37 FMVSS 301R-02 – Barrier Crash Testing [82]

European regulations only evaluate the structural body of the passenger vehicle's rear and front bumper through ECE R-42; Uniform provision concerning the approval of vehicles with regard to their front and rear protective devices. The regulation observer's behaviour of certain parts of the front and rear structure of passenger cars when involved in a collision at low speeds, 4 km/hr [83]. The test utilizes a small impactor which would not represent a full vehicle impact. The test is very unrealistic for this research in which focuses on a tractor-trailer impacting at higher speeds and larger impacting area.

The IIHS guideline that focuses on rear impact directs a focus on occupant safety through a simulation of a rear end impact at 32 km/hr. The testing evaluates the seats and head restraint with geometry rating, as well as utilizing a special dummy (BioRID) that has a realistic spine [84].

Conclusively there was no direct methodology to conform to for evaluating the FUPDs. As well there was no available physical data to reference the performance of the rear structure of the FEA vehicles. Utilizing the ideals of FMVSS 301R-02 – Barrier Crash may hold some value, however the limitations of the FEA models cannot exceed their validated performance of 64 km/hr. Therefore, it was decided to create an ideal testing method and evaluation metrics to observe the FUPDs performance and focus on occupant safety. Both Toyota Yaris and Ford Taurus was utilized in this section of experiments.

6.3.1 Virtual Experiment I – Dynamic Rear Impact Setup

For this experiment since there are no resources for procedure and evaluating dynamic rear impact tests for occupant safety, it was decided to utilize methodologies of the front impact experiments. To ensure accuracy and validity of the FEA models, the impact velocity was set to 64 km/hr. The experiment would be done in two overlap scenarios: head-on 100% overlap to observe the effects of an in lane hit from the tractor-trailer and a 50% overlap scenario to reflect a more severe impact rather than the FVMSS's 70% overlap. The FMVSS 301R-02 – Barrier Crash 70% ensures that the fuel tank and exhaust system is impacted during the test to evaluate on. However, this evaluate does not focus on the safety of the occupants and the structural integrity. A 50% impact would insure that the driver side wheel and rear rail take more of the energy and to analyze the FUPDs absorption at 50% overlap. Furthermore, the 100% overlap may be more comparable to the absorption at 70% overlap from the FUPDs.

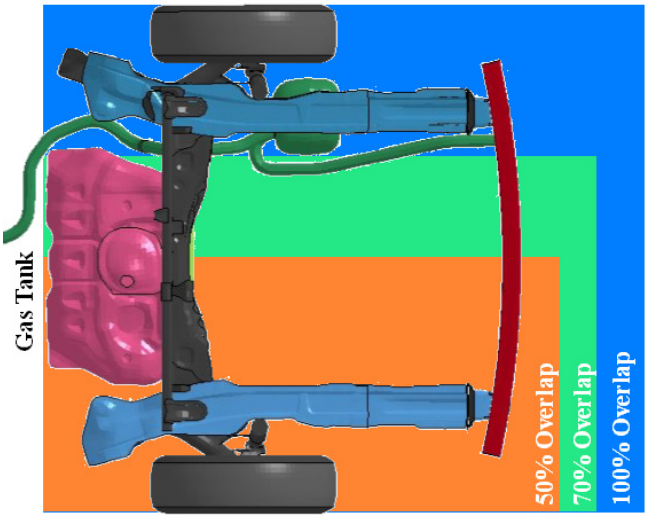

Figure 6-38 Overlap Coverage Toyota Yaris Rear Structure - Top View

As the component level VNL tractor-trailer was not mobilized to resemble a dynamic impact by giving it a velocity, the same ideal will be taken by from the side impact experiments. Utilizing the momentum of the passenger applied to the direction of the component level VNL tractor-trailer. Note the component level VNL structure was held at the end of the chassis rail.

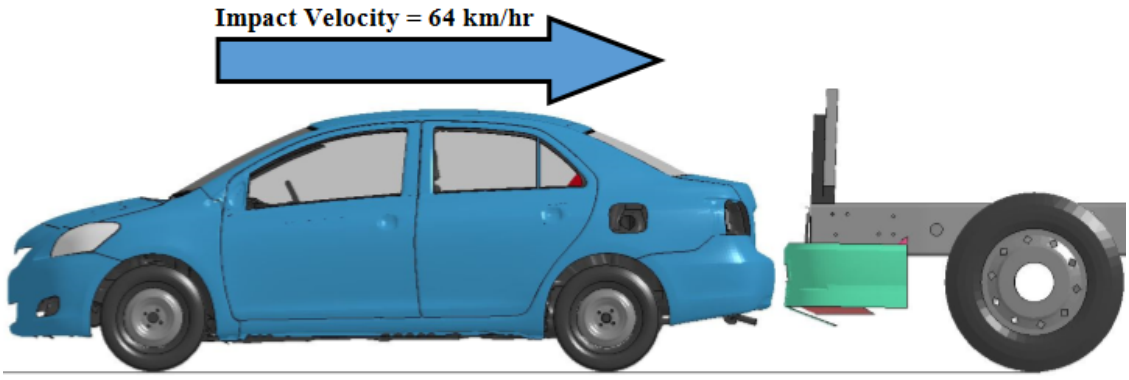

Figure 6-39 Experiment Setup with Component VNL – Side View

For a reference to the impact forces and intrusion measurements, the full FEA tractor-trailer was utilized to allow some reference. The tractor-trailer impacts the passenger vehicles at both 100% and 50% overlaps at 64 km/hr. The difference in the test was that it was designed to resemble the real world scenario. With the component level VNL structure being held in place it may resemble a braked vehicle impact. Therefore, in

this experiment the passenger vehicle was allowed to skid, with no brakes active along a high friction road.

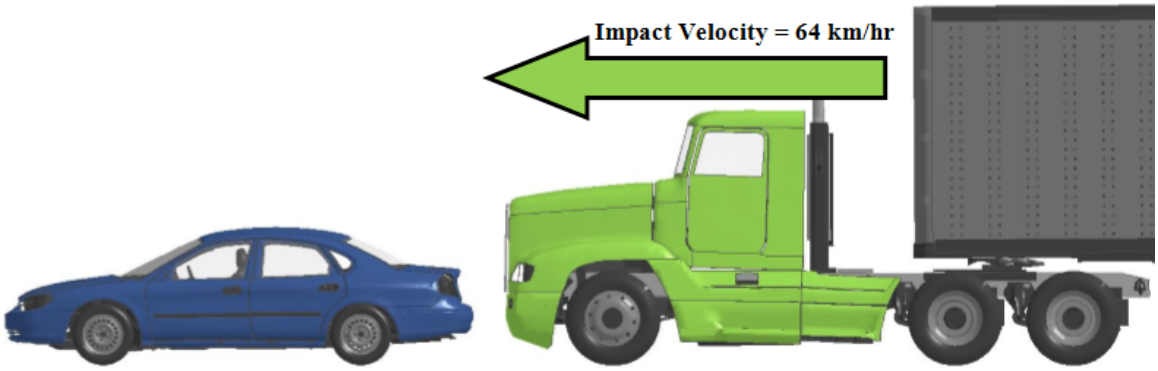

Figure 6-40 Tractor-Trailer vs. Ford Taurus Rear Impact Setup

The evaluation of the results from the rear impact took on a resemblance of the IIHS's guidelines for rating occupant compartment intrusion for front impacts metrics, section 0. Utilizing the impact force and deformation metrics ideals, from section 2.3.1, the metrics sets the deformation values to reflect the intrusion into the passenger vehicle with reference to the rear passenger head rest, Figure 6-41 and Figure 6-42 illustrate the graphical and top visual of the evaluation. Resulting with the Toyota Yaris with 1100mm from the rear plastic bumper and the Ford Taurus with 1600mm of trunk space.

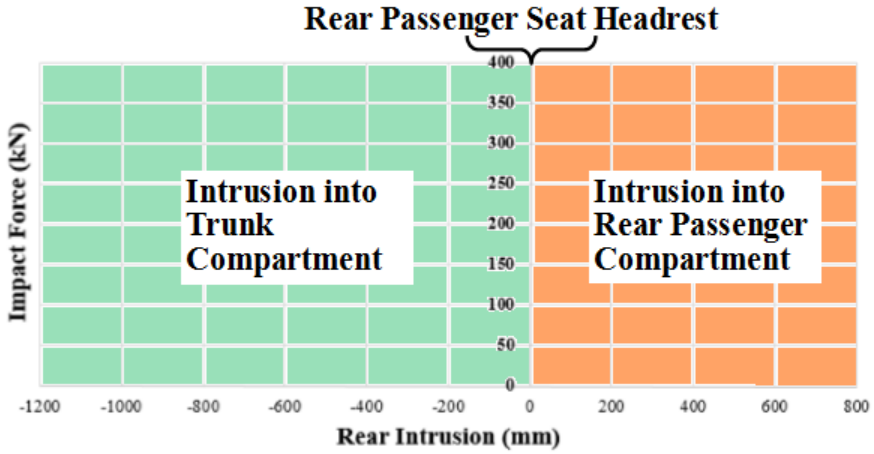

Figure 6-41 Metric for Evaluation Rear Impact Intrusion Results

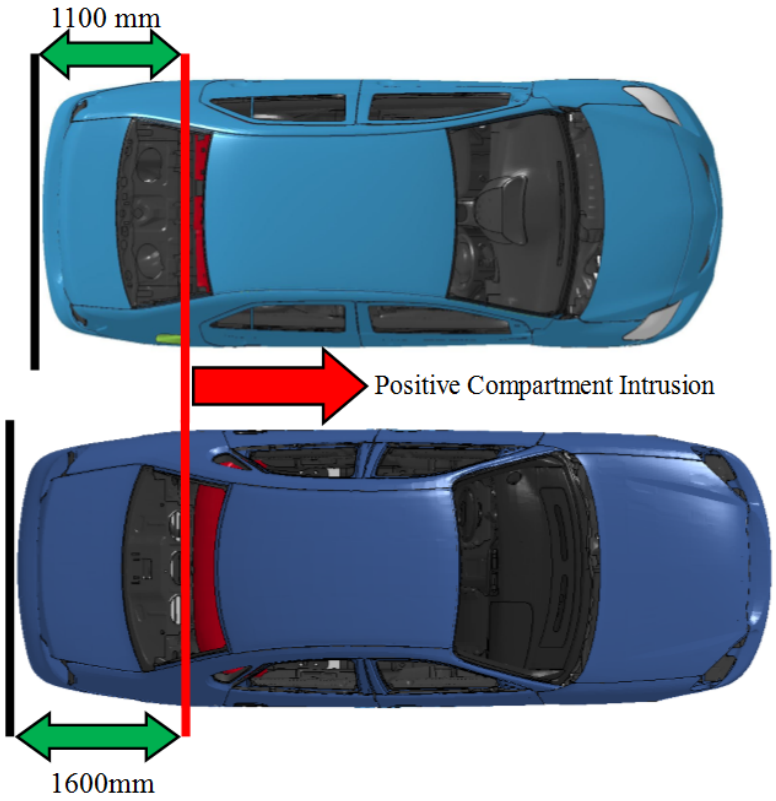

Figure 6-42 Rear Occupant Compartment Evaluation Referenced to the Rear Passenger Seat Head Rest (Dark Red) – Top View of the Toyota Yaris (Top) and Ford Taurus (Bottom)

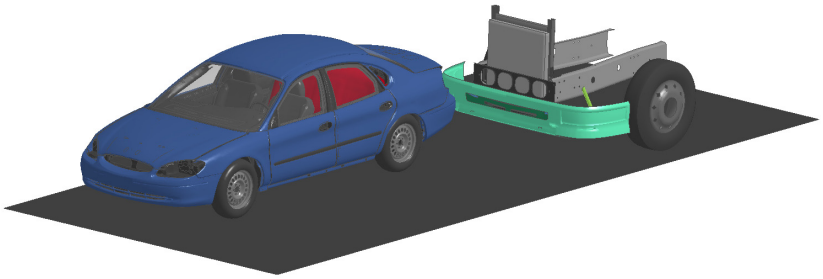

Figure 6-43 Experiment I Setup at 50% Overlap

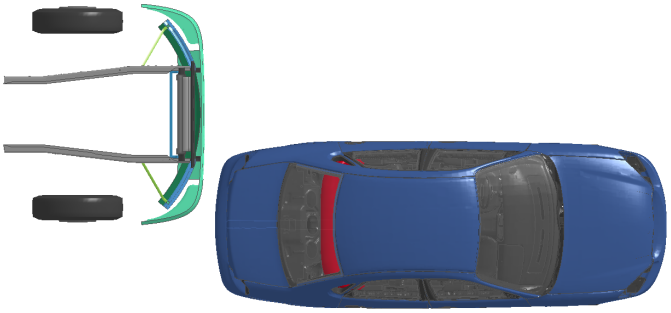

Figure 6-44 Experiment I Setup at 50% Overlap – Top View

6.3.2 Virtual Experiment I - Results

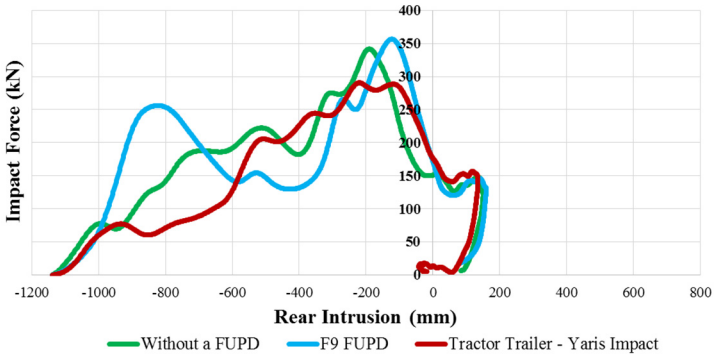

Figure 6-45 Yaris – Rear Impact – 100% Coverage (Head-on)

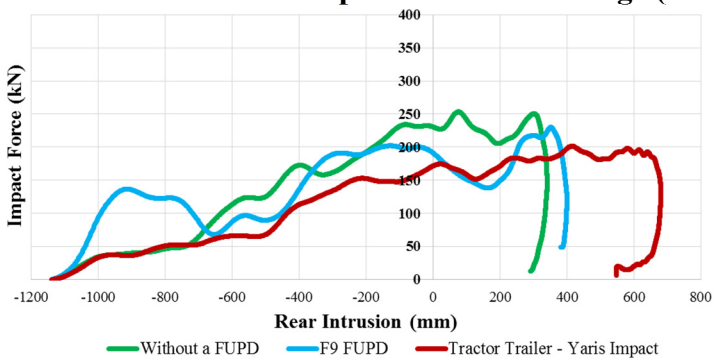

Figure 6-46 Yaris – Rear Impact – 50% Overlap

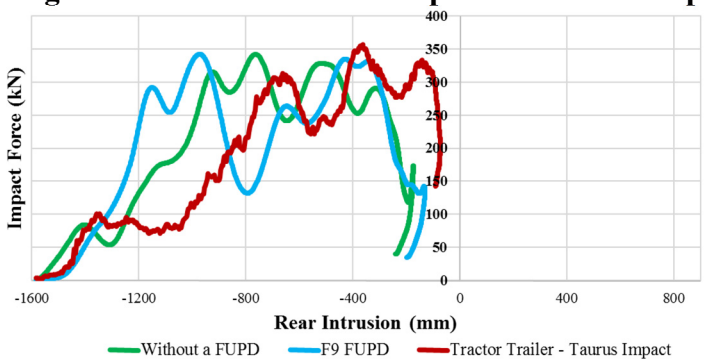

Figure 6-47 Taurus – Rear Impact – 100% Coverage (Head-on)

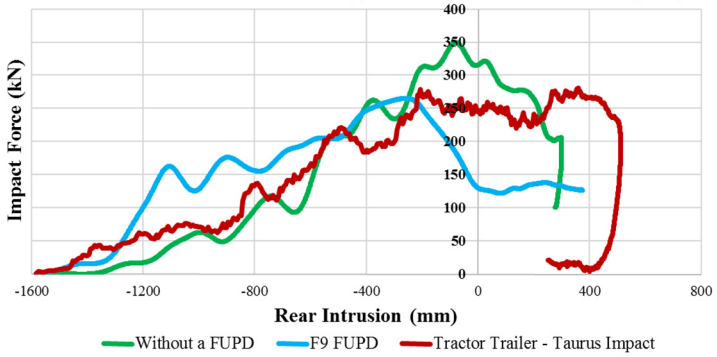

Figure 6-48 Taurus – Rear Impact – 50% Overlap

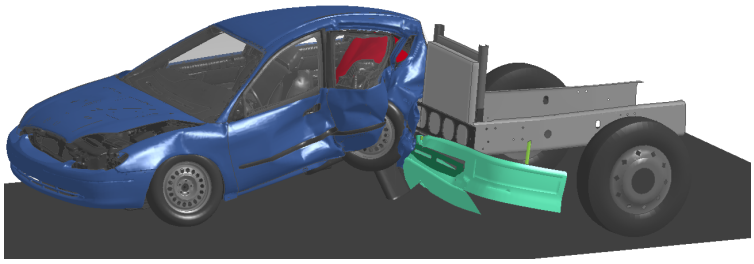

Figure 6-49 50% Overlap Rear Impact with a FUPDs – Ford Taurus

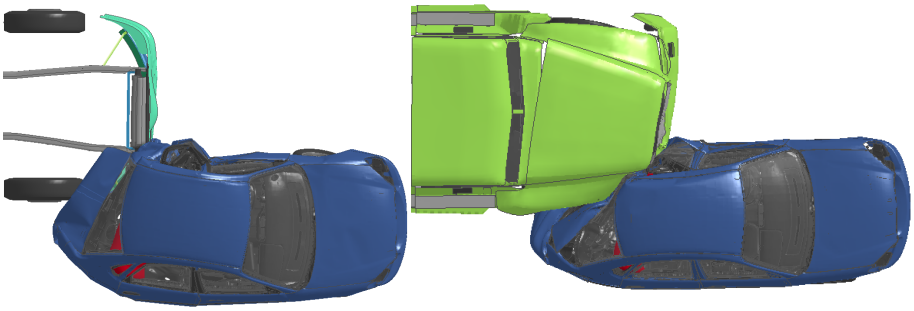

(a) VNL with a FUPDs (b) Tractor-trailer model

Figure 6-50 50% Overlap Rear Impact– Ford Taurus

6.3.3 Virtual Experiment I – Discussion

The rear impact environments utilizing the component level VNL resulted in similar results compared to the full FEA tractor-trailer impact. From the 100% coverage, Figure 6-45 and Figure 6-47, the impacts are similar in intrusion measurements and impact forces. However, the 50% overlap results in higher intrusion levels when utilizing the full tractor-trailer than the component level VNL. This can be attributable to the stationary nature of the passenger vehicle rebounding after the impact the component level VNL.

The 100% overlap of the Toyota Yaris and Ford Taurus results in the impact performances similar with and without a FUPDs, Figure 6-45 and Figure 6-47. The Toyota Yaris resulted in a failure in intrusion values with +175mm of intrusion into the rear passenger compartment. The FUPDs does not provide any improvement in occupant safety for the Yaris. The Ford Taurus proved to absorb the impact and result in a negative intrusion value only by 100mm, which would be a rather poor result. However, the FUPDs proves to allow for more intrusion. From these results it can be suggested either the FEA model is not suitable for rear deformation analysis, or the vehicles have very poor rear absorption structures. Since the materials and FEA environments are accurate and valid for the speeds,

and proven to be valid for front and side impacts deformations, it would be suggested that the rear structure of the vehicles are poorly designed for any rear impact.

At 50% overlap for both Toyota Yaris and Ford Taurus, Figure 6-46 and Figure 6-48, resulted in proving the performance of the FUPDs would cause more intrusion than without a FUPDs. With the Toyota Yaris, the FUPDs increased intrusion levels by 55mm than without a FUPDs. The Ford Taurus proved to cause very dissimilar events between with and without the FUPDs. It should be noted the F9 FUPDs simulation with the Ford Taurus did not completed to full time after various attempts due to instabilities in the solution at 12 seconds of the simulation. Furthermore, the solution yielded enough time pre-instabilities to evaluate acceptable data for that specific impact. The 50% overlap impact of the Ford Taurus also resulted with the VNL causing negative intrusion into the rear passenger compartment by +300mm. The addition of the FUPDs resulted in more intrusion than without a FUPDs, suggesting the results would outcome closer to that of the tractor-trailer.

Impact forces onto the vehicle and experienced by the passengers are relatively the equivalent between all cases of with and without FUPDs for its coverage. Therefore, force impact induced injuries may be studied without the need of analyzing the FUPDs.

Conclusively the FUPDs does not improve rear impact performance and causes a greater intrusion in overlap scenarios. The overall design of the FUPDs should not change to benefit the rear impact over the front impact. With that statement, a FUPDs designed with materials with enhanced absorption qualities may improve performance.

6.3.4 Section Discussion

This section was devoted to review the crashworthy performance of a FUPDs when the tractor-trailer impacts the rear end of a passenger vehicle. Rear impacts are the third highest fatal impact at 9.3%, however the event was the highest among injuries in Canada. It was vital to understand if the FUPDs would provide any improvement to help support the claim to overall safety improvement. Without any collision organization regulating or testing for high impact rear collisions for occupant intrusion a procedure and evaluation metric was created to analyze the FUPDs performance for rear impacts. Both component

level VNL models with and without a FUPDs was experimented on with the Toyota Yaris and Ford Taurus. The FUPDs did not improve crashworthiness in the event of a rear impact and cause more intrusion in overlapped impacts of the passenger vehicle. However, in a 100% coverage impact, in-lane impact, the FUPDs preformed similarly to without a FUPDs. Impact forces onto the vehicle and experienced by the passengers are relatively equivalent between cases of with and without FUPDs. Furthermore, force induced injuries may be studied without the need of analyzing the FUPDs.

6.4 CHAPTER SUMMARY

Within this chapter three topic were investigated and concluded on:

Heavy Breaking and Pitching Effects

- The FUPDs performances is maintained during pitching of either or both vehicles while heavy braking.
- Impacts are more severe when neither passenger vehicle and tractor-trailer pitch.

Side Impact Collisions (2V2D)

- The NCAC FEA Toyota Yaris model is structurally valid for side impact testing.
- The addition of a FUPDs improves crashworthiness of Side impacts.

Rear Impact Collisions (2V1D)

- A rear collision procedure and evaluation metric was created for investigating rear compartment intrusion for occupant safety.
- The addition FUPD does not change the outcome in a 100% overlap rear collision.
- Overlap collisions caused more intrusion to the occupant compartment of the vehicle with the addition of the FUPDs on a tractor-trailer.

CHAPTER 7
CONCLUSION AND FUTURE WORK

7.1 ACCOMPLISHMENTS & RECOMMENDATIONS

- Established a foundation for design and testing of FUPDs for use on Conventional Style Tractors, in North America
- Enhanced the tier design methodology embedded with advanced optimization methodology to guide engineering intuition
- Guards should have minimal frontal contact height of 240mm, with ground clearance set between 350mm to 400mm.
- All load points (P1, P2 and P3) are to be 160kN, and P1 could be greater.
- Set forth 2 Stage Design Optimization Methodology and successful application with crashworthy Materials.
    - System Mass reduction by 45%.
    - Material Cost reduction by 18%.
    - Maintained FUPD Performance while being light weight.
- The vertical impact section height be fully vertical for at least half of the frontal contact face before curving for aerodynamic design.
- The base curvature of the FUPD should be relatively near 45 degrees from the vertical section height.
- The outer curvature should be designed between 36 to 48 degrees from the chassis to promote “good” compatibility of overlap collisions.
- The side support structural member should be mounted lower to the chassis or on the leaf spring mount for improved strength of the member.
- The FUPDs performances is maintained during pitching of either or both vehicles while heavy braking.
- Impacts are more severe when neither passenger vehicle and tractor-trailer pitch.
- The NCAC FEA Toyota Yaris model is structurally valid for side impact testing.
- The addition of a FUPDs improves crashworthiness of side impacts.

- A rear collision procedure and evaluation metric was created for investigating rear compartment intrusion for occupant safety.
- The addition FUPD does not change the outcome in a 100% overlap rear collision. An impact with 50% overlap is more severe with an FUPD.
- Overlap collisions caused more intrusion to the occupant compartment of the vehicle with the addition of the FUPDs on a tractor-trailer.

7.2 CONCLUSIONS

The objective of the Front Underride Protection Devices project was to develop the knowledge and understanding of potential benefits to road safety when North American heavy vehicles are equipped with a FUPD. The efforts of the work were to ensure that the fundamentals of crashworthiness were built into the design of the FUPD. Ensuring that the FUPD structure was sacrificed optimally and robustly for the safety of the passenger vehicles occupants. These devices are passive structures equipped at the front of the tractor to ensure the impacting passenger vehicle does not become wedged underneath the tractor during a collision. The prevention of underriding has the potential of saving numerous lives when/if regulated in North America. With the support of Volvo Group Trucks Technology, the FUPDs design was focused on North America Conventional Style Tractors. The research contributes to the design of all heavy vehicles in North America to prevent underride.

Motivated by the lack of regulation for frontal collision protection on heavy vehicles in North America, the project builds and enhances on the European ECE R93 regulations to conform to North America style of Tractors. The modified ECE R93 for North America ensures the design of a FUPDs structural stiffness manages impact energies at direct and overlap impacts. Ideal compatibility geometry and loading requirements from regulations and publications were analyzed through Tier I design methodology with dynamic impacts of the passenger vehicles into rigid entities. Concluding that the FUPD should have a minimum section height of 240mm. In addition, the base of the FUPDs should have a ground clearance between 350mm to 400mm. It was recommended that all regulations limit the ground clearance to a maximum of 400mm, as greater clearances will

cause incompatibilities and underride. Regulations enforce quasistatic load magnitudes at three various locations to ensure structural stiffness is satisfied. ECE R93 loading conditions suggest for a direct head-on impact by regulating the FUPD to be constructed with a higher stiffness towards at the center of the tractor (P2) with a magnitude of 160kN (100% of the tractor weight). While regulating a lower stiffness on the outer side of the FUPD 80kN (P1 - 50% weight). However, it was concluded higher impacts at overlap conditions as the structural energy absorption of the passenger vehicle was lower. Therefore, the FUPD would need a higher structural stiffness. It was recommended that the ECE R93 P1 be increased to 160kN or more.

A 2 Stage Design Optimization Methodology was established to enhance Tier 2 of the design methodology. A computational effective optimization approach to designing FUPDs was established to embed the optimization of material selection for the objective to reduce weight, cost, and maintain performance under modified regulation requirements. Various grades of steels were gathered to build a collection of materials that could withstand the induced forces. The assembly of various materials optimized the FUPD to become a lightweight structure and verified for the crashworthiness through dynamic testing. The optimal design with a weight of 23.1 kg maintained the crashworthy performance of a FUPD weighing 65% more.

Due to the aerodynamic shape of North American Conventional Tractors, the geometry of the FUPD would need to conform to the aerodynamic curvatures. However, limitations were recommended to ensure aerodynamic curvatures does not induce underride. It was recommended that; The vertical impact section height be fully vertical for at least half of the frontal contact face before curving for aerodynamic design. The base curvature of the FUPD should be relatively near 45 degrees from the vertical section height. The outer curvature should be designed between 36 to 48 degrees from the chassis to promote “good” compatibility of overlap collisions. In addition, placement of the side support structure was investigated for the optimal position. It was recommended that the side support structural member should be mounted lower to the chassis or on the leaf spring mount for improved strength of the member.

With the focus of this research on the development of front underride protection devices for head-on collisions, the FUPDs performance would possibly be affected in other collisions scenarios. Heavy braking from either vehicle before an impact is a very plausible event to be considered in a frontal crash. Heavy braking causes the vehicle to dive/pitch and lower the front end of the vehicle in which may cause compatibility issues in the impact with the FUPD. From conclusions, the FUPD performance was not affected while heavy pitch of either or both vehicles. Side impact collisions from the tractor impacting the side of the passenger vehicle was investigated. The first notion of the study concluded on the validity of using the NCAC Toyota Yaris for side impact experiments, with acceptable measurements compared to physical testing. After validating the Toyota Yaris for side impacts, it was concluded that the FUPDs would improve impact compatibly in a side impact. The FUPDs reduced B-Pilar intrusion into the occupant's compartment greatly compared to without a FUPD. The final impact studied concluded on the tractor impacting the rear side of the passenger vehicle. Results concluded that a rear impact by a tractor with a FUPD would be similar without one.

7.3 FUTURE WORK

Future work for the front underride protection devices need to build upon the full 3 tier design methodology and the 2 stage design optimization with enhanced performance metrics. The research lacks the ability to analyze the forces/acceleration on the occupants due to inaccurate crash test dummy models, anthropomorphic test device (ATD). Once finite element analysis dummies are accurate enough to conclude on valid measurements, and not just trends, the research should be directed into lowering occupant injuries of the impact impulses.

More investigations into material application of the FUPDs is needed as there are a wide range of materials that could be used to reduce weight of the FUPD while ensuring the crashworthiness. The combination of utilizing both aluminum and steel should be investigated, ie. using foam aluminum inside of steel beams.

Regulated and recommended ECE R93 point load P3 magnitudes needs a more solidified conclusion; whether or not the magnitude should be 80kN, 160kN, or more. There are many parameters to be considered, such as with the absorption characteristics of the radiator, and energy management from impact. This type of investigation needs to be completed with deformable FUPDs to gage structural stiffness. Its recommended, from the authors experience, that the 80 kN magnitude should be adequate, however this should be confirmed.

Outside of the realm of structural design, the dynamic effects from the added weight to the front end of the chassis should be verified to ensure tractor dynamics are not affected.

PUBLICATIONS

Cook, A., El-Gindy, M., and Critchley, D., "Front Underride Protection Devices (FUPDs): Multi-Objective Optimization," *SAE 2015 World Congress & Exhibition, Occupant Protection: Structural Crashworthiness and Occupant Safety,* paper number: 2015-01-1488.

Cook, A., El-Gindy, M., Aveline, R. "Multi-Objective Optimization of Crashworthy Materials in Underride Protection Devices in Tractor-Trailers" International Journal of Crashworthiness, (submitted)

Cook, A., El-Gindy, M., Aveline, R. "Influence of Front Underride Protection Devices Performance in Disproportioned Collisions Scenarios" International Journal of Crashworthiness, (submitted)

Note parts of the above publications are by the author and is contained in this work. All of writing, testing, data and research conducted in this work and publications was completed by the author. The co-authors reviewed and provided technical support when needed to the work.

REFERENCES

[1] CANSIM, "Motor vehicle registrations, by province and territory," Statistics Canada, 2015.

[2] Bureau of Transportation Statistics, "National Transportation Statistics," U.S. Department of Transportation, Washington, 2015.

[3] D. Glassbrenner, "An Analysis of Recent Improvements to Vehicle Safety," U.S. Department of Transportation - National Highway Traffic Safety Administration, Washington, 2012.

[4] D. Kristy, "Head-On Crash Snarls Traffic On County Road 42," Windsor Star, Windsor, 2012.

[5] T. MacDonald, *Front Underride Protection Devices: Methods for Design and Testing,* Oshawa, ON: Dept. FEAS, University of Ontario Institute of Technology, 2014.

[6] M. Castellanos, M. El-Gindy, C. Fedishen, D. Maciejewski and A. Atahan, "Truck Front Underride Development: Literature Survery," *International Journal of Heavy Vehicle Systems,* vol. Volume, no. Issue, pp. 18-34, 2010.

[7] Road Safety and Motor Vehicle Regulation Directorate, "Heavy Truck Casualty Collisions 2001 - 2005," Transport Canada, Ottawa, 2010.

[8] European Parliament and the Council of the European Union, "Directive 2000/40/EC of the European Parliament and of the Council," *Official Journal of the European Communities,* pp. 9-28, 2000.

[9] UNECE, "Regulation No. 93 - Front Underrun Protection," 1994. [Online]. Available: http://www.unece.org/fileadmin/DAM/trans/main/wp29/wp29regs/R093e.pdf.

[10] Y. Sukeawa, *Japan's Approach to FUPD,* Japan Automobile Research Institute, 2006.

[11] Australia, "Vehicle Standard (Australian Design Rule 84/00 - Front Underrun Impact Protection) 2009," Minister for Infrastructue, Transport, Regional Development and Local Government, 2009.

[12] Government of India, "Automotive Industry Standard AIS-069," Automotive Reasearch Association of India, Pune, 2006.

[13] G. Baldwin, "Too Many Trucks on the Road?," Statistics Canada: Transportation Division, Ottawa, 2009.

[14] Insurance Institute for Highway Safety (IIHS), "Factality Facts - Large trucks 2013," [Online]. Available: http://www.iihs.org/iihs/topics/t/large-trucks/fatalityfacts/large-trucks. [Accessed 1 February 2016].

[15] "Large Truck Crash Overview 2011," U.S. Department of Transportation, Washington, 2013.

[16] TRL, TNO, Chalmers, BASt, UTAC, Volvo, GDV, DAF, DC, Scania, UPM, CIM, "Improvement of Vehicle Crash Compatibility through the Development of Crash Test Procedures," TRL and TNO, 2007.

[17] P. Galipeau-Bélair, *Design and Development of Side Underride Protection Devices (SUPD) for Heavy Vehicles,* Oshawa: Dept. FEAS, University of Ontario Institute of Technology, 2014.

[18] FKA, "Final Report: Design of a Tractor for Optimised Safety and Fuel Consumption," 2011. [Online]. Available: http://www.transportenvironment.org/sites/te/files/media/2012%2002%20FKA%20Smart%20Cab%20study_web.pdf.

[19] D. Freund, "HVTT11," 2010. [Online]. Available: http://hvttconference.com/hvtt11/proceedings/papers/2b1/2b1%20Paper.pdf.

[20] "Volvo Trucks," Volvo Trucks, 2015. [Online]. Available: https://www.flickr.com/photos/volvotrucks. [Accessed 1 February 2016].

[21] L. Hjelm and B. Bergqvist, "European Truck Aerodynamics - A Comparison Between Conventional and CoE Truck Aerodynamics and a Look into Future Trends and Possibilities," *The Aerodynamics of Heavy Vehicles II: Trucks, Buses and Trains,* pp. 469-477, 2009.

[22] "Set-Back or Set-Forward?," CAT, 9 Novemeber 2014. [Online]. Available: http://www.drivecat.com/blog/2014/11/set-back-or-set-forward/. [Accessed February 2016].

[23] National Highway Traffic Safety Administration, "Heavy-Vehicle Crash Data Collection And Analysis to Characterize Rear and Side Underride and Front Override in Fatal Truck Crashes," U.S. Department of Transportation, Washington, 2013.

[24] "Mach Trucks," 2015. [Online]. Available: http://www.macktrucks.com/. [Accessed 1 February 2016].

[25] "Fixed Rigid Barrier Collision Tests(SAE J 850)," SAE International , Detroit, 2015.

[26] Canadian Motor Vehicle Safety Standards, "Occupant Crash Protection (CMVSS No. 208, 0R)," Transport Canada, Ottawa, 2013.

[27] National Highway Traffic Safety Administration, "Occupant Crash Protection (FMVSS 208)," U.S. Department of Transportation, Washington, 2013.

[28] Insurance Institute for Highway Safety, "Frontal Crash Test," Arlington, 2016.

[29] C. PHILPOT, "Crash Course: How Current Impact Tests Make Cars Safer," Car and Driver, December 2012. [Online]. Available: http://www.caranddriver.com/features/crash-course-how-current-impact-tests-make-cars-safer-feature. [Accessed 1 January 2016].

[30] Economic Commission for Europe, "Frontal Collision Protection - ECE R94," Geneva, 2013.

[31] South Korea's Ministry of Land, Transport, and Maritime Affairs (KNCAP), "Regulations on New Car Assessment Program Testing, ETC. (Notice 2009-102)," Sejong City, 2009.

[32] J. Lambert and G. Rechnitzer, "Review of Truck Safety: Stage 1: Frontal, Side and Rear Underrun Protection," Monash University - Accident Research Centre, 2002.

[33] A. Krusper and R. Thomson, "Crash Compatibility Between Heavy Goods Vehicles and Passenger Cars: Structural Interaction Analysis and In-Depth Accident Analysis," in *International Conference on Heavy Vehicles*, Paris, 2008.

[34] J. Anderson, "Inventory of Current Underrun Devices," Cranfield Impact Centre, VC-Compat, 2003.

[35] "Test Method 223 Rear Impact Guard," Transport Canada: Standards Research and Development Branch, Ottawa, 2003.

[36] "FMVSS 223," NHTSA, [Online]. Available: http://www.nhtsa.gov/DOT/NHTSA/Vehicle%20Safety/Test%20Procedures/Associated%20Files/TP-223-00.pdf.

[37] "New crash tests: Underride guards on most big rigs leave passenger vehicle occupants at risk in certain crashes," Insurance Institute for Highway Safety, Arlington, 2013.

[38] "NHTSA signals plan to address deaths in underride crashes," Insurance Institute for Highway Safety, Arlington, 2014.

[39] "Rear underride guard mandate may extend to more trucks under NHTSA proposal," Insurance Institute for Highway Safety, Arlington, 2015.

[40] A. Krusper and R. Thomson, "Energy-Absorbing FUPDs and their Interactions with Fronts of Passenger Cars," *International Journal of Crashworthiness,* pp. 635-647, 2010.

[41] Livermore Software Technology Corporation, "LS-TaSC Topology and Shape Computations for LS-DYNA User's Manual," Livermore, California, 2011.

[42] Livermore Software Technology Corporation, "LS-DYNA Theory Manual," Livermore, California, 2006.

[43] "LS DYNA for Automotive Crash," Livermore Software Technology Corporation, [Online]. Available: http://www.lstc.com/.

[44] Livermore Software Technology Corporation, "LS-OPT User Manual," Livermore Software Technology Corporation, Livermore, 2013.

[45] "CarSim - TruckSim," Mechanical Simulation Corporation, 2016. [Online]. Available: https://www.carsim.com/.

[46] X.-S. Yang, Engineering Optimization: An Introduction with Metaheuristic Applications, Hoboken, NJ: John Wiley & Sons, Inc., 2010.

[47] A. Ryberg, R. Domeij Backryd and L. Nilsson, "Metamodel-Based Multidisciplinary Design Optimization for Automotive Applications," LiU-Tryck, Linköping, Sweden, 2012.

[48] S. Rao, Engineering Optimization, New Jersey: Wiley, 2009.

[49] R. D'Souza, C. Sekaran and A. Kandasamy, "Improved NSGA-II Based on a Novel Ranking Scheme," *Journal of Computing,* vol. 2, no. 2, February 2010.

[50] E. Zitzler, M. Laumanns and L. Thiele, "SPEA2: Improving the Strength Pareto Evolutionary Algorithm," Zurich, Switzerland, 2001.

[51] N. Stander, W. Roux, A. Basudhar, T. Eggleston, T. Goel and K. Craig, "LS-OPT User's Manual a Design Optimization and Probabilistic Analysis Tool for the Engineering Analyst -V5," Livermore Software Technology Corporation, Livermore, 2013.

[52] M. Jeanneau and P. Pichant, "La Revue de Metallurgie," *REV METALL,* vol. 97, no. 10, pp. 1143 - 1144, 2000.

[53] R. Kuziak, S. Kawalla and S. Waengler, "Advanced high strength steels for automotive industry," *ARCHIVES OF CIVIL AND MECHANICAL ENGINEERING,* vol. 8, no. 2, pp. 103-116, 2008.

[54] World Auto Steels, "Automotive Steel Definitions," 2016. [Online]. Available: http://www.worldautosteel.org/steel-basics/automotive-steel-definitions/. [Accessed 2016].

[55] World AutoSteel, "Steel Types," 2015. [Online]. Available: http://www.worldautosteel.org/steel-basics/steel-types/. [Accessed 2015].

[56] WorldAutoSteel, "Advanced High Strength Steel (AHSS) Application Guidelines V4.1," World Steel Association, 2009.

[57] V. Colla, M. De Sanctis, A. Dimatteo, G. S. A. Lovicu and R. Valentini, "Strain Hardening Behavior of Dual-Phase Steels," *The Minerals, Metals & Materials Society and ASM International,* 2009.

[58] AASHTO, "Manual for Assessing Safety Hardware," 2009.

[59] IIHS, "2010 Toytoa Yaris Full Vehicle Report," Insurance Institute for Highway Safety, 2016. [Online]. Available: http://www.iihs.org/iihs/ratings/vehicle/v/toyota/yaris-4-door-sedan/2010. [Accessed 1 January 2016].

[60] NCAC, "Developemt & Validation of a Finite Element Model for the 2010 Toyota Yaris Passenger Sedan - Technical Summary," 2011. [Online]. Available: http://www.ncac.gwu.edu/vml/models.html.

[61] NCAC, "2010 Toyota Yaris FE Model - Report," [Online]. Available: http://www.ncac.gwu.edu/vml/models.html.

[62] D. Marzougui, R. Samaha, C. Cui and C. Kan, "Extended Validation of the Finite Element Model for the 2001 Ford Taurus Passenger Sedan," NCAC, Ashburn, VA, 2012.

[63] NTRCI, "FEM Models for Semitrailer Trucks," [Online]. Available: http://tractor-trailer.model.ntrci.org/index.cgi?model=1&navv=0. [Accessed 2015].

[64] Insurance Institute for Highway Safety, "Moderate Overlap Frontal Crashworthiness Evaluation Guidelines for Rating Structural Performance," Arlington, 2011.

[65] Livermore Software Technology Corporation, "PrePost- IIHS," 2015.

[66] W. Witteman, "Improved Vehicle Crashworthiness Design by Control of the Energy Absorption for Different Collision Situations," Doctoral dissertation, Eindhoven University of Technology, Eindhoven, 1999.

[67] K Craft BullBars, "FUPD BullBar," 2016. [Online]. Available: http://www.kcraftbullbars.com.au/fupd-bullbars/. [Accessed 2016].

[68] Whitelock, "Whitelock Bull Bars," 2016. [Online]. Available: http://www.whitlockbullbars.com.au/. [Accessed 2016].

[69] Varmint Al, "Varmint Al's Engineering," 2015. [Online]. Available: http://www.varmintal.com/aengr.htm. [Accessed 2016].

[70] SSAB, [Online]. Available: http://www.ssab.com/.

[71] ArcelorMittal, "ArcelorMittal Corporate," 2015. [Online]. Available: http://corporate.arcelormittal.com/. [Accessed 2015].

[72] K. D. Kusano and H. Gabler, "Method for Estimating Time to Collision at Braking in Real-World, Lead Vehicle Stopped Rear-End Crashes for Use in Pre-Crash System Design," in *SAE International*, Detroit, 2011.

[73] R. Van Der Horst and J. H. Hogema, "Time-to-Collision and Collision Avoidance Systems," in *Proceedings 6th ICTCT Workshop*, Kuratorium fur Verkehrssicherheit, Salzburg, Austria. , 1994.

[74] J. Nickerson, "ctpost," 5 October 2010. [Online]. Available: http://www.ctpost.com/news/article/Bridgeport-woman-killed-on-I-95-crash-in-Norwalk-689031.php#photo-355805. [Accessed 1 January 2016].

[75] National Highway Traffic Safety Administration, "FMVSS No. 214, DYNAMIC SIDE IMPACT PROTECTION," U.S. Department of Transportation, Washington, 2012.

[76] National Agency for Automotive Safety & Victim's Aid, "Testing methods in other countries," [Online]. Available: http://www.nasva.go.jp/mamoru/en/assessment_car/crackup_other.html. [Accessed 1 January 2016].

[77] United Nations Economic Commission for Europe, "ECER95 The Protection of the Occupants in the Event of a Lateral Collision," Geneva, 2014.

[78] Insurance Institute for Highway Safety, "Side Impact Crashworthiness Evaluation Crash Test Protocol (Version VII)," Ruckersville, 2014.

[79] "IIHS Side Impact Testing Program Rating Guidelines - Presentation," Insurance Institute for Highway Safety, 2006.

[80] "Development & Validation of a Finite Element Model for the 2010 Toyota Yaris Passenger Sedan," The National Crash Analysis Center, Ashburn, VA, 2011.

[81] W. C. Holden, "1 killed after water truck rear-ends car in Weld County," FOX31 Denver KDVR-TV, Denver, 2014.

[82] National Highway Traffic Safety, "Laboratory Testing Procedure for FMVSS 301R - Fuel System Integrity - Rear Impact," U.S. DEPARTMENT OF TRANSPORTATION, Washington, 2007.

[83] Economic Commission for Europe, "Front and Rear Portection Devices (Bumpers, Etc)," Geneva , 2008.

[84] Insurance Institute for Highway Safety, "Vehicle seat/head restraint evaluation protocol, dynamic criteria," Arlington, 2016.